Physiological Roles of PKB Isoforms in Development, Growth and Glucose Metabolism

Inauguraldissertation

zur
Erlangung der Würde eines Doktors der Philosophie
vorgelegt der
Philosophisch-Naturwissenschaftlichen Fakultät
der Universität Basel

von

Bettina Dümmler
aus Küsnacht, Schweiz

Basel, 2007

Genehmigt von der Philosophisch-Naturwissenschaftlichen Fakultät auf Antrag von Dr. Brian Hemmings, Prof. Dr. Nancy Hynes, and Prof. Dr. Christoph Moroni.

Basel, den 21.11.2006

Prof. Dr. Hans-Peter Hauri
(Dekan)

TABLE OF CONTENT

ii. SUMMARY

Protein kinase B (PKB), also known as Akt, is a serine/threonine protein kinase that regulates key events in metabolism, proliferation, cell survival, and differentiation. Importantly, PKB is a major downstream effector of IGF1 and insulin signaling, implicating this kinase in growth control and insulin action. In mammals, there are three isoforms of PKB, PKBα/Akt1, PKBβ/Akt2, and PKBγ/Akt3. These are encoded by distinct genes but share similar structural organization. It has been proposed that such isoforms are uniquely adapted to transmit distinct biological signals. To identify specific physiological functions of the individual isoforms, we and others have generated animal models deficient in PKBα, PKBβ, and PKBγ: Mice lacking PKBα demonstrate increased perinatal mortality and a reduction in body weight, whereas PKBβ-deficient exhibit a diabetes-like syndrome with elevated fasting plasma glucose and peripheral insulin resistance; the present study shows a role of PKBγ in postnatal brain development.

These observations indicate that the PKB isoforms have some differential, non-redundant physiological functions. The relatively subtle phenotypes of these mice as well as the viability of the animals suggest, however, that for many functions PKB isoforms are able to compensate for each other. Certain physiological functions of PKB are thus revealed only when total PKB levels are below a critical threshold in particular cell types and tissues. In the present study we analyzed mice doubly deficient for PKBα/PKBγ and PKBβ/PKBγ, respectively, to identify the combined roles of these isoforms in PKB-mediated physiological processes.

We show that mice mutant in both PKBα and PKBγ die around embryonic day 12 with severe impairments in growth, cardiovascular development, and organization of the nervous system. In contrast, we found that PKB$\beta^{-/-}\gamma^{-/-}$ mice develop normally and survive with minimal dysfunctions despite a dramatic reduction of total PKB levels in all tissues. In PKB$\beta^{-/-}\gamma^{-/-}$ mice only the PKBα isoform remains to perform essential PKB functions and we show that minimal amounts of PKBα appear to be sufficient for full activation of many downstream targets. Interestingly, even the presence of only a single functional allele of

PKBα is sufficient for successful embryonic development and postnatal survival in mice. However, PKB$\beta^{-/-}\gamma^{-/-}$ mice are glucose and insulin intolerant and exhibit a ~25% reduction in body weights compared to wild-type mice. In addition, we found a substantial reduction in relative size and weight of brain and testis, demonstrating an *in vivo* role for both PKBβ and PKBγ in the determination of whole animal size and individual organ sizes.

Taken together, our results provide insights into the PKB isoform hierarchy and their relative importance during early development, growth, and glucose metabolism.

ii. ABBREVIATIONS

CDK	cyclin-dependent kinase
4EBP1	eIF4E binding protein 1
eIF4B	eukaryotic translation initiation factor 4B
GAP	GTPase activating protein
GSK3	glycogen synthase kinase 3
IGF1	insulin-like growth factor 1
IRS	insulin receptor substrate
mTOR	mammalian target of rapamycin
PDK1	3-phosphoinositide-dependent protein kinase 1
PH	pleckstrin homology
PI3K	phosphoinositide-3-kinase
PI(3,4,5)P3	phosphatidylinositol 3,4,5-triphosphate
PKB	protein kinase B
PRK2	protein kinase C-related kinase 2
PTEN	phosphatase and tensin homolog
Raptor	regulatory-associated protein of mTOR
Rictor	rapamycin-insensitive companion of mTOR
RTK	receptor tyrosine kinase
SH2	Src homology 2
S6K1	p70 ribosomal protein S6 kinase 1
TSC	tuberous sclerosis complex

Less frequently used abbreviations are defined upon their first use in the text.

I. INTRODUCTION

1. PKB isoforms and structure

PKB is a member of a family of protein kinases that originally contained cAMP-dependent kinase, cGMP-dependent kinase and protein kinase C (PKC), termed the AGC family. Other members of the AGC family include p70 ribosomal protein S6 kinase 1 (S6K1), protein kinase C-related kinase 2 (PRK2), and serum- and glucocorticoid-inducible kinase (SGK). The protein kinases of the AGC family show similarities in many structural and regulatory features. Highly similar in all AGC kinases is a flexible peptide loop (activation loop) proximal to the catalytic pocket of the kinase domain, and phosphorylation of this loop is required for the activation of virtually all AGC kinases. PKB is the cellular homologue of the transforming oncogene v-Akt, which was found in a retrovirus termed AKT8. This retrovirus was originally isolated from mice with a high incidence of spontaneous lymphoma. Close homologues of PKB have been identified in a variety of species, including birds, insects, nematodes, slime mold, and yeast (Fig. 1B).

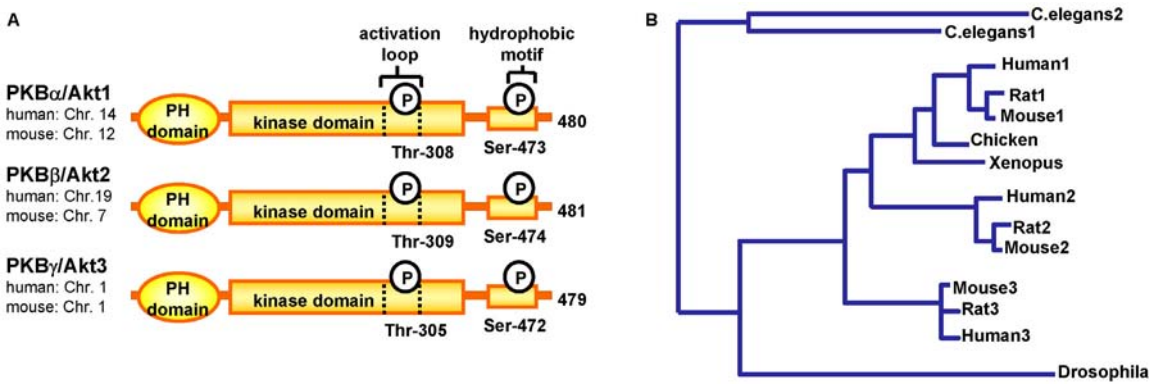

Fig, 1. (A) Domain structure and regulatory phosphorylation sites of PKB. All isoforms contain a pleckstrin homology (PH) domain, a catalytic domain and a C-terminal regulatory domain containing the hydrophobic motif. Phosphorylation of the activation loop and the hydrophobic motif (Thr308 and Ser473 in PKBα) are critical for kinase activation. (B) Phylogenetic tree of the PKB family. PKB has a high level of evolutionary conservation; mouse and human genomes encode three PKB genes (PKBα, PKBβ, PKBγ), the C.elegans genome encodes two (Akt1 and Akt2) and the drosophila genome only one (dPKB) (Adapted from Riehle *et al*., 2003).

There are three isoforms of PKB in mammals, termed PKBα (Akt1), PKBβ (Akt2), and PKBγ (Akt3). These are products of distinct genes but highly related, exhibiting greater than 80% sequence identity and sharing the same structural organization (Fig. 1A). Each isoform possesses an amino-terminal pleckstrin homology (PH) domain that binds to 3-phosphoinositides, a central catalytic domain, and a carboxy-terminal regulatory domain. Furthermore, all three isoforms possess two conserved phosphorylation sites, and phosphorylation of both sites is required for full activation of the kinase. The first one (Thr308 in PKBα) lies within the activation loop of the kinase domain and its phosphorylation induces a catalytically active conformation of the kinase. The second one lies within the regulatory domain in a 6-amino acid long sequence termed the hydrophobic motif (FPQFS^{473}Y).

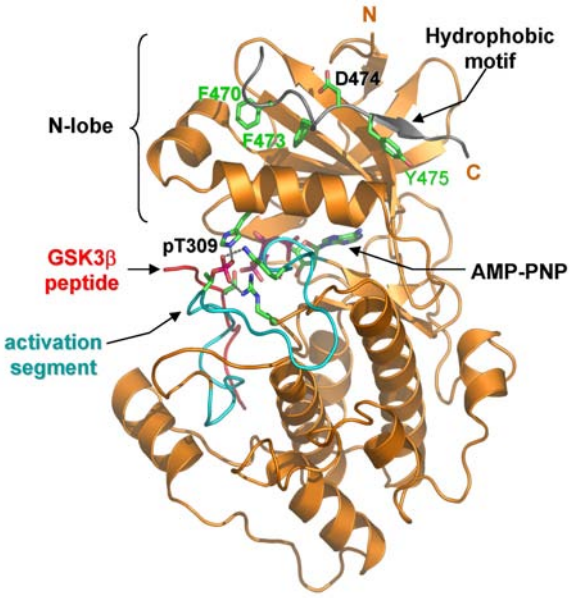

Fig. 2. Structure of activated PKB. The ribbon diagram shows an activated PKBβ ternary complex with GSK3-peptide (red) bound in the substrate-binding site and AMP-PNP (a hydrolysis-resistant ATP analogue) bound in the ATP-binding site. To obtain an active conformation, the hydrophobic motif of PKB was replaced with that of another AGC kinase, PRK2, and T309 in the activation segment (blue) was phosphorylated by PDK1. The hydrophobic motif of PRK2 contains an acidic residue (D474) in place of a phosphorylatable serine and binds constitutively to the N-lobe without needing phosphorylation. (Adapted from Yang *et al*., 2002).

Phosphorylation at Ser473 enables the hydrophobic motif to bind into a pocket[1] within the small lobe (N-lobe) of the kinase domain and thereby it stabilizes the active conformation of PKB. Binding of the phosphorylated hydrophobic motif to this pocket increases kinase activity of PKB by tenfold.

The crystal structure of the kinase domain of PKB has been solved, although this required deletion of the PH domain and substitution of the hydrophobic motif of PKB with the hydrophobic motif of PRK2 (Fig. 2)(116). All PKB isoforms are assumed to have identical or similar substrate specificity. The minimal consensus sequence for *in vitro* phosphorylation by PKB has been defined as ArgXArgXXSer/Thr-Hyd, where X is any amino acid and Hyd is a bulky hydrophobic residue.

[1] This structure has been termed the 'PRK2-interacting factor (PIF)-pocket' because it was initially identified on PDK1 as a binding site for the hydrophobic motif of PRK2.

2. The PI3K/PKB signaling pathway

The typical route of PKB activation is via receptor tyrosine kinases. Binding of ligands such as epidermal growth factor (EGF) and platelet-derived growth factor (PDGF) to their appropriate receptors leads to autophosphorylation of specific tyrosine residues on the intracellular portion of the receptor (Fig. 3). Recruitment of phosphoinositide 3-kinase (PI3K)[2] then occurs, via binding of the Src homology 2 (SH2) domains of its regulatory subunit, p85, to specific phosphotyrosine residues on the receptor. For insulin-receptor and IGF-receptor, recruitment of the p85 subunit to the receptor is largely mediated by an adaptor protein called IRS[3] (insulin receptor substrate). Binding of p85 subunit to phosphotyrosines on the receptor or IRS proteins leads to a conformational change in PI3K and consequently to activation of its catalytic subunit, p110. Activated PI3K phosphorylates inositol-containing membrane lipids at the 3'-OH position of the inositol ring, generating phosphatidylinositol 3,4,5-trisphosphate (PI(3,4,5)P3). Subsequently, inactive PKB is recruited from the cytosol to the membrane via binding of its PH domain to PI(3,4,5)P3.

Membrane recruitment brings PKB in close proximity to 3-phosphoinositide-dependent protein kinase (PDK1). PDK1 possesses a PH domain in its carboxy-terminus, which binds PI(3,4,5)P3 and localizes PDK1 at the membrane. Co-localization of the two proteins and the conformational change induced in PKB upon lipid binding then enable PDK1 to phosphorylate PKB on Thr308 in the activation loop. For full kinase activation, PKB requires phosphorylation of an additional site, Ser473, which is located in the

[2] There are several classes of phosphoinositide kinases. For growth factor signaling, the predominant enzymes that produce second messengers belong to the 3' family of phosphoinositide kinases, specifically the Class I subdivision. Class I PI3K is a heterodimeric complex comprising a 85-kDa regulatory subunit and a 110-kDa catalytic subunit. At least eight isoforms of p85 have been identified, which are derived from three distinct genes. The most ubiquitous regulatory subunit is p85α from the Pik3r1 gene. Furthermore, there are three different catalytic subunits, p110α, β, and δ, which are derived from three different genes and show different tissue distribution. The p110α and p110β forms are almost ubiquitous, whereas p110δ is restricted to leukocytes.

[3] IRS proteins have both PH domains and phosphotyrosine-binding domains (PTB domains) near the N-terminus that account for the high affinity of these proteins to the receptors. The centre and the C-terminus of the IRS proteins contain up to 20 potential tyrosine-phosphorylation sites that, after phosphorylation by the receptor, bind to intracellular molecules that contain SH2 domains.

hydrophobic motif domain. The identity of the kinase(s) mediating Ser473 phosphorylation on PKB is still controversial. Recent work has identified two kinases that can phosphorylate PKB on the hydrophobic motif: the mTOR-rictor complex and DNA-PK (DNA-dependent protein kinase) (33, 94). Most likely, these two upstream kinases mediate PKB activation in response to different stimuli. Following activation, PKB is detached from the plasma membrane and translocates to cytosol and nucleus to phosphorylate its substrates.

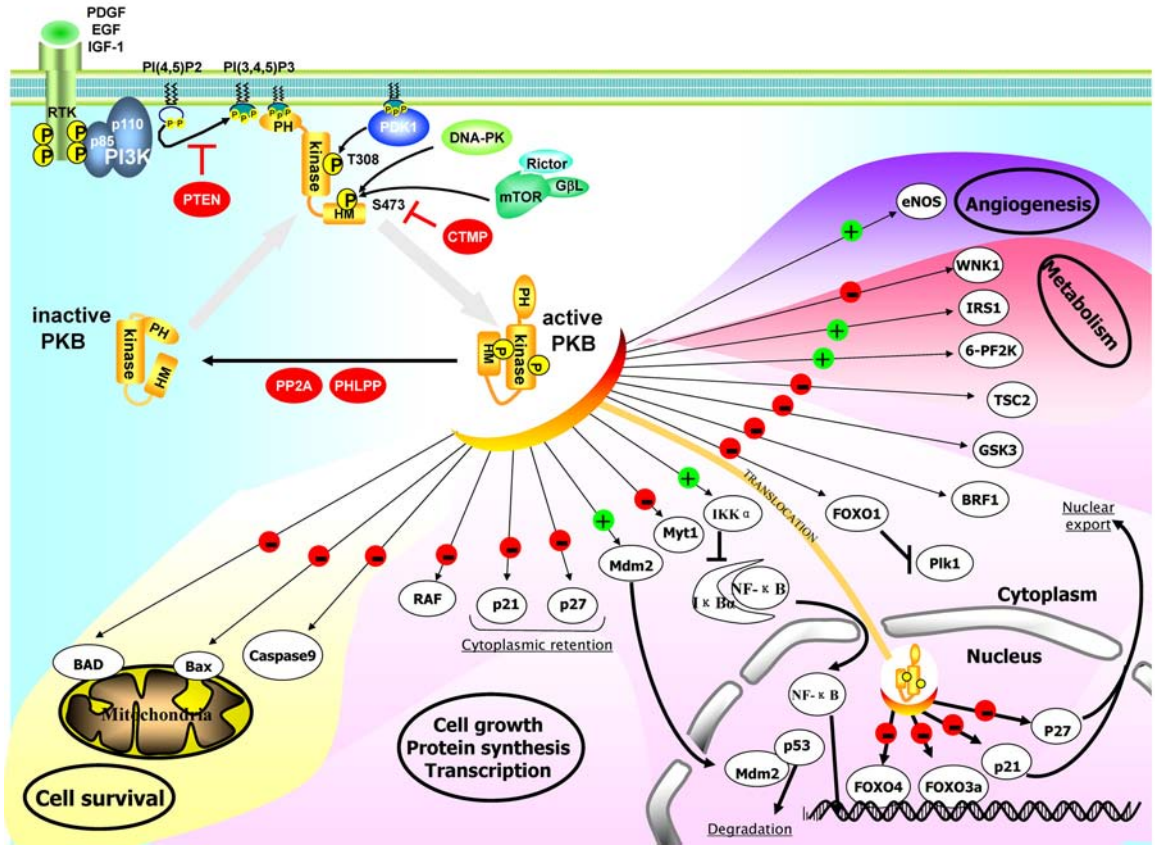

Fig. 3. Mechanism of PKB activation and downstream targets. PKB is activated via receptor tyrosine kinases (RTK) in a PI3K-dependent manner and phosphorylated on Thr308 and Ser473 by upstream kinases. Representative substrates of PKB in cytoplasm and nucleus are grouped according to their function. Activation (+) or inhibition (-) of the targets upon PKB-mediated phosphorylation is indicated. Abbreviations: BAD: Bcl-2 antagonist of cell death; BRF1: Butyrate response factor1; CTMP: C-terminal modulator protein; eNOS: endothelial cell nitric oxide synthase; FOXO1/3a/4: Forkhead Box O1/3a/4 (FOXO1/FKHR, FOXO3a/FKHRL1, and FOXO4/AFX); IKK: inhibitor kappa B kinase; Mdm2: mouse double minute 2; Myt1: membrane associated and tyrosine/threonine specific 1; NF-κB: nuclear factor-kappa B; PHLPP: PH domain and leucine rich repeat protein phosphatase; 6-PF2K: 6-phosphofructo-2-kinase/fructose-2,6-bisphosphatase; Plk1: Polo like kinase1; PP2A: protein phosphatase 2 subunit A; WNK1: with no lysine [K]1. (Adapted from Fayard *et al*., 2005)

3. Physiological functions of PKB

Up to date over 40 proteins have been identified as substrates for PKB (although some of them only *in vitro*) and the list is still increasing. The identification of PKB substrates and the role PKB-mediated phosphorylation plays in the regulation of these molecules have been a major focus of research in recent years. The long list of PKB substrates reflects the widely divergent cellular processes that PKB is implicated in, such as metabolism, differentiation, cell survival, and cell growth/proliferation. In the following, PKB function in cell growth/proliferation and in glucose metabolism is described.

3.1. Role of PKB in cell proliferation

Cell proliferation involves two distinct but intertwined processes: cell growth (increase in cell size) and cell division (i.e. progression through the cell cycle). Cell growth is characterized by elevated production of the translational apparatus that is needed to cope with the increasing demand for protein synthesis. A favourable metabolic state is necessary to accumulate enough cell mass and organelles to establish two daughter cells. Cell cycle progression includes activation of cyclin-dependent kinases (CDKs) that, in association with different cyclins, turn key switches throughout the cell cycle. PKB-mediated control of both cell growth and cell cycle progression is well established and involves regulation of many different targets (Fig. 4).

The PI3K/PKB pathway in cell cycle progression

PKB triggers a network that positively regulates G1/S cell cycle progression (59). For instance, PKB regulates the cell cycle inhibitors $p21^{Cip1}$ and $p27^{Kip1}$ (60, 109, 120). In quiescent cells $p27^{Kip1}$ and $p21^{Cip1}$ are localized in the nucleus and inhibit cell cycle progression by binding to cyclin-CDK complexes. Mitogenic stimuli activate PKB, which then phosphorylates $p21^{Cip1}$ and $p27^{Kip1}$ at specific sites within their nuclear localization sequences. Phosphorylation at these sites impairs nuclear import of $p21^{Cip1}$ and $p27^{Kip1}$ and liberates CDKs from inhibition.

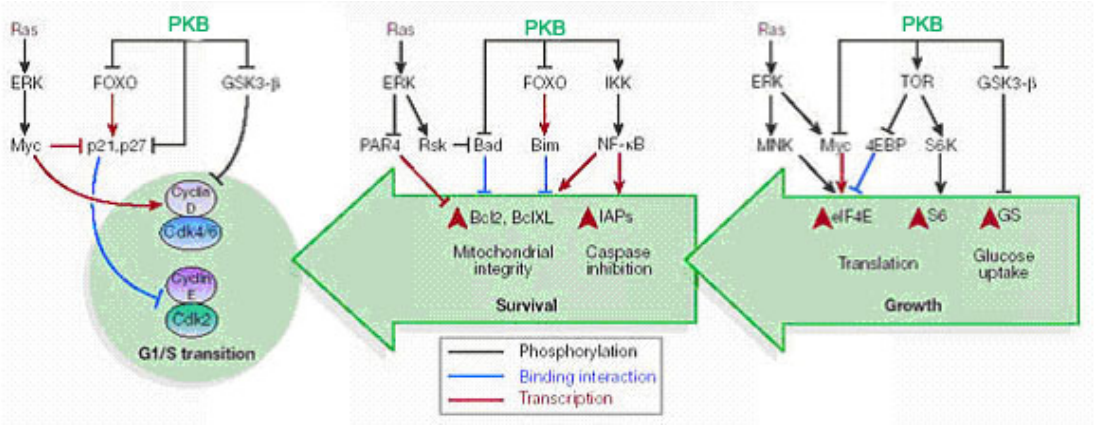

Fig. 4. Networks integrating growth, survival, and cell cycle progression signals. PKB controls key nodes in cell growth, survival, and cell cycle G1/S transition. Important PKB downstream targets are FOXO transcription factors, mTOR, GSK3β, and the CDK inhibitors $p21^{Cip1}$ and $p27^{Kip1}$. (Adapted from Massague *et al.*, 2004)

Another mechanism, by which PKB promotes cell cycle progression, is the indirect regulation of cyclin D1 protein stability. In quiescent cells cyclin D1 protein is unstable, as glycogen synthase kinase-3β (GSK3β)-mediated phosphorylation targets cyclin D1 for degradation by the proteasome. Active PKB negatively regulates GSK3 activity by phosphorylation and thereby prevents cyclin D1 degradation (30). Recent data also implicated PKB in G2/M transition. Okumura *et al.* found that PKB phosphorylates and thereby inactivates the Wee1 family kinase Myt1 in starfish oocytes (78). Myt1 mediates inhibitory phosphorylation of CDK1, which keeps the cyclin B-CDK1 complex in an inactive state. When Myt1 is inactivated, Cdc25 phosphatase can dephosphorylate CDK1 and the cyclin B-CDK1 complex can drive G2/M transition.

The TSC1/TSC2 complex connects the nutrient-mTOR and the PI3K/PKB growth pathways

Effective cell growth is a prerequisite for the cell cycle machinery to proceed through G1/S phase and initiate cell division. The major regulator of cell growth is a distinct signaling network, termed the mTOR (mammalian target of rapamycin) pathway. mTOR is a large protein with homology to members of the lipid kinase family and is active in presence of high nutrient levels (glucose and amino acids) in the cell. mTOR exists in two distinct multi-protein complexes

(93). One is composed of mTOR as well as GβL (G-protein β-subunit-like) and raptor (regulatory-associated protein of mTOR). The other complex contains also mTOR and GβL but, instead of raptor, a different protein called rictor (rapamycin-insensitive companion of mTOR). The mTOR-raptor complex is rapamycin sensitive, as rapamycin-FKBP12 can bind to it and inhibit mTOR kinase activity, whereas the mTOR-rictor complex is rapamycin-insensitive. The two complexes have different functions: mTOR-rictor has been shown to function as an upstream kinase for PKB (94) and regulator of cytoskeletal reorganization (47), whereas mTOR-raptor positively regulates cell growth and modulates a stunning number of other processes, including mRNA translation, ribosome biogenesis, nutrient metabolism and autophagy (37, 71).

The discovery of a regulatory link between PKB and mTOR-raptor revealed how mitogenic stimuli can promote mTOR-mediated cell growth via the PI3K/PKB pathway. Tuberous sclerosis complex (TSC) is an autosomal dominant disorder that is characterized by benign tumors (hamartomas) involving multiple organ systems. TSC is due to inactivating mutations in either of two genes, tuberous sclerosis complex 1 (TSC1) and tuberous sclerosis complex 2 (TSC2) (17, 58). The protein products of these genes form a complex, TSC1/TSC2, that inhibits growth. During the past few years enormous progress has been made in understanding the biochemical and signaling function of this complex. TSC2 is a GTPase-activating protein (GAP), and in unstimulated conditions the TSC1/TSC2 complex has a highly specific GAP activity towards a small G protein called Rheb (Ras homolog enriched in brain) (44, 95, 119). Rheb-GTP levels play a major role in regulating the state of activation of the mTOR-raptor complex: in the GTP-bound state, Rheb leads to an increase in the activation of the mTOR-raptor complex, whereas a functional TSC1/TSC2 complex maintains GDP-bound Rheb and thereby low levels of mTOR-raptor activity (63). In cells lacking either TSC1 or TSC2, there is absence of a functional TSC1/TSC2 complex and concomitantly an elevation of Rheb-GTP levels. This leads to high levels of growth factor-independent, deregulated mTOR-raptor activity and consequently to the growth and differentiation defects that are seen in TSC hamartomas. Several groups have now shown that TSC2 is directly phosphorylated by PKB on several sites and

that this PKB-mediated phosphorylation inhibits TSC1/TSC2 function as a Rheb-GAP (27, 45, 68, 84). The TSC1/TSC2 complex constitutes therefore the converging node through which PKB can connect with the mTOR pathway and regulate cell growth.

How does the mTOR pathway promote cell growth? Two mammalian proteins, eIF4E binding protein 1 (4EBP1) and S6K1, are known to link the mTOR-raptor complex to the control of mRNA translation. 4EBP1 is a repressor of translation; when hypophosphorylated in the absence of nutrients or growth factors, 4EBP1 associates with eIF4E[4] (eukaryotic translation initiation factor 4B), the mRNA cap binding protein, to inhibit cap-dependent translation. Binding of 4EBPs to eIF4E is regulated by ordered phosphorylation of critical residues on 4EBP1. The mTOR-raptor complex catalyzes phosphorylation of 4EBP1 on specific Ser/Thr sites, which leads to release of eIF4E from 4EBP1 and permits its participation in translation initiation complexes (75). In parallel, mTOR-raptor activates S6K1 (and likely the related S6K2) by phosphorylating it within the hydrophobic motif conserved in the AGC family of kinases (12). Although activation of S6K requires phosphorylation on many sites by several distinct kinases, mTOR-mediated phosphorylation on the hydrophobic motif site is absolutely required for S6K activity. How S6K1 substrates exactly contribute to cell size control remains to be determined but numerous reports have shown that absence or inactivation of S6K1 causes smaller cells, whereas activation of S6K1 stimulates cell growth (73, 90, 102). Several S6K1 substrates have been described, including the ribosomal S6 protein and the translational regulators eEF2 kinase and eIF4B (88). In addition, translational activation of 5'TOP mRNAs has been attributed to S6K activity (48). 5'TOP mRNAs encode many components of the translational apparatus (ribosomal proteins, elongation factors eEF1A and eEF2, and poly(A)-binding protein). Translational repression of 5'TOP mRNAs is apparent when proliferation of vertebrate cells is blocked by a wide variety of physiological signals (terminal differentiation, contact

[4] Initiation of translation is considered to be the rate-limiting step of translation. In the most general mechanism of translation initiation, the assembly of the eIF4F complex on the mRNA 5' cap structure is essential for the recruitment of the 40S small ribosomal subunit to the mRNA. The eIF4F complex is comprised of three polypeptides, among these is the cap-binding protein eIF4E, which is present in limiting amounts relative to other initiation factors. The availability of eIF4E is regulated by its interaction with the inhibitory proteins 4EBP1-3.

inhibition, serum starvation) or by cell cycle inhibitors (aphidicolin and nocodazole). More recent work however does not support a role of S6K1 in this process; Stolovich *et al.* found that translational activation of 5'TOP mRNAs requires neither S6K1 nor ribosomal protein S6 phosphorylation (104).

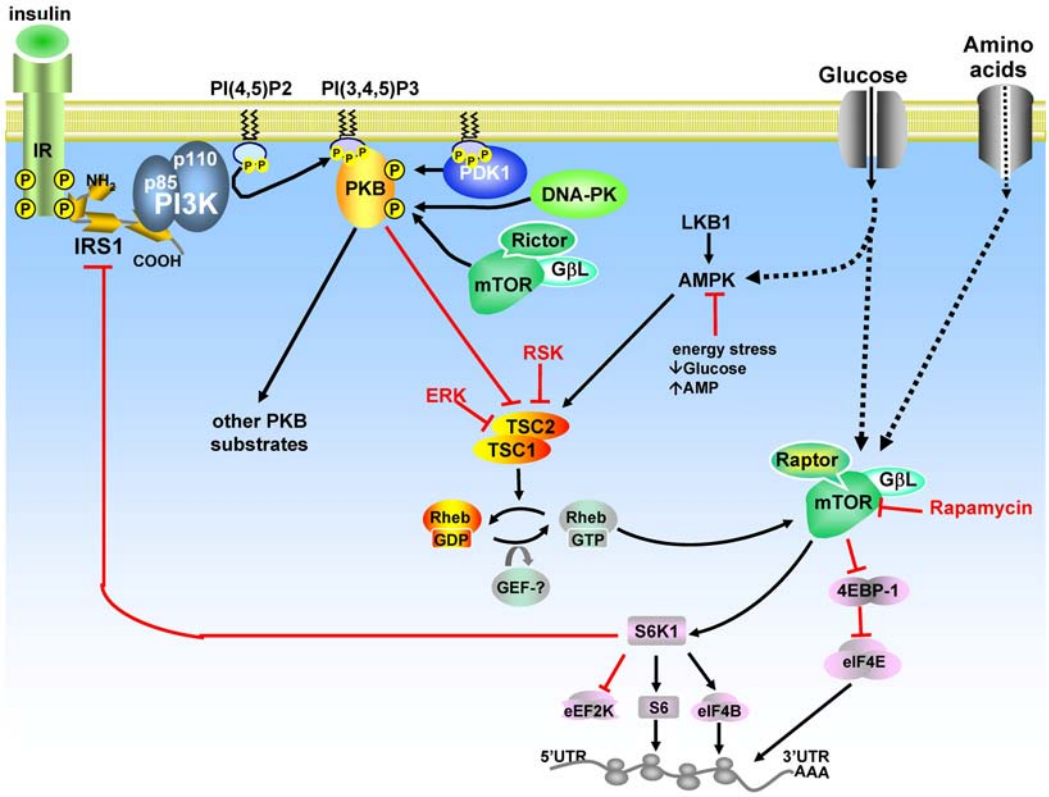

Fig. 5. The PI3K/PKB pathway promotes cell growth and translation via activation of the mTOR-raptor complex. In response to mitogens, activated PKB phosphorylates TSC2 on Ser939, Ser1130, and Thr1462, thereby inhibiting GAP function of the TSC1/TSC2 complex on Rheb and relieving inhibition on the mTOR-raptor complex. (Adapted from Um *et al.*, 2006).

Taken together, these results suggest the following model for growth signaling (Fig. 5). In the absence of growth-stimulatory signals, hypophosphorylated TSC1/TSC2 inhibits mTOR-raptor, so that translation regulated by eIF4E and S6K1 is minimal. When stimulated by growth factors, activated PI3K/PKB signaling results in the phosphorylation and inhibition of the TSC1/TSC2 complex and thus the derepression of mTOR-raptor. mTOR-raptor then phosphorylates S6K1 and 4EBP1, translation rates increase and growth ensues. Interestingly, the mTOR-raptor complex also initiates feedback inhibition of PKB which is, at least in part, mediated by an inhibitory effect of

S6K on IRS1 (38). Although up to date rather speculative, another mechanism of feedback inhibition could occur via a shift in the equilibrium between mTOR-raptor and mTOR-rictor complex formations. PKB-mediated inhibition of TSC1/TSC2 complex may promote the assembly of active mTOR-raptor complexes and thereby antagonize formation of mTOR-rictor complexes. As mentioned above, mTOR-rictor complex may be the principal Ser473 kinase in PKB activation following growth factor stimulation, and reduction of mTOR-rictor complex formation would therefore also reduce PKB activity.

Of note, the TSC1/TSC2 complex receives inputs from at least two other major signaling pathways, besides the PI3K/PKB pathway, that regulate its function as a GTPase activating protein by kinase-mediated phosphorylation events. First, there is regulation of the mTOR pathway by the MAP (mitogen-activated protein) kinase pathway at the TSC1/TSC2 level; both ERK (extracellular signal-regulated kinase) and its downstream target RSK1 (p90 ribosomal protein S6 kinase 1) phosphorylate TSC2 (at sites distinct from the major PKB sites) and thereby negatively regulate the Rheb-GAP activity of the TSC1/TSC2 complex (64, 89). Second, the cellular energy-sensing kinase AMPK (AMP-activated protein kinase) can also phosphorylate TSC2 but, in contrast to the phosphorylation of TSC2 by PKB, AMPK-mediated phosphorylation somehow enhances the ability of TSC1/TSC2 to act as a Rheb-GAP and therefore blocks Rheb-dependent mTOR activation under conditions of energy stress (46). Apparently, the TSC1/TSC2 complex serves as the converging point for the AMPK (nutrient) and PKB (growth factor) signaling in higher eukaryotes.

3.2. Role of PKB in glucose homeostasis

In humans as well as in other species, the ingestion of food provides the fundamental source of energy for various cellular activities. The intake of food and the ability of controlling the plasma levels of substrates for energy production involve complex mechanisms that ensure a constantly adequate supply of metabolites both in fasting and fed state. Postprandial blood glucose levels are mainly controlled by secretion of the peptide hormone insulin, which acts as a highly potent physiological anabolic agent. It promotes the storage

and synthesis of lipids, protein, and carbohydrates and inhibits their breakdown and release into circulation (Fig. 6).

The first step by which insulin increases energy storage or utilization involves the regulated transport of glucose into the cells. In muscle and adipose tissues, a unique member of the facilitative glucose transporter (GLUT) family, GLUT4, is highly expressed and responsible for insulin-stimulated glucose uptake in these tissues (11). In unstimulated cells, GLUT4 is stored in intracellular vesicles. Binding of insulin to its receptor initiates translocation of GLUT4 from its storage vesicles to the plasma membrane and thereby increases glucose entry into the cell 10-40 fold.

.

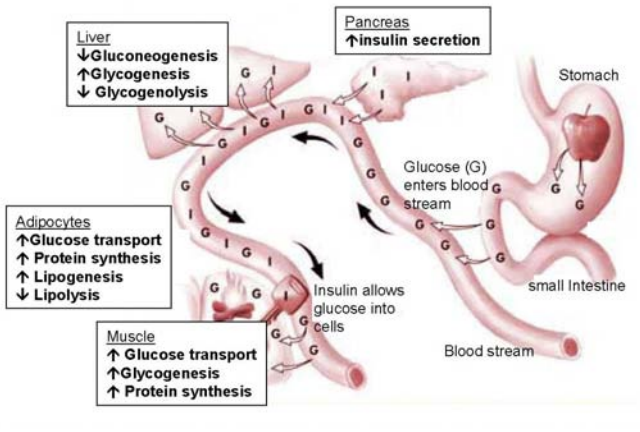

Fig. 6. Insulin regulates energy metabolism following food intake. Insulin (I) secretion from pancreatic β-cells depends on the abundance of ingested and circulating nutrients. In its target tissues (mainly liver, fat, and skeletal muscle) it promotes the uptake and storage of glucose (G), amino acids, and fat, whilst simultaneously antagonizing the catabolism of fuel reserves. In target cells, the PI3K/PKB pathway is a major mediator of the metabolic actions of insulin. (Adapted from Mayo Foundation for Medical Education and Research).

The PI3K/PKB pathway is a major mediator of the metabolic actions of insulin and plays an essential role in glucose uptake and GLUT4 translocation. PKB becomes strongly activated upon insulin stimulation and overexpression of PKB was shown to be sufficient to drive GLUT4 translocation (54). Although it is still not clear how PKB impinges on GLUT4 cycling, there is evidence for at least two PKB substrates to be involved in insulin-stimulated glucose transport. The first is AS160 (Akt substrate 160), a Rab-GAP that contains five sites that

conform to the PKB substrate consensus sequence (RXRXX[pS/pT]) and whose phosphorylation has been shown to be increased by insulin. Rab GTPases are key players in membrane trafficking events and have been shown to have critical roles in vesicle formation, fusion, and movement. The Rab protein regulated by AS160 is yet to be identified; however, it has been demonstrated that a mutant AS160 lacking the PKB phosphorylation sites blocks the ability of insulin to stimulate the exocytosis of GLUT4 (91). A second PKB substrate that plays a role in insulin-regulated GLUT4 trafficking is PI5-kinase (PIKfyve) (10). PIKfyve may have a role in the sorting of GLUT4 from internalized endosomes into GLUT4 storage vesicles. Another PKB substrate that seems to be involved in the regulation of insulin-stimulated GLUT4 translocation is Synip (115). However, the relevance of Synip phosphorylation is controversial because substitution of the PKB-phosphorylated residue to alanine does not prevent insulin-dependent GLUT4 accumulation at the cell surface.

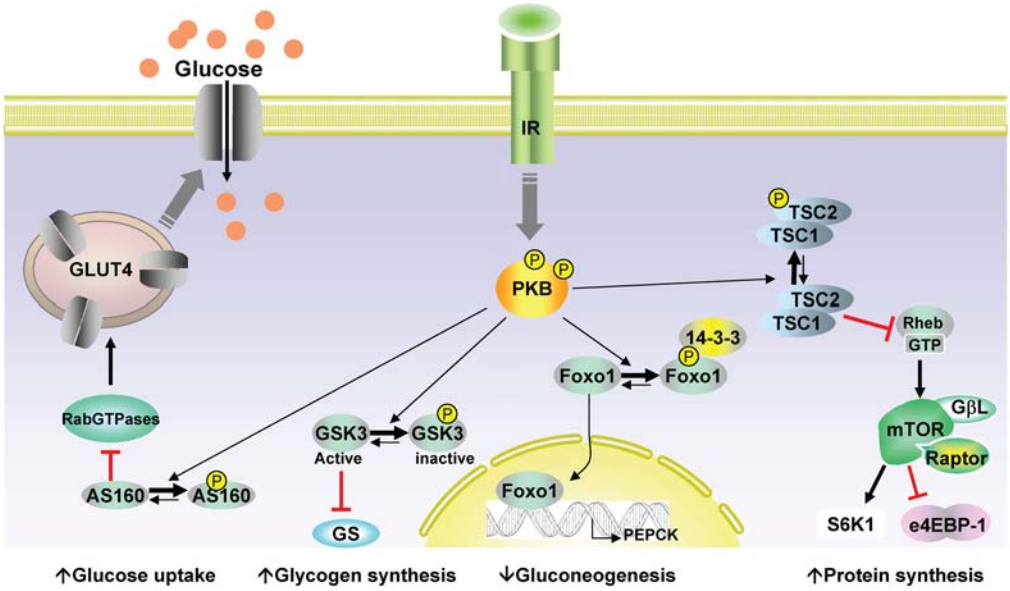

Fig. 6. Schematic model for PKB-mediated insulin actions. In muscle and fat cells, GLUT4 redistributes from intracellular storage vesicle to the plasma membrane, resulting in increased glucose flux into the cells. Protein synthesis is promoted via the mTOR pathway and glycogen synthesis is stimulated via activation of glycogen synthase (GS). In liver, PKB suppresses transcription of phosphoenolpyruvate carboxykinase (PEPCK), which is the rate limiting enzyme in gluconeogenesis.

Furthermore, in response to insulin, PKB promotes glycogen synthesis via phosphorylation and inactivation of GSK3 (26). In unstimulated cells, glycogen synthase, the enzyme mediating incorporation of glucose from uridine diphosphoglucose into glycogen, is kept in an inactive state via GSK3-mediated phosphorylation. Activated PKB phosphorylates and thereby inactivates GSK3, thus promoting dephosphorylation of glycogen synthase and increased glycogen synthesis.

Of note, atypical members of the protein kinase C family (ζ and λ) have been proposed as alternative mediators of insulin induced glucose transport (55).

4. Role of PKB in disease

Aberrant signaling via the PI3K/PKB pathway plays a central role in the development and progression of two major diseases, type 2 diabetes mellitus and cancer (Fig. 7).

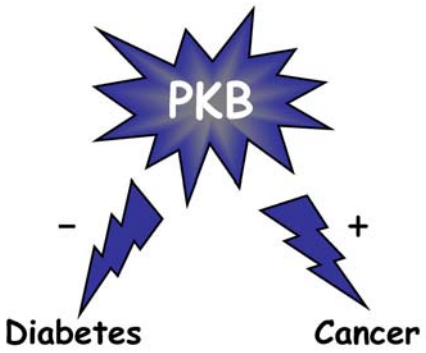

Fig. 7. Aberrant PKB activity in disease. Hypoactivation of PKB is implicated in type 2 diabetes mellitus and hyperactivation of PKB is one of the most common molecular alterations in human malignancy.

4.1 Pathology of type 2 diabetes and molecular mechanisms in insulin resistance and β cell failure

Type 2 diabetes mellitus is a polygenic, multifactorial disease with a pathology that includes both a diminished ability of cells to respond to insulin (termed "insulin resistance") and defective insulin secretion by pancreatic β cells. It afflicts an estimated 6% of the adult population in Western society and its worldwide frequency is expected to continue to grow (39). Insulin resistance typically heralds the onset of type 2 diabetes; it can often be detected years prior to onset of clinical disease (111). In pre-type 2 diabetic individuals, pancreatic β cells are capable of secreting increased amounts of insulin as a compensatory response to overcome the defect in insulin action; hyperinsulinemia ensues to maintain normal blood glucose levels. Ultimately, however, this balance between insulin resistance and insulin secretion can exhaust, and the full phenotype of type 2 diabetes develops (34). Dysfunctional glucose uptake into muscle and adipose tissue, in conjunction with an oversupply of glucose from the liver, results in high circulating plasma glucose levels that cause many severe complications. Untreated type 2 diabetes can

result in renal failure, vascular disease (including coronary artery disease), and vision damage.

The molecular defects underlying peripheral insulin resistance and relative failure of the pancreatic β cells in type 2 diabetes are still unclear and may be diverse. Most likely, a combination of acquired and genetic alterations accounts for the development of the disease. Functional studies have demonstrated numerous quantitative and qualitative abnormalities in the insulin signaling pathways of patients displaying insulin-resistance, including down-regulation of the insulin receptor, decreased insulin receptor phosphorylation and tyrosine kinase activity, reduced levels of active intermediates in the insulin signaling pathway, and impairment of GLUT4 translocation (15, 79, 83).

A relatively new area in type 2 diabetes research is the regulation of β cell mass plasticity and its relevance in the onset of disease. Decreased β cell mass is a universal observation in both human patients and rodent disease models with obesity-linked type 2 diabetes (85). It is caused by a marked increase in β cell apoptosis that outweighs the rate of β cell replication and neogenesis. Currently, it is unclear what instigates an increased rate of β cell apoptosis during the pathogenesis of type 2 diabetes; however, both chronic exposure to elevated levels of fatty acids and prolonged fluctuations of high circulating glucose levels have a prominent influence. Recent studies have implicated signal transduction via IGF1→ IRS2[5] (insulin receptor substrate 2)→ PI3K/PKB as critical to the control of β cell survival (100). For instance, targeted disruption of IRS2 in mice results in both peripheral insulin resistance and and increased rate of pancreatic β-cell apoptosis; ultimately these mice become profoundly diabetic (113). In contrast, $IRS1^{-/-}$ mice also display peripheral insulin resistance but do not become diabetic, because the β cell mass can in presence of functional IRS2 signaling expand and compensate for

[5] Several insulin receptor substrate (IRS) proteins have been identified in mammals (IRS1-IRS6). IRS1 and IRS2 are widely distributed, whereas IRS3 is largely limited to adipocytes and brain, and IRS4 is expressed primarily in embryonic tissues or cell lines. Although they are highly homologous, studies in knockout mice and cell lines indicate that the various IRS proteins serve complementary, rather than redundant, roles in insulin/IGF1 signaling. Of note, IRS proteins also undergo serine phosphorylation in response to stimuli, which in general seem to negatively regulate IRS signaling. Serine phosphorylation of IRS1 is increased in insulin-resistant states but its exact role in the pathophysiology of insulin resistance is still not completely understood.

the insulin resistance (106). PKB appears to be a key downstream mediator of IRS signaling in both β cell survival and insulin sensitivity. Activation of PKB provides protection from apoptosis through phosphorylation and inhibition of pro-apoptotic proteins, such as BAD, and increases expression of PDX1 (pancreas-duodenum homeobox-1), an important proliferation and survival factor in β cell (49, 85).

4.2 Activation of PKB in cancer

The PI3K/PKB pathway is an important driver of cell proliferation, cell growth, and cell survival, all events that favor tumorigenesis. Accordingly, constitutive or increased activity of the PI3K/PKB-dependent signaling cascade presents a major means whereby tumor cells achieve uncontrolled proliferation - and PKB is one of the most frequently hyperactivated protein kinases in human cancer (Table1). Hyperactive PKB is, due to its anti-apoptotic activity, also linked to the resistance of many cancers to treatment with cytotoxic agents. Aberrant activation of PKB in human cancer can occur by diverse mechanisms. PTEN (phosphatase and tensin homolog) is a lipid phosphatase that negatively regulates the PI3K singnaling pathway and normally limits PKB activation. In a large number of cancers PTEN is mutated, deleted, or otherwise inactivated, which results in accumulation of high levels of $PI(3,4,5)P_3$ and constitutive activation of PKB. PTEN inactivation occurs with a high incidence in prostate and endometrial cancers, glioblastoma, and melanoma (14, 28, 92). Amplification and overexpression of the gene encoding the p110α catalytic subunit of PI3K is also observed in a subset of human cancers (13, 81, 101), as well as increased receptor tyrosine kinase activation (e.g. heterodimeric ErbB-2/ErbB-3 receptor activation) (3, 96); both leading to deregulated PKB activation. Lastly, PKB gene amplification as well as mRNA or protein overexpression has been found in a variety of human cancers (21, 77, 114).

The observed dependence of certain tumors on PKB signaling for survival and growth make components of the PI3K/PKB pathway appealing targets for novel anticancer therapies. In the last several years, through combinatorial chemistry and high-throughput screening, a number of inhibitors of the PKB pathway

have been identified. Potential targets for selective inhibition include upstream receptor tyrosine kinases, PI3K, PDK1, PKB itself, and mTOR kinase (20, 57); the different therapeutic targets of the PI3K/PKB pathway are summarized in Fig. 8.

Table 1. PKB activation in human cancers

Tumor type	% Tumors with hyperactive PKB
Glioma	~55
Thyroid carcinoma	80-100
Breast carcinoma	20-55
Small-cell lung carcinoma	~60
Non-small-cell lung carcinoma	30-75
Gastric carcinoma	~80
Gastrointestinal stromal tumors	~30
Pancreatic carcinoma	30-70
Bile duct carcinoma	~85
Ovarian carcinoma	40-70
Endometrial carcinoma	>35
Prostate carcinoma	45-55
Renal cell carcinoma	~40
Anaplastic large-cell lymphoma	100
Acute myeloid leukemia	~70
Multiple myeloma	~90
Malignant mesothelioma[a]	~65
Malignant melanoma[b]	43-67

[a] Altomare et al., 2005; [b] Reviewed in Robertson, 2005; remaining cancer types reviewed in Bellacosa et al., 2005. (Adapted from Altomare et al., 2005).

Most small molecule inhibitors against kinases bind in the enzyme active site and display ATP-competitive behavior. So far, due to the fact that there is a high degree of homology in the ATP-binding pockets between PKB, PKA and PKC, no ATP-competitive inhibitors have been identified that are specific against PKB. However, recently a group from Merck research laboratories described novel allosteric PKB inhibitors that are highly specific for PKB and even isoform-selective (5, 61). Binding of these inhibitors appears to promote an inactive conformation of the kinase. Although promising results were

achieved in cell culture experiments, the poor solubility and pharmacokinetic properties of these inhibitors have so far precluded their evaluation in animal models.

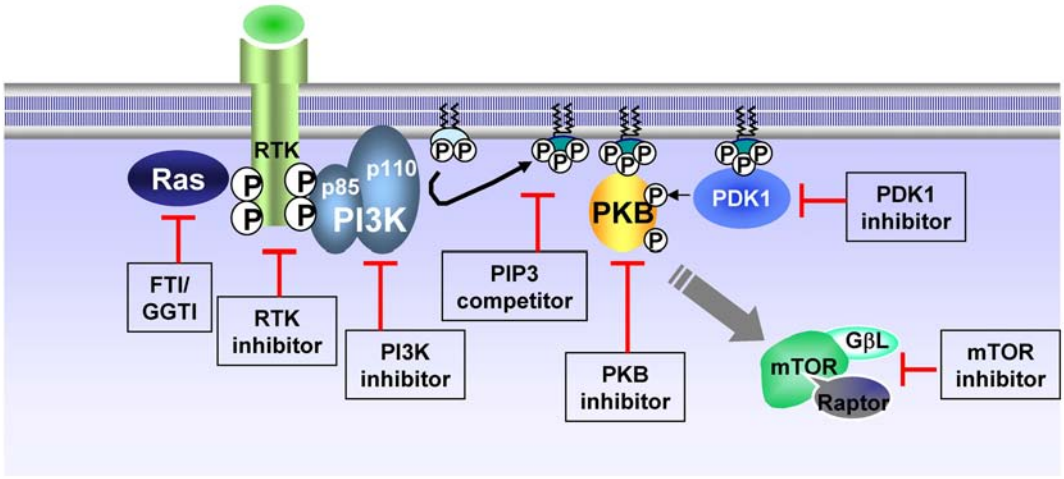

Fig. 8. Therapeutic targeting of the PI3K/PKB pathway. Receptor tyrosine kinase inhibitors (RTK inhibitors) include small-molecule tyrosine kinase inhibitors and humanized antibodies against the extracellular receptor domains. Farnesyltransferase inhibitors (FTI) and geranylgeranyltransferase inhibitors (GGTI) and are a new class of anticancer drugs (inhibitors of prenylation); the mechanism of their antitumor activity is still unclear. PI3K inhibitors include Wortmannin and LY294002, which are relatively non-specific for members of the PI3K family, and several new, more selective compounds. Wortmannin inhibits PI3K activity by binding covalently to a conserved lysine residue in the ATP-binding site of the enzyme whereas LY294002 is a reversible ATP-competitive inhibitor. PDK1 inhibitors include the staurosporine derivative UCN-01, which forms a complex with the kinase domain of PDK1. PIP3 competitors bind to the PH domain of PKB and decrease its localization at the plasma membrane. Recently, highly specific allosteric PKB inhibitors were identified that seem to stabilize PKB in an inactive conformation that is not capable of being activated by PDK1. mTOR inhibitors include rapamycin and its derivatives. Rapamycin binds to FKBP-12 and this complex can inhibit mTOR kinase activity. (Adapted from Cheng *et al*., 2005).

Two mTOR inhibitors, the rapamycin derivatives CCI-779 (Wyeth Ayerst) and RAD001 (Novartis Pharma) are currently being assessed in clinical trials in phase III and phase I/II, respectively (7). They appear to have anti-tumor activity for a wide range of malignancies; it seems that the maintenance of tumors that harbour hyperactive PI3K/PKB signaling requires intact mTOR signaling. Furthermore, three small-molecule PDK1 inhibitors (BX-795, BX-912, and BX-320) have recently been identified that may have clinical utility as anticancer agents, and a staurosporine derivative (UCN-01) which also potently inhibit PDK1 is currently in clinical trials. A recent study found several modified phosphatidylinositol ether lipid analogues that could act as PI(3,4,5)P3

competitors and bind to the PH domain of PKB (and presumably to other PH-domain containing proteins). These PI(3,4,5)P3 competitors can inhibit PKB and selectively induce apoptosis in cancer cell lines with high levels of endogenous PKB activity (16).

5. Insights from PKB mutant mice

Targeted deletion of PKB isoforms in mice and as well the generation of transgenic mice expressing constitutively active PKB in specific organs (i.e. in heart, thymus, mammary gland, pancreas, and prostate) have made it possible to identify biological processes controlled by individual PKB isoforms. The three PKB isoforms appear to have some differential, non-redundant physiological functions. PKBα (and to a lesser extent also PKBβ and PKBγ) seems to be an essential regulator of cell proliferation and cell size. Mice lacking PKBα display a reduction in body weight of 20-30%, whereas an increase in PKBα activity in specific organs or tissues increases cell number and cell size (9, 19, 23, 24, 67, 69, 103, 108, 118). In addition, PKBα was shown to be an important regulator in adipocyte differentiation (6). PKBβ appears to be required for the maintenance of normal glucose homeostasis. PKBβ-deficient mice display glucose intolerance, insulin resistance, dyslipidemia, and hyperglycemia – and in a substantial portion of PKBβ-deficient mice this phenotype progresses to a severe form of diabetes that is accompanied by β cell failure. Interestingly, PKB isoforms are not functionally redundant in glucose homeostasis. Studies in embryonic fibroblasts derived from PKBα and PKBβ knockout mice, as well as knockdown studies in 3T3L1 adipocytes using siRNA, indicate that PKBβ is the major isoform mediating insulin-induced glucose uptake and loss of PKBβ function cannot be rescued by expression of PKBα (4, 22, 35, 50). The phenotypes of different PKB mutant mice are summarized in Table 2 and the phenotypes of mice deficient in PKBγ, PKBα/PKBγ, and PKBβ/PKBγ are described in detail in the result section.

Table 2. Phenotypes of PKB mutant mice

Targeted tissues	PKB	General findings and references
all	PKBα-deficient	Increased neonatal lethality, small body size, placental defect, and impaired adipogenesis (6, 19, 23, 118)
all	PKBβ-deficient	Fasting hyperglycemia, glucose intolerance, insulin resistance, and age-dependent loss of adipose tissue (22, 35).

all	PKBγ-deficient	Reduced brain weight (decreases in both cell size and cell number) (32, 107).
all	PKBαβ-deficient	Mice die shortly after birth with multiple defects: small body size, impaired skin development, skeletal muscle atrophy, delayed bone development, and impeded adipogenesis (82).
all	PKBαγ-deficient	Lethal at embryonic stage (day E12). Severe impairments in growth, cardiovascular development, and organization of the nervous system (117).
all	PKBβγ-deficient	Mice are viable but exhibit impaired glucose homeostasis and reduce brain and testis weights.
Heart	constitutively active PKBα	Increased basal glucose uptake and myocardial contractility, cardiac hypertrophy, increased cell size of cardiomyocytes. In some cases cardiac dilatation and death. α-myosin heavy chain promoter was used for tissue-specific expression. (24, 25, 52, 69, 70, 103)
Thymus	constitutively active PKBα; (one study with constitutively active PKBβ)	Active PKB prevents apoptosis in T cells. Tumor induction (thymomas and lymphomas) and larger cell size of thymocytes; isolated thymocytes display increased cell cycle progression. CD2 promoter and lck promoter were used for T cell-specific expression. (51, 67, 72, 76, 80, 87).
Mammary gland	constitutively active PKBα	Increased fat content in milk, delayed involution after lactation; constitutively active PKB contributes to tumor development when co-expressed with ErbB2. MMTV promoter was used for tissue-specific expression. (1, 41, 42, 98, 99)
Pancreas	constitutively active PKBα	Larger islets due to increase in cell size and cell number, elevated insulin secretion. Rat insulin promoter was used for β cell-specific expression. (9, 108).
Pancreas	kinase-dead mutant of PKBα	Impaired glucose tolerance due to defective insulin secretion; Rat insulin promoter was used for β cell-specific expression (8).
Prostate	constitutively active PKBα	Prostatic intraepithelial neoplasia (PIN) (66). Probasin promoter was used for prostate-specific expression.

Two forms of PKBα have been commonly used for plasmid construction to generate mice with constitutively active PKB: a myristylated version (Myr-PKB) engineered by adding a Lck or Src myristylation signal sequence to the N-terminus of PKB, which leads to a hyperactivated form of the kinase; and a constitutively active variant of PKB in which the two regulatory sites of PKB are mutated to acidic residues to mimic the doubly phosphorylated form of the kinase (i.e. T308D /S473D in PKBα). The kinase-dead mutant of PKB has a mutation in the ATP-binding site (K179M) and acts in a dominant negative manner. Abbreviations: lck: lymphocyte-specific kinase; MMTV: mouse mammary tumor virus.

Although mice deficient in individual PKB isoforms show distinct phenotypes, these differences have yet to be correlated to differences at the level of

substrate selectivity or signaling functions of the different isoforms. It is likely that there are some isoform-specific substrates but the abundance of each PKB isoform in a given cell type or tissue (Fig. 9) and perhaps specific intracellular localizations may also in part account for the different phenotypes observed in the mutant mice.

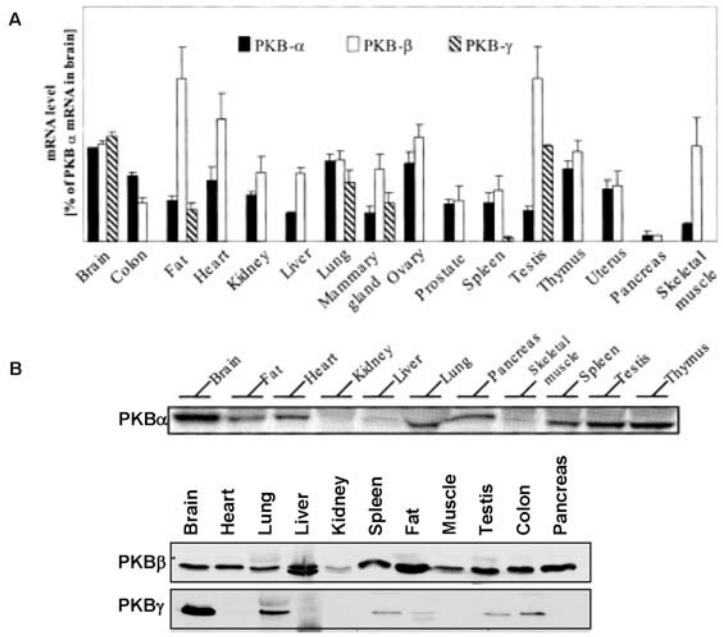

Fig. 9. Tissue distribution of PKB isoforms in adult mice. (A) Quantitative PCR analysis of mRNA encoding the three PKB isoforms (adapted from Yang *et al.*, 2003). (B) Protein expression of PKB isoforms in various tissues as detected by isoform-specific antibodies (PKBα expression blot is adapted from Yang *et al*., 2003; PKBβ and PKBγ blots are from B.Duemmler, unpublished).

Although constitutively active PKB alone leads only in rare cases to tumorigenesis (lymphomas and prostatic intraepithelial neoplasia have been observed (66, 67, 72, 87)), a recent study demonstrated that PKB deficiency can markedly decrease the incidence and development of tumors in PTEN$^{+/-}$ mice. Haplodeficiency of PTEN elicits in mice a wide range of tumors with a high tumor incidence in prostate, endometrium, thyroid, adrenal medulla, and the intestine (29, 105). Chen *et al.* crossed these mice with PKBα-deficient mice and could show that PKBα-deficiency markedly decrease the incidence and development of tumors in all of the above tissues (18). Considered that

PTEN inactivation occurs at a high frequency in human cancers, these results have important implications for cancer therapy. They provide genetic evidence that a deficiency in PKBα is effective in inhibiting neoplasia induced by PTEN inactivation. Partial inhibition of PKB activity or inhibition of individual PKB isoforms could thus potentially be used for cancer therapy without severe side effects.

6. Aims of this thesis

The general aim of this thesis is to identify physiological functions of PKB by generation and analysis of loss-of-function mouse models. Emphasis is placed on identifying isoform-specific functions and as well functional overlap in-between the isoforms. Because the three isoforms have overlapping expression patterns in mice (Fig. 9), absence of one isoform may be compensated by the remaining other isoform(s). Some physiological functions of PKB are thus only revealed in mice with combined deficiencies in PKB isoforms. The mice generated and analyzed here are deficient in PKBβ/PKBγ, PKBγ, and PKBα/PKBγ, respectively.

II. RESULTS

Part 1:

Life with a single isoform of Akt: Mice lacking Akt2 and Akt3 are viable but display impaired glucose homeostasis and growth deficiencies

Dummler B, Tschopp O, Hynx D, Yang ZZ, Dirnhofer S, Hemmings BA.
Mol Cell Biol, 2006, 26: 8042-8051.

MOLECULAR AND CELLULAR BIOLOGY, Nov. 2006, p. 8042–8051 Vol. 26, No. 21
0270-7306/06/$08.00+0 doi:10.1128/MCB.00722-06

Life with a Single Isoform of Akt: Mice Lacking Akt2 and Akt3 Are Viable but Display Impaired Glucose Homeostasis and Growth Deficiencies▽†

Bettina Dummler,[1] Oliver Tschopp,[1] Debby Hynx,[1] Zhong-Zhou Yang,[1] Stephan Dirnhofer,[2] and Brian A. Hemmings[1]*

Friedrich Miescher Institute for Biomedical Research, Maulbeerstrasse 66, Basel CH-4058, Switzerland,[1] and Institute of Pathology, University of Basel, Schönbeinstrasse 40, Basel CH-4031, Switzerland[2]

Received 26 April 2006/Returned for modification 1 June 2006/Accepted 13 August 2006

To address the issues of isoform redundancy and isoform specificity of the Akt family of protein kinases in vivo, we generated mice deficient in both Akt2 and Akt3. In these mice, only the Akt1 isoform remains to perform essential Akt functions, such as glucose homeostasis, proliferation, differentiation, and early development. Surprisingly, we found that *Akt2*$^{-/-}$ *Akt3*$^{-/-}$ and even *Akt1*$^{+/-}$ *Akt2*$^{-/-}$ *Akt3*$^{-/-}$ mice developed normally and survived with minimal dysfunctions, despite a dramatic reduction of total Akt levels in all tissues. A single functional allele of Akt1 appears to be sufficient for successful embryonic development and postnatal survival. This is in sharp contrast to the previously described lethal phenotypes of *Akt1*$^{-/-}$ *Akt2*$^{-/-}$ mice and *Akt1*$^{-/-}$ *Akt3*$^{-/-}$ mice. However, *Akt2*$^{-/-}$ *Akt3*$^{-/-}$ mice were glucose and insulin intolerant and exhibited an ~25% reduction in body weight compared to wild-type mice. In addition, we found substantial reductions in relative size and weight of the brain and testis in *Akt2*$^{-/-}$ *Akt3*$^{-/-}$ mice, demonstrating an in vivo role for both Akt2 and Akt3 in the determination of whole animal size and individual organ sizes.

The coordination between signal specificity and kinome redundancy is a fundamental issue in cell biology that is not yet fully understood. Although most of the major kinase families are conserved among metazoans, the vertebrate genome contains distinctly more genes encoding protein kinases than do those of worms or flies (24). Duplications of gene loci in vertebrates have led to the expansion of individual kinases into several homologous isoforms and brought about a concomitant increase in signaling complexity. It has been proposed that such isoforms are uniquely adapted to transmit distinct biological signals.

The Akt protein signaling kinase (also known as protein kinase B [PKB]) has a high level of evolutionary conservation and plays a key role in the conserved phosphoinositide 3-kinase (PI3K) signaling pathway (27). In mammals, Akt is implicated in the regulation of widely divergent cellular processes, such as metabolism, differentiation, proliferation, and apoptosis (3, 20). Accordingly, activation of Akt is promoted by numerous stimuli, including growth factors, hormones, and cytokines. There are three isoforms of Akt in mammals, termed Akt1/PKBα, Akt2/PKBβ, and Akt3/PKBγ. These isoforms are products of distinct genes but are highly related, exhibiting >80% protein sequence identity and sharing the same structural organization. To understand the specific physiological functions of the individual isoforms, animal models deficient in Akt1, Akt2, or Akt3 have been generated. Mice lacking Akt1 demonstrate increased perinatal mortality and reductions in body weight of 20 to 30% (6, 8, 38). In contrast, Akt2-deficient mice are born in the expected Mendelian ratio and display normal growth, but they exhibit a diabetes-like syndrome with an elevated fasting plasma glucose level, elevated hepatic glucose output, and peripheral insulin resistance (7, 15). Akt3-deficient mice exhibit a reduction in brain weight resulting from decreases in both cell size and cell number but maintain normal glucose homeostasis and body weights (13, 33). These observations indicate that the three Akt isoforms have some differential, nonredundant physiological functions. The relatively subtle phenotypes of mice lacking individual Akt isoforms as well as the viability of the animals suggest, however, that for many functions Akt isoforms are able to compensate for each other. To address the issue of isoform redundancy, mice with combined Akt deficiencies have been generated. Mice lacking both Akt1 and Akt2 develop to term but die shortly after birth and display multiple defects. They exhibit a severe growth deficiency (body weights at birth are ~50% of normal weights), skeletal muscle atrophy, impaired skin development, and a delay in ossification (25). Mice mutant in both Akt1 and Akt3 die around embryonic day 12, with severe impairments in growth, cardiovascular development, and organization of the nervous system (37). Such data obtained from double knockout mice argue strongly for partially overlapping functions of Akt isoforms in vivo. Certain physiological functions of Akt are thus revealed only when total Akt levels are below a critical threshold in particular cell types and tissues. Here we report the generation of *Akt2*$^{-/-}$ *Akt3*$^{-/-}$ mice to determine the combined roles of these isoforms in Akt-related physiological processes, such as glucose metabolism, development, and growth. It was surprising to us that compound *Akt2*$^{-/-}$ *Akt3*$^{-/-}$ mice and even mice retaining only

* Corresponding author. Mailing address: Friedrich Miescher Institute for Biomedical Research, Maulbeerstrasse 66, Basel CH-4058, Switzerland. Phone: 41 61 697 4872. Fax: 41 61 697 3976. E-mail: brian.hemmings@fmi.ch.

† Supplemental material for this article may be found at http://mcb.asm.org/.

▽ Published ahead of print on 21 August 2006.

one functional allele of Akt1 (*Akt1*$^{+/-}$ *Akt2*$^{-/-}$ *Akt3*$^{-/-}$) were viable and did not display any gross abnormalities. The body size of *Akt2*$^{-/-}$ *Akt3*$^{-/-}$ mice was reduced at birth and throughout postnatal life, and they exhibited severe glucose and insulin intolerance.

MATERIALS AND METHODS

Mice. Akt3 mutant mice were generated as described previously (33). For the generation of Akt2 mutant mice, an ~9.4-kb mouse genomic DNA fragment containing exons 3 and 4 of the *Akt2* gene was subcloned into pBluescript, and a NotI site was generated in exon 4 by PCR. An ~5-kb IRES-*lacZ*-Neo^r cassette was inserted into the NotI site, resulting in partial deletion of exon 4 and a frameshift in the open reading frame of the *Akt2* gene. The resulting targeting vector was linearized with SalI and electroporated into 129/Ola embryonic stem (ES) cells. Screening of ES cell clones was performed by Southern blotting. DNAs were digested with EcoRI and probed with an external probe (see Fig. S2a, probe A, in the supplemental material). An internal probe (see Fig. S2a, probe B, in the supplemental material) was then used on BamHI-digested DNAs for further characterization of ES cell clones positive for homologous recombination. Correctly targeted ES cells were used to generate chimeras. Male chimeras were mated with wild-type C57BL/6 females to obtain *Akt2*$^{+/-}$ mice, which were intercrossed to produce Akt2 homozygous mutants. Progeny were genotyped for the presence of a targeted *Akt2* allele by multiplex PCR. The following primers were used for genotyping: P1-as, 5′-CTCAGGGACACCCAT GTGTGGCTGC-3′; P2/KO-s, 5′-GCTGCCTCGTCCTGCAGTTCATTC-3′; and P3/WT-s, 5′-CCACAGGCAGCAGAAAGGAA-3′. One primer set amplifies a 600-bp fragment from the targeted allele, and the second primer set amplifies a 360-bp fragment from the wild-type allele. *Akt2*$^{-/-}$ *Akt3*$^{+/+}$ mice were crossed with *Akt2*$^{+/+}$*Akt3*$^{-/-}$ mice to obtain *Akt2*$^{+/-}$ *Akt3*$^{+/-}$ offspring, which were mated to generate *Akt2*$^{-/-}$ *Akt3*$^{-/-}$ mice as well as the wild-type, *Akt2*$^{-/-}$, and *Akt3*$^{-/-}$ littermates used in the study. Both starting strains were on a mixed 129 Ola and C57BL/6 background. For the generation of *Akt1*$^{+/-}$ *Akt2*$^{-/-}$ *Akt3*$^{-/-}$ mice, *Akt2*$^{-/-}$ *Akt3*$^{-/-}$ mice were mated with *Akt1*$^{+/-}$ *Akt3*$^{-/-}$ mice (37), and resulting *Akt1*$^{+/-}$ *Akt2*$^{+/-}$ *Akt3*$^{-/-}$ progeny were intercrossed. Mice were housed according to the Swiss Animal Protection Laws in groups with 12-h dark-light cycles and with free access to food and water. All procedures were conducted with the relevant approval of the appropriate authorities.

Cell culture. Cerebellar granule cells were isolated and cultured as previously described (28). Cells were counted and plated on poly-D-lysine-coated six-well plates in culture medium (basal Eagle medium containing 10% fetal bovine serum, 100 U of penicillin-streptomycin, 2 mM glutamine, and 25 mM KCl). After 24 h, 10 μM cytosine arabinoside was added to the medium to inhibit the proliferation of nonneuronal cells. After 2 days in culture, cells were starved by serum deprivation for 12 h and then stimulated with 100 nM insulin.

Western blot analysis. For Western blot analysis, protein lysates were prepared by homogenization of various organs in lysis buffer (50 mM Tris-HCl, pH 8.0, 120 mM NaCl, 1% NP-40, 40 mM β-glycerophosphate, 10% glycerol, 4 μM leupeptin, 0.05 mM phenylmethylsulfonyl fluoride, 1 mM benzamidine, 50 mM NaF, 1 mM Na_3VO_4, 5 mM EDTA, 1 μM Microcystin LR). Homogenates were centrifuged twice (13,000 rpm for 10 min at 4°C) to remove cell debris. Protein concentrations were determined using the Bradford assay. Proteins (50 μg per sample) were separated by 15%, 10%, or 6% sodium dodecyl sulfate-polyacrylamide gel electrophoresis and then transferred to Immobilon-P polyvinylidene difluoride membranes (Millipore). Akt isoform-specific antibodies were obtained by immunizing rabbits with isoform-specific peptides as previously described (38). Antibodies against total Akt, phospho-Akt (Ser473), phospho-glycogen synthase kinase 3α/β (phospho-GSK3α/β [Ser21/9]), phospho-GSK3β (Ser9), total GSK3β, phospho-TSC2 (Thr1462), phospho-p70 S6K (Thr389), and total 4E-BP1 were purchased from Cell Signaling Technologies. Anti-Foxo3a and anti-phospho-Foxo3a (Thr32) antibodies were obtained from Upstate Biotechnology. A rat monoclonal anti-α-tubulin (YL1/2)-producing hybridoma cell line was obtained from the American Type Culture Collection. Anti-TSC2 antibody was generated as previously described (35) and kindly provided by K. Molle (Biozentrum, University of Basel, Switzerland). For quantitation, Western blots were scanned using a GS-800 Bio-Rad densitometer with a resolution of 63.5 μm by 63.5 μm, and bands were quantified using Proteomweaver 4.0.0.5 (Bio-Rad). As shown in Fig. S1 in the supplemental material, the anti-total Akt and anti-phospho-Akt (Ser473) antibodies utilized in this study show equal affinities towards Akt1 and Akt3 but a lower affinity towards Akt2. As a consequence, the total Akt and phospho-Akt levels that were detected in our study with these antibodies may slightly understate the magnitude of the differences between wild-type and *Akt2*$^{-/-}$ *Akt3*$^{-/-}$ mice.

Histology and TUNEL assays. For histological analysis, organs were dissected and fixed in 4% paraformaldehyde–phosphate-buffered saline overnight at 4°C. After dehydration in ethanol, samples were embedded in paraffin. Tissues were cut into 6-μm-thick sections and stored for staining. For hematoxylin-eosin (Sigma) and cresyl violet (Sigma) staining, sections were deparaffinized and stained. A terminal deoxynucleotidyltransferase-mediated dUTP-biotin nick end labeling (TUNEL) assay was performed as previously described (37). For quantitation of apoptosis in testes, sections of testes derived from wild-type and *Akt2*$^{-/-}$ *Akt3*$^{-/-}$ mice were subjected to TUNEL assay, and the number of TUNEL-positive cells per area was counted (for each mouse, an area of ~20 to 40 mm^2 of stained testis sections was analyzed).

Testosterone measurement. Blood samples were collected from tail veins of 10-week-old male mice. Samples were allowed to clot at room temperature, and serum was separated by centrifugation. To account for the pulsatile secretion of testosterone, three separate samples were taken from each mouse on the same day (spaced 3 h apart) and pooled. A commercial enzyme-linked immunosorbent assay kit (DRG Instruments GmbH, Marburg, Germany) was used to measure testosterone in serum following the manufacturer's recommendations.

Glucose and insulin tolerance test. All mice used for glucose and insulin tolerance tests were offspring from doubly heterozygous parents. Note that glucose and insulin tolerance was not affected in doubly heterozygous mice, and an influence of the mother on the diabetic phenotype of the offspring could therefore be excluded. Three-month-old mice of the selected genotypes were made to fast overnight; for glucose tolerance tests, glucose (2 g/kg of body weight) (D-(+)-glucose anhydrous; Fluka) was given orally, and for insulin tolerance tests, insulin (1 U/kg) (human recombinant insulin; Sigma) was administered by intraperitoneal injection. Blood samples were collected at the indicated times from tail veins, and glucose levels were determined using Glucometer Elite (Bayer). Similarly, random-fed and fasting blood glucose levels were determined for 3-month-old mice by the collection of blood samples from tail veins, with glucose levels determined as described above. Blood insulin levels were measured with an ultrasensitive mouse insulin enzyme-linked immunosorbent assay (Immunodiagnostic Systems).

In vivo insulin stimulation. In vivo insulin stimulation was performed on ~8-week-old male mice. Following an overnight fast, a bolus of insulin (1 mU/g or 10 mU/g, as indicated) (human recombinant insulin; Sigma) or saline solution was injected via the inferior vena cava into terminally anesthetized mice. White adipose tissue, liver, skeletal muscle, and whole brain were harvested after 12 min of stimulation and immediately snap frozen in liquid nitrogen. Tissues were homogenized thereafter and lysed as described above.

Statistics. Data are provided as arithmetic means ± standard errors of the means (SEM), and n represents the number of independent experiments. All data were tested for significance using one-way analysis of variance (ANOVA) and a paired or unpaired Student t test, as applicable. Only results with P values of <0.05 were considered statistically significant.

RESULTS

A single functional allele of Akt1 is sufficient for successful embryonic development and postnatal survival in mice lacking Akt2 and Akt3. Considering the lethal phenotypes and multiple developmental defects of *Akt1*$^{-/-}$ *Akt2*$^{-/-}$ and *Akt1*$^{-/-}$ *Akt3*$^{-/-}$ mice, Akt isoforms appear to play essential roles in various aspects of embryonic development (25, 37). Moreover, the *Akt* genes seem to compensate functionally for one another in vivo, as no developmental deficiencies have been observed in any mice lacking only one isoform of the Akt family (6–8, 13, 15, 33). We wanted to evaluate the impact of combined Akt2 and Akt3 deficiencies on the viability and embryonic development of mice. *Akt2*$^{-/-}$ mice were generated by targeted disruption of exon 4 of the *Akt2* gene (see Fig. S2a in the supplemental material). In mice homozygous for the targeted allele, expression of the Akt2 protein was not detectable with isoform-specific antisera (see Fig. S2c in the supplemental material). Thus, the targeted disruption resulted in a functional null allele. *Akt2*$^{-/-}$ *Akt3*$^{+/+}$ mice were crossed with *Akt2*$^{+/+}$

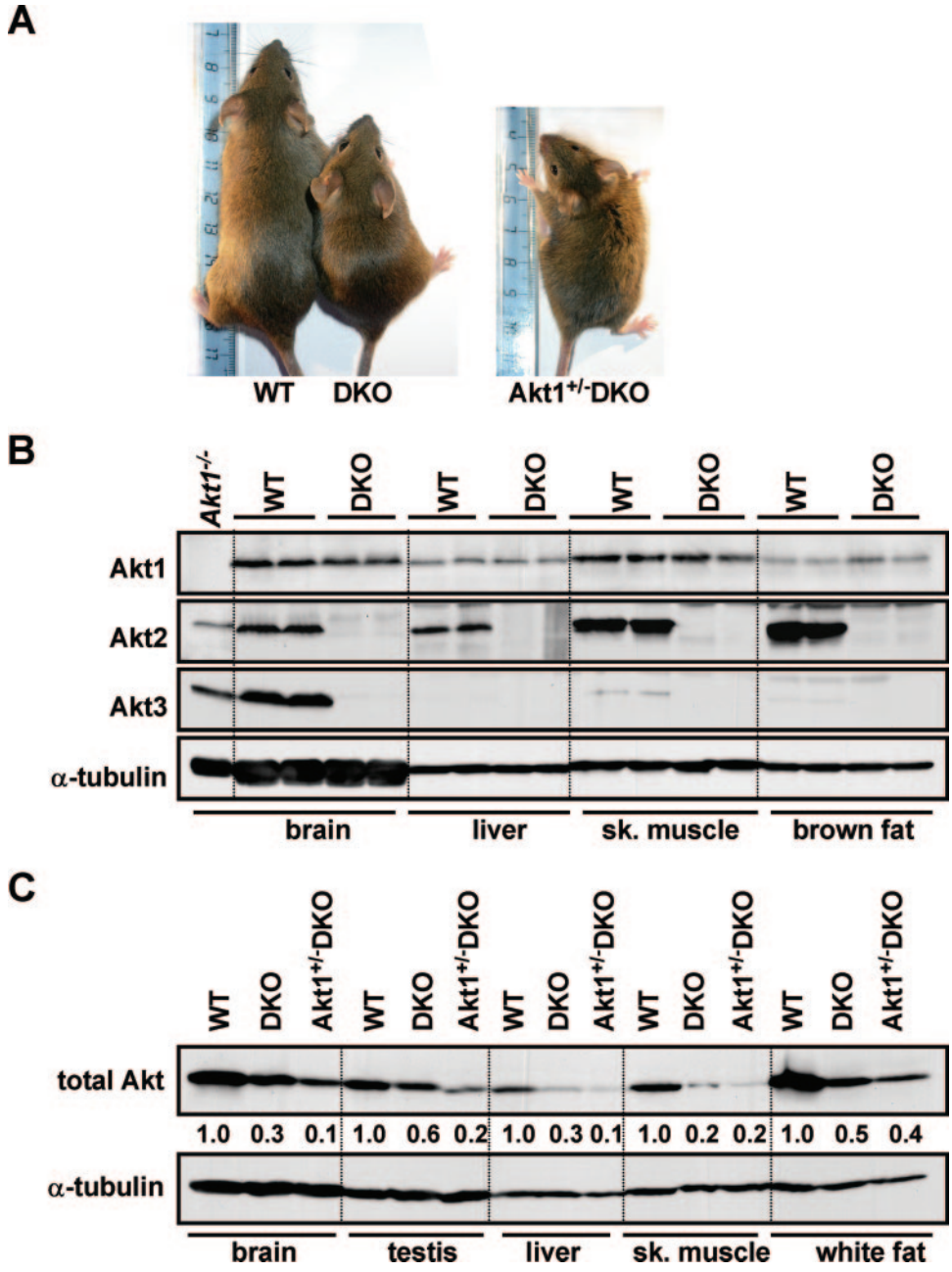

FIG. 1. (A) Top view of wild-type (WT), *Akt2*$^{-/-}$ *Akt3*$^{-/-}$ (DKO), and *Akt1*$^{+/-}$ *Akt2*$^{-/-}$ *Akt3*$^{-/-}$ (Akt1$^{+/-}$DKO) mice (12-week-old male mice; the WT and DKO mice were from the same litter). Note that the pictures are illustrative of the viability of mutant mice rather than a size comparison. (B) Akt1 protein levels in 4-day-old wild-type (WT) and *Akt2*$^{-/-}$ *Akt3*$^{-/-}$ (DKO) pups. The indicated tissues from wild-type and DKO pups were lysed and blotted with antibodies specific for Akt1, Akt2, and Akt3. As a loading control, the expression of α-tubulin was detected on the same membrane. Duplicates are from independent samples. (C) Stepwise reduction of total Akt levels in wild-type (WT), *Akt2*$^{-/-}$ *Akt3*$^{-/-}$ (DKO), and *Akt*$^{+/-}$ *Akt2*$^{-/-}$ *Akt3*$^{-/-}$ (Akt$^{+/-}$DKO) mice. Tissues from 3-month-old mice of the indicated genotypes were lysed and blotted with an Akt antibody that recognizes all three isoforms. As a loading control, the expression of α-tubulin was detected on the same membrane. Bands were quantified, and indicated values represent total Akt expression relative to wild-type expression levels, normalized to the α-tubulin control. The experiment was performed twice with independent samples and with similar results.

Akt3$^{-/-}$ mice to obtain *Akt2*$^{+/-}$ *Akt3*$^{+/-}$ mice. These doubly heterozygous mice were intercrossed to generate *Akt2*$^{-/-}$ *Akt3*$^{-/-}$ mice. Surprisingly, *Akt2*$^{-/-}$ *Akt3*$^{-/-}$ offspring were viable and showed no obvious abnormalities, except for their smaller size (Fig. 1A). Examination of >500 pups from matings between *Akt2*$^{+/-}$ *Akt3*$^{+/-}$ mice showed the expected Mendelian distribution for *Akt2*$^{-/-}$ *Akt3*$^{-/-}$ progeny and the other resulting genotypes (see Table S1 in the supplemental material). We investigated whether upregulation of the remaining Akt isoform in these mice, Akt1, could account for the mild phenotype of *Akt2*$^{-/-}$ *Akt3*$^{-/-}$ mice. Immunoblotting of protein extracts from various tissues of 4-day-old *Akt2*$^{-/-}$ *Akt3*$^{-/-}$

mice with an isoform-specific antibody against Akt1 revealed no significant increase in Akt1 protein levels compared to those in wild-type littermates (Fig. 1B). Since we had previously observed that in neonates the tissue distribution of Akt isoforms differs from that in adult mice (37), we also examined Akt1 expression levels in tissues of adult *Akt2*$^{-/-}$ *Akt3*$^{-/-}$ mice. As in neonates, Akt1 was not upregulated in tissues of adult *Akt2*$^{-/-}$ *Akt3*$^{-/-}$ mice (data not shown). We therefore excluded the possibility that a compensatory upregulation of Akt1 could influence the phenotype of *Akt2*$^{-/-}$ *Akt3*$^{-/-}$ mice.

Next, we asked the question of whether Akt1 affects mouse development in a dose-dependent fashion. To evaluate the impact of a decrease in the Akt1 dose, we crossed our *Akt2*$^{-/-}$ *Akt3*$^{-/-}$ mice with *Akt1*$^{+/-}$ *Akt3*$^{-/-}$ mice (38). Resulting *Akt1*$^{+/-}$ *Akt2*$^{+/-}$ *Akt3*$^{-/-}$ mice were subsequently intercrossed to obtain mice containing only one functional allele of *Akt1* (*Akt1*$^{+/-}$ *Akt2*$^{-/-}$ *Akt3*$^{-/-}$ mice). We did not obtain any *Akt1*$^{-/-}$ *Akt2*$^{-/-}$ *Akt3*$^{-/-}$ mice, as a combined deficiency of Akt1 and Akt3 is lethal at embryonic stage E12 (37). However, we obtained viable *Akt1*$^{+/-}$ *Akt2*$^{-/-}$ *Akt3*$^{-/-}$ mice from these crosses (Fig. 1A; see Table S2 in the supplemental material). Approximately 14% of the mice in the analyzed cohort (n = 105) were *Akt1*$^{+/-}$ *Akt2*$^{-/-}$ *Akt3*$^{-/-}$ mutants. As shown in Fig. 1C, a stepwise reduction in functional *Akt* alleles was reflected by a concomitant reduction in total Akt protein levels. For instance, in both brain and liver, there was an ~3-fold reduction of total Akt levels in *Akt2*$^{-/-}$ *Akt3*$^{-/-}$ mice and an ~10-fold reduction of total Akt levels in *Akt1*$^{+/-}$ *Akt2*$^{-/-}$ *Akt3*$^{-/-}$ mice compared to wild-type levels (Fig. 1C). *Akt1*$^{+/-}$ *Akt2*$^{-/-}$ *Akt3*$^{-/-}$ mice developed normally, with no obvious defects except for a severe growth deficiency, with body weights at the age of 12 weeks reduced ~40% compared to those of wild-type mice (17.1 ± 1.7 g versus 29.1 ± 0.7 g, respectively [n = 5]; $P <$ 0.01). Taken together, these findings demonstrate that Akt1 (even in the case where only one allele is present) is sufficient to enable successful embryonic development and postnatal survival in mice lacking Akt2 and Akt3.

Growth deficiency and substantially reduced brain and testis mass in *Akt2*$^{-/-}$ *Akt3*$^{-/-}$ mice. It was previously shown that disruption of the *Akt1* gene in mice leads to growth retardation (6, 8, 38), and Akt3-deficient mice were shown to have a reduction in brain size (13, 33). In progeny of *Akt2*$^{+/-}$ *Akt3*$^{+/-}$ intercrosses, we observed that the combined deletion of Akt2 and Akt3 resulted in a growth deficiency in both male and female *Akt2*$^{-/-}$ *Akt3*$^{-/-}$ mice. One-week-old male *Akt2*$^{-/-}$ *Akt3*$^{-/-}$ mice were ~28% smaller than their wild-type littermates (3.81 ± 0.21 g versus 5.26 ± 0.14 g; $P < 0.001$), and an average decrease in body weight of 25% persisted throughout the examined 3-month life period of male *Akt2*$^{-/-}$ *Akt3*$^{-/-}$ mice (Fig. 2). For female *Akt2*$^{-/-}$ *Akt3*$^{-/-}$ mice, a significant decrease in body weight was evident only from the fourth week of age onward, with an average decrease of 14% compared to wild-type littermates. Consistent with previous reports, single knockouts of either Akt2 or Akt3 did not significantly affect animal size compared to wild-type littermates (data not shown) (7, 33). Comparisons of selected organ weights (brain, heart, lung, thymus, liver, spleen, kidney, and testis) from 3-month-old *Akt2*$^{-/-}$ *Akt3*$^{-/-}$, *Akt2*$^{-/-}$, *Akt3*$^{-/-}$, and wild-type littermate mice revealed an ~35% reduction in brain weights of

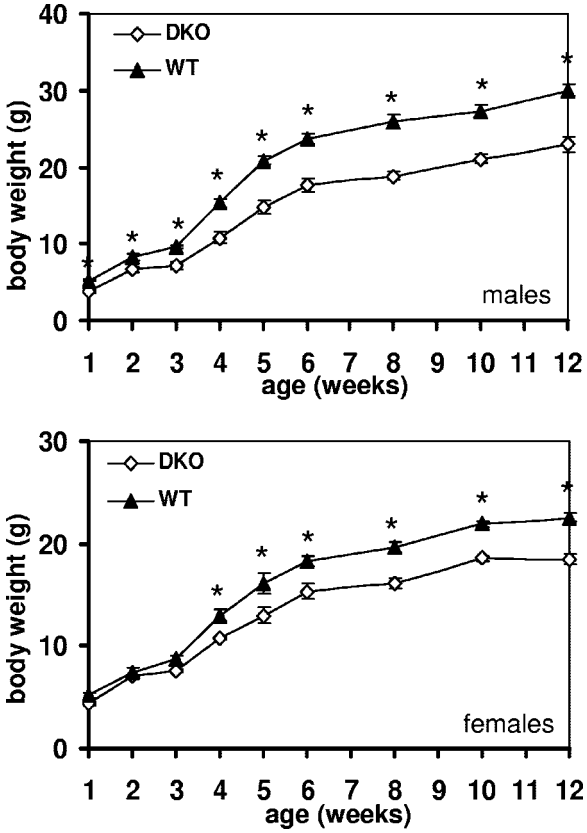

FIG. 2. Growth deficiency in *Akt2*$^{-/-}$ *Akt3*$^{-/-}$ (DKO) mice. Body weights of male (upper panel) and female (lower panel) wild-type (filled triangles) and *Akt2*$^{-/-}$ *Akt3*$^{-/-}$ (open diamonds) littermate mice were determined at the indicated time points. The graph depicts arithmetic means ± SEM (n = 8 for each group). Significantly different values for *Akt2*$^{-/-}$ *Akt3*$^{-/-}$ mice versus the wild type, as determined by one-way ANOVA, are indicated (*, $P < 0.05$).

Akt2$^{-/-}$ *Akt3*$^{-/-}$ mice (0.31 ± 0.01 g versus 0.49 ± 0.01 g; $P <$ 0.001) and an ~40% reduction in testis weights (0.12 ± 0.01 g versus 0.20 ± 0.01 g; $P < 0.001$) compared to those of wild-type mice (Fig. 3A and B). While most organs of *Akt2*$^{-/-}$ *Akt3*$^{-/-}$ mice were decreased proportionally to the reduced body weights, the relative weights of brains and testes were reduced by 18.8% ± 1.7% and 28.5% ± 2.7%, respectively (Fig. 3A and B). The prominent size reduction in the testes prompted us to measure serum testosterone levels in 10-week-old male *Akt2*$^{-/-}$ *Akt3*$^{-/-}$ and wild-type mice. In *Akt2*$^{-/-}$ *Akt3*$^{-/-}$ mice, testosterone levels were ~70% lower than those measured in wild-type mice (1.4 ± 0.5 ng/ml versus 4.7 ± 1.2 ng/ml [n = 5]; $P < 0.05$). In addition, we compared ovary weights in 3-month-old *Akt2*$^{-/-}$ *Akt3*$^{-/-}$ and wild-type females. We observed an ~26% reduction in absolute weights of ovaries of *Akt2*$^{-/-}$ *Akt3*$^{-/-}$ mice (13.3 ± 1.3 mg versus 18.2 ± 1.0 mg [n = 5]; $P <$ 0.05); however, there was no significant difference from the wild type in the organ/body weight ratio.

The PI3K/Akt pathway also plays a critical role in cell survival and apoptosis, and therefore we assessed whether an increased rate of spontaneous apoptosis could account for the smaller sizes of testes in *Akt2*$^{-/-}$ *Akt3*$^{-/-}$ mice. TUNEL assays were performed on testis sections from adult *Akt2*$^{-/-}$ *Akt3*$^{-/-}$

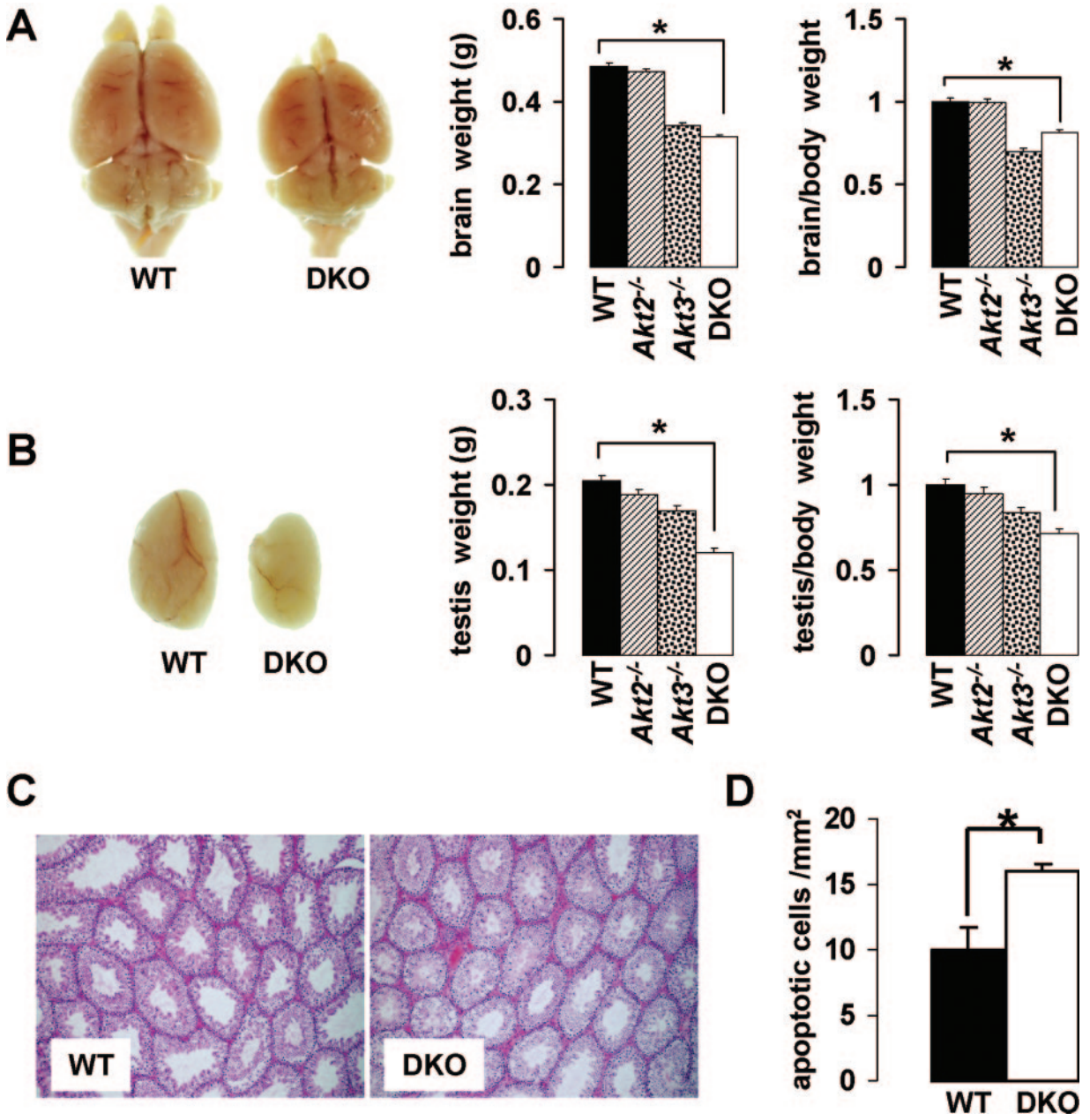

FIG. 3. Selective reduction of brain and testis size in $Akt2^{-/-}$ $Akt3^{-/-}$ mice. (A) Brains were dissected from 3-month-old male wild-type (WT) and $Akt2^{-/-}$ $Akt3^{-/-}$ (DKO) littermate mice (left). Mean absolute brain weights (middle) and brain weights relative to body weight (right) of 3-month-old male mice of the indicated genotypes are shown ($n = 8$; *, $P < 0.001$). (B) Testes were dissected from 3-month-old wild-type and $Akt2^{-/-}$ $Akt3^{-/-}$ littermate mice (left). Mean absolute testis weights (middle) and testis weights relative to body weight (right) of 3-month-old mice of the indicated genotypes are depicted ($n = 14$; *, $P < 0.001$). Relative weights are percentages relative to the wild type (WT = 1). Error bars represent SEM. (C) Morphology of testes from wild-type and $Akt2^{-/-}$ $Akt3^{-/-}$ littermate mice. Representative sections stained with hematoxylin and eosin show morphologically normal seminiferous tubules. (D) Spontaneous apoptosis in testes of $Akt2^{-/-}$ $Akt3^{-/-}$ mice. The graph shows a comparison of TUNEL-positive cell numbers in testis sections from $Akt2^{-/-}$ $Akt3^{-/-}$ mice and their wild-type littermates ($n = 3$; *, $P < 0.05$).

mice and their wild-type littermates. Generally, the rate of spontaneous apoptosis was low for both genotypes, but the testes of $Akt2^{-/-}$ $Akt3^{-/-}$ mice showed an ~1.5-fold increase in TUNEL-positive cells compared to wild-type littermates (Fig. 3D). In addition, areas of seminiferous tubules were reduced ~24% in $Akt2^{-/-}$ $Akt3^{-/-}$ mice compared to those in wild-type littermates (0.76 ± 0.05 versus 1.0 ± 0.05 [$n = 4$]; $P < 0.05$). However, histopathological analysis of testes from $Akt2^{-/-}$ $Akt3^{-/-}$, $Akt2^{-/-}$, $Akt3^{-/-}$, and wild-type littermate mice (3-month-old mice; $n = 5$ to 8 mice per genotype) revealed no morphological abnormalities (Fig. 3C). Furthermore, both male and female $Akt2^{-/-}$ $Akt3^{-/-}$ mice were fertile, although litter sizes from such crossings were smaller (data not shown).

Akt1 is sufficient for phosphorylation of key downstream targets in brains and testes of *Akt2*$^{-/-}$ *Akt3*$^{-/-}$ mice. We were interested to know how Akt signaling was affected in the brains and testes of *Akt2*$^{-/-}$ *Akt3*$^{-/-}$ mice. First, we assessed steady-state phosphorylation/activation levels of Akt in brains and testes of adult *Akt2*$^{-/-}$ *Akt3*$^{-/-}$ and wild-type mice by immunoblotting protein extracts with an antibody against phospho-Ser473. This phosphorylation site is a distinctive indicator of Akt activation status, and the antibody detects phosphorylation of this site in all three Akt isoforms. In the testes of *Akt2*$^{-/-}$ *Akt3*$^{-/-}$ mice, steady-state phosphorylation of Akt was reduced ~10-fold compared to that in wild-type littermate controls and represented residual Akt1 activity (Fig. 4A and B). Interestingly, we found that in vivo insulin stimulation could increase the phosphorylation of Akt in testes of wild-type mice, although this induction was less prominent than that in a classical insulin-responsive tissue, such as the liver, and was scarcely detectable in *Akt2*$^{-/-}$ *Akt3*$^{-/-}$ mice (see Fig. S3 in the supplemental material). Similarly, phosphorylation of Akt in the brain was severely reduced (Fig. 5C shows phospho-Akt under fasting and insulin-stimulated conditions; data for steady state not shown).

Next, we generated primary cultures of cerebellar granule cells to study inducible Akt activation in an in vitro cellular system. In wild-type cerebellar granule cells, the expression of all three Akt isoforms could be detected by isoform-specific antibodies (data not shown), and there was no compensatory upregulation of Akt1 in cells of *Akt2*$^{-/-}$ *Akt3*$^{-/-}$ mice (Fig. 4C). Cerebellar granule cell cultures were deprived of serum for 12 h and then stimulated with 100 nM insulin. After serum deprivation, phospho-Akt levels were >10-fold lower in *Akt2*$^{-/-}$ *Akt3*$^{-/-}$ cells than in wild-type cells, and after stimulation, phospho-Akt levels increased in both wild-type and *Akt2*$^{-/-}$ *Akt3*$^{-/-}$ cells but remained ~2-fold lower in *Akt2*$^{-/-}$ *Akt3*$^{-/-}$ cells (Fig. 4C). We then assessed the phosphorylation levels of several downstream targets of Akt. GSK3 is a key molecule implicated in neuronal survival, protein synthesis, and glycogen synthesis (10–12), whereas tuberous sclerosis complex 2 (TSC2) is a critical target of Akt in mediating cell growth (17, 23, 26) and p70 S6 kinase (S6K) is a downstream component of the PI3K/Akt/TSC pathway (19, 22). Both GSK3 and TSC2 are well-established Akt substrates. In contrast, the regulation of S6K is more complex, as both PI3K-dependent and -independent signaling pathways are involved in its activation (5, 9, 14). Upon insulin stimulation, a clear induction in phosphorylation of all three downstream targets could be observed in cerebellar granule cells, but interestingly, no differences in phosphorylation levels were apparent in *Akt2*$^{-/-}$ *Akt3*$^{-/-}$ cells compared to wild-type cells (Fig. 4C). Similarly, no significant differences in phosphorylation levels of these downstream targets were apparent in the testis (Fig. 4B). We also assessed phosphorylation of the Akt substrate Foxo3a and of the mammalian target of rapamycin (mTOR) substrate 4E-binding protein 1 in testes of *Akt2*$^{-/-}$ *Akt3*$^{-/-}$ mice but found no marked differences compared to the wild type (see Fig. S3 in the supplemental material). In summary, residual Akt1 activity appears be sufficient to phosphorylate these downstream targets under both steady-state and induced conditions in *Akt2*$^{-/-}$ *Akt3*$^{-/-}$ mice.

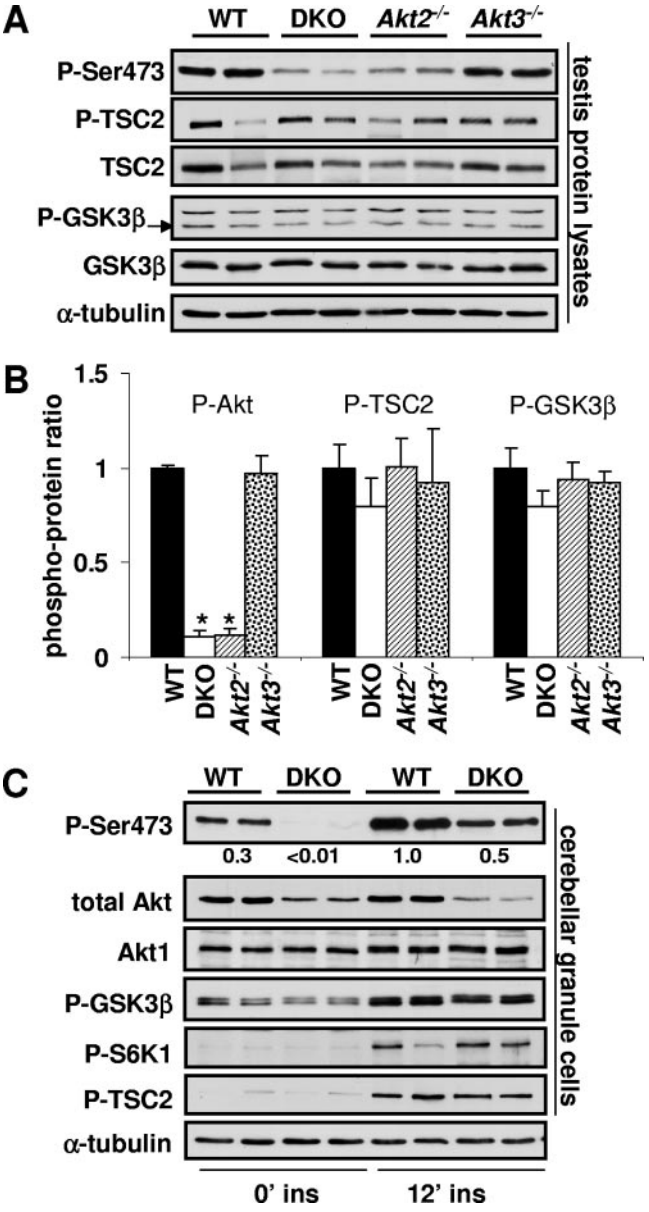

FIG. 4. Phospho-Western blot analysis of downstream targets of Akt. (A) Representative blot showing steady-state phosphorylation of downstream targets of Akt in testes of wild-type (WT), *Akt2*$^{-/-}$, *Akt3*$^{-/-}$, and *Akt2*$^{-/-}$ *Akt3*$^{-/-}$ (DKO) littermate mice. (B) Quantification of phosphorylated Akt and downstream targets. Values are the means for three mice per genotype, error bars depict SEM, and phospho-protein/total protein ratios are relative to the wild-type ratio. Phospho-Akt values were normalized to α-tubulin. (C) Primary cerebellar granule cell cultures of wild-type (WT) and *Akt2*$^{-/-}$ *Akt3*$^{-/-}$ (DKO) mice were serum starved overnight and then stimulated with 100 nM insulin for 12 min. Lysates were analyzed for the phosphorylation status of the indicated downstream targets of Akt. Phospho-Akt bands (P-Ser473) were quantified, and indicated values represent the means for two mice per genotype. Values are relative to stimulated phospho-Akt levels in the wild type and were normalized to the α-tubulin control.

Perturbation of glucose metabolism in *Akt2*$^{-/-}$ *Akt3*$^{-/-}$ mice. The Akt2 isoform of the Akt family has a major role in the regulation of glucose metabolism (36). It is the predominant isoform expressed in insulin-responsive tissues and is in-

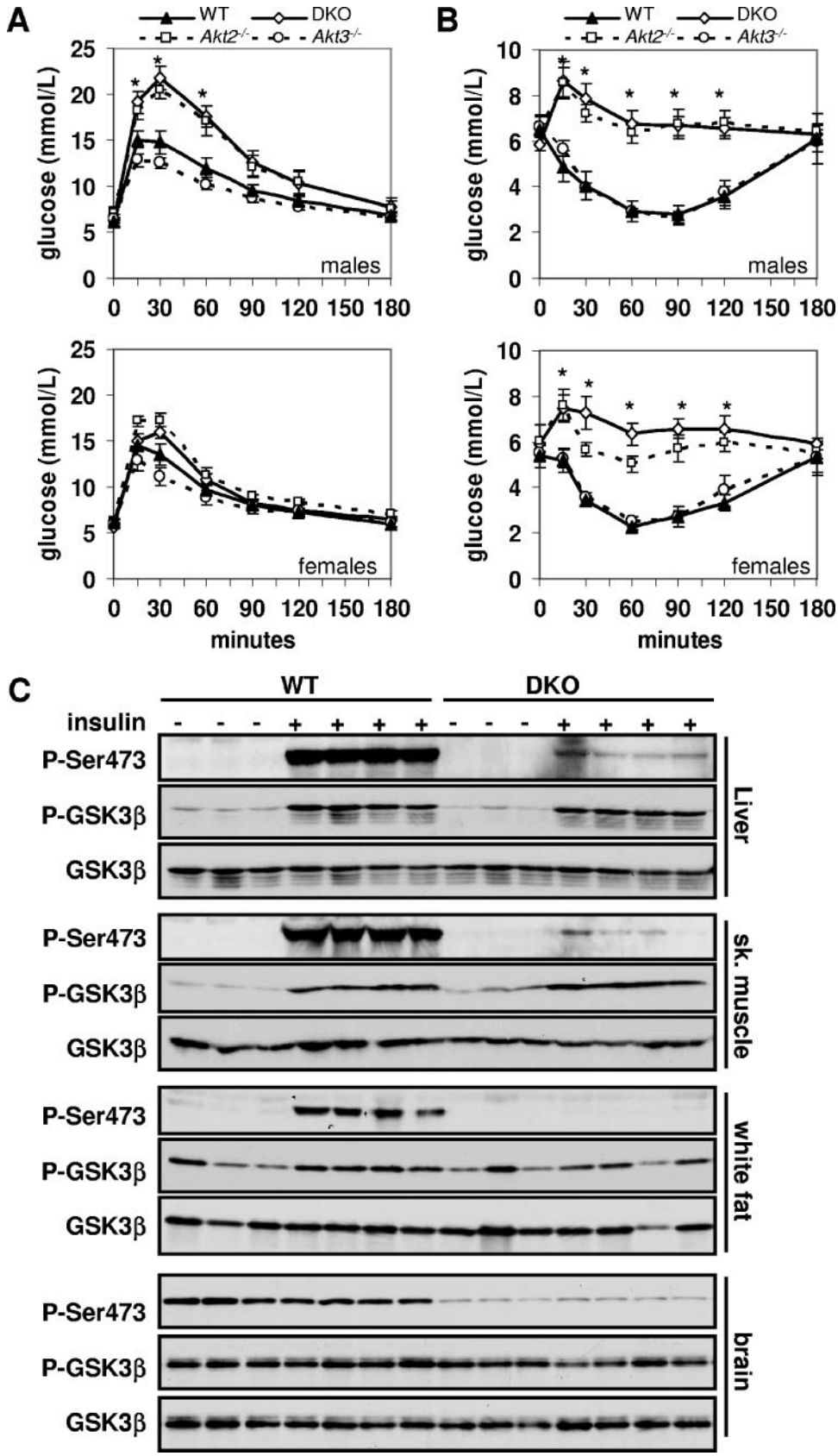

FIG. 5. Glucose metabolism in *Akt2*$^{-/-}$ *Akt3*$^{-/-}$ mice. (A) A glucose tolerance test was performed on 12-week-old male (upper panel) and female (lower panel) mice of the indicated genotypes. The graph depicts arithmetic means ± SEM (n = 8 to 12 for each group) of plasma glucose

volved in the regulation of insulin-stimulated glucose transport, lipogenesis, and glycogen synthesis (1, 7, 15). To investigate glucose metabolism in *Akt2*$^{-/-}$ *Akt3*$^{-/-}$ mice, glucose tolerance and insulin tolerance tests were performed on 3-month-old mice obtained from doubly heterozygous intercrosses (Fig. 5A and B). For the glucose tolerance test, glucose (2 mg/g of body weight) was administered orally to fasted *Akt2*$^{-/-}$ *Akt3*$^{-/-}$, *Akt2*$^{-/-}$, *Akt3*$^{-/-}$, and wild-type littermate mice. For all four genotypes, blood glucose levels peaked 15 to 30 min after glucose administration and returned to baseline after 3 h. *Akt3*$^{-/-}$ mice had similar glucose excursions as wild-type mice. However, in male *Akt2*$^{-/-}$ *Akt3*$^{-/-}$ mice, blood glucose levels rose faster, and at 30 min they were ~50% higher than those of wild-type mice (21.8 ± 1.3 mM versus 14.8 ± 1.2 mM; $P < 0.01$) (Fig. 5A). *Akt2*$^{-/-}$ mice had similar blood glucose levels as *Akt2*$^{-/-}$ *Akt3*$^{-/-}$ mice at all time points. The susceptibility to glucose intolerance was gender dependent because in female mice of all four genotypes, blood glucose levels were not statistically different ($P < 0.05$). Generally, female mice manifest better glucose tolerance than do male mice (16). For assessment of insulin sensitivity, insulin (1 mU/g of body weight) was administered by intraperitoneal injection to fasted *Akt2*$^{-/-}$ *Akt3*$^{-/-}$, *Akt2*$^{-/-}$, *Akt3*$^{-/-}$, and wild-type littermate mice. In wild-type and *Akt3*$^{-/-}$ mice, insulin elicited a >50% decrease in blood glucose levels 60 to 90 min after administration. After 90 min, glucose levels began to recover and reached baseline values 3 h after insulin administration. In contrast, blood glucose levels remained close to baseline levels at all measured time points in *Akt2*$^{-/-}$ *Akt3*$^{-/-}$ and *Akt2*$^{-/-}$ mice. The reduced insulin sensitivity was evident in both male and female mice of the *Akt2*$^{-/-}$ *Akt3*$^{-/-}$ and *Akt2*$^{-/-}$ genotypes.

To further explore the observed differences in glucose disposal, fasting and fed blood glucose and plasma insulin levels were examined in 3-month-old male *Akt2*$^{-/-}$ *Akt3*$^{-/-}$, *Akt2*$^{-/-}$, and wild-type littermate mice. Plasma insulin levels were significantly higher in *Akt2*$^{-/-}$ *Akt3*$^{-/-}$ mice than in the wild type, under both random feeding (4.6- ± 1.6-fold; $P < 0.05$) and fasting (1.9- ± 0.3-fold; $P < 0.05$) conditions (see Table S3 in the supplemental material). In addition, hyperglycemia was observed in *Akt2*$^{-/-}$ *Akt3*$^{-/-}$ mice under random feeding conditions (1.7-fold ± 0.2-fold increase; $P < 0.05$), whereas fasting blood glucose levels were not significantly different from the wild-type levels. We also assessed the percentage of nonenzymatically glycated hemoglobin (hemoglobin A1c [HbA1c]) in male mice of all four genotypes. This value provides an integrated measure of blood glucose levels during a period of approximately 1 month prior to sample removal. Despite the defects in glucose homeostasis, HbA1c levels were similar in both *Akt2*$^{-/-}$ and *Akt2*$^{-/-}$ *Akt3*$^{-/-}$ mice to those in wild-type mice (see Table S3 in the supplemental material). Next, we performed in vivo insulin stimulation in these mice to investigate the induction of Akt phosphorylation in insulin-responsive tissues. Wild-type and *Akt2*$^{-/-}$ *Akt3*$^{-/-}$ mice were made to fast overnight and then injected with a bolus of insulin (10 mU/g) or a saline control. Twelve minutes after injection, insulin-responsive tissues (liver, skeletal muscle, and white fat tissue) were collected. In wild-type mice, Akt became strongly phosphorylated upon insulin stimulation in all three tissues (Fig. 5C). In *Akt2*$^{-/-}$ *Akt3*$^{-/-}$ mice, inducible Akt could also be detected, but phospho-Akt levels were ~10- to 20-fold lower than those in wild-type mice (see Fig. S4 in the supplemental material for quantitation). As a readout for Akt1 activity in *Akt2*$^{-/-}$ *Akt3*$^{-/-}$ mice, we assessed phospho-GSK3β levels in insulin-responsive tissues. Phosphorylation of GSK3β was induced robustly in the liver and skeletal muscle following insulin stimulation, and phosphorylation levels were similar in both *Akt2*$^{-/-}$ *Akt3*$^{-/-}$ and wild-type mice. There was no apparent induction of phospho-GSK3β in white fat in our experimental settings. Peripherally injected insulin was recently shown to also induce Akt phosphorylation in the brain, suggesting an in vivo regulation of the Akt signaling pathway in mouse brain in response to changes in glucose metabolism (29). However, within 12 min of intravenous insulin injection, we could not detect any induction of phospho-Akt in the brain (Fig. 5C), although phospho-Akt levels were consistently lower in *Akt2*$^{-/-}$ *Akt3*$^{-/-}$ mice than in wild-type mice.

DISCUSSION

In order to fully evaluate the impact of the Akt kinase pathway on physiological processes, combined ablation of its isoforms is necessary. Complete inhibition of Akt activity appears to be incompatible with cell survival, but we were able to generate viable Akt mutant mice that contain only a single Akt isoform. Our results provide strong genetic evidence that the Akt1 isoform of the Akt family is sufficient to perform all essential Akt functions in embryonic development and postnatal survival. We observed that *Akt2*$^{-/-}$ *Akt3*$^{-/-}$ mice and even *Akt1*$^{+/-}$ *Akt2*$^{-/-}$ *Akt3*$^{-/-}$ mice, which retain only one functional allele of *Akt1* and have total Akt levels that are up to 10-fold lower than those in wild-type mice, can develop normally and survive with minimal dysfunctions. This is in sharp contrast to the lethal phenotype of mice that contain only Akt3 (*Akt1*$^{-/-}$ *Akt2*$^{-/-}$ mice) or Akt2 (*Akt1*$^{-/-}$ *Akt3*$^{-/-}$ mice) (25, 37). These mice have multiple developmental defects that culminate in lethality at embryonic stage E12 (*Akt1*$^{-/-}$ *Akt3*$^{-/-}$ mice) or the neonatal stage (*Akt1*$^{-/-}$ *Akt2*$^{-/-}$ mice).

concentrations following per os glucose administration (2 g/kg body weight). (B) An insulin tolerance test was performed on 15-week-old male (upper panel) and female (lower panel) mice of the indicated genotypes. The graph depicts arithmetic means ± SEM ($n = 8$ to 10 each group) of plasma glucose concentrations following intraperitoneal injection of insulin (1 mU/g body weight). All genotypes were littermate offspring of *Akt2*$^{+/-}$ *Akt3*$^{+/-}$ matings. Significantly different values obtained for *Akt2*$^{-/-}$ *Akt3*$^{-/-}$ mice (DKO) versus wild-type mice (WT), as determined by one-way ANOVA, are indicated (*, $P < 0.05$). In all four graphs, differences in *Akt2*$^{-/-}$ *Akt3*$^{-/-}$ versus *Akt2*$^{-/-}$ mice were not significant. (C) Active Akt and GSK3β in insulin-responsive tissues of wild-type and *Akt2*$^{-/-}$ *Akt3*$^{-/-}$ mice after in vivo insulin stimulation. Three-month-old male mice were made to fast overnight and injected with either saline (−) or insulin (10 mU/g body weight). After 12 min, the indicated tissues were harvested. Lysates were immunoblotted with the indicated antibodies. Samples are from individual mice ($n = 3$ for saline controls; $n = 4$ for insulin stimulation).

Significantly, combined deficiency of Akt2 and Akt3 affects the determination of whole animal size and individual organ sizes, indicating that Akt1 is not able to fully compensate for the lack of the other isoforms in growth signaling. Akt is a crucial downstream effector of IGF-1 signaling (2, 21). Consistent with a function in cell growth and proliferation, various reports have shown that the expression of activated Akt in specific mouse organs increases organ size (18, 30, 34), whereas ablation of Akt can cause reductions in whole animal growth and/or specific organ sizes (6, 8, 13, 15, 33). In *Akt2*$^{-/-}$ *Akt3*$^{-/-}$ mice, we observed a substantial reduction (25% in males) in body weights compared to those of wild-type mice. Interestingly, no growth deficiencies have been observed in either Akt2 or Akt3 single-knockout phenotypes for the same strain background. However, a mild growth deficiency was shown for *Akt2*$^{-/-}$ mice with a pure DBA/1lacj background (16%) (15). In addition, Akt2 and Akt3 appear to be involved in the regulation of brain and testis size, as the weights of both organs were severely reduced in *Akt2*$^{-/-}$ *Akt3*$^{-/-}$ mice. A testicular phenotype has also been described for *Akt1*$^{-/-}$ mice, which exhibit several morphological abnormalities in the testis (6). In contrast, we found no morphological abnormalities in testes of *Akt2*$^{-/-}$ *Akt3*$^{-/-}$ mice but observed a severe reduction in serum testosterone levels. Interestingly, relative to body weight, brain size was not further reduced in *Akt2*$^{-/-}$ *Akt3*$^{-/-}$ mice compared to Akt3-deficient mice, despite a high expression of Akt2 in the brain (25% of total Akt [13]) which is abrogated in *Akt2*$^{-/-}$ *Akt3*$^{-/-}$ mice. This argues for a selective influence of Akt3 on the regulation of brain size, rather than the size being a result of the total Akt dose in the tissue. Furthermore, Akt3 appears not to contribute to glucose homeostasis in mice, as a combined disruption of Akt2 and Akt3 did not noticeably exacerbate the glucose and insulin intolerance observed in *Akt2*$^{-/-}$ mice.

Detection of active Akt by a phospho-Ser473 antibody showed substantially reduced levels of total active Akt in various tissues of *Akt2*$^{-/-}$ *Akt3*$^{-/-}$ mice both at the steady state and when induced. Surprisingly, phosphorylation levels of critical downstream targets, such as GSK3, TSC2, and S6K, were similar in the *Akt2*$^{-/-}$ *Akt3*$^{-/-}$ mice to those in wild-type controls. Very low levels of active Akt1, the residual isoform, appear to be sufficient to phosphorylate certain downstream targets. However, we cannot formally exclude that these targets may be phosphorylated by another compensatory mechanism. For instance, S6K and p90 ribosomal S6 kinases (RSK) are two other insulin-stimulated protein kinases that can catalyze the phosphorylation of GSK3 in vitro (10, 31, 32). Although Akt appears to be the major kinase phosphorylating GSK3 in vivo upon insulin stimulation (4, 11), S6K and/or RSK may constitute a compensatory mechanism by which GSK3 becomes phosphorylated in Akt-deficient mice.

In conclusion, we provide genetic evidence for a dominant role of Akt1 in embryonic development and postnatal survival. We show that minimal amounts of Akt1 appear to be sufficient for full activation of many downstream targets. In addition, we identify redundant and nonredundant functions of the Akt2 and Akt3 isoforms in growth and glucose metabolism and provide insights into Akt isoform hierarchy.

ACKNOWLEDGMENTS

We thank J. F. Spetz and P. Kopp for their assistance with ES cell culture and embryonic aggregation and R. Portmann for help with Western blot quantifications.

B.D. is supported by the Swiss Cancer League (KFS 1167-09-2001 and KFS 01002-02-2000), O.T. is supported by the Novartis Stiftung für Medizinisch-Biologische Forschung, and Z.Z.Y. is supported, in part, by a grant from Bundesamt für Bildung und Wissenschaft (BBW 98.0176). The Friedrich Miescher Institute for Biomedical Research is funded by the Novartis Research Foundation.

REFERENCES

1. **Bae, S. S., H. Cho, J. Mu, and M. J. Birnbaum.** 2003. Isoform-specific regulation of insulin-dependent glucose uptake by Akt/protein kinase B. J. Biol. Chem. **278:**49530–49536.
2. **Baker, J., J. P. Liu, E. J. Robertson, and A. Efstratiadis.** 1993. Role of insulin-like growth factors in embryonic and postnatal growth. Cell **75:**73–82.
3. **Brazil, D. P., Z. Z. Yang, and B. A. Hemmings.** 2004. Advances in protein kinase B signalling: AKTion on multiple fronts. Trends Biochem. Sci. **29:** 233–242.
4. **Chang, P. Y., Y. Le Marchand-Brustel, L. A. Cheatham, and D. E. Moller.** 1995. Insulin stimulation of mitogen-activated protein kinase, p90rsk, and p70 S6 kinase in skeletal muscle of normal and insulin-resistant mice. Implications for the regulation of glycogen synthase. J. Biol. Chem. **270:**29928–29935.
5. **Cheatham, B., C. J. Vlahos, L. Cheatham, L. Wang, J. Blenis, and C. R. Kahn.** 1994. Phosphatidylinositol 3-kinase activation is required for insulin stimulation of pp70 S6 kinase, DNA synthesis, and glucose transporter translocation. Mol. Cell. Biol. **14:**4902–4911.
6. **Chen, W. S., P. Z. Xu, K. Gottlob, M. L. Chen, K. Sokol, T. Shiyanova, I. Roninson, W. Weng, R. Suzuki, K. Tobe, T. Kadowaki, and N. Hay.** 2001. Growth retardation and increased apoptosis in mice with homozygous disruption of the Akt1 gene. Genes Dev. **15:**2203–2208.
7. **Cho, H., J. Mu, J. K. Kim, J. L. Thorvaldsen, Q. Chu, E. B. Crenshaw III, K. H. Kaestner, M. S. Bartolomei, G. I. Shulman, and M. J. Birnbaum.** 2001. Insulin resistance and a diabetes mellitus-like syndrome in mice lacking the protein kinase Akt2 (PKB beta). Science **292:**1728–1731.
8. **Cho, H., J. L. Thorvaldsen, Q. Chu, F. Feng, and M. J. Birnbaum.** 2001. Akt1/PKBalpha is required for normal growth but dispensable for maintenance of glucose homeostasis in mice. J. Biol. Chem. **276:**38349–38352.
9. **Chung, J., T. C. Grammer, K. P. Lemon, A. Kazlauskas, and J. Blenis.** 1994. PDGF- and insulin-dependent pp70S6k activation mediated by phosphatidylinositol-3-OH kinase. Nature **370:**71–75.
10. **Cross, D. A. E., D. R. Alessi, P. Cohen, M. Andjelkovich, and B. A. Hemmings.** 1995. Inhibition of glycogen synthase kinase-3 by insulin mediated by protein kinase B. Nature **378:**785–789.
11. **Cross, D. A. E., P. W. Watt, M. Shaw, J. van der Kaay, C. P. Downes, J. C. Holder, and P. Cohen.** 1997. Insulin activates protein kinase B, inhibits glycogen synthase kinase-3 and activates glycogen synthase by rapamycin-insensitive pathways in skeletal muscle and adipose tissue. FEBS Lett. **406:** 211–215.
12. **Dudek, H., S. R. Datta, T. F. Franke, M. J. Birnbaum, R. Yao, G. M. Cooper, R. A. Segal, D. R. Kaplan, and M. E. Greenberg.** 1997. Regulation of neuronal survival by the serine-threonine protein kinase Akt. Science **275:** 661–665.
13. **Easton, R. M., H. Cho, K. Roovers, D. W. Shineman, M. Mizrahi, M. S. Forman, V. M. Lee, M. Szabolcs, R. de Jong, T. Oltersdorf, T. Ludwig, A. Efstratiadis, and M. J. Birnbaum.** 2005. Role for Akt3/protein kinase Bgamma in attainment of normal brain size. Mol. Cell. Biol. **25:**1869–1878.
14. **Fingar, D. C., S. Salama, C. Tsou, E. Harlow, and J. Blenis.** 2002. Mammalian cell size is controlled by mTOR and its downstream targets S6K1 and 4EBP1/eIF4E. Genes Dev. **16:**1472–1487.
15. **Garofalo, R. S., S. J. Orena, K. Rafidi, A. J. Torchia, J. L. Stock, A. L. Hildebrandt, T. Coskran, S. C. Black, D. J. Brees, J. R. Wicks, J. D. McNeish, and K. G. Coleman.** 2003. Severe diabetes, age-dependent loss of adipose tissue, and mild growth deficiency in mice lacking Akt2/PKB beta. J. Clin. Investig. **112:**197–208.
16. **Goren, H. J., R. N. Kulkarni, and C. R. Kahn.** 2004. Glucose homeostasis and tissue transcript content of insulin signaling intermediates in four inbred strains of mice: C57BL/6, C57BLKS/6, DBA/2, and 129X1. Endocrinology **145:**3307–3323.
17. **Inoki, K., Y. Li, T. Zhu, J. Wu, and K. L. Guan.** 2002. TSC2 is phosphorylated and inhibited by Akt and suppresses mTOR signalling. Nat. Cell Biol. **4:**648–657.
18. **Kim, Y. K., S. J. Kim, A. Yatani, Y. Huang, G. Castelli, D. E. Vatner, J. Liu, Q. Zhang, G. Diaz, R. Zieba, J. Thaisz, A. Drusco, C. Croce, J. Sadoshima, G. Condorelli, and S. F. Vatner.** 2003. Mechanism of enhanced cardiac function in mice with hypertrophy induced by overexpressed Akt. J. Biol. Chem. **278:**47622–47628.
19. **Kwiatkowski, D. J., H. Zhang, J. L. Bandura, K. M. Heiberger, M. Glogauer,**

N. el-Hashemite, and H. Onda. 2002. A mouse model of TSC1 reveals sex-dependent lethality from liver hemangiomas, and up-regulation of p70S6 kinase activity in Tsc1 null cells. Hum. Mol. Genet. **11:**525–534.
20. **Lawlor, M. A., and D. R. Alessi.** 2001. PKB/Akt: a key mediator of cell proliferation, survival and insulin responses? J. Cell Sci. **114:**2903–2910.
21. **Liu, J. P., J. Baker, A. S. Perkins, E. J. Robertson, and A. Efstratiadis.** 1993. Mice carrying null mutations of the genes encoding insulin-like growth factor I (Igf-1) and type 1 IGF receptor (Igf1r). Cell **75:**59–72.
22. **Manning, B. D., and L. C. Cantley.** 2003. Rheb fills a GAP between TSC and TOR. Trends Biochem. Sci. **28:**573–576.
23. **Manning, B. D., A. R. Tee, M. N. Logsdon, J. Blenis, and L. C. Cantley.** 2002. Identification of the tuberous sclerosis complex-2 tumor suppressor gene product tuberin as a target of the phosphoinositide 3-kinase/Akt pathway. Mol. Cell **10:**151–162.
24. **Manning, G., G. D. Plowman, T. Hunter, and S. Sudarsanam.** 2002. Evolution of protein kinase signaling from yeast to man. Trends Biochem. Sci. **27:**514–520.
25. **Peng, X. D., P. Z. Xu, M. L. Chen, A. Hahn-Windgassen, J. Skeen, J. Jacobs, D. Sundararajan, W. S. Chen, S. E. Crawford, K. G. Coleman, and N. Hay.** 2003. Dwarfism, impaired skin development, skeletal muscle atrophy, delayed bone development, and impeded adipogenesis in mice lacking Akt1 and Akt2. Genes Dev. **17:**1352–1365.
26. **Potter, C. J., L. G. Pedraza, and T. Xu.** 2002. Akt regulates growth by directly phosphorylating Tsc2. Nat. Cell Biol. **4:**658–665.
27. **Scheid, M. P., and J. R. Woodgett.** 2001. PKB/AKT: functional insights from genetic models. Nat. Rev. Mol. Cell. Biol. **2:**760–768.
28. **Schubert, M., D. P. Brazil, D. J. Burks, J. A. Kushner, J. Ye, C. L. Flint, J. Farhang-Fallah, P. Dikkes, X. M. Warot, C. Rio, G. Corfas, and M. F. White.** 2003. Insulin receptor substrate-2 deficiency impairs brain growth and promotes tau phosphorylation. J. Neurosci. **23:**7084–7092.
29. **Schubert, M., D. Gautam, D. Surjo, K. Ueki, S. Baudler, D. Schubert, T. Kondo, J. Alber, N. Galldiks, E. Kustermann, S. Arndt, A. H. Jacobs, W. Krone, C. R. Kahn, and J. C. Bruning.** 2004. Role for neuronal insulin resistance in neurodegenerative diseases. Proc. Natl. Acad. Sci. USA **101:**3100–3105.
30. **Shioi, T., J. R. McMullen, P. M. Kang, P. S. Douglas, T. Obata, T. F. Franke, L. C. Cantley, and S. Izumo.** 2002. Akt/protein kinase B promotes organ growth in transgenic mice. Mol. Cell. Biol. **22:**2799–2809.
31. **Sutherland, C., and P. Cohen.** 1994. The alpha-isoform of glycogen synthase kinase-3 from rabbit skeletal muscle is inactivated by p70 S6 kinase or MAP kinase-activated protein kinase-1 in vitro. FEBS Lett. **338:**37–42.
32. **Sutherland, C., I. A. Leighton, and P. Cohen.** 1993. Inactivation of glycogen synthase kinase-3 beta by phosphorylation: new kinase connections in insulin and growth-factor signalling. Biochem. J. **296:**15–19.
33. **Tschopp, O., Z. Z. Yang, D. Brodbeck, B. A. Dummler, M. Hemmings-Mieszczak, T. Watanabe, T. Michaelis, J. Frahm, and B. A. Hemmings.** 2005. Essential role of protein kinase B gamma (PKB gamma/Akt3) in postnatal brain development but not in glucose homeostasis. Development **132:**2943–2954.
34. **Tuttle, R. L., N. S. Gill, W. Pugh, J. P. Lee, B. Koeberlein, E. E. Furth, K. S. Polonsky, A. Naji, and M. J. Birnbaum.** 2001. Regulation of pancreatic beta-cell growth and survival by the serine/threonine protein kinase Akt1/PKBalpha. Nat. Med. **7:**1133–1137.
35. **van Slegtenhorst, M., M. Nellist, B. Nagelkerken, J. Cheadle, R. Snell, A. van den Ouweland, A. Reuser, J. Sampson, D. Halley, and P. van der Sluijs.** 1998. Interaction between hamartin and tuberin, the TSC1 and TSC2 gene products. Hum. Mol. Genet. **7:**1053–1057.
36. **Whiteman, E. L., H. Cho, and M. J. Birnbaum.** 2002. Role of Akt/protein kinase B in metabolism. Trends Endocrinol. Metab. **13:**444–451.
37. **Yang, Z. Z., O. Tschopp, N. Di-Poi, E. Bruder, A. Baudry, B. Dummler, W. Wahli, and B. A. Hemmings.** 2005. Dosage-dependent effects of Akt1/protein kinase Balpha (PKBalpha) and Akt3/PKBgamma on thymus, skin, and cardiovascular and nervous system development in mice. Mol. Cell. Biol. **25:**10407–10418.
38. **Yang, Z. Z., O. Tschopp, M. Hemmings-Mieszczak, J. Feng, D. Brodbeck, E. Perentes, and B. A. Hemmings.** 2003. Protein kinase B alpha/Akt1 regulates placental development and fetal growth. J. Biol. Chem. **278:**32124–32131.

II. RESULTS

Part 2:

Essential role of protein kinase B gamma (PKBgamma/Akt3) in postnatal brain development but not in glucose homeostasis.

Tschopp O, Yang ZZ, Brodbeck D, Dummler BA, Hemmings-Mieszczak M, Watanabe T, Michaelis T, Frahm J, Hemmings BA.

Development 2005, 132:2943-2954

Essential role of protein kinase Bγ (PKBγ/Akt3) in postnatal brain development but not in glucose homeostasis

Oliver Tschopp[1], Zhong-Zhou Yang[1], Daniela Brodbeck[1], Bettina A. Dummler[1], Maja Hemmings-Mieszczak[2], Takashi Watanabe[3], Thomas Michaelis[3], Jens Frahm[3] and Brian A. Hemmings[1,*]

[1]Friedrich Miescher Institute for Biomedical Research, Maulbeerstrasse 66, CH-4058 Basel, Switzerland
[2]Novartis Pharma AG, Lichtstrasse 35, CH-4056, Basel, Switzerland
[3]Biomedizinische NMR Forschungs GmbH am Max-Planck-Institut für biophysikalische Chemie, 37070 Göttingen, Germany
*Author for correspondence (e-mail: brian.hemmings@fmi.ch)

Accepted 14 April 2005

Development 132, 2943-2954
Published by The Company of Biologists 2005
doi:10.1242/dev.01864

Summary

Protein kinase B is implicated in many crucial cellular processes, such as metabolism, apoptosis and cell proliferation. In contrast to *Pkbα* and *Pkbβ*-deficient mice, *Pkbγ*$^{-/-}$ mice are viable, show no growth retardation and display normal glucose metabolism. However, in adult *Pkbγ* mutant mice, brain size and weight are dramatically reduced by about 25%. In vivo magnetic resonance imaging confirmed the reduction of *Pkbγ*$^{-/-}$ brain volumes with a proportionally smaller ventricular system. Examination of the major brain structures revealed no anatomical malformations except for a pronounced thinning of white matter fibre connections in the corpus callosum. The reduction in brain weight of *Pkbγ*$^{-/-}$ mice is caused, at least partially, by a significant reduction in both cell size and cell number. Our results provide novel insights into the physiological role of PKBγ and suggest a crucial role in postnatal brain development.

Key words: *Pkbγ/Akt3* knockout, Brain development, Apoptosis

Introduction

Protein kinase B (PKB/Akt) is a second messenger-regulated kinase that has been implicated in many crucial cellular processes, such as glucose metabolism, transcription, cell proliferation, apoptosis, migration and growth (Brazil and Hemmings, 2001; Chan et al., 1999; Datta et al., 1999; Kandel and Hay, 1999; Scheid and Woodgett, 2001). Deregulation of PKB activity contributes to cell transformation and diabetes (Brazil and Hemmings, 2001; Nicholson and Anderson, 2002). In mammalian cells, three closely related isoforms of the PKB family have been identified and termed PKBα/Akt1, PKBβ/Akt2 and PKBγ/Akt3 (Brodbeck et al., 1999; Cheng et al., 1992; Jones et al., 1991a; Jones et al., 1991b; Masure et al., 1999; Nakatani et al., 1999). These proteins are products of three separate genes located on distinct chromosomes and are widely expressed with a few isoform-specific features (Altomare et al., 1998; Yang et al., 2003). All three members of the PKB family contain a highly conserved N-terminal pleckstrin homology (PH) domain, a central catalytic domain and a short C-terminal regulatory domain (Hanada et al., 2004).

PKB is activated by numerous stimuli, including growth factors, hormones and cytokines (Brazil and Hemmings, 2001; Chan et al., 1999; Datta et al., 1999). Activation of PKB occurs in response to signalling via phosphoinositide 3 kinase (PI3K) and requires the membrane-bound second messenger phosphatidylinositol-3,4,5-triphosphate [PtdIns(3,4,5)P_3 or PIP3] (Burgering and Coffer, 1995; Cross et al., 1995; Franke et al., 1995). The current model for PKB regulation proposes that PtdIns(3,4,5)P_3, generated following PI3K activation, interacts with the PH domain of PKB, recruiting the inactive kinase from the cytoplasm to the plasma membrane and promoting a conformational change that allows phosphorylation on two regulatory sites by upstream kinases at the plasma membrane. One of these critical phosphorylation sites resides in the activation loop of the kinase domain (Thr308 in PKBα) and the other is located in the C-terminal regulatory domain (Ser-473 in PKBα), termed the hydrophobic motif (Alessi et al., 1996; Brodbeck et al., 1999; Meier et al., 1997). The upstream kinase that phosphorylates Thr308 in the activation loop of the kinase domain of PKBα in a PIP3-dependent-manner has been identified and termed 3-phosphoinositide-dependent kinase 1 (PDK1) (Alessi et al., 1997; Stokoe et al., 1997). Thr308 phosphorylation is necessary and sufficient for PKB activation; however, maximal activation requires additional phosphorylation at Ser473 (Alessi et al., 1996; Yang et al., 2002a; Yang et al., 2002b). Several different protein kinases and mechanisms have been proposed for the phosphorylation of the hydrophobic motif (Brazil and Hemmings, 2001; Yang et al., 2002b).

Mice with targeted disruption of *Pkbα* and/or *Pkbβ* have been obtained recently with *Pkbα* mutant mice displaying an increased neonatal lethality and a reduction in body weight of ~30% (Chen et al., 2001; Cho et al., 2001b; Yang et al., 2003). Moreover, loss of *Pkbα* leads to placental hypotrophy with impaired vascularisation (Yang et al., 2003). By contrast, *Pkbβ*-deficient mice are born with the expected Mendelian ratio and exhibit a diabetes-like syndrome with elevated fasting plasma glucose, hepatic glucose output, peripheral insulin resistance and an compensatory increase of islet mass (Cho et

al., 2001a). Compared with *Pkbα* mutant mice, *Pkbβ*-deficient mice are only mildly growth retarded (Cho et al., 2001a; Garofalo et al., 2003). However, mice lacking both isoforms die after birth, probably owing to respiratory failure (Peng et al., 2003). *Pkbαβ* double mutant newborns display a severe reduction in body weight (≈50%), prominent atrophy of the skin and skeletal muscle, as well as impaired adipogenesis and delayed ossification.

Here, we report the generation and characterisation of mice with targeted disruption of the *Pkbγ* gene. Compared with *Pkbα*$^{-/-}$ and *Pkbβ*$^{-/-}$ mice, *Pkbγ* mutant mice display a distinct phenotype without increased perinatal mortality, growth retardation or altered glucose metabolism. However, loss of PKBγ profoundly affects postnatal brain growth. Brains from adult *Pkbγ* mutant mice show a dramatic reduction in size and weight. Taken together, our results reveal a novel and important physiological role for PKBγ in postnatal brain development.

Materials and methods

Targeted disruption of the Pkbγ gene by homologous recombination

An ~11-kb *Hin*dIII fragment was subcloned containing exons 4 and 5 of *Pkbγ*. A *Nco*I site was generated in exon 4 for insertion of a ~5-kb IRES-*lacZ*-Neo cassette. The targeting vector was linearised with *Sal*I and electroporated into 129/Ola ES cells. An external probe was used for ES cell screening following *Xba*I digestion. An internal probe and a *lacZ*-Neo probe were used to characterize ES clones positive for homologous recombination (data not shown). Correctly targeted ES cells were used to generate chimeras. Male chimeras were mated with wild-type C57BL/6 females to obtain *Pkbγ*$^{+/-}$ mice. *Pkbγ*$^{+/-}$ mice have been backcrossed twice with pure C57BL/6 mice and the progeny of *Pkbγ*$^{+/-}$ intercrosses have ~75% C57BL/6 genetic background. Progeny were genotyped by multiplex PCR with the following three primers: (1) *P35*, GGTTCTGTGGGAGGTA-GTTCTC; (2) Neo-2, GCAATCCATCTTGTTCAATGGCCG; and (3) E4γ, CCATCGGTCGGCTACGGCTTGG.

Quantitative real time PCR

The levels of PKB isoforms in wild-type and mutant mice were determined by quantitative Q-RT-PCR. The experiment was performed as described previously (Yang et al., 2003). Briefly, total RNA was purified using Trizol Reagent (Invitrogen). For the Q-PCR reaction, 50 ng total RNA was mixed with 5′ and 3′ primers, Taqman probe, MuLV reverse transcriptase, RNase inhibitor and the components of the TaqMan PCR reagent kit (Eurogentec) in a total volume of 25 μl following the TaqMan PCR reagent kit protocol.

Western blot analysis

For Western blot analysis, protein lysates were processed as previously described (Yang et al., 2003). PKB isoform-specific antibodies were obtained by immunizing rabbits with isoform-specific peptides as previously described (Yang et al., 2003). Antibodies against phospho-PKB (Ser473), phospho-GSK3α/β (Ser21/9), phospho-TSC2 (Thr1462) and phospho-p70S6K were purchased from Cell Signalling Technologies. Antibodies against p27 and ERK were purchased from Santa Cruz Biotechnology. The antibody against phospho-ERK (Thr202/Tyr204) was purchased from Promega and the Pan-Actin antibody was obtained from NeoMarkers. Western blots were scanned using a GS-800 BioRad densitometer with a resolution of 63.5 μm × 63.5 μm and bands were quantified using Proteomweaver 3.0.0.6 (Definiens).

Histological examination

For histological analysis, animals were perfused with phosphate-buffered saline and 4% paraformaldehyde in phosphate-buffered saline. Organs were dissected and kept in the same fixation solution overnight at 4°C. Samples were embedded in paraffin following dehydration in ethanol. Tissues were cut into 6 μm sections and stored for staining. For Haematoxylin-Eosin and Cresyl-Violet (Sigma) staining, sections were freed of paraffin and stained.

Cell number determination

To determine the number of cells in a whole brain, the DNA content was determined as described by Labarca and Paigen (Labarca and Paigen, 1980). This method is based on the enhancement of fluorescence after binding of bisbenzimid (Riedel-de Haen) to DNA. A linear standard curve (1-10 μg/ml) was prepared to calculate the DNA concentration. The relative cell size in posterior cortex was measured on plane-matched, parasagittal brain sections stained with DAPI (Biotium). Image-Pro® Plus (Media Cybernetics) was used to count the cell number and to calculate the mean area occupied by one cell. The relative cell size is expressed as percent of wild type.

In vivo magnetic resonance imaging (MRI)

MRI studies of 4-month-old female *Pkbγ* wild-type (n=5) and mutant mice (n=5) were performed at 2.35 T using a MRBR 4.7/400 mm magnet (Magnex Scientific, Abingdon, England) equipped with BGA20 gradients (100 mT m^{-1}) and a DBX system (Bruker Biospin, Ettlingen, Germany). For in vivo examinations, animals were anaesthetized (1.0-1.5% halothane in 70:30 N_2O:O_2) and treated as previously described (Natt et al., 2002). Briefly, radiofrequency (rf) excitation and signal reception were accomplished with use of a Helmholtz coil (∅ 100 mm) and a surface coil (∅ 20×12 mm), respectively. Three-dimensional T_1-weighted (rf-spoiled 3D FLASH, repetition time TR=17 mseconds, echo time TE=7.6 mseconds, flip angle 25°, measuring time 84 minutes) and T_2-weighted MRI data sets (3D fast spin-echo, TR/TE=3000/98 mseconds, measuring time 58 minutes) were acquired with an isotropic resolution of 117 μm. Volumetric assessments were obtained by analysing T_1-weighted images using software provided by the manufacturer (Paravision, Bruker Biospin, Ettlingen, Germany). After manually outlining the whole brain and the ventricular spaces in individual sections, respective areas were calculated (in mm^2), summed and multiplied by the section thickness.

Neuronal cell culture

E16.5 murine hippocampal neurons were isolated from timed matings. Cells were kept in culture for 7 days on polylysine coverslips coated with B27/Neurobasal (GIBCO Life Technologies). At day 7, cultures were treated with glutamate (15 mM/24 hours), staurosporine (50 nM/12 hours) or were left untreated. For the detection of apoptotic cells, five fixed cultures per genotype were stained using a TUNEL-assay (Roche) according to the manufacturer's instructions and counterstained with DAPI (Biotium). At least 200 cells per culture were counted and the percentage of apoptotic cells was calculated.

Glucose and insulin tolerance test

Mice were housed according to the Swiss Animal Protection Laws in groups with 12 hours dark/light cycles and with free access to food and water. All procedures were conducted with the approval of the appropriate authorities.

Random-fed and fasting blood glucose levels were determined in 5- to 6-month-old mice. Blood samples were collected from tail veins and glucose levels were determined using Glucometer Elite (Bayer). Mice (aged 5-6 months) were fasted overnight before the start of the glucose and insulin tolerance tests. Glucose (2 g/kg) was given orally to conscious mice. Insulin (1 U/kg) was administered by intraperitoneal injection to conscious mice. Blood samples were collected at indicated times from tail veins and glucose levels were determined using Glucometer Elite (Bayer). Blood glucose levels were expressed as percentage of initial value. Blood insulin levels

were measured with a Mouse ultra-sensitive insulin ELISA (Immunodiagnostic Systems).

Microarray analysis

Microarray analysis was performed using murine MOE430A GeneChips™ (Affymetrix). Total RNA (10 μg) was reverse transcribed using the SuperScript Choice system for cDNA synthesis (Life Technologies) and biotin-labelled cRNA generated using the Enzo BioArray High Yield RNA transcript labelling kit (Enzo Diagnostics) following the manufacturer's protocol. cRNA fragmentation and hybridisation were performed as recommended by Affymetrix. Expression data were calculated using the RMA algorithm from BioConductor (Irizarry et al., 2003). A gene was considered to be significantly altered in its expression if it had an Affymetrix change *P*-value of less than 0.003 for either increase or decrease in at least two-thirds of replicate comparisons and it had a minimum expression value of 100 in at least one condition. A fold-change threshold of 1.5 was then applied and the resulting genes were subjected to a one-way ANOVA with a *P*-value cut-off of 0.05. A Benjamini and Hochberg multiple testing correction and a Tukey post-hoc test were applied.

Statistical analysis

To compare body weight, brain weight and volume, brain/body weight ratio, DNA content, cell number and percentage of apoptotic cells between $Pkb\gamma^{+/+}$ and $Pkb\gamma^{-/-}$, an unpaired Students *t*-test was performed. *P* values under 0.05 were considered as significant and values below 0.01 as highly significant.

Results

Targeting strategy and confirmation of genotype

$Pkb\gamma^{-/-}$ mice were generated by targeted disruption of exon 4 as shown in (Fig. 1A). The ablation of *Pkbγ* was confirmed by PCR, Q-RT-PCR and Western blot analysis using brain tissue samples from *Pkbγ* wild-type ($Pkb\gamma^{+/+}$), heterozygous ($Pkb\gamma^{+/-}$) and mutant ($Pkb\gamma^{-/-}$) mice (Fig. 1B). Quantitative RT-PCR displayed complete ablation of the PKBγ mRNA in brain samples of *Pkbγ* mutant mice (n=3, data not shown). To confirm the absence of PKBγ at the protein level, Western blot analysis was performed with an isoform-specific anti-PKBγ antibody. In contrast to $Pkb\gamma^{+/+}$ brain tissue samples, PKBγ was not detectable in samples derived from mutant mice (Fig. 1C). In addition, Western blot analysis with antibodies specific for PKBα and PKBβ, respectively, showed no compensatory upregulation of PKBα and/or PKBβ, respectively, in the brain of $Pkb\gamma^{-/-}$ mice (Fig. 1D).

Distribution of PKBγ in wild-type tissues

It has been reported that the PKBα and β isoform are widely expressed in all organs, but with some isoform-specific features (Altomare et al., 1998; Yang et al., 2003). Less is known about the tissue distribution of the PKBγ isoform. Previous reports suggest that PKBγ has a more restricted distribution with high levels in the adult brain and foetal heart and low levels in liver and skeletal muscle (Brodbeck et al., 1999; Masure et al., 1999; Yang et al., 2003). We assessed the distribution of PKBγ mRNA in 15 major tissues of adult mice by quantitative RT-PCR and normalised to the level of PKBγ in the brain (Fig. 2A). PKBγ mRNA was found at the highest level in brain and testis, and at lower levels in lung, mammary gland, fat and spleen.

To investigate whether PKBγ ablation leads to compensatory increase in PKBα and/or PKBβ, total RNA isolated from brain, testis, lung, mammary gland, fat and spleen of three *Pkbγ* wild-type and three mutant mice was subjected to quantitative RT-PCR. The levels of PKBα and β were normalised to the level of PKBα in wild-type brain and set as 100%. Overall, no marked upregulation of PKBα and/or PKBβ was observed, including the brain (Fig. 2B,C). These results are consistent with Western blot analysis of protein extracts of brains from *Pkbγ* wild-type and mutant mice (Fig. 1D). To investigate the distribution and levels of individual PKB isoforms within the brain, protein lysates were prepared from ten anatomically and functionally different regions. In general, all three isoforms were expressed in all examined regions but with certain isoform-specific features (Fig. 2D). PKBα is expressed in all regions at similar levels, whereas PKBβ is expressed at moderate levels in cortex, cerebellum, hippocampus and olfactory bulb, and at lower levels in the hypothalamus, midbrain, brain stem and spinal cord. PKBγ is expressed in all examined regions but at higher levels in the cortex and in the cerebellum.

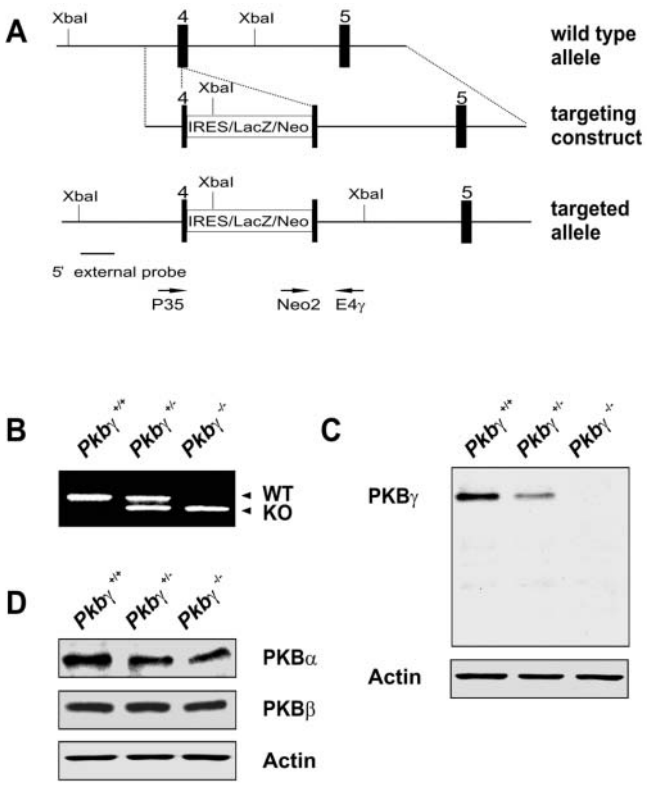

Fig. 1. Targeting strategy and confirmation of genotype. (A) The genomic organization of the *Pkbγ* wild-type allele (top) was disrupted using a targeting vector with an IRES-*lacZ*-Neo-cassette (middle). Targeting of the wild-type allele leads to disruption of exon 4 of the *Pkbγ* gene (bottom). Arrowheads indicate the localization of the primers for the PCR reaction. (B) The genotype of mice was determined by PCR. Representative results from $Pkb\gamma^{+/+}$, $Pkb\gamma^{+/-}$ and $Pkb\gamma^{-/-}$ mice are shown. (C) The levels of PKBγ in the brains of $Pkb\gamma^{+/+}$, $Pkb\gamma^{+/-}$ and $Pkb\gamma^{-/-}$ mice were determined by western blot analysis using a PKBγ-specific antibody. (D) The levels of PKBα and PKBβ, respectively, were determined in brain lysates from $Pkb\gamma^{+/+}$, $Pkb\gamma^{+/-}$ and $Pkb\gamma^{-/-}$ mice using PKBα- and PKBβ-specific antibodies.

Signalling in *Pkbγ* mutant mice

The phosphorylation/activation state of PKB in protein extracts from brains of 3-month-old $Pkb\gamma^{+/+}$ and $Pkb\gamma^{-/-}$ mice was analysed using an antibody specific for the phosphorylation site (anti-phospho-Ser-473) in the hydrophobic motif of the regulatory domain of all three isoforms (Fig. 3A). As expected, levels of activated PKB (quantification was done using actin as loading control) in $Pkb\gamma^{-/-}$ mice was significantly lower than in $Pkb\gamma^{+/+}$ littermate controls (100% versus 38%), but was not completely abolished (Fig. 3B). The phosphorylation levels of glycogen synthase kinase 3 (GSK3), tuberous sclerosis complex 2 (TSC2), p70S6K, ERK and p27 in $Pkb\gamma^{-/-}$ mice were not significantly changed when compared with wild-type littermate controls (levels of phosphorylated protein were normalised with the level of unphosphorylated protein). We repeated this experiment using brain samples of 14 days old mice and obtained comparable results with significantly reduced levels of total phosphorylated PKB and unchanged levels of phosphorylated substrates (data not shown).

Several recent studies emphasize the importance of insulin-like growth factor 1 (IGF1) signalling in the survival and proliferation of oligodendrocytes and myelination in the central nervous system (D'Ercole et al., 2002). Mice lacking IGF1 also have reduced brain weight and reduced size of the corpus callosum and anterior commissure (Ye et al., 2002). Therefore, we performed a western blot analysis with cell lineage-specific markers using antibodies against myelin basic protein (oligodendrocytes), glial fibrillary acidic protein

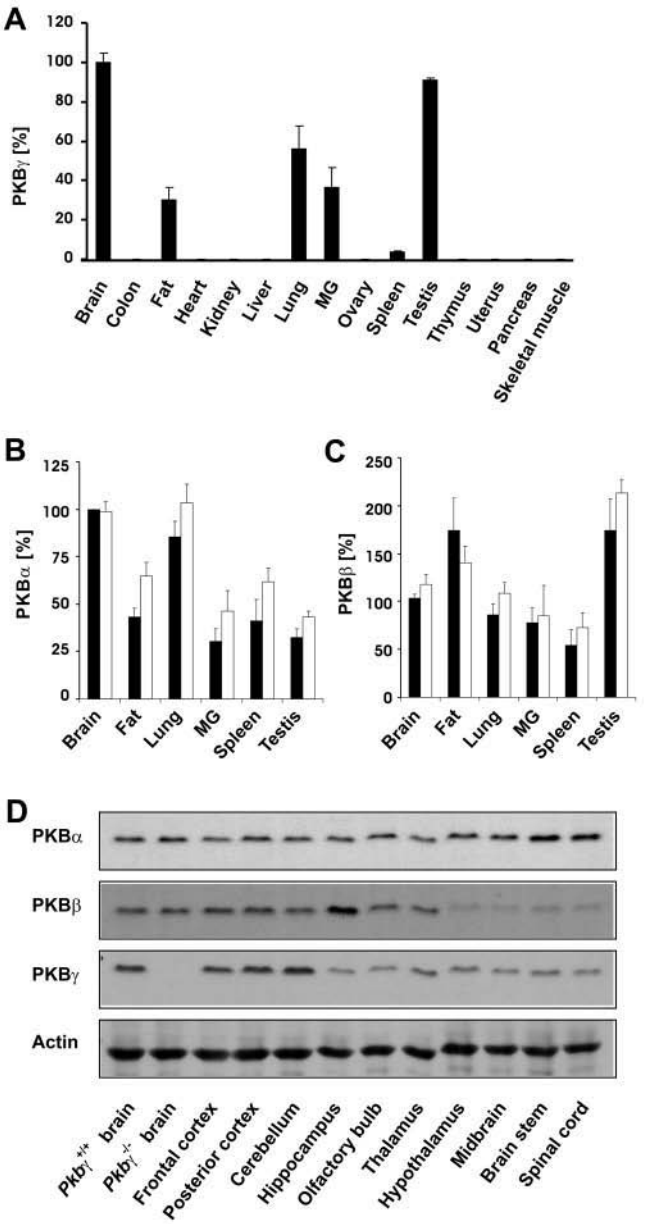

Fig. 2. Tissue distribution of PKBγ and levels of PKBα and PKBβ in *Pkbγ* mutant mice. (A) The mRNA level of PKBγ was determined in 15 different organs from adult $Pkb\gamma^{+/+}$ mice. Total RNA was isolated from three adult mice and the levels were normalized to the level of PKBγ in the brain (100%). MG, mammary gland. Error bars represent s.d. mRNA levels of (B) PKBα and (C) PKBβ were determined using total RNA from six different organs of adult *Pkbγ* wild-type (n=3; black bars) and mutant mice (n=3; white bars). mRNA levels of PKBα and PKBβ were normalized to the level of PKBα in wild-type brain (100%). Error bars represent s.d. (D) Western blot analysis of PKBα, β and γ within ten different brain regions using isoform specific antibodies.

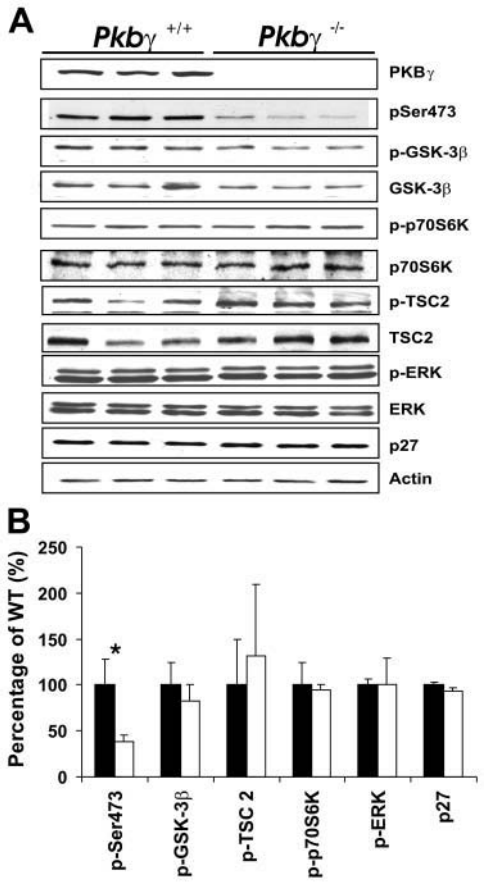

Fig. 3. Phospho-western blot analysis of brains from *Pkbγ* mutant mice. (A) Brains of three wild-type and three mutant mice were analysed for phosphorylation status of proteins involved in PKB signalling. p, indicates phosphorylated protein. (B) Western blot quantification. Levels of p-Ser473 and p27 were normalized to the level of actin, all phosphorylated proteins were normalized to the level of unphosphorylated protein. *P<0.05. Error bars represent s.d.

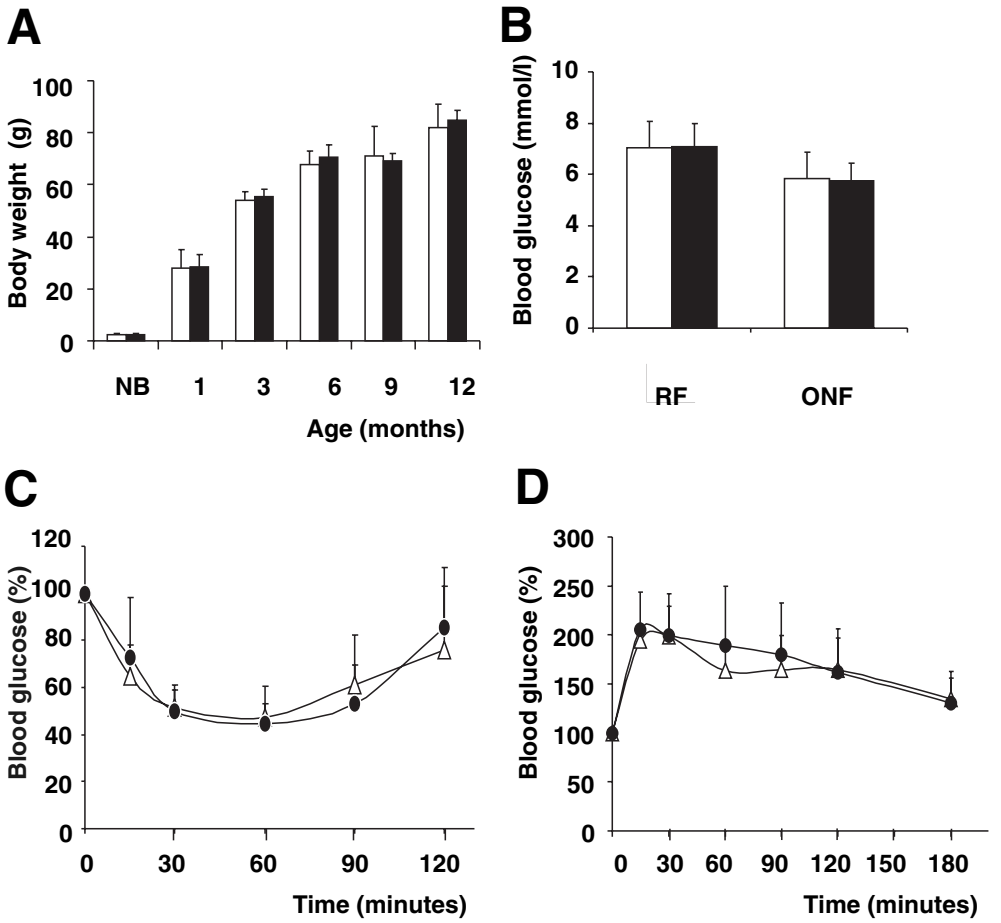

Fig. 4. Dispensable role of PKBγ for body weight and glucose metabolism. (A) Body weights of male $Pkb\gamma^{+/+}$ (white bars) and $Pkb\gamma^{-/-}$ (black bars) mice were measured at different points in time (n=5-8 animals per genotype). Error bars represent s.d. NB, newborn. (B) Blood glucose concentrations from random-fed (RF) and overnight fasted (ONF) mice (n=8; 6 months old; $Pkb\gamma^{+/+}$ white bars and $Pkb\gamma^{-/-}$ black bars). Error bars represent s.d. (C) Insulin tolerance test. Animals (n=6; 6 months old; $Pkb\gamma^{+/+}$ white triangles and $Pkb\gamma^{-/-}$ black circles) were fasted overnight and insulin (1 U/kg) was administered by intraperitoneal injection. (C) Glucose concentrations were determined at indicated time points from whole blood collected from tail veins. Values were normalized to the starting glucose concentration at the administration of insulin. Error bars represent s.d. (D) Glucose tolerance test. Animals (n=6; 5-6 months old; $Pkb\gamma^{+/+}$ white triangles and $Pkb\gamma^{-/-}$ black circles) were fasted overnight and glucose (2 g/kg) was orally administered. Blood glucose concentrations were sampled at the indicated times. Values were normalized to the starting glucose concentration at the administration of glucose. Error bars represent s.d.

(astrocytes) and M-neurofilaments (neurons). Significantly, no obvious differences in the expression levels of these marker proteins were observed when comparing samples of $Pkb\gamma^{+/+}$ and $Pkb\gamma^{-/-}$ mice (n=5 per genotype, data not shown).

PKBγ is not required for postnatal survival, fertility, body weight and glucose metabolism

There was no evidence for increased mortality of $Pkb\gamma^{-/-}$ mice after birth in an analysis of more than 400 pups (aged 3-4 weeks) [$Pkb\gamma^{+/+}$: $Pkb\gamma^{+/-}$: $Pkb\gamma^{-/-}$=104 (25.6%): 206 (50.7%): 96 (23.6%)]. As PKBγ is highly expressed in the testis, fertility of mutant mice was tested using male $Pkb\gamma^{-/-}$ × female $Pkb\gamma^{+/+}$ and female $Pkb\gamma^{-/-}$ × male $Pkb\gamma^{+/+}$ matings. Both male and female mutant mice matings gave normal pregnancies and births, indicating that fertility is not impaired in either male or female *Pkbγ* mutant mice (data not shown).

As PKB has been implicated in the regulation of cell and organ growth, body weight was measured in male *Pkbγ* mutant mice and wild-type littermate controls (n=5-8 per group) at different time points (Chen et al., 2001; Cho et al., 2001b; Peng et al., 2003; Yang et al., 2003). Body weight did not differ significantly between male *Pkbγ* mutant mice and wild-type controls at any time point (Fig. 4A). A similar result was obtained with female $Pkb\gamma^{-/-}$ mice and $Pkb\gamma^{+/+}$ controls (n=5-8 per group, data not shown), indicating that PKBγ does not play a significant role in the overall growth of mice.

To investigate a potential role of PKBγ in the regulation of glucose metabolism, blood glucose levels were measured in adult (5-6 months) *Pkbγ* mutant mice under random-fed and fasting condition, and compared with age- and gender-matched wild-type controls. Interestingly, both random-fed and fasting blood glucose levels, were not significantly different between wild-type and mutant mice (Fig. 4B). Additionally, blood insulin levels in random-fed condition did not differ significantly between $Pkb\gamma^{+/+}$ and $Pkb\gamma^{-/-}$ mice (1.32±0.08 μg/l versus 1.30±0.13 μg/l; n=6). To further investigate glucose metabolism, overnight fasted mice were challenged with insulin (insulin tolerance test) or glucose (glucose tolerance test). To test the insulin responsiveness, insulin (1 U/kg) was applied by intraperitoneal injection und blood glucose levels were measured at indicated time points using blood from tail veins. No obvious differences of blood glucose levels in the insulin tolerance test were found between the groups with mutant and control mice (Fig. 4C). Additionally, mice were challenged with orally applied glucose (2 g/kg) and blood glucose levels were measured at indicated time. Compared with wild-type mice, $Pkb\gamma^{-/-}$ mice displayed a very similar response to the glucose load (Fig. 4D). Taken together, these results suggest that PKBγ does not play a significant role in the maintenance of glucose homeostasis.

Essential role of PKBγ in postnatal brain development

Next, adult $Pkb\gamma^{+/+}$ and $Pkb\gamma^{-/-}$ mice were dissected and all major organs were investigated macroscopically. Compared with $Pkb\gamma^{+/+}$ littermate controls, the overall size of brains from

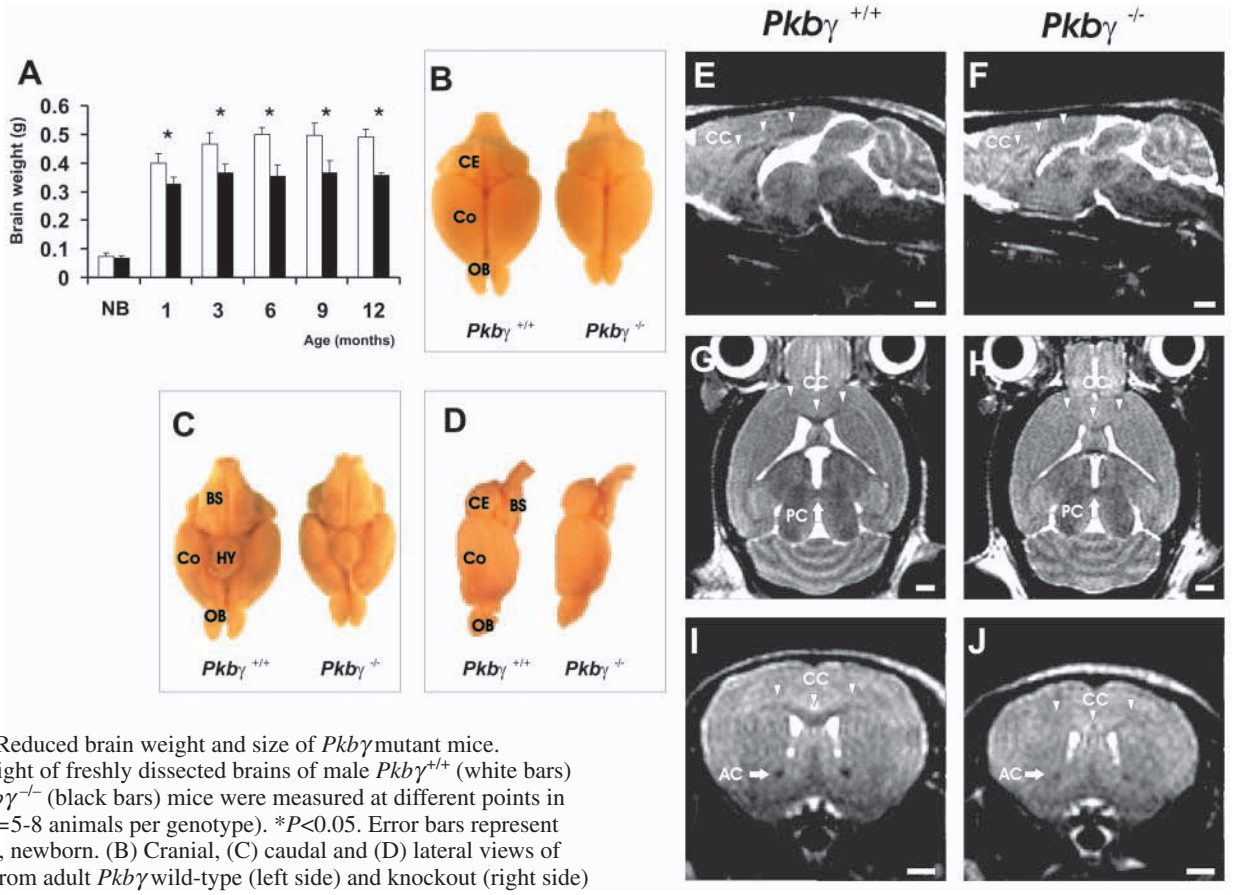

Fig. 5. Reduced brain weight and size of *Pkbγ* mutant mice. (A) Weight of freshly dissected brains of male *Pkbγ*$^{+/+}$ (white bars) and *Pkbγ*$^{-/-}$ (black bars) mice were measured at different points in time (n=5-8 animals per genotype). *P<0.05. Error bars represent s.d. NB, newborn. (B) Cranial, (C) caudal and (D) lateral views of brains from adult *Pkbγ* wild-type (left side) and knockout (right side) mice. Co, cortex; CE, cerebellum; OB, olfactory bulb; BS, brainstem; HY, hypothalamus. (E-J) Representative sections from T_2-weighted 3D MRI data sets acquired in vivo from the brains of *Pkbγ*$^{+/+}$ (E,G,I) and P*kbγ*$^{-/-}$ mice (F,H,J) from *Pkbγ*$^{+/-}$ matings in sagittal (E,F), horizontal (G,H) and coronal (I,J) orientation. CC, corpus callosum; AC, anterior commissure; PC, posterior commissure. Scale bar: 1 mm.

adult *Pkbγ*$^{-/-}$ mice was strikingly reduced. A representative example is shown in Fig. 5B-D. Furthermore, the weights of freshly dissected brains of *Pkbγ* wild-type and *Pkbγ* mutant mice were measured at different ages (Fig. 5A). Compared with age- and gender-matched wild-type littermate controls, brains from adult *Pkbγ*$^{-/-}$ mice (3-12 months old) exhibited a highly significant reduction in weight of about 25% (range 22%-29%), affecting both males and females (data for females not shown, n=5-8). Interestingly, at birth, brain weight did not differ significantly between *Pkbγ*$^{+/+}$ and *Pkbγ*$^{-/-}$ mice. The reduction in brain size and weight was first observed at the age of 1 month, but was less pronounced compared with adult mice (≈18%). In contrast to *Pkbα*, *Pkbβ* and *IgfI*-null mutant mice (Beck et al., 1995; Cheng et al., 1998; Garofalo et al., 2003; Powell-Braxton et al., 1993), the brain/body weight ratio of *Pkbγ* mutant mice was also significantly reduced to a similar extent.

In vivo magnetic resonance imaging (MRI) of *Pkbγ*$^{-/-}$ mice

MRI is an excellent non-invasive technique for studying brain anatomy in transgenic and mutant mice (Kooy et al., 2001; Natt et al., 2002). For further characterization of *Pkbγ* mutant brain anatomy, five adult female mutant and five age and gender matched wild-type littermate controls (with the same genetic background) from *Pkbγ*$^{+/-}$ matings were examined using high-resolution 3D MRI as previously described (Natt et al., 2002). Fig. 5E-J shows representative T_2-weighted images of *Pkbγ*$^{+/+}$ and *Pkbγ*$^{-/-}$ brains in a sagittal, horizontal, and coronal section orientation. Complementary in vivo volumetry based on T_1-weighted 3D MRI confirmed the much smaller brain size of all five *Pkbγ* mutant mice. Compared with wild-type littermates, whole brain volume in *Pkbγ*$^{-/-}$ mice was significantly reduced by about 24% (513±14 mm^3 versus 391±16 mm^3, P<0.01; n=5). Although several brain regions were affected, including olfactory bulb, cortex and hippocampal formation, no alteration in the structural organization of the brain was observed, confirming the macro-pathological findings. Moreover, because the volume of the ventricular spaces in *Pkbγ*$^{-/-}$ mice was reduced (7.85±2.2 mm^3 versus 5.55±2.8 mm^3) in proportion to that of the whole brain and MRI revealed no enlargement of the subarachnoid space, the occurrence of an internal or external hydrocephalus is excluded as a cause of reduced brain size. Interestingly, in contrast to any wild-type littermate controls, all five *Pkbγ*$^{-/-}$ mice presented with a marked thinning of the corpus callosum (downward arrowheads in Fig. 5E,F). White matter fibres connections are depicted as hypointense structures in T_2-weighted images. Although unequivocally identifiable in *Pkbγ*$^{+/+}$ mice (Fig. 5E,G,I), the corpus callosum is partly indistinguishable from surrounding grey matter in *Pkbγ*$^{-/-}$ mice (Fig. 5F,H,J). Anterior

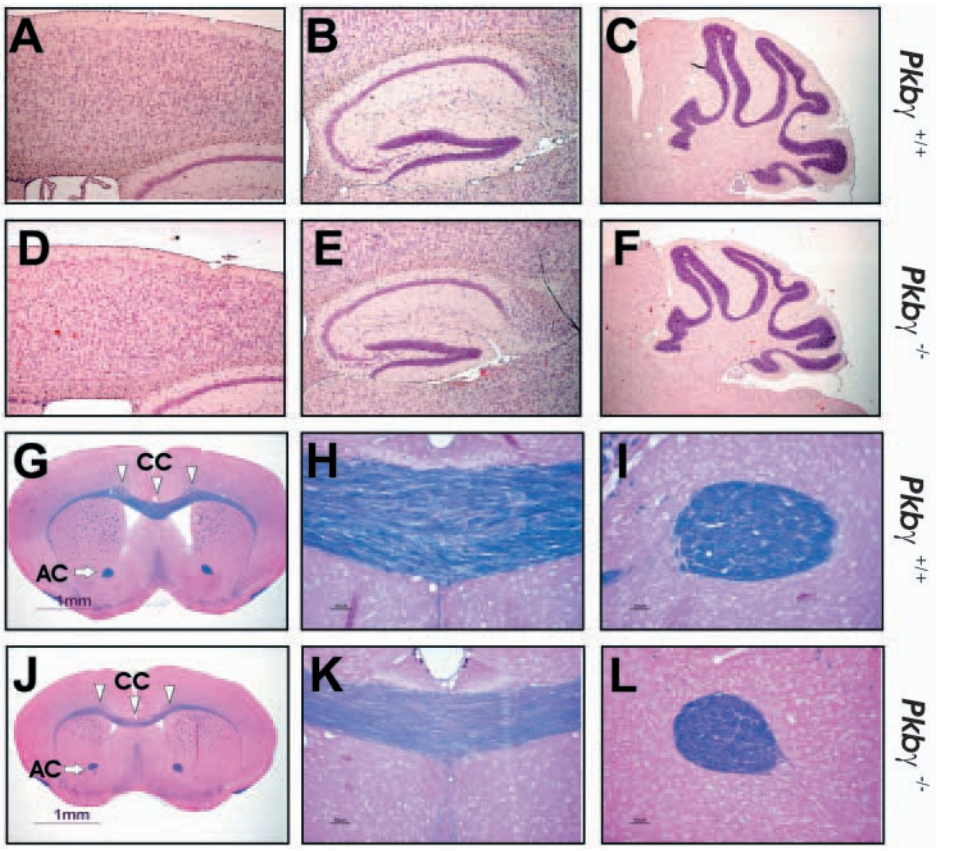

Fig. 6. Histology of brains from *Pkbγ* mutant mice. Representative sections (HE staining) of the cortex (A,D), hippocampus (B,E) and cerebellum (C,F) from adult $Pkb\gamma^{+/+}$ (A-C) and $Pkb\gamma^{-/-}$ (D-F) mice in parasagittal orientation. Representative sections stained for myelin (Luxol-Fast Blue/Eosin) of whole brain (G,J), corpus callosum (H,K) and anterior commissure (I,L) from $Pkb\gamma^{+/+}$ (G-I) and $Pkb\gamma^{-/-}$ mice (J-L) in coronal orientation. White matter structures are labelled as follows: CC, corpus callosum; AC, anterior commissure.

and posterior commissures as well as the hippocampal fimbria are less prominently affected.

Histology of $Pkb\gamma^{-/-}$ mouse brains

Histological examination of $Pkb\gamma^{-/-}$ brain was performed to investigate changes at the microscopic level. Various brain regions, including cerebellum, hippocampus and corpus callosum, were examined following Haematoxylin/Eosin staining (Fig. 6A-F). With the exception of the reduced size of all regions, no abnormalities in the overall structure of the different brain regions were observed. In line with the in vivo MRI findings, the thickness of the corpus callosum in *Pkbγ* mutant mice was markedly reduced (downward arrowheads in Fig. 6G,J). Additionally, myelin staining with luxol Fast Blue revealed not only a reduction in thickness of the corpus callosum but also less intense staining of the structure (Fig. 6H,K).

Cell number in the brains of $Pkb\gamma^{-/-}$ mice

Next, we indirectly assessed the cell number by measuring the amount of DNA in whole brains derived from $Pkb\gamma^{+/+}$ and $Pkb\gamma^{-/-}$ mice. The amount of DNA is considered as an indicator of cell number, whereas the amount of DNA per gram of tissue is an indicator of cell density which is reciprocal to cell volume (Zamenhof, 1976). The DNA contents of brains from newborns and 1-month-old mice were determined using the method described by Labarca and Paigen (Labarca and Paigen, 1980). Briefly, this method is based on the enhancement of fluorescence after binding of bisbenzimid to DNA. Compared with wild-type control samples, whole brain DNA content of $Pkb\gamma^{-/-}$ newborns did not differ significantly, indicating that cell number was not changed. Similarly, the DNA content per gram of brain tissue was comparable between *Pkbγ* wild-type and mutant mice, indicating a comparable cell size. In contrast to newborns, the DNA content in brains of 1-month-old *Pkbγ* mutant mice was slightly, but significantly, reduced compared with the $Pkb\gamma^{+/+}$ controls (Table 1). However, the DNA content per gram of tissue was, significantly increased in samples from $Pkb\gamma^{-/-}$ compared with wild-type littermate controls, indicative of increased cell density (and reduced cell size).

Additionally, the relative cell size in the posterior cortex of adult mice (3 months) was determined based on histological slides stained with DAPI. Cells were analysed using Image-Pro Plus in a defined field of view (≈1000 per field), and the area occupied by one cell was subsequently calculated. In line with the results of the DNA content experiment, the relative cell size was significantly and consistently reduced in *Pkbγ* mutant mice (100±10% versus 80±7%; n=5 per genotype; P<0.05). Taken together, the results show that both cell size and cell number contribute to the reduction in brain size observed in mutant mice, but the relative contribution of cell size reduction plays a more important part.

Susceptibility to glutamate and staurosporine induced cell death

It is established that the PI3K/PKB pathway plays a crucial role in cell survival in the central nervous system (Datta et al., 1999; Dudek et al., 1997; Kim et al., 2002). To investigate the potential role of PKBγ in apoptosis, primary cell cultures were established from $Pkb\gamma^{+/+}$ and $Pkb\gamma^{-/-}$ hippocampal neurons. Immunocytochemistry at day 28 using antibodies against tau (for axons) and Map2C (for dendrites) did not reveal any obvious defects in the differentiation of $Pkb\gamma^{-/-}$ hippocampal neurons (Fig. 7A-D). Consistent with the analysis of the expression pattern of PKB isoforms in various brain regions (Fig. 2D), we found that PKBα, PKBβ and PKBγ, respectively, were expressed in cultured wild-type primary hippocampal neurons. In accordance with the result of Fig. 1D, we did not

Table 1. Cell number in the brain of *Pkbγ* wild-type and mutant mice

	Age			
	Newborns		One month old	
	Pkbγ$^{+/+}$	Pkbγ$^{-/-}$	*Pkbγ*$^{+/+}$	*Pkbγ*$^{-/-}$
Body weight (g)	1.21±0.23	1.31±0.14 (107%)	14.1±2.5	13.0±2.3 (92%)
Brain weight (g)	0.071±0.001	0.069±0.006 (98%)	0.41±0.03	0.32±0.03 (78%)*
Brain/body weight ratio	0.059±0.011	0.054±0.008 (90%)	0.030±0.004	0.025±0.003 (85%)*
DNA/brain (mg)	0.59±0.04	0.56±0.12 (96%)	1.38±0.03	1.29±0.07 (93%)*
DNA/g of tissue (mg)	8.53±1.64	8.11±1.29 (95%)	3.38±0.20	4.04±0.47 (119%)*

The cell number in whole brains of *Pkbγ*$^{+/+}$ and *Pkbγ*$^{-/-}$ mice was determined in newborns and 1-month-old animals. Brain weight, brain/body weight and DNA content (parameter of cell number) per brain were significantly reduced in *Pkbγ*$^{-/-}$ mice at 1 month, but not in newborns. The DNA content per gram of tissue, a parameter of cell density, was significantly increased in *Pkbγ* mutant mice at 1 month, but not in newborns (*P<0.05).

find a compensatory upregulation of PKBα and PKBβ in *Pkbγ*-deficient cells (Fig. 7E). To test the potential role of PKBγ in the survival of hippocampal neurons, cell cultures were challenged with glutamate (15 mM/24 hours) or staurosporine (50 nM/12 hours) after 7 days in culture. Apoptotic cells were detected using the TUNEL assay. In untreated cells cultures, no significant difference in the percentage of apoptotic cells between *Pkbγ*$^{+/+}$ and *Pkbγ*$^{-/-}$ hippocampal neurons was observed (Fig. 7F). After treatment with glutamate or staurosporine, the percentage of apoptotic cells was significantly increased (51% and 24%, respectively, P<0.01) in cultures from *Pkbγ*$^{-/-}$ hippocampal neurons (Fig. 7F).

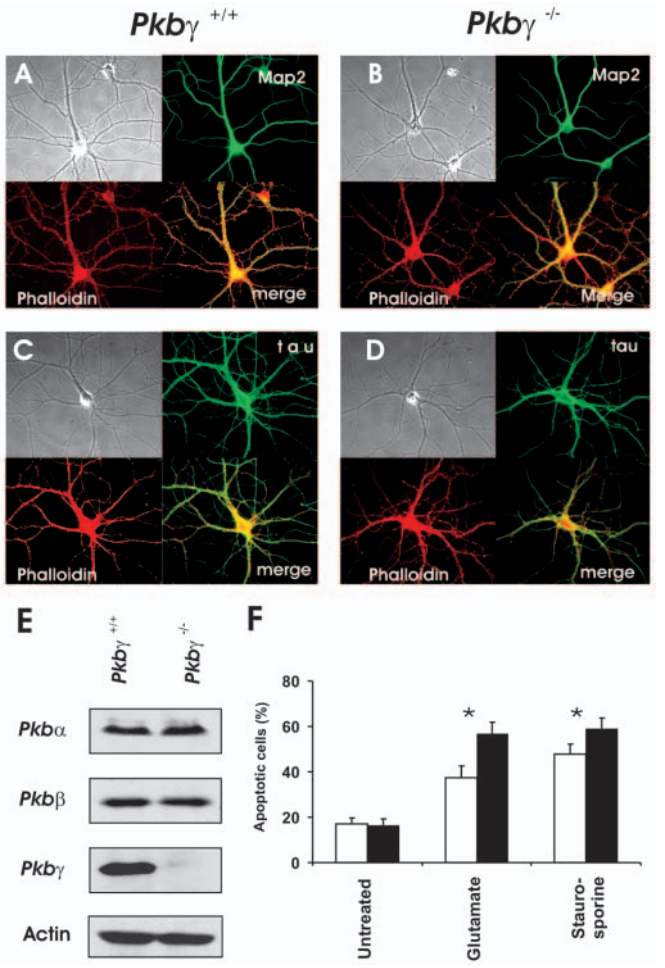

Additionally, we analysed the number of apoptotic cells from adult brains (n=5 per genotype) using TUNEL staining on parasagittal sections. Similar to the results of untreated cultures, we did not find any difference between *Pkbγ*$^{+/+}$ and *Pkbγ*$^{-/-}$ mice (data not shown).

Microarray analysis of *Pkbγ*$^{-/-}$ brains

In the CNS, a considerable amount of cellular and physiological events occur during postnatal development, such as neuronal outgrowth, differentiation, synaptogenesis and maturation. To investigate a potential role of PKBγ in these events, we analyzed gene expression patterns in brains of *Pkbγ*$^{+/+}$ and *Pkbγ*$^{-/-}$ mice at different time points during postnatal brain development, i.e. day 1, day 7 and day 30. RNA was extracted from whole mice brains and microarray analysis was performed on three individual brains per genotype and time point using murine Affymetrix GeneChips™. Changes below 1.5-fold increase were considered insignificant, and differentially regulated genes were subjected to a one-way ANOVA analysis (Table 2). As the brain consists of various heterogeneous cell populations, any change of expression occurring in a specific cell type will be quenched in the pool of whole brain RNA. It is therefore likely that the real expression changes in specific tissues are higher than apparent in this experiment. Among the 17,000 expressed genes, we found 37 genes to be differentially expressed in *Pkbγ*$^{-/-}$ brains versus *Pkbγ*$^{+/+}$ brains. Of these, 16 genes were upregulated and 21 genes downregulated. Among the genes with changed expression are several transcription factors and genes implicated in cell cycle and proliferation. Significantly, one of the most interesting findings is that at P30, several genes involved in synaptic transmission (pre- and postsynaptic), including ionotropic glutamate receptor (NMDAR1), potassium-chloride co-transporter 2 (KCC2), chapsyin 110 [channel-associated protein of synapses, 110 kDa (DLG2)] and

Fig. 7. Increased susceptibility to glutamate and staurosporine induced cell death. (A-D) Primary hippocampal neurons were established from E16.5 embryos and kept in culture for 28 days. Immunocytochemistry was performed using antibodies against dendritic (Map2C) or axonal (tau) proteins. (E) PKBα, PKBβ and PKBγ expression in *Pkbγ* wild-type and mutant hippocampal neurons. (F) Seven-day-old cultures were treated with glutamate (15 mM/24 hours) or with staurosporine (50 nM/12 hours) or were left untreated (*Pkbγ*$^{+/+}$ white bars and *Pkbγ*$^{-/-}$ black bars). Apoptotic cells were identified by TUNEL-assay and at least 200 cells per culture were counted (n=5 cultures per treatment and genotype). *P<0.05. Error bars represent s.d.

Table 2. Microarray analysis of Pkbγ mutant brain

Gene name	GenBank Accession Number	Fold change in expression: Day 1	Day 7	Day 30	Function
RIO kinase 3 (yeast)	AK004748	5.47*	0.59	1.52*	Chromatin condensation
Kinesin family member 5B	BF099632	2.24*	0.72	1.03	Microtubule based transport
Small EDRK-rich factor 1	AA709993	1.69*	1.14	1.06	
CD24a antigen	BB560574	1.57*	1.33	1.12	Cell proliferation
SRp20, splicing factor, arginine/serine-rich 3	AV135383	1.53*	1.32	0.91	mRNA splicing
WNK1 (protein kinase, lysine deficient 1)	BI692255	1.53*	1.00	0.93	Blood pressure
ATPase, Na^+/K^+ transporting, alpha 2 polypeptide	BQ175915	2.23*	2.93*	1.71*	Nt uptake, K^+ uptake
SRY-box containing gene 11	BG072739	0.96	1.82*	0.95	Transcription
Histone 1, H2af	W91024	1.04	1.60*	1.16	Nucleosome structure
Upstream transcription factor 1	AF479773	1.53*	1.55*	1.45	Transcription
Early B-cell factor 3	AK014058	1.13	1.54*	0.76	Transcription
RNA-binding region (RNP1, RRM) containing 2	BB436856	1.40	1.53*	1.46	Transcription
CDC28 protein kinase regulatory subunit 2	NM_025415	1.09	1.53*	1.20	Cell cycle
Procollagen, type III, alpha 1	BG968894	1.08	1.09	2.10*	Cell adhesion
Surfeit gene 4	AI788623	1.20	1.23	1.83*	Membrane protein
$GABA_A$ receptor, subunit alpha 6	NM_008068	1.06	0.57*	0.92	Synaptic transmission
ATPase, Na^+/K^+ transporting, alpha 2 polypeptide	AI845177	0.72	0.66*	0.56*	Nt uptake, K^+ uptake
Kinesin family member 5A	NM_008447	1.04	0.80	0.53*	Microtubule based transport
ADP-ribosylation factor 3	NM_007478	1.05	0.80	0.56*	Protein transport
Contactin associated protein 1	NM_016782	0.96	0.96	0.57*	Cell adhesion
Fibroblast growth factor 1	BM932451	0.86	0.95	0.59*	Angiogenesis, cell proliferation
Growth arrest specific 7	NM_008088	0.89	0.89	0.59*	Neurite outgrowth
Ca^{2+}/calmodulin-dependent protein kinase II alpha	X14836	1.04	0.69	0.59*	Cell cycle, synaptic plasticity
K^+/Cl^- co-transporter (KCC2/SLC12A5)	AF332064	1.13	0.90	0.62*	Synaptic transmission
Glutamate receptor, ionotropic, NMDA1 (ζ1)	NM_008169	0.96	0.80	0.63*	Synaptic transmission
Synaptotagmin 2	AF257304	1.02	1.00	0.64*	Synaptic transmission
Fascin homolog 1, actin bundling protein	BE952057	1.06	0.86	0.64*	Actin binding
Potassium voltage-gated channel, beta member 2	L48983	0.87	0.86	0.64*	Ion transport
Protein tyrosine phosphatase, receptor type, F	NM_011213	0.98	1.03	0.65*	Cell adhesion
Coronin, actin binding protein 1C	AW548837	0.97	0.94	0.65*	Actin assembly
Chapsyn-110 [discs, large homolog 2 (DLG2)]	BB622767	1.29	0.80	0.65*	Synaptic transmission

Genes with altered expression in male $Pkb\gamma^{-/-}$ mice (n=3) compared with $Pkb\gamma^{+/+}$ animals at different time points during postnatal brain development.
*Significant changes (1.5 fold).
Nt, neurotransmitter.

synaptotagmin 2 (SYT2), have significantly reduced expression levels in *Pkbγ* mutant brains. Additionally, Ca^{2+}/calmodulin-dependent protein kinase II α (CaMKII), an enzyme that is essential in synaptic plasticity and memory formation, was found at reduced expression levels (Ninan and Arancio, 2004).

Discussion

Here, we report the phenotypic consequences of the ablation of the *Pkbγ* gene. Mice with targeted disruption of all single PKB isoform were generated and all demonstrated a distinct phenotype. Mice deficient in *Pkbα* are smaller with a 30% reduction in body size and partial neonatal lethality, which might be caused by placental insufficiency (Chen et al., 2001; Cho et al., 2001b; Yang et al., 2003). By contrast, *Pkbβ* knockout mice exhibited a diabetes-like syndrome with hyperglycemia and impaired insulin action in fat, liver and skeletal muscle and, depending on the genetic background, mild growth retardation (Cho et al., 2001; Garofalo et al., 2003). Recently, Peng and colleagues reported the generation of *Pkbαβ* double mutant mice with severe intrauterine growth retardation that die shortly after birth with multiple defects in skin, bone and fat tissue (Peng et al., 2003). However, our results demonstrate that *Pkbγ*-deficient mice display a distinct phenotype without increased mortality, growth retardation and altered glucose homeostasis. Inactivation of the *Pkbγ* gene leads to a considerable reduction in total phosphorylated/activated PKB in the mutant brain without any compensatory increase of the α and β isoforms (assessed at the mRNA and protein levels), suggesting a failure to fully compensate for the loss of PKBγ. This result is consistent with findings in *Pkbα* and *Pkbβ* mutant mice, where no compensatory upregulation of 2 remaining isoforms was found (Cho et al., 2001b; Garofalo et al., 2003; Yang et al., 2003). It has been speculated that the distinct phenotypes of *Pkbα* and *Pkbβ* mutant mice are due to specific and distinct functions of the different PKB isoforms. By contrast, Peng and colleagues proposed that the individual phenotypes are due to loss of the dominant isoform in a specific tissue, which leads to significant reduction of total activated PKB below a crucial level (Peng et al., 2003). For example, the observed diabetes mellitus-like syndrome of $Pkb\beta^{-/-}$ mice could be due to ablation of the dominant isoform in the classical insulin-responsive tissues such as fat, liver and muscle. Moreover, the loss of a second isoform would have an additive effect in reducing the level of total PKB and, therefore, would intensify the phenotype. This possibility is supported by the observation of *Pkbαβ* double knockout mice (Peng et al., 2003) and our unpublished data on the *Pkbαγ* double mutant mice (Z.-Z.Y. and B.A.H., unpublished). Ablation of a single copy of *Pkbγ* in *Pkbα*-deficient mice ($Pkb\alpha^{-/-}$ $Pkb\gamma^{+/-}$) led to a higher perinatal mortality compared with *Pkbα* single mutant

mice and the ablation of both *Pkbγ* alleles in *Pkbα*$^{-/-}$ mice led to more pronounced dwarfism and intra-uterine death of all *Pkbα*$^{-/-}$*Pkbγ*$^{-/-}$ double mutant animals. However, it cannot be confirmed yet whether the observed phenotypes are due to a combination of reduced level of activated PKB and the loss of isoform-specific functions.

The IGF1/PI3K/PKB pathway plays a crucial role in mammalian brain development and function (D'Ercole et al., 2002; Rodgers and Theibert, 2002). Besides the severe growth retardation, adult mice with IGF1 deficiency exhibit a significant (38%) brain weight reduction (Beck et al., 1995). Similar to the *Pkbγ* mutant mice, all brain parts of the *Igf1*$^{-/-}$ mice were affected but the general anatomical organisation was normal. Furthermore, ablation of IGF1 resulted in a cell type-dependent loss of neurons, as well as a reduced total number of oligodendrocytes and hypomyelination (Beck et al., 1995; Ye et al., 2002). In addition, targeted deletion of IRS2 in mice also produced a pronounced brain growth deficiency, but in contrast to *Pkbγ* mutants, the reduction was already apparent during embryonic (E15.5) development (Schubert et al., 2003). By contrast, an increased brain mass was observed in mice overexpressing IGF1 (Mathews et al., 1988; Ye et al., 1995). Moreover, mice with brain-specific deletion of PTEN, a negative regulator of the PI3K/PKB pathway, exhibited an enlarged brain with seizures and ataxia resembling Lhermitte-Duclos disease (Backman et al., 2001; Kwon et al., 2001). Less is known about the consequences of *Pkbα* and *Pkbβ* inactivation for mouse brain development. Compared with *Pkbγ*$^{-/-}$ mice, adult *Pkbα* and *Pkbβ* mutant mice showed only a slight decrease in brain weight (Garofalo et al., 2003; Yang et al., 2004). In both *Pkbα* and *Pkbβ* mutant mice, no changes in the gross brain morphology were reported.

However, inactivation of the *Pkbγ* gene resulted in a significant reduction of brain weight and size. Interestingly, *Pkbγ* deficiency did not affect the general anatomical organization of the brain. In vivo 3D MRI and histological analysis excluded the absence of a specific brain region as the main cause of the weight reduction, consistent with the result of the broad expression profile among brain regions. More specifically, the proportionally reduced ventricular system rules out major disturbances in production, circulation and absorption of cerebrospinal fluid as a cause of reduced cell size/number in *Pkbγ*$^{-/-}$ mice. The biological relevance of the MRI signal alterations in white matter such as the corpus callosum requires further investigation. Nevertheless, it should be noted that the in vivo MRI results are consistent with a pronounced, but not complete, deficit in myelin deposition (Boretius, 2003), which is also strongly supported by the histological findings for myelin staining. In agreement with our results, mice deficient in IGF1, a potent activator of PKBγ, the myelin-rich white matter regions, including corpus callosum and anterior commissure, were overproportionally reduced by about 70% (Beck et al., 1995). By contrast, mice overexpressing IGF1 display an increased brain weight and the corpus callosum of the *Igf1* transgenic mice was increased in excess of proportionality (Carson et al., 1993).

The PI3-K/PKB signalling pathway plays a crucial role in the determination of cell size (Scanga et al., 2000; Shioi et al., 2002; Tuttle et al., 2001; Verdu et al., 1999). Results from transgenic mice overexpressing PKB show larger cardiac myocytes and thymocytes, or hypertrophy and hyperplasia in the pancreas (Kovacic et al., 2003; Mangi et al., 2003). An increase in neuronal soma size was observed in mice with brain-specific deletion of PTEN (Backman et al., 2001; Kwon et al., 2001). By contrast, the size of skeletal muscle cells in *Pkbαβ* double mutant mice was dramatically reduced (Peng et al., 2003). Our results show that both cell number and cell size are affected, but that reduced cell size contributes more than the reduced cell number. Additionally, it has been shown that the mTOR signalling pathway is also involved in the determination of cell size (Montagne et al., 1999; Oldham et al., 2000; Zhang et al., 2000). PKB modulates mTOR activity by phosphorylating TSC2, with a subsequent disruption of the TSC1-TSC2 interaction (Inoki et al., 2002; Potter et al., 2003).

Recent publications have linked PI3-K/PKB with synaptic plasticity and memory (Dash et al., 2004; Kelly and Lynch, 2000; Lin et al., 2001; Robles et al., 2003; Sanna et al., 2002). Wang and colleagues demonstrated that the A-type γ-aminobutyric acid receptors ($GABA_AR$), which mediate fast inhibitory synaptic transmission, is phosphorylated by PKB (Wang et al., 2003). Phosphorylation of $GABA_AR$ leads to an increased number of receptor on the cell membrane and an increased synaptic transmission. Additionally, Lin et al. established a role of the PI3-K/PKB pathway in fear conditioning in the amygdala (Lin et al., 2001). As we found several genes involved in neuronal circuit activity in our microarray experiment, future behavioural and electrophysiological studies of *Pkbγ* mutant brains will elucidate the specific role of PKBγ in synaptic transmission, learning and memory.

In summary, we have demonstrated that *Pkbγ*-deficient mice display a phenotype distinct from *Pkbα* and *Pkbβ* mutant mice. Our results provide novel insights into the physiological function of PKBγ and suggest a crucial role in postnatal brain development of mammals. Identification of PKBγ specific substrates involved in postnatal brain development is now of critical importance.

The authors thank Michael Leitges (Max-Planck-Institut für Experimentelle Endokrinologie, Hannover, Germany) for providing the IRES/*lacZ*/Neo targeting cassette. From the FMI we acknowledge J. F. Spetz and P. Kopp for ES cell culture and generation of chimera, D. Hynx for animal care, H. Brinkhaus for help with neuronal cell culture, E. Oakeley and H. Angliker for microarray analysis, M. Sticker for helpful advice in histology and R. Portmann for advice on Western blot quantification. O.T. is supported by the Novartis Stiftung für Medizinisch-Biologische Forschung, Z.Z.Y. is funded in part by a grant from Bundesamt für Bildung und Wissenschaft (BBW #98.0176) and B.D. by the Swiss Cancer League (KFS 1167-09-2001 and KFS 01002-02-2000). The Friedrich Miescher Institute for Biomedical Research is funded by the Novartis Research Foundation.

References

Alessi, D. R., Andjelkovic, M., Caudwell, B., Cron, P., Morrice, N., Cohen, P. and Hemmings, B. A. (1996). Mechanism of activation of protein kinase B by insulin and IGF-1. *EMBO J.* **15**, 6541-6551.

Alessi, D. R., Deak, M., Casamayor, A., Caudwell, F. B., Morrice, N., Norman, D. G., Gaffney, P., Reese, C. B., MacDougall, C. N., Harbison, D. et al. (1997). 3-Phosphoinositide-dependent protein kinase-1 (PDK1): structural and functional homology with the Drosophila DSTPK61 kinase. *Curr. Biol.* **7**, 776-789.

Altomare, D. A., Lyons, G. E., Mitsuuchi, Y., Cheng, J. Q. and Testa, J. R. (1998). Akt2 mRNA is highly expressed in embryonic brown fat and the AKT2 kinase is activated by insulin. *Oncogene* **16**, 2407-2411.

Backman, S. A., Stambolic, V., Suzuki, A., Haight, J., Elia, A., Pretorius, J., Tsao, M. S., Shannon, P., Bolon, B., Ivy, G. O. et al. (2001). Deletion of Pten in mouse brain causes seizures, ataxia and defects in soma size resembling Lhermitte-Duclos disease. *Nat. Genet.* **29**, 396-403.

Beck, K. D., Powell-Braxton, L., Widmer, H. R., Valverde, J. and Hefti, F. (1995). Igf1 gene disruption results in reduced brain size, CNS hypomyelination, and loss of hippocampal granule and striatal parvalbumin-containing neurons. *Neuron* **14**, 717-730.

Boretius, S., Merkler, D., Awn, N., Stadelmann, C., Natt, O., Watanabe, T., Michaelis, T., Frahms, J. and Brück, W. (2003). How do T1-, T2- and MT-weighted images reflect de- and remyelination? In vivo MRI of mice treated with the demyelinating neurotoxic agent cuprizone. *Proc. Intl. Soc. Magn. Reson. Med.* **12**, 280.

Brazil, D. P. and Hemmings, B. A. (2001). Ten years of protein kinase B signalling: a hard Akt to follow. *Trends Biochem. Sci.* **26**, 657-664.

Brodbeck, D., Cron, P. and Hemmings, B. A. (1999). A human protein kinase Bgamma with regulatory phosphorylation sites in the activation loop and in the C-terminal hydrophobic domain. *J. Biol. Chem.* **274**, 9133-9136.

Burgering, B. M. and Coffer, P. J. (1995). Protein kinase B (c-Akt) in phosphatidylinositol-3-OH kinase signal transduction. *Nature* **376**, 599-602.

Carson, M. J., Behringer, R. R., Brinster, R. L. and McMorris, F. A. (1993). Insulin-like growth factor I increases brain growth and central nervous system myelination in transgenic mice. *Neuron* **10**, 729-740.

Chan, T. O., Rittenhouse, S. E. and Tsichlis, P. N. (1999). AKT/PKB and other D3 phosphoinositide-regulated kinases: kinase activation by phosphoinositide-dependent phosphorylation. *Annu. Rev. Biochem.* **68**, 965-1014.

Chen, W. S., Xu, P. Z., Gottlob, K., Chen, M. L., Sokol, K., Shiyanova, T., Roninson, I., Weng, W., Suzuki, R., Tobe, K. et al. (2001). Growth retardation and increased apoptosis in mice with homozygous disruption of the Akt1 gene. *Genes Dev.* **15**, 2203-2208.

Cheng, C. M., Joncas, G., Reinhardt, R. R., Farrer, R., Quarles, R., Janssen, J., McDonald, M. P., Crawley, J. N., Powell-Braxton, L. and Bondy, C. A. (1998). Biochemical and morphometric analyses show that myelination in the insulin-like growth factor 1 null brain is proportionate to its neuronal composition. *J. Neurosci.* **18**, 5673-5681.

Cheng, J. Q., Godwin, A. K., Bellacosa, A., Taguchi, T., Franke, T. F., Hamilton, T. C., Tsichlis, P. N. and Testa, J. R. (1992). AKT2, a putative oncogene encoding a member of a subfamily of protein-serine/threonine kinases, is amplified in human ovarian carcinomas. *Proc. Natl. Acad. Sci. USA* **89**, 9267-9271.

Cho, H., Mu, J., Kim, J. K., Thorvaldsen, J. L., Chu, Q., Crenshaw, E. B., 3rd, Kaestner, K. H., Bartolomei, M. S., Shulman, G. I. and Birnbaum, M. J. (2001a). Insulin resistance and a diabetes mellitus-like syndrome in mice lacking the protein kinase Akt2 (PKB beta). *Science* **292**, 1728-1731.

Cho, H., Thorvaldsen, J. L., Chu, Q., Feng, F. and Birnbaum, M. J. (2001b). Akt1/PKBalpha is required for normal growth but dispensable for maintenance of glucose homeostasis in mice. *J. Biol. Chem.* **276**, 38349-38352.

Cross, D. A., Alessi, D. R., Cohen, P., Andjelkovich, M. and Hemmings, B. A. (1995). Inhibition of glycogen synthase kinase-3 by insulin mediated by protein kinase B. *Nature* **378**, 785-789.

Dash, P. K., Mach, S. A., Moody, M. R. and Moore, A. N. (2004). Performance in long-term memory tasks is augmented by a phosphorylated growth factor receptor fragment. *J. Neurosci. Res.* **77**, 205-216.

Datta, S. R., Brunet, A. and Greenberg, M. E. (1999). Cellular survival: a play in three Akts. *Genes Dev.* **13**, 2905-2927.

D'Ercole, A. J., Ye, P. and O'Kusky, J. R. (2002). Mutant mouse models of insulin-like growth factor actions in the central nervous system. *Neuropeptides* **36**, 209-220.

Dudek, H., Datta, S. R., Franke, T. F., Birnbaum, M. J., Yao, R., Cooper, G. M., Segal, R. A., Kaplan, D. R. and Greenberg, M. E. (1997). Regulation of neuronal survival by the serine-threonine protein kinase Akt. *Science* **275**, 661-665.

Franke, T. F., Yang, S. I., Chan, T. O., Datta, K., Kazlauskas, A., Morrison, D. K., Kaplan, D. R. and Tsichlis, P. N. (1995). The protein kinase encoded by the Akt proto-oncogene is a target of the PDGF-activated phosphatidylinositol 3-kinase. *Cell* **81**, 727-736.

Garofalo, R. S., Orena, S. J., Rafidi, K., Torchia, A. J., Stock, J. L., Hildebrandt, A. L., Coskran, T., Black, S. C., Brees, D. J., Wicks, J. R. et al. (2003). Severe diabetes, age-dependent loss of adipose tissue, and mild growth deficiency in mice lacking Akt2/PKB beta. *J. Clin. Invest.* **112**, 197-208.

Hanada, M., Feng, J. and Hemmings, B. A. (2004). Structure, regulation and function of PKB/AKT – a major therapeutic target. *Biochim. Biophys. Acta.* **1697**, 3-16.

Inoki, K., Li, Y., Zhu, T., Wu, J. and Guan, K. L. (2002). TSC2 is phosphorylated and inhibited by Akt and suppresses mTOR signalling. *Nat. Cell Biol.* **4**, 648-657.

Irizarry, R. A., Bolstad, B. M., Collin, F., Cope, L. M., Hobbs, B. and Speed, T. P. (2003). Summaries of Affymetrix GeneChip probe level data. *Nucleic Acids Res.* **31**, e15.

Jones, P. F., Jakubowicz, T. and Hemmings, B. A. (1991a). Molecular cloning of a second form of rac protein kinase. *Cell Regul.* **2**, 1001-1009.

Jones, P. F., Jakubowicz, T., Pitossi, F. J., Maurer, F. and Hemmings, B. A. (1991b). Molecular cloning and identification of a serine/threonine protein kinase of the second-messenger subfamily. *Proc. Natl. Acad. Sci. USA* **88**, 4171-4175.

Kandel, E. S. and Hay, N. (1999). The regulation and activities of the multifunctional serine/threonine kinase Akt/PKB. *Exp. Cell Res.* **253**, 210-229.

Kelly, A. and Lynch, M. A. (2000). Long-term potentiation in dentate gyrus of the rat is inhibited by the phosphoinositide 3-kinase inhibitor, wortmannin. *Neuropharmacology* **39**, 643-651.

Kim, A. H., Yano, H., Cho, H., Meyer, D., Monks, B., Margolis, B., Birnbaum, M. J. and Chao, M. V. (2002). Akt1 regulates a JNK scaffold during excitotoxic apoptosis. *Neuron* **35**, 697-709.

Kooy, R. F., Verhoye, M., Lemmon, V. and Van Der Linden, A. (2001). Brain studies of mouse models for neurogenetic disorders using in vivo magnetic resonance imaging (MRI). *Eur. J. Hum. Genet.* **9**, 153-159.

Kovacic, S., Soltys, C. L., Barr, A. J., Shiojima, I., Walsh, K. and Dyck, J. R. (2003). Akt activity negatively regulates phosphorylation of AMP-activated protein kinase in the heart. *J. Biol. Chem.* **278**, 39422-39427.

Kwon, C. H., Zhu, X., Zhang, J., Knoop, L. L., Tharp, R., Smeyne, R. J., Eberhart, C. G., Burger, P. C. and Baker, S. J. (2001). Pten regulates neuronal soma size: a mouse model of Lhermitte-Duclos disease. *Nat. Genet.* **29**, 404-411.

Labarca, C. and Paigen, K. (1980). A simple, rapid, and sensitive DNA assay procedure. *Anal. Biochem.* **102**, 344-352.

Lin, C. H., Yeh, S. H., Lu, K. T., Leu, T. H., Chang, W. C. and Gean, P. W. (2001). A role for the PI-3 kinase signaling pathway in fear conditioning and synaptic plasticity in the amygdala. *Neuron* **31**, 841-851.

Mangi, A. A., Noiseux, N., Kong, D., He, H., Rezvani, M., Ingwall, J. S. and Dzau, V. J. (2003). Mesenchymal stem cells modified with Akt prevent remodeling and restore performance of infarcted hearts. *Nat. Med.* **9**, 1195-1201.

Masure, S., Haefner, B., Wesselink, J. J., Hoefnagel, E., Mortier, E., Verhasselt, P., Tuytelaars, A., Gordon, R. and Richardson, A. (1999). Molecular cloning, expression and characterization of the human serine/threonine kinase Akt-3. *Eur. J. Biochem.* **265**, 353-360.

Mathews, L. S., Hammer, R. E., Behringer, R. R., D'Ercole, A. J., Bell, G. I., Brinster, R. L. and Palmiter, R. D. (1988). Growth enhancement of transgenic mice expressing human insulin-like growth factor I. *Endocrinology* **123**, 2827-2833.

Meier, R., Alessi, D. R., Cron, P., Andjelkovic, M. and Hemmings, B. A. (1997). Mitogenic activation, phosphorylation, and nuclear translocation of protein kinase Bbeta. *J. Biol. Chem.* **272**, 30491-30497.

Montagne, J., Stewart, M. J., Stocker, H., Hafen, E., Kozma, S. C. and Thomas, G. (1999). Drosophila S6 kinase: a regulator of cell size. *Science* **285**, 2126-2129.

Nakatani, K., Sakaue, H., Thompson, D. A., Weigel, R. J. and Roth, R. A. (1999). Identification of a human Akt3 (protein kinase B gamma) which contains the regulatory serine phosphorylation site. *Biochem. Biophys. Res. Commun.* **257**, 906-910.

Natt, O., Watanabe, T., Boretius, S., Radulovic, J., Frahm, J. and Michaelis, T. (2002). High-resolution 3D MRI of mouse brain reveals small cerebral structures in vivo. *J. Neurosci. Methods* **120**, 203-209.

Nicholson, K. M. and Anderson, N. G. (2002). The protein kinase B/Akt signalling pathway in human malignancy. *Cell Signal* **14**, 381-395.

Ninan, I. and Arancio, O. (2004). Presynaptic CaMKII is necessary for synaptic plasticity in cultured hippocampal neurons. *Neuron* **42**, 129-141.

Oldham, S., Montagne, J., Radimerski, T., Thomas, G. and Hafen, E. (2000). Genetic and biochemical characterization of dTOR, the Drosophila homolog of the target of rapamycin. *Genes Dev.* **14**, 2689-2694.

Peng, X. D., Xu, P. Z., Chen, M. L., Hahn-Windgassen, A., Skeen, J., Jacobs, J., Sundararajan, D., Chen, W. S., Crawford, S. E., Coleman, K. G. et al. (2003). Dwarfism, impaired skin development, skeletal muscle

atrophy, delayed bone development, and impeded adipogenesis in mice lacking Akt1 and Akt2. *Genes Dev.* **17**, 1352-1365.

Potter, C. J., Pedraza, L. G., Huang, H. and Xu, T. (2003). The tuberous sclerosis complex (TSC) pathway and mechanism of size control. *Biochem. Soc. Trans.* **31**, 584-586.

Powell-Braxton, L., Hollingshead, P., Warburton, C., Dowd, M., Pitts-Meek, S., Dalton, D., Gillett, N. and Stewart, T. A. (1993). IGF-I is required for normal embryonic growth in mice. *Genes Dev.* **7**, 2609-2617.

Robles, Y., Vivas-Mejia, P. E., Ortiz-Zuazaga, H. G., Felix, J., Ramos, X. and Pena de Ortiz, S. (2003). Hippocampal gene expression profiling in spatial discrimination learning. *Neurobiol. Learn Mem.* **80**, 80-95.

Rodgers, E. E. and Theibert, A. B. (2002). Functions of PI 3-kinase in development of the nervous system. *Int. J. Dev. Neurosci.* **20**, 187-197.

Sanna, P. P., Cammalleri, M., Berton, F., Simpson, C., Lutjens, R., Bloom, F. E. and Francesconi, W. (2002). Phosphatidylinositol 3-kinase is required for the expression but not for the induction or the maintenance of long-term potentiation in the hippocampal CA1 region. *J. Neurosci.* **22**, 3359-3365.

Scanga, S. E., Ruel, L., Binari, R. C., Snow, B., Stambolic, V., Bouchard, D., Peters, M., Calvieri, B., Mak, T. W., Woodgett, J. R. et al. (2000). The conserved PI3′K/PTEN/Akt signaling pathway regulates both cell size and survival in Drosophila. *Oncogene* **19**, 3971-3977.

Scheid, M. P. and Woodgett, J. R. (2001). PKB/AKT: functional insights from genetic models. *Nat. Rev. Mol. Cell Biol.* **2**, 760-768.

Schubert, M., Brazil, D. P., Burks, D. J., Kushner, J. A., Ye, J., Flint, C. L., Farhang-Fallah, J., Dikkes, P., Warot, X. M., Rio, C. et al. (2003). Insulin receptor substrate-2 deficiency impairs brain growth and promotes tau phosphorylation. *J. Neurosci.* **23**, 7084-7092.

Shioi, T., McMullen, J. R., Kang, P. M., Douglas, P. S., Obata, T., Franke, T. F., Cantley, L. C. and Izumo, S. (2002). Akt/protein kinase B promotes organ growth in transgenic mice. *Mol. Cell Biol.* **22**, 2799-2809.

Stokoe, D., Stephens, L. R., Copeland, T., Gaffney, P. R., Reese, C. B., Painter, G. F., Holmes, A. B., McCormick, F. and Hawkins, P. T. (1997). Dual role of phosphatidylinositol-3,4,5-trisphosphate in the activation of protein kinase B. *Science* **277**, 567-570.

Tuttle, R. L., Gill, N. S., Pugh, W., Lee, J. P., Koeberlein, B., Furth, E. E., Polonsky, K. S., Naji, A. and Birnbaum, M. J. (2001). Regulation of pancreatic beta-cell growth and survival by the serine/threonine protein kinase Akt1/PKBalpha. *Nat. Med.* **7**, 1133-1137.

Verdu, J., Buratovich, M. A., Wilder, E. L. and Birnbaum, M. J. (1999). Cell-autonomous regulation of cell and organ growth in Drosophila by Akt/PKB. *Nat. Cell Biol.* **1**, 500-506.

Wang, Q., Liu, L., Pei, L., Ju, W., Ahmadian, G., Lu, J., Wang, Y., Liu, F. and Wang, Y. T. (2003). Control of synaptic strength, a novel function of Akt. *Neuron* **38**, 915-928.

Yang, J., Cron, P., Good, V. M., Thompson, V., Hemmings, B. A. and Barford, D. (2002a). Crystal structure of an activated Akt/Protein Kinase B ternary complex with GSK3-peptide and AMP-PNP. *Nat. Struct. Biol.* **9**, 940-944.

Yang, J., Cron, P., Thompson, V., Good, V. M., Hess, D., Hemmings, B. A. and Barford, D. (2002b). Molecular mechanism for the regulation of protein kinase B/Akt by hydrophobic motif phosphorylation. *Mol. Cell* **9**, 1227-1240.

Yang, Z. Z., Tschopp, O., Hemmings-Mieszczak, M., Feng, J., Brodbeck, D., Perentes, E. and Hemmings, B. A. (2003). Protein kinase B alpha/Akt1 regulates placental development and fetal growth. *J. Biol. Chem.* **278**, 32124-32131.

Yang, Z. Z., Tschopp, O., Baudry, A., Dummler, B., Hynx, D. and Hemmings, B. A. (2004). Physiological functions of protein kinase B/Akt. *Biochem. Soc. Trans.* **32**, 350-354.

Ye, P., Carson, J. and D'Ercole, A. J. (1995). In vivo actions of insulin-like growth factor-I (IGF-I) on brain myelination: studies of IGF-I and IGF binding protein-1 (IGFBP-1) transgenic mice. *J. Neurosci.* **15**, 7344-7356.

Ye, P., Li, L., Richards, R. G., DiAugustine, R. P. and D'Ercole, A. J. (2002). Myelination is altered in insulin-like growth factor-I null mutant mice. *J. Neurosci.* **22**, 6041-6051.

Zamenhof, S. and van Marthens, E. (1976). Neonatal and adult brain parameters in mice selected for adult brain weight. *Dev. Psychobiol.* **9**, 587-593.

Zhang, H., Stallock, J. P., Ng, J. C., Reinhard, C. and Neufeld, T. P. (2000). Regulation of cellular growth by the Drosophila target of rapamycin dTOR. *Genes Dev.* **14**, 2712-2724.

II. RESULTS

Part 3:

Dosage-dependent effects of Akt1/protein kinase Balpha (PKBalpha) and Akt3/PKBgamma on thymus, skin, and cardiovascular and nervous system development in mice.

Yang ZZ, Tschopp O, Di-Poi N, Bruder E, Baudry A, Dummler B, Wahli W, Hemmings BA.
Mol Cell Biol 2005, 25:10407-10418

MOLECULAR AND CELLULAR BIOLOGY, Dec. 2005, p. 10407–10418 Vol. 25, No. 23
0270-7306/05/$08.00+0 doi:10.1128/MCB.25.23.10407–10418.2005

Dosage-Dependent Effects of Akt1/Protein Kinase Bα (PKBα) and Akt3/PKBγ on Thymus, Skin, and Cardiovascular and Nervous System Development in Mice

Zhong-Zhou Yang,[1] Oliver Tschopp,[1] Nicolas Di-Poï,[2] Elisabeth Bruder,[3] Anne Baudry,[1] Bettina Dümmler,[1] Walter Wahli,[2] and Brian A. Hemmings[1]*

Friedrich Miescher Institute for Biomedical Research, Maulbeerstrasse 66, Basel CH-4058,[1] Center for Integrative Genomics, Biology Building, University of Lausanne, Lausanne CH-1015,[2] and Institute of Pathology, University of Basel, Schönbeinstrasse 40, Basel CH-4031,[3] Switzerland

Received 28 July 2005/Returned for modification 28 August 2005/Accepted 14 September 2005

Akt/protein kinase B (PKB) plays a critical role in the regulation of metabolism, transcription, cell migration, cell cycle progression, and cell survival. The existence of viable knockout mice for each of the three isoforms suggests functional redundancy. We generated mice with combined mutant alleles of *Akt1* and *Akt3* to study their effects on mouse development. Here we show that *Akt1*$^{-/-}$ *Akt3*$^{+/-}$ mice display multiple defects in the thymus, heart, and skin and die within several days after birth, while *Akt1*$^{+/-}$ *Akt3*$^{-/-}$ mice survive normally. Double knockout (*Akt1*$^{-/-}$ *Akt3*$^{-/-}$) causes embryonic lethality at around embryonic days 11 and 12, with more severe developmental defects in the cardiovascular and nervous systems. Increased apoptosis was found in the developing brain of double mutant embryos. These data indicate that the *Akt1* gene is more essential than *Akt3* for embryonic development and survival but that both are required for embryo development. Our results indicate isoform-specific and dosage-dependent effects of *Akt* on animal survival and development.

In mammals, Akt1, Akt2, and Akt3 (also called protein kinase Bα [PKBα], PKBβ, and PKBγ) proteins have similar domain structures and can be activated by numerous growth factors in a phosphatidylinositol 3-kinase-dependent manner (1, 3, 4, 15, 23). Once activated, Akt phosphorylates and controls the activities of a diverse group of substrates involved in many cellular and physiological processes, such as cell survival, cell cycle progression, cell growth, metabolism, and angiogenesis (3, 10, 17, 23).

Although many proteins have been identified as Akt substrates, the challenge that remains is to show that they actually have an important impact on physiological processes in organisms. Recently, targeted deletion of specific isoforms of Akt in mice has proved to be a powerful tool for elucidating the physiological roles of Akt proteins (5, 7, 8, 13, 16, 25, 27, 28). Characterization of such knockout mice has yielded intriguing and surprising results. We and others found that ~40% of *Akt1* knockout mice die at a neonatal stage with growth retardation, but the other ~60% of *Akt1* knockout mice survive apparently normally. This suggests that the other two remaining *Akt* isoforms can, in part, compensate for the loss of one *Akt*. Knockout of each single isoform gives rise to a distinct phenotype. In general, *Akt1* null mice are growth retarded, which may result from placental insufficiency, while *Akt2*-deficient mice suffer from a type 2 diabetes-like syndrome and *Akt3* null mice show impaired brain development (5, 7, 8, 13, 16, 25, 27, 28). These observations indicate that the three Akt isoforms have different nonredundant physiological functions. The relatively normal development and distinct physiological functions exhibited by single knockouts may be explained by differences in the tissue distribution and expression levels of these isoforms. We found that Akt1 is the major isoform in placenta and that placenta lacking this protein cannot form a proper vascular labyrinth; this may restrict nutrient supply to the fetus and impair growth (28). Similarly, in the major insulin-responsive tissues of fat, skeletal muscle, and liver, Akt2 is the predominant isoform (2, 7, 28). In the case of Akt3, which shows a more restricted level of expression with the brain containing the highest levels and has lower levels of expression in other tissues, ablation of this isoform affects postnatal brain development (13, 25).

We predicted that simultaneous inactivation of two *Akt* isoforms in mice would severely affect development and survival. To test this hypothesis, we crossed *Akt1* with *Akt3* knockout mice to generate compound (combined mutation of four alleles of *Akt1* and *Akt3*) and double knockout (DKO) mice. Our results show that the *Akt1* gene is more essential than the *Akt3* gene for survival and that both proteins are required for normal embryo development. Our studies demonstrate isoform-specific and dosage-dependent effects of *Akt* genes on animal survival and development.

MATERIALS AND METHODS

Preparation of murine embryonic fibroblasts (MEFs) and Western analysis. MEFs were prepared from embryonic day 10.5 (E10.5) to E13.5 embryos as previously described (14). Western analysis and the antibody that recognizes both mouse Akt1 and Akt3 have been described previously (25, 28). The isoform-specific antibodies for mouse Akt1, Akt2, and Akt3 have been described already (25). Antibodies for pSer473 were purchased from Cell Signaling Technology. Actin antibody was purchased from Neomarkers.

Mice. Mice were housed in accordance with the Swiss Animal Protection Ordinance in groups with 12-h dark-light cycles and with free access to food and

* Corresponding author. Mailing address: Friedrich Miescher Institute for Biomedical Research, P.O. Box 2543, Maulbeerstrasse 66, Basel CH-4002, Switzerland. Phone: 41-61-697-4872. Fax: 41-61-697-3976. E-mail: brian.hemmings@fmi.ch.

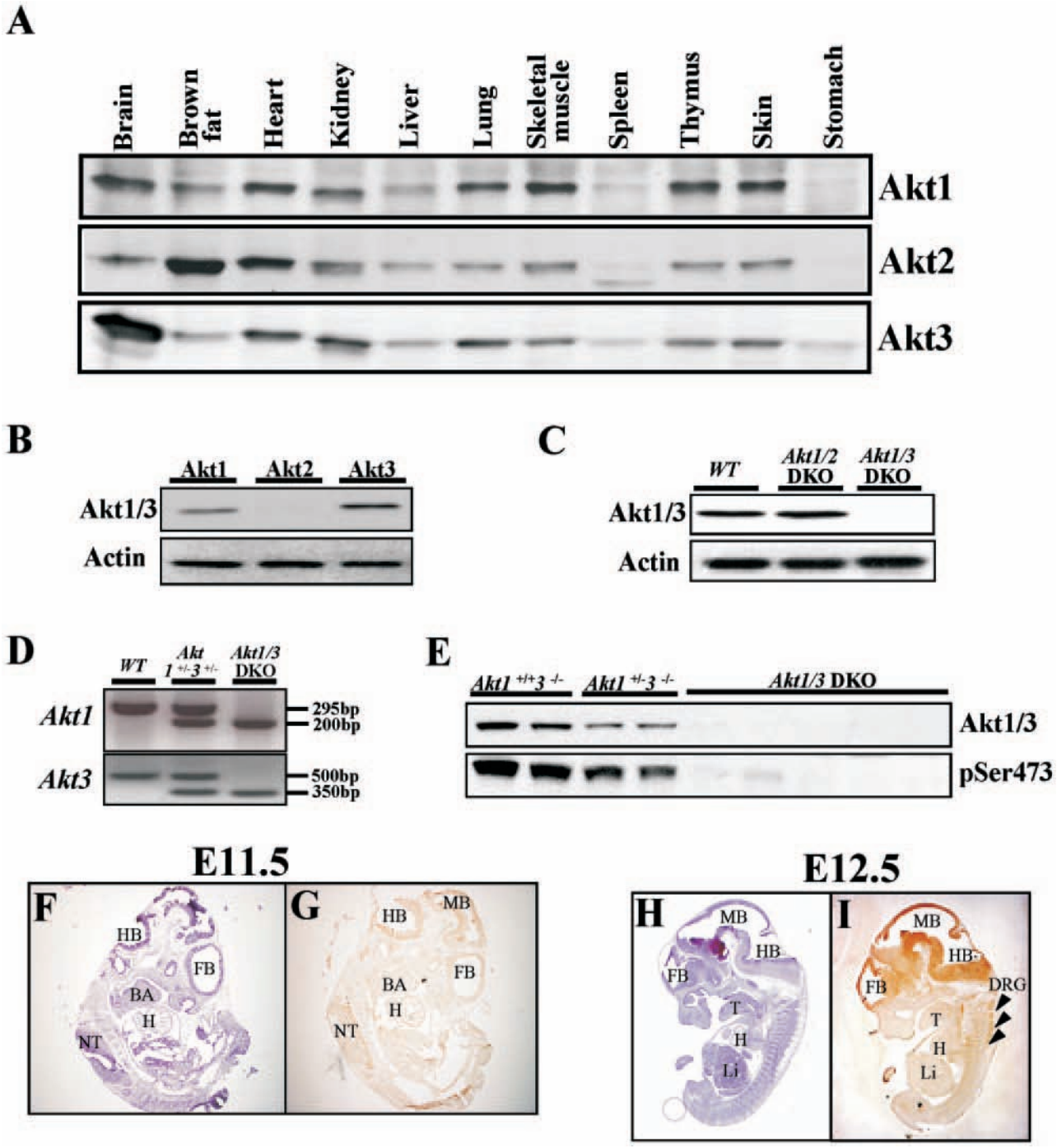

FIG. 1. Expression Akt isoforms in neonates, Akt1/Akt3 localization in E11.5 to E12.5 embryos, generation of *Akt1*/*Akt3* compound, and double knockout mice. (A) Expression patterns of Akt isoforms in neonates. Four wild-type mice from two litters were sacrificed, and their tissues were pooled for lysate preparation. Forty micrograms of total protein was used for Western analysis with the indicated isoform-specific antibodies. (B) Akt1/Akt3 antibody specificity. Mouse Akt1, Akt2, and Akt3 cDNAs cloned in pCMV5 were expressed in HEK293 cells, and cell lysates were prepared for Western analysis. Immunoblot analysis was carried out with an affinity-purified Akt1/Akt3 antibody that recognizes Akt1 and Akt3. Actin levels were determined to control for equal loading. (C) Absence of Akt1 and Akt3 proteins in DKO mouse embryonic fibroblasts (MEFs). MEFs were prepared from wild-type, *Akt1*/*Akt3* DKO, or *Akt2*/*Akt3* DKO embryos, and cell lysates derived from these cells were used for Western analysis using the antibody as described in the legend to panel B with actin as control. (D) PCR genotyping for *Akt1* and *Akt3* loci. WT, wild type; DKO, double knockout. (E) Absence of Akt1 and Akt3 proteins in DKO mouse tissue (placenta). Total phospho-Akt is substantially decreased. (F to I) HE and immunohistochemical staining of E11.5 and E12.5 embryos with the Akt1/Akt3 antibody. Panels F and G are for the E11.5 embryo and H and I are for the E12.5 embryo; F and H show hematoxylin and eosin staining, and G and I show immunohistochemical staining. Akt1 or Akt3 (or both) is expressed in both the central and peripheral nervous systems of brain, neural tube, and heart. Arrowheads indicate various ganglia. Abbreviations: HB, hindbrain; MB, midbrain; FB, forebrain; BA, branchial arch; H, heart; NT, neural tube; CG, cranial ganglia; DRG, dorsal root ganglia; Li, liver; T, tongue.

TABLE 1. Progeny of *Akt1*$^{+/-}$ *Akt3*$^{+/-}$ matings[a]

Genotype	$1^{+/+}$ $3^{+/+}$	$1^{+/+}$ $3^{+/-}$	$1^{+/+}$ $3^{-/-}$	$1^{+/-}$ $3^{+/+}$	$1^{+/-}$ $3^{+/-}$	$1^{+/-}$ $3^{-/-}$	$1^{-/-}$ $3^{+/+}$	$1^{-/-}$ $3^{+/-}$	$1^{-/-}$ $3^{-/-}$
No. of animals	27	34	20	31	74	37	11	3	0
%	11.3	14.3	8.4	13	31	15.5	4.6	1.3	0
Theoretical %	6.3	12.5	6.3	12.5	25	12.5	6.3	12.5	6.3

[a] Total number analyzed, 237.

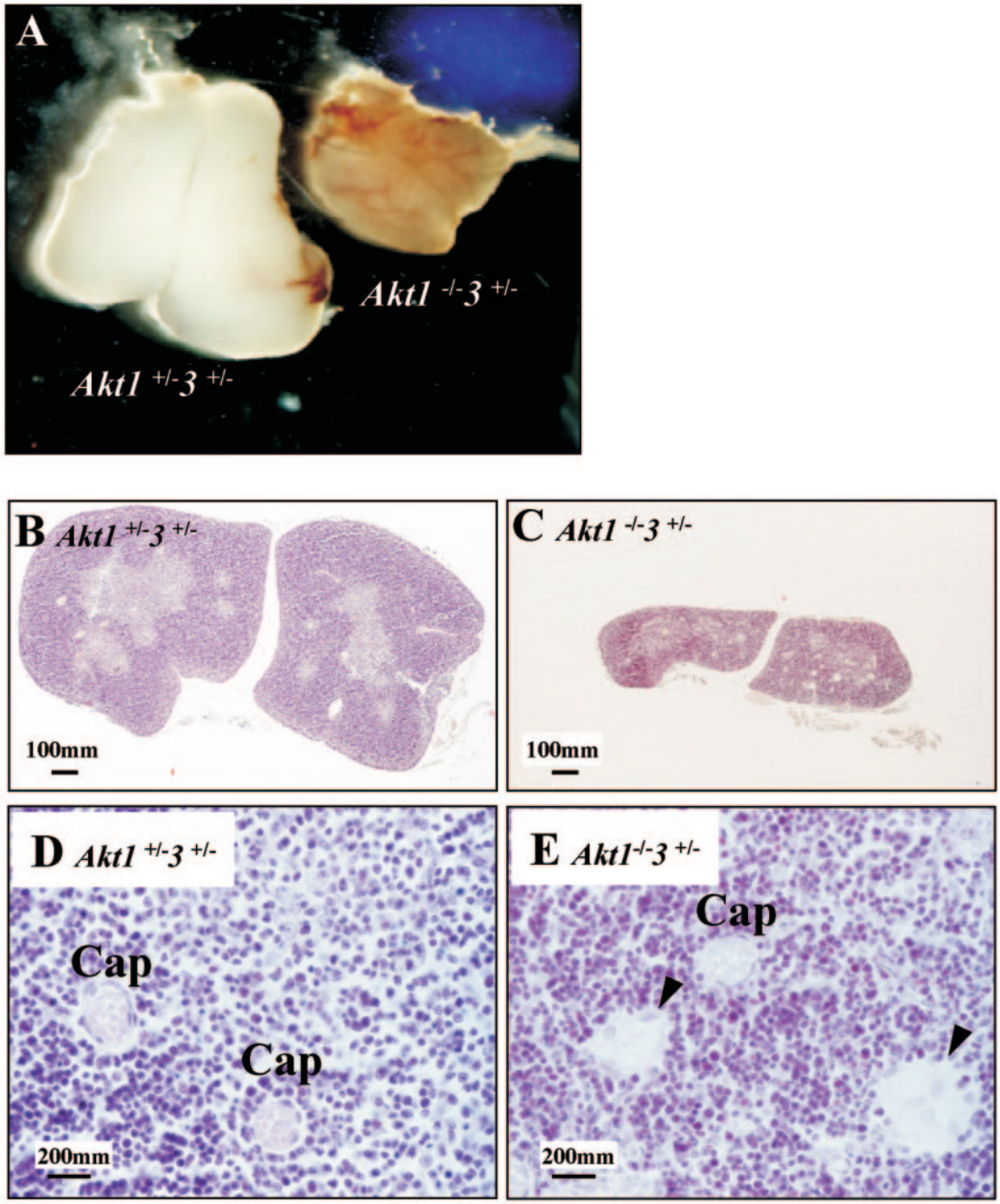

FIG. 2. Defects in the thymus from *Akt1*$^{-/-}$ *Akt3*$^{+/-}$ mice. (A) Thymi from P3 *Akt1*$^{+/-}$ *Akt3*$^{+/-}$ and *Akt1*$^{-/-}$ *Akt3*$^{+/-}$ littermates. (B to E) HE staining of the thymus from panel A. Panels B and C are lower-magnification images of panels D and E. Arrowheads in panel E indicate the Hassall's corpuscle-like structures in the *Akt1*$^{-/-}$ *Akt3*$^{+/-}$ mice which are not found in wild-type mouse thymus. Cap, capillary blood vessel. Magnification for panels B and C, ×40; for panels D and E, ×400.

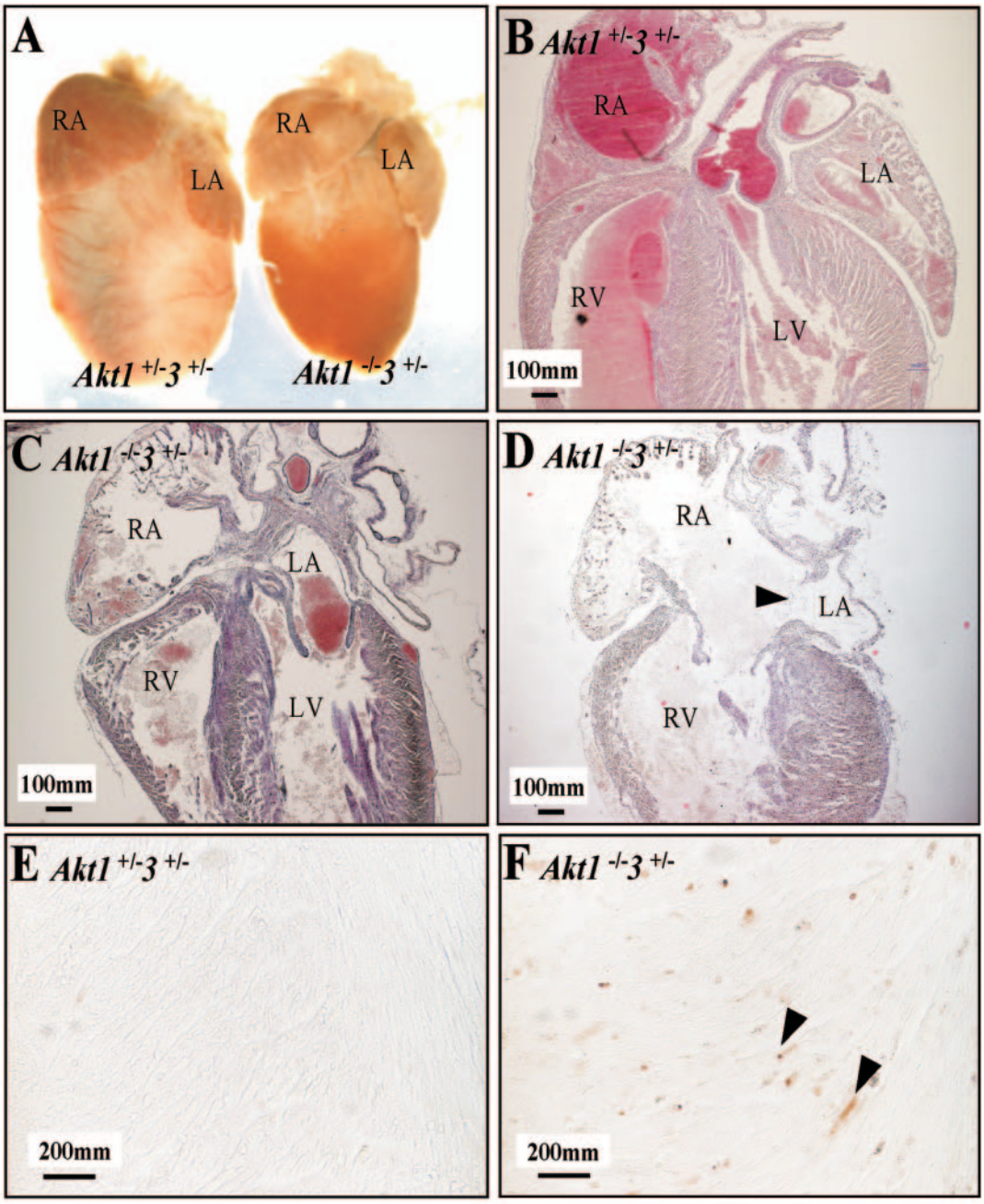

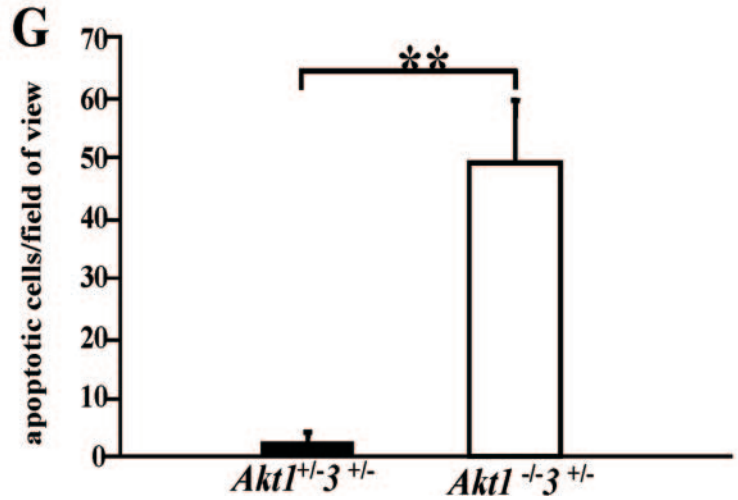

water. All procedures were conducted with relevant authority approval. $Akt1^{-/-}$ and $Akt3^{-/-}$ mice have been described previously (25, 28). All mice had a 129 Ola and C57BL/6 mixed background.

BrdU incorporation. E10.5 to E11.5 pregnant mice were injected intraperitoneally with bromodeoxyuridine (BrdU) (1 mg per 20 g of body weight). The mice were sacrificed 2 h later, and embryos together with placenta were dissected (25, 28).

Hematoxylin-eosin (HE) and immunohistochemisty (IHC). The HE and IHC protocols were as described previously (25, 28). For IHC, sections were incubated at 4°C overnight with antibodies for Akt1 and Akt3, BrdU (AbCam Ltd.), platelet endothelial cell adhesion molecule (PECAM) (Pharmingen), skin markers of keratin 10 (K10) and K14, and involucrin (BABCO). The sections were then processed as described in the protocol of the Vectastain ABC kit (Vector Laboratories).

Terminal deoxynucleotidyltransferase-mediated dUTP-biotin nick end labeling (TUNEL staining). Paraffin-embedded sections were treated with 20 μg/ml proteinase K for 10 min at 37°C (omitted for cryosections). Endogenous peroxidase was inactivated by treatment with 3% H_2O_2 in 100% methanol for 30 min at room temperature. The sections were then equilibrated with 1× terminal deoxynucleotidyl transferase (TdT) buffer for 15 min at room temperature and incubated with TdT and biotinylated dUTP (TdT reaction) for 1 h at 37°C. The reaction was stopped by washing with 1× SSC (1× SSC is 0.15 M NaCl plus 0.015 M sodium citrate). A Vectastain ABC kit (Vector Laboratories) was used as described by the manufacturer for color development.

Quantification and statistics. Quantification of skin thickness and hair follicles was performed with three double-heterozygous (DH) ($Akt1^{+/-}$ $Akt3^{+/-}$) and three $Akt1^{-/-}$ $Akt3^{+/-}$ mice as described previously (11). For the TUNEL assay of heart, five fields of each section were counted for apoptotic cells. The *t* test was used for statistical analysis. Similar scoring was performed for placental vasculature.

RESULTS

Tissue distribution of Akt isoforms in neonates and midgestation embryos. We first investigated the expression patterns of the three isoforms in neonates and surprisingly show that the expression of the Akt3 isoform is more widely expressed than it is in adults (Fig. 1A). Similar to adult mice, Akt3 is highest in the brain and Akt2 is highest in fat as reported previously (7, 13, 25, 28). However, Akt1 and Akt3 are abundant in kidney and skeletal muscle, whereas they are nearly absent in adult mice (Fig. 1A). The ubiquitous expression pattern of the three Akt proteins in neonates indicates that all three isoforms are apparently required for early development.

These isoform-specific antibodies could not be used for immunohistochemistry (IHC) because of nonspecific background staining. Therefore, we used an antibody that specifically recognized both Akt1 and Akt3 (labeled Akt1/Akt3 antibody in Fig. 1B and C) that was originally developed against the carboxyl-terminal peptide sequence of porcine Akt1 (18). This affinity-purified antibody recognized mouse Akt1 and Akt3 but not Akt2 (Fig. 1B) and could be used for IHC.

At E11.5, the level of Akt1 or Akt3 protein (or both) is high in the brain, neural tube, and heart (Fig. 1F and G). At E12.5, the signals are predominantly localized in the developing brain and various ganglia, and the levels (indicated by the staining signal) increased compared to that at E11.5 (Fig. 1H and I). The tissue distribution patterns indicate that the two proteins are important for brain and cardiovascular development at E11.5 to E12.5.

Generation of Akt1 and Akt3 double mutant mice. *Akt1*, *Akt2*, and *Akt3* genes have been successfully targeted in our laboratory by homologous recombination (25, 28; B. A. Dümmler, unpublished data). In the present work, we first mated $Akt1^{-/-}$ males with $Akt3^{-/-}$ females to generate $Akt1^{+/-}$ $Akt3^{+/-}$ (DH) mice. Intercrossing of these DH mice gave rise to offspring with nine genotypes (Table 1). Genotyping of these mice was carried out by independent PCR for the *Akt1* and *Akt3* loci as previously described (25, 28) (Fig. 1D). Western blot analysis confirmed the absence of the two proteins in the MEFs and tissues from Akt1/Akt3 DKO mice (Fig. C and 1E).

***Akt1*$^{-/-}$ *Akt3*$^{+/-}$ mice die at an early age and *Akt1*/*Akt3* double knockout mice are embryonic lethal.** Among the nine genotypes, only $Akt1^{-/-}$ $Akt3^{+/-}$ and DKO mice had survival problems, whereas all others were produced in numbers consistent with the expected Mendelian ratio (Table 1). More than 90% of $Akt1^{-/-}$ $Akt3^{+/-}$ mice were lost by the time of genotyping, and we did not observe any DKO mice at the time of genotyping (Table 1). We next determined at what stage $Akt1^{-/-}$ $Akt3^{+/-}$ mice and DKO mice die. For $Akt1^{-/-}$ $Akt3^{+/-}$ mice, we set up matings between $Akt1^{+/-}$ $Akt3^{-/-}$ males and $Akt1^{-/-}$ females. Theoretically, offspring of this mating are half $Akt1^{-/-}$ $Akt3^{+/-}$ and half DH (1:1). Of the 20 newborns collected from four litters, 8 were DH and 12 were $Akt1^{-/-}$ $Akt3^{+/-}$, which is consistent with the expected Mendelian ratio. Therefore, $Akt1^{-/-}$ $Akt3^{+/-}$ mice appear to develop to term. In a follow-up study, we found that the majority of $Akt1^{-/-}$ $Akt3^{+/-}$ mice died several days after birth.

We next determined the stage of DKO embryonic lethality. No double knockout embryos were found at E14.5. At E12.5, some double knockout embryos had already decayed, leaving only the placenta and body remnants (progeny of $Akt1^{+/-}$ $Akt3^{-/-}$ intercross mice were the following: for genotype $Akt1^{+/+}$ $Akt3^{-/-}$, 15 mice; for genotype $Akt1^{+/-}$ $Akt3^{-/-}$, 12 mice; for genotype $Akt1^{-/-}$ $Akt3^{-/-}$, 13 mice [7 of the $Akt1^{-/-}$ $Akt3^{-/-}$ mice were dead and partially decayed). DKO embryos dissected at E11.5 displayed severely retarded development (data not shown). When E10.5 embryos were dissected and genotyped, double knockout embryos were found with morphology comparable to that of $Akt1^{+/-}$ $Akt3^{-/-}$ littermates. These data indicate that double knockout mutants die around E11 to E12.

Thus, Akt3 appears to be redundant for the survival of Akt1 mutant mice. In contrast, Akt1 mutant mice ($Akt1^{-/-}$) showed a 40% loss after birth, with the mortality of $Akt1^{-/-}$ $Akt3^{+/-}$ mice increased to more than 90%.

FIG. 3. Structural defects in the heart from $Akt1^{-/-}$ $Akt3^{+/-}$ mice. (A) The hearts of $Akt1^{-/-}$ $Akt3^{+/-}$ mice are smaller than those of the controls, but the atria are as big as those of the controls. (B to D) Sagittal sections of the hearts. (B to D) HE staining of hearts from panel A. (C and D) Enlargement of the right side of $Akt1^{-/-}$ $Akt3^{+/-}$ hearts and apparent atria septum defects in $Akt1^{-/-}$ $Akt3^{+/-}$ hearts (P3). The wall of the right atrium of the $Akt1^{-/-}$ $Akt3^{+/-}$ heart is thin due to enlargement (C and D). The arrowhead in panel D indicates atria septum defects. (E and F) TUNEL assay. Arrowheads indicate apoptotic cells. (G) Quantification of apoptosis. Error bars indicate standard deviation. **, $P < 0.01$. RA, right atrium; RV, right ventricle; LA, left atrium. Magnification for panels B to D, ×40; for panels E and F, ×400.

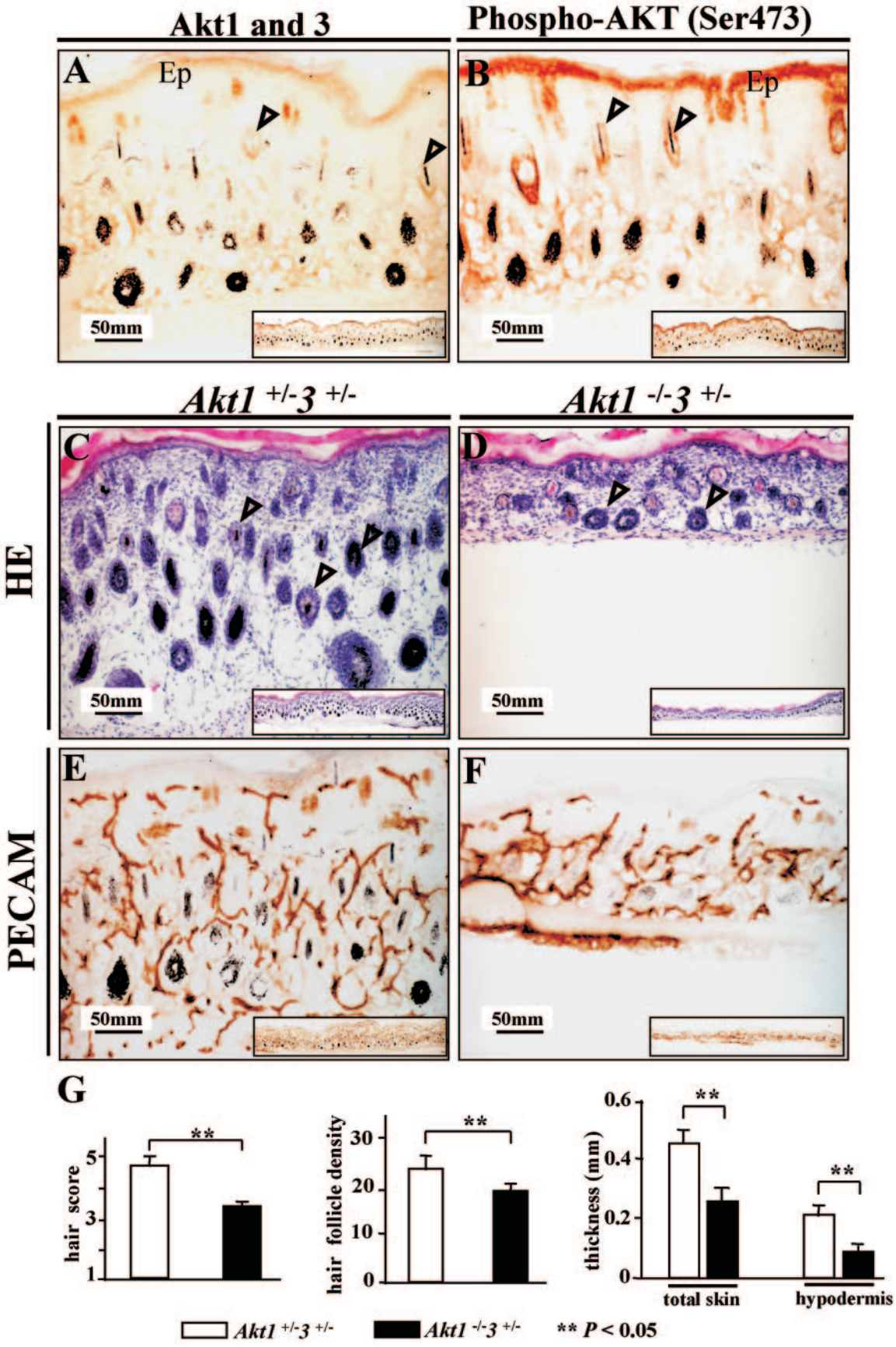

Multiple defects in the thymus, heart, and skin of *Akt1*$^{-/-}$ *Akt3*$^{+/-}$ mice. Nearly all *Akt1*$^{-/-}$ *Akt3*$^{+/-}$ mice died within a few days after birth. To determine possible causes of death, we first performed systemic anatomic organ analysis of postnatal day 3 (P3) viable *Akt1*$^{-/-}$ *Akt3*$^{+/-}$ mice and their DH littermates (the latter mice survive normally and were, therefore, used as the control). Generally, most organs from *Akt1*$^{-/-}$ *Akt3*$^{+/-}$ mice analyzed were proportionally smaller than those of DH controls.

Strikingly, *Akt1*$^{-/-}$ *Akt3*$^{+/-}$ mice also displayed nonproportional hypotrophy of the thymus, heart, and skin. We have studied the six thymi from two litters of P3 mice (three *Akt1*$^{-/-}$ *Akt3*$^{+/-}$ and three DH). The thymus of *Akt1*$^{-/-}$ *Akt3*$^{+/-}$ mice is hypotrophic and much smaller than the control (Fig. 2A to C). There are many Hassall's corpuscle-like structures (arrowheads in Fig. 2E) formed in the thymus of *Akt1*$^{-/-}$ *Akt3*$^{+/-}$ mice, but they were not seen in the DH control (Fig. 2D).

To analyze heart development, we used eight *Akt1*$^{-/-}$ *Akt3*$^{+/-}$ and three *Akt1*$^{-/-}$ mice (similar numbers for control) from newborn to P8. The hearts of *Akt1*$^{-/-}$ *Akt3*$^{+/-}$ mice were smaller than those of controls, the difference being mainly in the ventricles (Fig. 3A). Further histological study of these P3 hearts and other P3 hearts from wild-type mice revealed that *Akt1*$^{-/-}$ *Akt3*$^{+/-}$ hearts had dilated (enlarged) atria and ventricles, especially on the right side (Fig. 3C and D). In addition, we found a range of defects in *Akt1*$^{-/-}$ *Akt3*$^{+/-}$ hearts, including atria septum defect, muscular ventricle septum defect, ventricle septum vascular anomaly, and thickened valves (data not shown). Small ventricle size and insufficient contractility of cardiomyocytes of *Akt1*$^{-/-}$ *Akt3*$^{+/-}$ hearts may lead to the retention of blood in the right side of the heart and cause the atria septum to open. One *Akt1*$^{-/-}$ *Akt3*$^{+/-}$ mouse that died after 8 days exhibited a significantly enlarged right atrium and ventricle (data not shown). Trichrome staining revealed a large area of necrosis (data not shown). TUNEL staining of the heart identified a large number of apoptotic cells outside of the necrotic area (Fig. 3F and G). Histological structure of the lung of *Akt1*$^{-/-}$ *Akt3*$^{+/-}$ mice was similar to that of controls (data not shown). The data presented are representative of the phenotype observed for these mice.

Previously, we observed impaired hair follicle development in *Akt1*$^{-/-}$ mice by HE staining (11). We performed immunohistochemical and HE analyses to evaluate the structure and development of the skin of *Akt1*$^{-/-}$ *Akt3*$^{+/-}$ mice. We have analyzed 11 *Akt1*$^{-/-}$ *Akt3*$^{+/-}$ mice (and a similar number for control) from E16.5 to P8 for skin development. The thin-skin phenotype observed was found in nearly all the mice examined.

Immunohistochemical staining showed Akt1 and Akt3 to be localized mainly in the keratinocytes of epidermis and follicles at P2 (Fig. 4A), which coincided with phospho-Ser473 staining (Fig. 4B). HE staining revealed a reduction in the thickness of *Akt1*$^{-/-}$ *Akt3*$^{+/-}$ skin at P2 and P8 (Fig. 4C). Thickness of the hypodermis and total skin, total number of hair follicles (or hair follicle density), and hair morphogenesis of skin samples from three *Akt1*$^{-/-}$ *Akt3*$^{+/-}$ mice and three controls (*Akt*α$^{+/-}$ *Akt3*$^{+/-}$) at P3 were all significantly different (Fig. 4G). Cell differentiation is normal in *Akt1*$^{-/-}$ *Akt3*$^{+/-}$ skin based on keratin 14 (K14), keratin 10 (K10), and involucrin staining (data not shown). Although all skin layers were present in *Akt1*$^{-/-}$ *Akt3*$^{+/-}$ mice, individual skin layers were much thinner than in the wild type. Thus, the skin as a whole was much thinner. Hair follicles were distinctly reduced in size in *Akt1*$^{-/-}$ *Akt3*$^{+/-}$ animals, and there were fewer (black) hair fibers (data not shown). The impaired skin development of *Akt1*$^{-/-}$ *Akt3*$^{+/-}$ mice may be attributable to decreased vasculature revealed by PECAM (CD31) staining (24) (Fig. 4E and F). This provides further evidence for Akt1- and Akt3-dependent regulation of angiogenesis and vascular formation.

Abnormal development of DKO embryos. At E11.5, some DKO embryos displayed apparent vascular defects and hemorrhages. E10.5 DKO embryos displayed morphology comparable to that of the control. Therefore, we studied embryonic development of E10.5 DKO embryos to understand the ensuing embryo lethality. We analyzed four to five mutant embryos (similar for control) at E10.5 and E12.5. The data presented are representative of the phenotype observed.

Vascular structure was studied using PECAM staining (24). We found a significant decrease in vasculature of DKO embryos compared with controls (Fig. 5A to H). Fine (capillary) vessels were abundant in the head (neuroepithelium) and body trunk of the control but were not apparent in DKO embryos (Fig. 5A to D). Furthermore, DKO embryos displayed hypoplastic branchial arches (Fig. 5G), fused or dilated arch arteries, and the absence of fine vessels (Fig. 5H).

Previously, we observed reduced vasculature in *Akt1*$^{-/-}$ placenta (28), and a more significant vascular defect was found in DKO placenta (Fig. 5J and K). In addition, reduced cell proliferation was detected in DKO placenta (Fig. 5M).

The predominant expression of Akt1 or Akt3 (or both) in the nervous system at E11.5 to E12.5 suggests an important role of these two proteins in the maintenance of brain development. However, there was no significant difference between DKO and wild-type control mice with cell proliferation displayed by BrdU staining (data not shown).

An increase of apoptotic cells was detected using the TUNEL assay in the neuroepithelium and in the neurons of various ganglia in DKO embryos compared to the wild type (Fig. 6A to H). These results indicate that Akt1 and Akt3 contribute to the development of the nervous system by maintenance of cell survival.

FIG. 4. Histology of *Akt1*$^{-/-}$ *Akt3*$^{+/-}$ skin. (A and B) Immunohistochemical staining of Akt1/Akt3 and phospho-Akt (Ser473) in control skin. (A) Akt1/Akt3 localization. The two proteins are mainly localized in the keratinocytes of the epidermis (Ep) and hair follicles (arrowheads). (B) Phospho-Akt (Ser473) in control skin. Localization of phospho-Akt is similar to that of Akt1/Akt3. (C and D) HE staining. Skin of *Akt1*$^{-/-}$ *Akt3*$^{+/-}$ mice is much thinner than that of control littermates and has fewer hair follicles (arrowheads). (E and F) PECAM (CD31) staining to display the vasculature. *Akt1*$^{-/-}$ *Akt3*$^{+/-}$ skin has fewer vessels than the control. Insets in all panels are lower magnification images showing a larger part of the skin. (G) Quantification of skin thickness and hair follicles. HE staining sections from three *Akt1*$^{-/-}$ *Akt3*$^{+/-}$ mice and three *Akt1*$^{+/-}$ *Akt3*$^{+/-}$ littermates (P3) were measured for thickness and hair follicle density. Error bars are standard deviation, and two asterisks indicate a significant difference between the two genotypes ($P < 0.05$). Magnification, ×200.

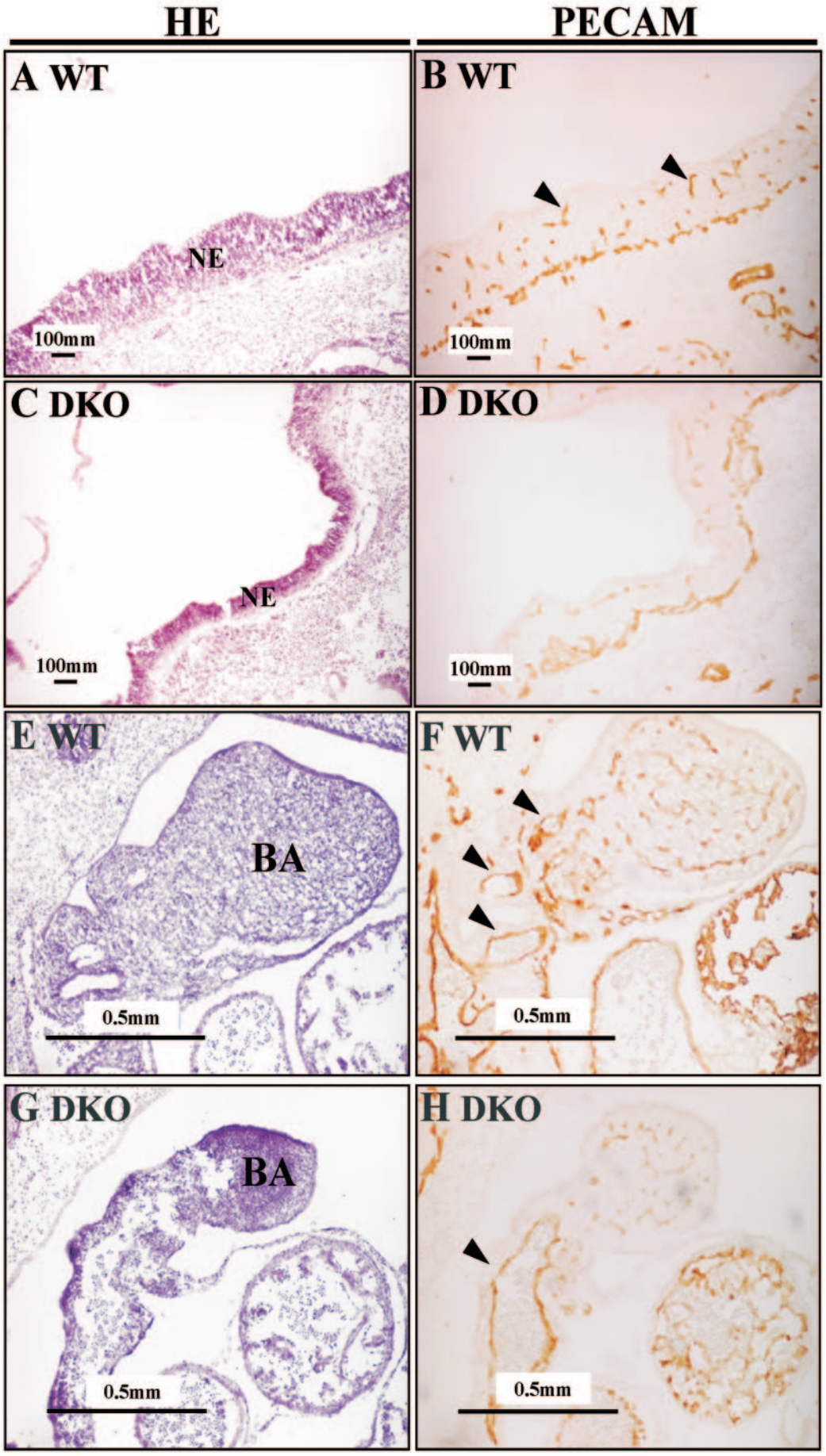

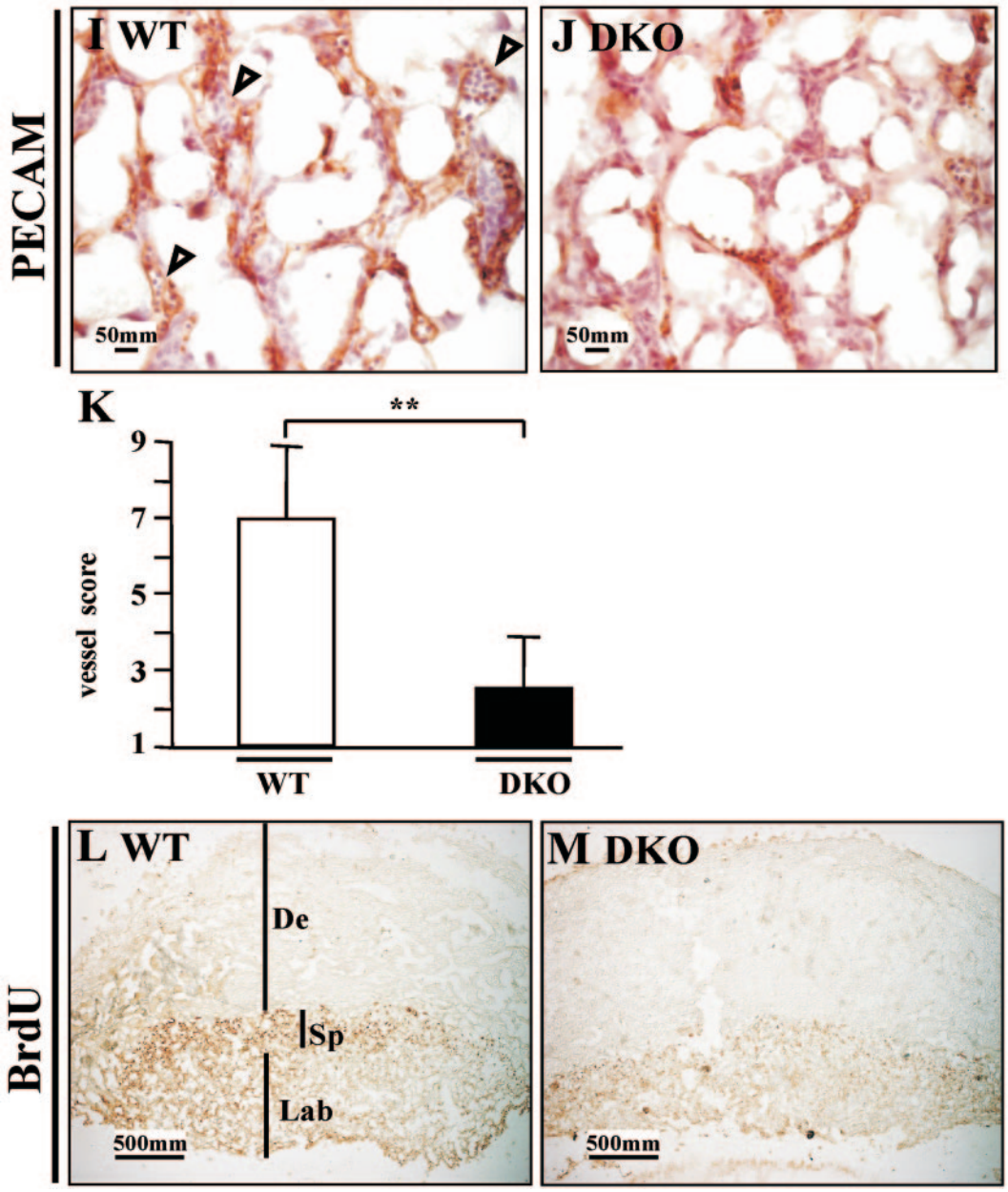

FIG. 5. Analysis of the vascular system of DKO embryos. (A to H) Left panels are HE staining to show the morphology, and the right panels are PECAM staining to display vasculature. (A to D) Fine vessels (capillary) in the neuroepithelium of hindbrain. Arrowheads indicate the small vessels (capillary). Small vessels are abundant in the control and are evenly distributed, while these vessels are scarce in DKO embryos. (E to H) Branchial arches and their arteries. In the control, first, second, and third arch arteries can be seen (arrowheads), and small vessels are rich in mesenchymal tissue (F). However, the branchial arches of DKO mice are hypoplastic, with little mesenchymal tissue, and the large arch arteries cannot be distinguished (arrowhead). Small vessels are also scarce in DKO branchial arches. Abbreviations: NE, neuroepithelium; BA, branchial arch; WT, wild type. Magnification, ×100. (I to M) Histological analysis of DKO placenta. (I and J) E12.5 placentas. PECAM staining displays fetal vessels in the labyrinth. In the wild type (I), fetal vessels are well formed and filled with fetal nucleated erythroid cells (arrowheads), while in DKO mice (J) these vessels are rare, although the epithelial cells can be seen. (K) Quantification of fetal vessels in wild-type and DKO placenta. The double asterisks indicates a significant difference ($P < 0.05$). (L and M) E10.5 placentas. BrdU staining. DKO placenta shows a substantial reduction of proliferation, especially in the spongiotrophoblast layer (Sp). De, decidua; Lab, labyrinth. Magnification, ×40.

DISCUSSION

With neonatal mice, we found that the three Akt proteins are widely expressed in contrast to results obtained in the adult mice, where the Akt3 protein expression is quite restricted. Our findings provide important insights and help better understand the developmental defects in *Akt1*/*Akt3* compound mutant mice and *Akt1*/*Akt2 Akt1*/*Akt3* DKO mice. In the single knockouts of *Akt* isoforms, *Akt2* and *Akt3* null mice have no neonatal survival disadvantages (7, 16, 25, 27). Nevertheless, we and others have observed that 40% of *Akt1* null mice fail to

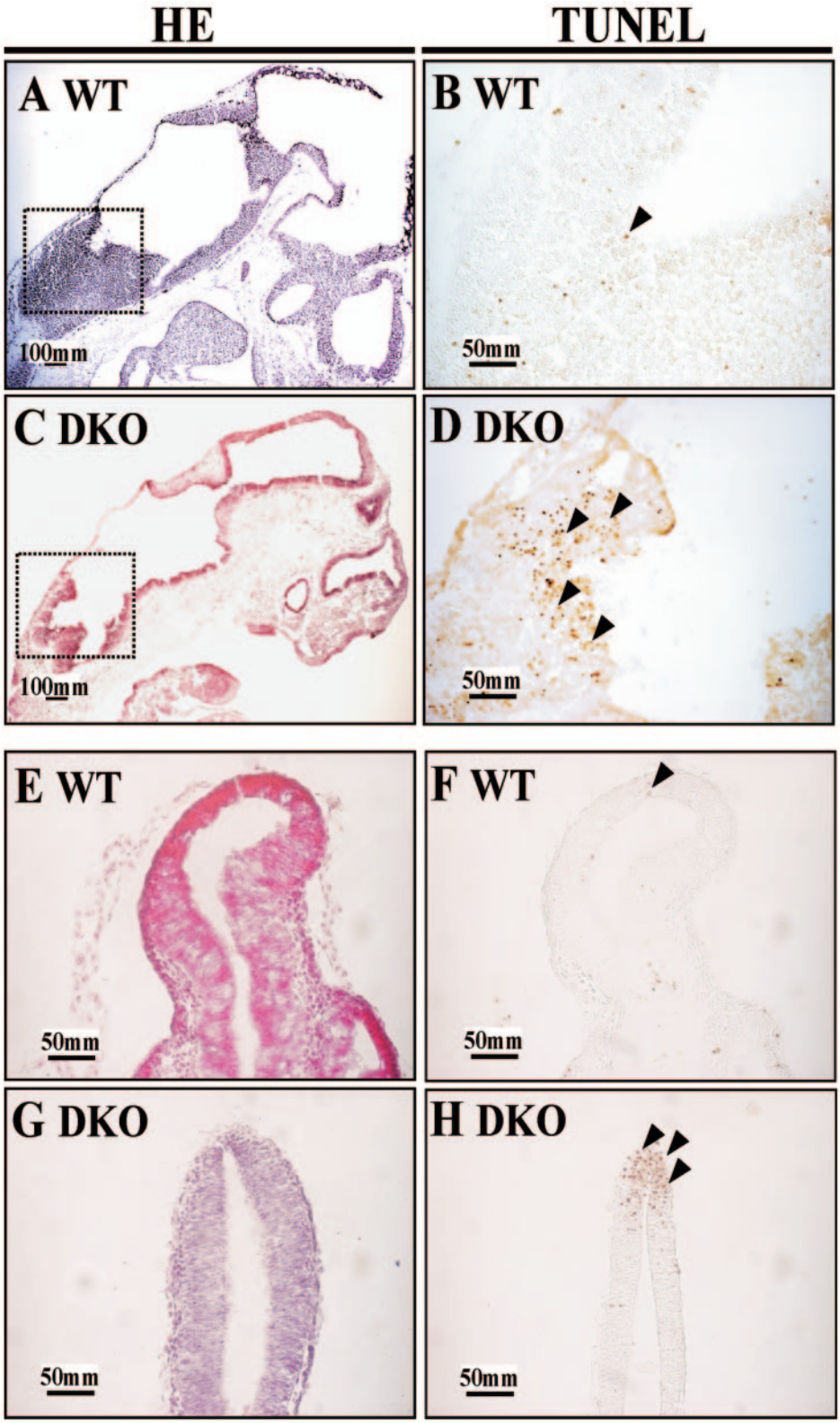

FIG. 6. Apoptosis in wild-type (WT) and DKO embryos. The left panels are HE staining, and the right panels are TUNEL staining. In the wild type, very few apoptotic cells can be seen in the neuroepithelium, but there are many in DKO neuroepithelium (arrowheads indicate apoptotic cells). (A to D) E10.5; (E to H) E9.5. Magnification for panels A and B, ×40; for panels C to F, ×200.

survive past the neonatal period (8). This raises the intriguing possibility that the *Akt1* gene is the most critical isoform of the three for early mouse development. Nearly all $Akt1^{-/-}$ $Akt3^{+/-}$ mice died at an early age, while $Akt1^{+/-}$ $Akt3^{-/-}$ mice survived normally. This suggests that the *Akt1* gene is more essential than *Akt3* for mouse survival. In a recent report, *Akt1*/*Akt2* double knockout mice developed to term but died shortly after birth with severe developmental defects, including dwarfism, skeletal deformity, and skin abnormalities (22). We found that $Akt1^{-/-}$ $Akt3^{+/-}$ mice have severe growth deficiencies, and nearly all died young with multiple organ and tissue pathologies. Mice lacking both *Akt1* and *Akt3* genes died at approximately E11 to E12 and displayed multiple fatal developmental defects. *Akt1*/*Akt2* double knockout mice with only *Akt3* developed to term (22), but *Akt1*/*Akt3* DKO mice (i.e., only *Akt2* was expressed) did not develop beyond the midterm (E12). This indicates a more critical role for *Akt3* than *Akt2* in early animal development and survival. Thus, the order of apparent importance of the three *Akt* genes in mouse development and survival is *Akt1* > *Akt3* > *Akt2*. The phenotypes observed with *Akt1*/*Akt3* DKO and *Akt1*/*Akt2* DKO mice are largely due to loss of *Akt1* function. Taken together, these results indicate that the three *Akt* genes have isoform-specific and dosage-dependent effects on mouse survival and development.

In this study, we found that *Akt1* and *Akt3* have essential roles in cardiovascular development and function. The probable cause of sudden death of $Akt1^{-/-}$ $Akt3^{+/-}$ mice is heart failure, possibly as a result of defective heart development and cardiomyocyte function (6). *Akt1*/*Akt3* DKO mice embryonic lethality could also be attributed to cardiovascular anomalies. These embryos died at around E12, with significant vascular reduction in embryo and placenta; large vessels in the branchial arches and dorsal aorta were also abnormal. As these large branchial arch and dorsal aorta arteries are converted to aortic artery and other large arteries, the developmental defects of these vessels at E12 inhibits further development of mice and enhances morbidity (9, 20, 21).

Our studies of *Akt1*/*Akt3* DKO mice also indicate that *Akt1* and *Akt3* are critical for nervous system development. Previously, we found that Akt3 protein levels are the highest in the brain, and deletion of this isoform substantially impaired brain development (13, 25). In *Akt1*/*Akt3* DKO embryos, many apoptotic cells were found in the neuroepithelium and neurons of ganglia. Therefore, *Akt1* and *Akt3* are indispensable for nervous system development in the embryo through their maintenance of cell survival (12, 29, 30).

Another interesting finding is the Hassall's corpuscle-like structures in, $Akt1^{-/-}$ $Akt3^{+/-}$ thymus, as this structure is well developed in the thymus of humans and guinea pigs but poorly developed in the thymus of mice and rats (26). In humans, the Hassall's corpuscles have been proposed to remove apoptotic thymocytes (26). Previously, Hay's group found increased apoptotic thymocytes in Akt1 null mice (5). The formation and function of these structures in $Akt1^{-/-}$ $Akt3^{+/-}$ thymus need to be studied further.

In conclusion, our results indicate that *Akt1* and *Akt3* genes apparently regulate multiple developmental processes in mice. *Akt1* and *Akt3* genes share some redundant functions required to maintain mouse development and survival. However, these two proteins seem to play distinct roles based on the phenotypes of the individual knockouts. To rigorously understand the causes of the different phenotypes, it will be necessary to identify the specific Akt substrates involved in the development of the different organs.

ACKNOWLEDGMENTS

We thank D. Hynx (FMI) for management of the mouse colonies and J. Günthard and T. Dieterle at the Children's Hospital and Canton Hospital, Basel, Switzerland, for consultation on $Akt1^{-/-}$ $Akt3^{+/-}$ heart phenotype. We are grateful to B. Sücürü and E. Fayard for antibody preparation. The Friedrich Miescher Institute for Biomedical Research is a part of the Novartis Research Foundation.

B.D. is supported by the Swiss Cancer League (KFS 1002-02-2000).

REFERENCES

1. **Alessi, D., M. Andjelkovic, B. Caudwell, P. Cron, N. Morrice, P. Cohen, and B. A. Hemmings.** 1996. Mechanism of activation of protein kinase B by insulin and IGF1. EMBO J. **15:**6541–6551.
2. **Altomare, D. A., G. E. Lyons, Y. Mitsuuchi, J. Q. Cheng, and J. R. Testa.** 1998. Akt2 mRNA is highly expressed in embryonic brown fat and the AKT2 kinase is activated by insulin. Oncogene **16:**2407–2411.
3. **Brazil, D. P., and B. A. Hemmings.** 2001. Ten years of protein kinase B signalling: a hard Akt to follow. Trends Biochem. Sci. **26:**657–664.
4. **Burgering, B. M., and P. J. Coffer.** 1995. Protein kinase B (c-Akt) in phosphatidylinositol-3-OH kinase signal transduction. Nature **376:**599–602.
5. **Chen, W. S., P.-Z. Xu, K. Gottlob, M.-L. Chen, K. Sokol, T. Shiyanova, I. Roninson, W. Weng, R. Suzuki, K. Tobe, T. Kadowaki, and N. Hay.** 2001. Growth retardation and increased apoptosis in mice with homozygous disruption of the akt1 gene. Genes Dev. **15:**2203–2208.
6. **Chien, K. R., and E. N. Olson.** 2002. Converging pathways and principles in heart development and disease: CV@CSH. Cell **110:**153–162.
7. **Cho, H., J. Mu, J. K. Kim, J. L. Thorvaldsen, Q. Chu, E. B. Crenshaw III, K. H. Kaestner, M. S. Bartolomei, G. I. Shulman, and M. J. Birnbaum.** 2001. Insulin resistance and a diabetes mellitus-like syndrome in mice lacking the protein kinase Akt2 (PKBβ). Science **292:**1728–1731.
8. **Cho, H., J. L. Thorvaldsen, Q. Chu, F. Feng, and M. J. Birnbaum.** 2001. Akt1/PKBα is required for normal growth but dispensable for maintenance of glucose homeostasis in mice. J. Biol. Chem. **276:**38349–38352.
9. **Conway, S. J., A. Kruzynska-Frejtag, P. L. Kneer, M. Machnicki, and S. V. Koushik.** 2003. What cardiovascular defect does my prenatal mouse mutant have, and why? Genesis **35:**1–21.
10. **Datta, S. R., A. Brunet, and M. E. Greenberg.** 1999. Cellular survival: a play in three Akts. Genes Dev. **13:**2905–2927.
11. **Di-Poi, N., C. Y. Ng, N. S. Tan, Z. Yang, B. A. Hemmings, B. Desvergne, L. Michalik, and W. Wahli.** 2005. Epithelium-mesenchyme interactions control the activity of peroxisome proliferator-activated receptor β/δ during hair follicle development. Mol. Cell. Biol. **25:**1696–1712.
12. **Dudek, H., S. R. Datta, T. F. Franke, M. J. Birnbaum, R. Yao, G. M. Cooper, R. A. Segal, D. R. Kaplan, and M. E. Greenberg.** 1997. Regulation of neuronal survival by the serine-threonine protein kinase Akt. Science **275:**661–665.
13. **Easton, R. M., H. Cho, K. Roovers, D. W. Shineman, M. Mizrahi, M. S. Forman, V. M.-Y. Lee, M. Szabolcs, R. de Jong, T. Oltersdorf, T. Ludwig, A. Efstratiadis, and M. J. Birnbaum.** 2005. Role for Akt3/protein kinase Bγ in attainment of normal brain size. Mol. Cell. Biol. **25:**1869–1878.
14. **Feng, J., R. Tamaskovic, Z. Yang, D. P. Brazil, A. Merlo, D. Hess, and B. A. Hemmings.** 2004. Stabilization of Mdm2 via decreased ubiquitination is mediated by protein kinase B/Akt-dependent phosphorylation. J. Biol. Chem. **279:**35510–35517.
15. **Franke, T. F., S. I. Yang, T. O. Chan, K. Datta, A. Kazlauskas, D. K. Morrison, D. R. Kaplan, and P. N. Tsichlis.** 1995. The protein kinase encoded by the Akt proto-oncogene is a target of the PDGF-activated phosphatidylinositol 3-kinase. Cell **81:**727–736.
16. **Garofalo, R. S., S. J. Orena, K. Rafidi, A. J. Torchia, J. L. Stock, A. L. Hildebrandt, T. Coskran, S. C. Black, D. J. Brees, J. R. Wicks, J. D. McNeish, and K. G. Coleman.** 2003. Severe diabetes, age-dependent loss of adipose tissue, and mild growth deficiency in mice lacking Akt2/PKBβ. J. Clin. Investig. **112:**197–208.
17. **Hanada, M., J. Feng, and B. A. Hemmings.** 2004. Structure, regulation and function of PKB/AKT–a major therapeutic target. Biochimica et Biophysica Acta Proteins Proteom. **1697:**3–16.
18. **Jones, P., T. Jakubowicz, F. Pitossi, F. Maurer, and B. Hemmings.** 1991. Molecular cloning and identification of a serine/threonine protein kinase of the second-messenger subfamily. Proc. Natl. Acad. Sci. USA **88:**4171–4175.
19. **Lawlor, M. A., and D. R. Alessi.** 2001. PKB/Akt: a key mediator of cell proliferation, survival and insulin responses? J. Cell Sci. **114:**2903–2910.

20. **Liu, C., W. Liu, J. Palie, M. F. Lu, N. A. Brown, and J. F. Martin.** 2002. Pitx2c patterns anterior myocardium and aortic arch vessels and is required for local cell movement into atrioventricular cushions. Development **129:** 5081–5091.
21. **Papaioannou, V. E., and R. R. Behringer.** 2005. Mouse phenotypes, a handbook of mutation analysis. Cold Spring Harbor Laboratory Press, Cold Spring Harbor, N.Y.
22. **Peng, X.-d., P.-Z. Xu, M.-L. Chen, A. Hahn-Windgassen, J. Skeen, J. Jacobs, D. Sundararajan, W. S. Chen, S. E. Crawford, K. G. Coleman, and N. Hay.** 2003. Dwarfism, impaired skin development, skeletal muscle atrophy, delayed bone development, and impeded adipogenesis in mice lacking Akt1 and Akt2. Genes Dev. **17:**1352–1365.
23. **Scheid, M. P., and J. R. Woodgett.** 2001. PKB/AKT: functional insights from genetic models. Nat. Rev. Mol. Cell Biol. **2:**760–768.
24. **Stainier, D. Y., R. K. Lee, and M. C. Fishman.** 1994. Platelet endothelial cell adhesion molecule-1 (PECAM-1/CD31): alternatively spliced, functionally distinct isoforms expressed during mammalian cardiovascular development. Development **120:**2539–2553.
25. **Tschopp, O., Z.-Z. Yang, D. Brodbeck, B. Duemmler, M. Hemmings-Mieszczak, T. Watanabe, T. Michaelis, J. Frahm, and B. A. Hemmings.** 2005. Essential role of protein kinase Bγ (PKBγ/Akt3) in postnatal brain development, but not for glucose homeostasis. Development **132:**2943–2954.
26. **Watanabe, N., Y. H. Wang, H. K. Lee, T. Ito, Y. H. Wang, W. Cao, and Y. J. Liu.** 2005. Hassall's corpuscles instruct dendritic cells to induce CD4+ CD25+ regulatory T cells in human thymus. Nature **436:**1181–1185.
27. **Yang, Z.-Z., O. Tschopp, A. Baudry, B. Duemmler, D. Hynx, and B. A. Hemmmngs.** 2004. Physiological function of PKB/Akt. Biochem. Soc. Trans. **32:**350–354.
28. **Yang, Z.-Z., O. Tschopp, M. Hemmings-Mieszczak, J. Feng, D. Brodbeck, E. Perentes, and B. A. Hemmings.** 2003. Protein kinase Bα/Akt1 regulates placental development and fetal growth. J. Biol. Chem. **278:**32124–32131.
29. **Yuan, J., M. Lipinski, and A. Degterev.** 2003. Diversity in the mechanisms of neuronal cell death. Neuron **40:**301–413.
30. **Yuan, J., and B. A. Yankner.** 2000. Apoptosis in the nervous system. Nature **407:**802–809.

III. DISCUSSION

Since its discovery more than 15 years ago, the signaling kinase PKB has been recognized as a central player in a diverse array of cellular processes. PKB lies at the crossroads of multiple cellular signaling pathways and acts as a transducer of many functions initiated by growth factor receptors that activate PI3K. Importantly, deregulation of PKB activity is implicated in human diseases, especially in cancer and type 2 diabetes. The members of the PKB family of protein kinases are attractive targets for pharmacological intervention and knowledge of the precise individual roles of each isoform may be useful for the design of PKB-based therapeutics.

It is still unclear whether PKBα, PKBβ, and PKBγ are functionally redundant or whether each isoform performs specific functional roles. To elucidate specific physiological roles of the different PKB isoforms, we generated and analyzed loss-of-function mouse models of PKBγ, PKBα/PKBγ, and PKBβ/PKBγ.

PKB function in somatic growth and organ size

Our analysis of the PKBγ$^{-/-}$ phenotype has provided a function for this protein kinase in the attainment of normal brain size, influencing both cell size and number in the mouse brain. The requirement of functional PKBγ appears to be remarkably organ-specific, as PKBγ$^{-/-}$ mice display normal body size and no other abnormalities. Furthermore, this appears to be a PKBγ-specific non-redundant function as (a) neither PKBα$^{-/-}$ (19) nor PKBβ$^{-/-}$ (22, 35) mice exhibit reduced brain weights and (b) relative brain weights of the here analyzed PKBβ$^{-/-}$PKBγ$^{-/-}$ mice were not decreased compared to those of PKBγ$^{-/-}$ mice, indicating that the absence of an additional PKB isoform does not intensify the small-brain phenotype of PKBγ$^{-/-}$ mice.

Particular organ sizes appear to be regulated by specific isoforms. For instance, while PKBγ influences brain size, PKBβ$^{-/-}$PKBγ$^{-/-}$ mice display reduced relative

weights of testes, and PKBα$^{-/-}$PKBβ$^{-/-}$ mice show decreased myocyte size in skeletal muscle and a decreased cell number in skin (82). There are organ-specific differences in the modes of mass reduction in PKB mutant mice (i.e. decreased cell number, cell size, or both). However, these differences may reflect the growth potential for particular organs (e.g. proliferative capacity throughout life or postnatal growth exclusively through increases in cell size). Comparison of the phenotypes of mice deficient in IGF1 receptor (IGF1r), IRS proteins, and PKB isoforms allows some conclusions about the relevant signaling pathways for somatic growth and growth of particular organs. Both IGF1r$^{-/-}$ and IRS1$^{-/-}$ mice display severely reduced body size (2, 62). In contrast, IRS2$^{-/-}$ mice reach nearly normal size but have an impairment of brain growth secondary to a decrease in neuronal proliferation (97). Thus, the IGF1→IRS2→PKBγ pathway may be responsible for the effects of IGF1 on brain size, whereas IRS1 mediates the effect of IGF1 on somatic growth.

The most important PKB isoform for somatic growth is PKBα. PKBα$^{-/-}$ mice are about 20% smaller than wild type littermates and organs weights are reduced proportionally to the reduced body weights (19, 23, 118). Interestingly, somatic growth is not exclusively influenced by PKBα. Deletion of either PKBβ or PKBγ in PKBα$^{-/-}$ mice intensifies the growth deficiency seen in PKBα null mice. PKBα$^{-/-}$PKBβ$^{-/-}$ mice have a birth weight ~50% of that of wild type littermates (82) and PKBα$^{-/-}$PKBγ$^{-/-}$ embryos (lethal at day E12) display severely retarded development. In addition, we observed a ~25% reduction in body weights of PKBβ$^{-/-}$PKBγ$^{-/-}$ mice compared to wild types. Thus, all three isoforms influence somatic growth, although PKBα appears to be the major contributor, and the three isoforms can partial compensation for each other in this function.

A very recent publication has shown that PKBα and PKBβ may play differential and opposing roles in the modulation of p21^{Cip1} localization and cell proliferation. Heron-Milhavet *et al.* show differential interaction of PKBα and PKBβ with the cell cycle inhibitor p21^{Cip1} (40). Whereas PKBα promotes proliferation by mediating phosphorylation of p21^{Cip1} on Thr145 and its release from CDK2, PKBβ binds p21^{Cip1} in the region of the phosphorylation site, induces accumulation of p21^{Cip1} in the nucleus and ultimately cell cycle exit.

This data was obtained mainly by siRNA knock down experiments and overexpression of the isoforms in mouse myoblasts and fibroblast cell lines. The physiological relevance of these findings is still an open question and is only partially supported by the phenotypes we observed in our PKB mutant mice. Although PKBα appears to be the predominant isoform regulating somatic growth, there is no indication for PKBβ being a negative regulator of cell proliferation. However, we did not yet investigate $p21^{Cip1}$ localization in our PKB mutant mice.

PKB function in embryonic development and postnatal survival

PKB$\alpha^{-/-}$ mice display an increased neonatal lethality and about 30% of these mice die shortly after birth (19, 118). A potential cause of death in these animals may be the growth retardation of PKB$\alpha^{-/-}$ mice, which is resulting from placental insufficiency and also embryo-intrinsic mechanisms (118). Mice with a PKB$\alpha^{-/-}$PKB$\gamma^{-/-}$ genotype display lethality already at embryonic day E12; PKB$\alpha^{-/-}$PKB$\gamma^{-/-}$ embryos show multiple severe developmental defects in the cardiovascular and nervous system. PKB$\alpha^{-/-}$PKB$\beta^{-/-}$ mice finish gestation but die shortly after birth with developmental defects in skin, skeletal muscle and bone (82).

Considering the lethal phenotypes and multiple developmental defects of PKB$\alpha^{-/-}$PKB$\gamma^{-/-}$ and PKB$\alpha^{-/-}$PKB$\beta^{-/-}$ mice, PKB isoforms appear to play essential roles in various aspects of embryonic development. However, PKB$\beta^{-/-}$PKB$\gamma^{-/-}$ and even PKB$\alpha^{+/-}$PKB$\beta^{-/-}$PKB$\gamma^{-/-}$ mice, which retain only one functional allele of PKBα, can develop normally and survive with minimal dysfunctions. Interestingly, we found no compensatory upregulation of PKBα protein in PKB$\beta^{-/-}$PKB$\gamma^{-/-}$ mice, neither in adult animals nor in neonates. PKBα appears thus to play a dominant role in embryonic development and postnatal survival: it is sufficient (even when expressed at very low levels as in PKB$\alpha^{+/-}$PKB$\beta^{-/-}$PKB$\gamma^{-/-}$) to perform all essential PKB functions in these processes.

PKB function in glucose metabolism

Various lines of evidence have confirmed an isoform-specific role of PKBβ in insulin-stimulated glucose uptake. PKBβ$^{-/-}$ mice are glucose and insulin intolerant (22, 35) whereas PKBα$^{-/-}$ mice display normal glucose homeostasis (23). In accordance with this, studies in adipocytes derived from embryonic fibroblasts of PKBα$^{-/-}$PKBβ$^{-/-}$ mice have shown that impaired glucose uptake can be rescued in these cells by re-expression of PKBβ whereas re-expression of PKBα at comparable levels was ineffective (4).

We found that the PKBγ isoform is, like PKBα, dispensable for glucose homeostasis. PKBγ$^{-/-}$ mice have similar glucose excursions in glucose and insulin tolerance tests as wild type. In addition, absence of PKBγ does not intensify the diabetes-like phenotype of PKBβ$^{-/-}$ mice, as PKBβ$^{-/-}$PKBγ$^{-/-}$ mice have similar glucose excursions in glucose and insulin tolerance tests as PKBβ$^{-/-}$ mice.

Of note, PKB signal transduction is also critical for β cell growth and survival. We assessed hyperinsulinemia in both PKBβ$^{-/-}$ and PKBβ$^{-/-}$PKBγ$^{-/-}$ mice, indicating that the pancreatic β cells are trying to compensate for the peripheral insulin resistance in these mice. Most likely the higher plasma insulin levels are due to increased secretion of insulin rather than an increase in β cell mass. Garofalo *et al.* showed that PKBβ$^{-/-}$ mice were not able to increase β cell mass in response to the peripheral insulin resistance, and six-month-old male PKBβ$^{-/-}$ mice presented increased β cell apoptosis accompanied with β cell failure (35). Upstream, the signaling pathway mediating β cell growth and survival appears to involve IGF1 receptor and IRS2 (112). IRS2$^{-/-}$ mice are insulin resistant and develop diabetes due to a concomitant reduction in β cell mass (56, 113). This phenotype is even more severe in IGF1r$^{+/-}$IRS2$^{-/-}$ mice (112). The β cell phenotype of PKBβ$^{-/-}$ mice strongly resembles the one of IRS2$^{-/-}$ mice but is less severe, indicating that in PKBβ$^{-/-}$ mice the other PKB isoforms allow some signaling downstream of IRS2.

Downstream signaling of PKB in mutant mice

Although many downstream targets of PKB that mediate cell growth, proliferation, and insulin signaling are known and their functions well established, it is not always possible to correlate the deficiencies observed in PKB mutant mice with a reduction in phosphorylation of these targets. For example, we could not detect any reduction in the phosphorylation levels of the growth-relevant downstream targets TSC2 and S6K1 in neither cerebellar neurons of PKB$\beta^{-/-}$PKB$\gamma^{-/-}$ mice nor whole brains of PKB$\gamma^{-/-}$ mice; although these mice exhibit a prominent reduction in neuronal cell size and number. However, Peng *et al.* found reduced TSC2 phosphorylation in primary cultures of PKB$\alpha^{-/-}$PKB$\beta^{-/-}$ MEFs (82).

It has been proposed that PKB isoforms display differential activation in insulin responsive tissues. For instance, insulin-stimulated activation of the three isoforms of PKB was studied in primary hepatocytes and activation of PKBα appeared to be 4-fold higher than PKBβ activity, while PKBγ activity was lowest (110). We found that insulin-induced PKB activation, as measured by Ser473 phosphorylation, was more than 10-fold reduced in livers of PKB$\beta^{-/-}$ and PKB$\beta^{-/-}$PKB$\gamma^{-/-}$ mice compared to wild type levels. However, when we examined insulin-induced phosphorylation levels of the PKB substrate GSK3β in those mice, we found no reduction of phospho-GSK3β levels in PKB$\beta^{-/-}$ and PKB$\beta^{-/-}$PKB$\gamma^{-/-}$ mice compared to wild type. It is not quite clear yet why a striking decrease in total levels of activated PKB should not be followed by reduced phosphorylation of PKB substrates. It may be that in PKB$\beta^{-/-}$PKB$\gamma^{-/-}$ mice the remaining PKBα isoform is even at minimal amounts sufficient to phosphorylate many downstream targets. Alternatively, compensation for the deletion of PKB isoforms could occur via other kinases or relevant substrates may be affected in particular developmental stages only.

IV. REFERENCES

1. **Ackler, S., S. Ahmad, C. Tobias, M. D. Johnson, and R. I. Glazer.** 2002. Delayed mammary gland involution in MMTV-AKT1 transgenic mice. Oncogene **21:**198-206.

2. **Araki, E., M. A. Lipes, M.-E. Patti, J. C. Bruning, B. Haag Iii, R. S. Johnson, and C. R. Kahn.** 1994. Alternative pathway of insulin signalling in mice with targeted disruption of the IRS-1 gene. Nature **372:**186.

3. **Bacus, S. S., D. A. Altomare, L. Lyass, D. M. Chin, M. P. Farrell, K. Gurova, A. Gudkov, and J. R. Testa.** 2002. AKT2 is frequently upregulated in HER-2/neu-positive breast cancers and may contribute to tumor aggressiveness by enhancing cell survival. Oncogene **21:**3532-40.

4. **Bae, S. S., H. Cho, J. Mu, and M. J. Birnbaum.** 2003. Isoform-specific regulation of insulin-dependent glucose uptake by Akt/protein kinase B. J Biol Chem **278:**49530-6.

5. **Barnett, S. F., M. T. Bilodeau, and C. W. Lindsley.** 2005. The Akt/PKB family of protein kinases: a review of small molecule inhibitors and progress towards target validation. Curr Top Med Chem **5:**109-25.

6. **Baudry, A., Z. Z. Yang, and B. A. Hemmings.** 2006. PKBalpha is required for adipose differentiation of mouse embryonic fibroblasts. J Cell Sci **119:**889-97.

7. **Bellacosa, A., C. C. Kumar, A. Di Cristofano, and J. R. Testa.** 2005. Activation of AKT kinases in cancer: implications for therapeutic targeting. Adv Cancer Res **94:**29-86.

8. **Bernal-Mizrachi, E., S. Fatrai, J. D. Johnson, M. Ohsugi, K. Otani, Z. Han, K. S. Polonsky, and M. A. Permutt.** 2004. Defective insulin secretion and increased susceptibility to experimental diabetes are induced by reduced Akt activity in pancreatic islet beta cells. J Clin Invest **114:**928-36.

9. **Bernal-Mizrachi, E., W. Wen, S. Stahlhut, C. M. Welling, and M. A. Permutt.** 2001. Islet beta cell expression of constitutively active Akt1/PKB alpha induces striking hypertrophy, hyperplasia, and hyperinsulinemia. J Clin Invest **108:**1631-8.

10. **Berwick, D. C., G. C. Dell, G. I. Welsh, K. J. Heesom, I. Hers, L. M. Fletcher, F. T. Cooke, and J. M. Tavare.** 2004. Protein kinase B phosphorylation of PIKfyve regulates the trafficking of GLUT4 vesicles. J Cell Sci **117:**5985-93.

11. **Bryant, N. J., R. Govers, and D. E. James.** 2002. Regulated transport of the glucose transporter GLUT4. Nat Rev Mol Cell Biol **3:**267-77.

12. **Burnett, P. E., R. K. Barrow, N. A. Cohen, S. H. Snyder, and D. M. Sabatini.** 1998. RAFT1 phosphorylation of the translational regulators p70 S6 kinase and 4E-BP1. Proc Natl Acad Sci U S A **95:**1432-7.

13. **Byun, D. S., K. Cho, B. K. Ryu, M. G. Lee, J. I. Park, K. S. Chae, H. J. Kim, and S. G. Chi.** 2003. Frequent monoallelic deletion of PTEN and its reciprocal associatioin with PIK3CA amplification in gastric carcinoma. Int J Cancer **104:**318-27.

14. **Cantley, L. C., and B. G. Neel.** 1999. New insights into tumor suppression: PTEN suppresses tumor formation by restraining the phosphoinositide 3-kinase/AKT pathway. Proc Natl Acad Sci U S A **96:**4240-5.

15. **Caro, J. F., M. K. Sinha, S. M. Raju, O. Ittoop, W. J. Pories, E. G. Flickinger, D. Meelheim, and G. L. Dohm.** 1987. Insulin receptor kinase in human skeletal muscle from obese subjects with and without noninsulin dependent diabetes. J Clin Invest **79:**1330-7.

16. **Castillo, S. S., J. Brognard, P. A. Petukhov, C. Zhang, J. Tsurutani, C. A. Granville, M. Li, M. Jung, K. A. West, J. G. Gills, A. P. Kozikowski, and P. A. Dennis.** 2004. Preferential inhibition of Akt and killing of Akt-dependent cancer cells by rationally designed phosphatidylinositol ether lipid analogues. Cancer Res **64:**2782-92.

17. **Cheadle, J. P., M. P. Reeve, J. R. Sampson, and D. J. Kwiatkowski.** 2000. Molecular genetic advances in tuberous sclerosis. Hum Genet **107:**97-114.

18. **Chen, M. L., P. Z. Xu, X. D. Peng, W. S. Chen, G. Guzman, X. Yang, A. Di Cristofano, P. P. Pandolfi, and N. Hay.** 2006. The deficiency of Akt1 is sufficient to suppress tumor development in Pten+/- mice. Genes Dev **20:**1569-74.

19. **Chen, W. S., P. Z. Xu, K. Gottlob, M. L. Chen, K. Sokol, T. Shiyanova, I. Roninson, W. Weng, R. Suzuki, K. Tobe, T. Kadowaki, and N. Hay.** 2001. Growth retardation and increased apoptosis in mice with homozygous disruption of the Akt1 gene. Genes Dev **15:**2203-8.

20. **Cheng, J. Q., C. W. Lindsley, G. Z. Cheng, H. Yang, and S. V. Nicosia.** The Akt//PKB pathway: molecular target for cancer drug discovery. **24:**7482.

21. **Cheng, J. Q., B. Ruggeri, W. M. Klein, G. Sonoda, D. A. Altomare, D. K. Watson, and J. R. Testa.** 1996. Amplification of AKT2 in human pancreatic cells and inhibition of AKT2 expression and tumorigenicity by antisense RNA. Proc Natl Acad Sci U S A **93:**3636-41.

22. **Cho, H., J. Mu, J. K. Kim, J. L. Thorvaldsen, Q. Chu, E. B. Crenshaw, 3rd, K. H. Kaestner, M. S. Bartolomei, G. I. Shulman, and M. J. Birnbaum.** 2001. Insulin resistance and a diabetes mellitus-like syndrome in mice lacking the protein kinase Akt2 (PKB beta). Science **292:**1728-31.

23. **Cho, H., J. L. Thorvaldsen, Q. Chu, F. Feng, and M. J. Birnbaum.** 2001. Akt1/PKBalpha is required for normal growth but dispensable for maintenance of glucose homeostasis in mice. J Biol Chem **276:**38349-52.

24. **Condorelli, G., A. Drusco, G. Stassi, A. Bellacosa, R. Roncarati, G. Iaccarino, M. A. Russo, Y. Gu, N. Dalton, C. Chung, M. V. Latronico, C. Napoli, J. Sadoshima, C. M. Croce, and J. Ross, Jr.** 2002. Akt induces enhanced myocardial contractility and cell size in vivo in transgenic mice. Proc Natl Acad Sci U S A **99:**12333-8.

25. **Cook, S. A., T. Matsui, L. Li, and A. Rosenzweig.** 2002. Transcriptional effects of chronic Akt activation in the heart. J Biol Chem **277:**22528-33.

26. **Cross, D. A. E., D. R. Alessi, P. Cohen, M. Andjelkovich, and B. A. Hemmings.** 1995. Inhibition of glycogen synthase kinase-3 by insulin mediated by protein kinase B. Nature **378:**785.

27. **Dan, H. C., M. Sun, L. Yang, R. I. Feldman, X. M. Sui, C. C. Ou, M. Nellist, R. S. Yeung, D. J. Halley, S. V. Nicosia, W. J. Pledger, and J. Q. Cheng.** 2002. Phosphatidylinositol 3-kinase/Akt pathway regulates tuberous sclerosis tumor suppressor complex by phosphorylation of tuberin. J Biol Chem **277:**35364-70.

28. **Di Cristofano, A., and P. P. Pandolfi.** 2000. The multiple roles of PTEN in tumor suppression. Cell **100:**387-90.

29. **Di Cristofano, A., B. Pesce, C. Cordon-Cardo, and P. P. Pandolfi.** 1998. Pten is essential for embryonic development and tumour suppression. Nat Genet **19:**348-55.

30. **Diehl, J. A., M. Cheng, M. F. Roussel, and C. J. Sherr.** 1998. Glycogen synthase kinase-3beta regulates cyclin D1 proteolysis and subcellular localization. Genes Dev **12:**3499-511.

31. **Dormer, P., E. Spitzer, M. Frankenberger, and E. Kremmer.** 2004. Erythroid differentiation regulator (EDR), a novel, highly conserved factor I. Induction of haemoglobin synthesis in erythroleukaemic cells. Cytokine **26:**231-42.

32. **Easton, R. M., H. Cho, K. Roovers, D. W. Shineman, M. Mizrahi, M. S. Forman, V. M. Lee, M. Szabolcs, R. de Jong, T. Oltersdorf, T. Ludwig, A. Efstratiadis, and M. J. Birnbaum.** 2005. Role for Akt3/protein kinase Bgamma in attainment of normal brain size. Mol Cell Biol **25:**1869-78.

33. **Feng, J., J. Park, P. Cron, D. Hess, and B. A. Hemmings.** 2004. Identification of a PKB/Akt hydrophobic motif Ser-473 kinase as DNA-dependent protein kinase. J Biol Chem **279:**41189-96.

34. **Ferrannini, E.** 1998. Insulin resistance versus insulin deficiency in non-insulin-dependent diabetes mellitus: problems and prospects. Endocr Rev **19:**477-90.

35. **Garofalo, R. S., S. J. Orena, K. Rafidi, A. J. Torchia, J. L. Stock, A. L. Hildebrandt, T. Coskran, S. C. Black, D. J. Brees, J. R. Wicks, J. D. McNeish, and K. G. Coleman.** 2003. Severe diabetes, age-dependent loss of adipose tissue, and mild growth deficiency in mice lacking Akt2/PKB beta. J Clin Invest **112:**197-208.

36. **Gawienowski, A. M., P. J. Orsulak, M. Stacewicz-Sapuntzakis, and B. M. Joseph.** 1975. Presence of sex pheromone in preputial glands of male rats. J Endocrinol **67:**283-8.

37. **Hannan, K. M., Y. Brandenburger, A. Jenkins, K. Sharkey, A. Cavanaugh, L. Rothblum, T. Moss, G. Poortinga, G. A. McArthur, R. B. Pearson, and R. D. Hannan.** 2003. mTOR-dependent regulation of ribosomal gene transcription requires S6K1 and is mediated by phosphorylation of the carboxy-terminal activation domain of the nucleolar transcription factor UBF. Mol Cell Biol **23:**8862-77.

38. **Harrington, L. S., G. M. Findlay, A. Gray, T. Tolkacheva, S. Wigfield, H. Rebholz, J. Barnett, N. R. Leslie, S. Cheng, P. R. Shepherd, I. Gout, C. P. Downes, and R. F. Lamb.** 2004. The TSC1-2 tumor suppressor controls insulin-PI3K signaling via regulation of IRS proteins. J Cell Biol **166:**213-23.

39. **Harris, M. I., K. M. Flegal, C. C. Cowie, M. S. Eberhardt, D. E. Goldstein, R. R. Little, H. M. Wiedmeyer, and D. D. Byrd-Holt.** 1998. Prevalence of diabetes, impaired fasting glucose, and impaired glucose tolerance in U.S. adults. The Third National Health and Nutrition Examination Survey, 1988-1994. Diabetes Care **21:**518-24.

40. **Heron-Milhavet, L., C. Franckhauser, V. Rana, C. Berthenet, D. Fisher, B. A. Hemmings, A. Fernandez, and N. J. Lamb.** 2006. Only Akt1 is required for proliferation while Akt2 promotes cell cycle exit through p21 binding. Mol Cell Biol.

41. **Hutchinson, J., J. Jin, R. D. Cardiff, J. R. Woodgett, and W. J. Muller.** 2001. Activation of Akt (protein kinase B) in mammary epithelium provides a critical cell survival signal required for tumor progression. Mol Cell Biol **21:**2203-12.

42. **Hutchinson, J. N., J. Jin, R. D. Cardiff, J. R. Woodgett, and W. J. Muller.** 2004. Activation of Akt-1 (PKB-alpha) can accelerate ErbB-2-mediated mammary tumorigenesis but suppresses tumor invasion. Cancer Res **64:**3171-8.

43. **Ingersoll, D. W., K. T. Morley, M. Benvenga, and C. Hands.** 1986. An accessory sex gland aggression-promoting chemosignal in male mice. Behav Neurosci **100:**777-82.

44. **Inoki, K., Y. Li, T. Xu, and K. L. Guan.** 2003. Rheb GTPase is a direct target of TSC2 GAP activity and regulates mTOR signaling. Genes Dev **17:**1829-34.

45. **Inoki, K., Y. Li, T. Zhu, J. Wu, and K. L. Guan.** 2002. TSC2 is phosphorylated and inhibited by Akt and suppresses mTOR signalling. Nat Cell Biol **4:**648-57.

46. **Inoki, K., T. Zhu, and K. L. Guan.** 2003. TSC2 mediates cellular energy response to control cell growth and survival. Cell **115:**577-90.

47. **Jacinto, E., R. Loewith, A. Schmidt, S. Lin, M. A. Ruegg, A. Hall, and M. N. Hall.** 2004. Mammalian TOR complex 2 controls the actin cytoskeleton and is rapamycin insensitive. Nat Cell Biol **6:**1122-8.

48. **Jefferies, H. B., S. Fumagalli, P. B. Dennis, C. Reinhard, R. B. Pearson, and G. Thomas.** 1997. Rapamycin suppresses 5'TOP mRNA translation through inhibition of p70s6k. Embo J **16:**3693-704.

49. **Jetton, T. L., J. Lausier, K. LaRock, W. E. Trotman, B. Larmie, A. Habibovic, M. Peshavaria, and J. L. Leahy.** 2005. Mechanisms of compensatory beta-cell growth in insulin-resistant rats: roles of Akt kinase. Diabetes **54:**2294-304.

50. **Jiang, Z. Y., Q. L. Zhou, K. A. Coleman, M. Chouinard, Q. Boese, and M. P. Czech.** 2003. Insulin signaling through Akt/protein kinase B analyzed by small interfering RNA-mediated gene silencing. Proc Natl Acad Sci U S A **100:**7569-74.

51. **Jones, R. G., A. R. Elford, M. J. Parsons, L. Wu, C. M. Krawczyk, W. C. Yeh, R. Hakem, R. Rottapel, J. R. Woodgett, and P. S. Ohashi.** 2002. CD28-dependent activation of protein kinase B/Akt blocks Fas-mediated apoptosis by preventing death-inducing signaling complex assembly. J Exp Med **196:**335-48.

52. **Kim, Y. K., S. J. Kim, A. Yatani, Y. Huang, G. Castelli, D. E. Vatner, J. Liu, Q. Zhang, G. Diaz, R. Zieba, J. Thaisz, A. Drusco, C. Croce, J. Sadoshima, G. Condorelli, and S. F. Vatner.** 2003. Mechanism of enhanced cardiac function in mice with hypertrophy induced by overexpressed Akt. J Biol Chem **278:**47622-8.

53. **Knobbe, C. B., J. Reifenberger, B. Blaschke, and G. Reifenberger.** 2004. Hypermethylation and transcriptional downregulation of the carboxyl-terminal modulator protein gene in glioblastomas. J Natl Cancer Inst **96:**483-6.

54. **Kohn, A. D., S. A. Summers, M. J. Birnbaum, and R. A. Roth.** 1996. Expression of a constitutively active Akt Ser/Thr kinase in 3T3-L1 adipocytes stimulates glucose uptake and glucose transporter 4 translocation. J Biol Chem **271:**31372-8.

55. **Kotani, K., W. Ogawa, M. Matsumoto, T. Kitamura, H. Sakaue, Y. Hino, K. Miyake, W. Sano, K. Akimoto, S. Ohno, and M. Kasuga.** 1998. Requirement of atypical protein kinase clambda for insulin stimulation of glucose uptake but not for Akt activation in 3T3-L1 adipocytes. Mol Cell Biol **18:**6971-82.

56. **Kubota, N., K. Tobe, Y. Terauchi, K. Eto, T. Yamauchi, R. Suzuki, Y. Tsubamoto, K. Komeda, R. Nakano, H. Miki, S. Satoh, H. Sekihara, S. Sciacchitano, M. Lesniak, S. Aizawa, R. Nagai, S. Kimura, Y. Akanuma, S. I. Taylor, and T. Kadowaki.** 2000. Disruption of insulin receptor substrate 2 causes type 2 diabetes because of liver insulin resistance and lack of compensatory beta-cell hyperplasia. Diabetes **49:**1880-9.

57. **Kumar, C. C., and V. Madison.** 2005. AKT crystal structure and AKT-specific inhibitors. Oncogene **24:**7493-501.

58. **Kwiatkowski, D. J., and B. D. Manning.** 2005. Tuberous sclerosis: a GAP at the crossroads of multiple signaling pathways. Hum Mol Genet **14 Spec No. 2:**R251-8.

59. **Liang, J., and J. M. Slingerland.** 2003. Multiple roles of the PI3K/PKB (Akt) pathway in cell cycle progression. Cell Cycle **2:**339-45.

60. **Liang, J., J. Zubovitz, T. Petrocelli, R. Kotchetkov, M. K. Connor, K. Han, J. H. Lee, S. Ciarallo, C. Catzavelos, R. Beniston, E. Franssen, and J. M. Slingerland.** 2002. PKB/Akt phosphorylates p27, impairs nuclear import of p27 and opposes p27-mediated G1 arrest. Nat Med **8:**1153-60.

61. **Lindsley, C. W., Z. Zhao, W. H. Leister, R. G. Robinson, S. F. Barnett, D. Defeo-Jones, R. E. Jones, G. D. Hartman, J. R. Huff, H. E. Huber, and M. E. Duggan.** 2005. Allosteric Akt (PKB) inhibitors: discovery and SAR of isozyme selective inhibitors. Bioorg Med Chem Lett **15:**761-4.

62. **Liu, J. P., J. Baker, A. S. Perkins, E. J. Robertson, and A. Efstratiadis.** 1993. Mice carrying null mutations of the genes encoding insulin-like growth factor I (Igf-1) and type 1 IGF receptor (Igf1r). Cell **75:**59-72.

63. **Long, X., Y. Lin, S. Ortiz-Vega, K. Yonezawa, and J. Avruch.** 2005. Rheb binds and regulates the mTOR kinase. Curr Biol **15:**702-13.

64. **Ma, L., Z. Chen, H. Erdjument-Bromage, P. Tempst, and P. P. Pandolfi.** 2005. Phosphorylation and functional inactivation of TSC2 by Erk implications for tuberous sclerosis and cancer pathogenesis. Cell **121:**179-93.

65. **Maira, S. M., I. Galetic, D. P. Brazil, S. Kaech, E. Ingley, M. Thelen, and B. A. Hemmings.** 2001. Carboxyl-terminal modulator protein (CTMP), a negative regulator of PKB/Akt and v-Akt at the plasma membrane. Science **294:**374-80.

66. **Majumder, P. K., J. J. Yeh, D. J. George, P. G. Febbo, J. Kum, Q. Xue, R. Bikoff, H. Ma, P. W. Kantoff, T. R. Golub, M. Loda, and W. R. Sellers.** 2003. Prostate intraepithelial neoplasia induced by prostate restricted Akt activation: the MPAKT model. Proc Natl Acad Sci U S A **100:**7841-6.

67. **Malstrom, S., E. Tili, D. Kappes, J. D. Ceci, and P. N. Tsichlis.** 2001. Tumor induction by an Lck-MyrAkt transgene is delayed by mechanisms controlling the size of the thymus. Proc Natl Acad Sci U S A **98:**14967-72.

68. **Manning, B. D., A. R. Tee, M. N. Logsdon, J. Blenis, and L. C. Cantley.** 2002. Identification of the tuberous sclerosis complex-2 tumor suppressor gene product tuberin as a target of the phosphoinositide 3-kinase/akt pathway. Mol Cell **10:**151-62.

69. **Matsui, T., L. Li, J. C. Wu, S. A. Cook, T. Nagoshi, M. H. Picard, R. Liao, and A. Rosenzweig.** 2002. Phenotypic spectrum caused by transgenic overexpression of activated Akt in the heart. J Biol Chem **277:**22896-901.

70. **Matsui, T., T. Nagoshi, E. G. Hong, I. Luptak, K. Hartil, L. Li, N. Gorovits, M. J. Charron, J. K. Kim, R. Tian, and A. Rosenzweig.**

2006. Effects of chronic Akt activation on glucose uptake in the heart. Am J Physiol Endocrinol Metab **290:**E789-97.

71. **Meijer, A. J., and P. Codogno.** 2004. Regulation and role of autophagy in mammalian cells. Int J Biochem Cell Biol **36:**2445-62.

72. **Mende, I., S. Malstrom, P. N. Tsichlis, P. K. Vogt, and M. Aoki.** 2001. Oncogenic transformation induced by membrane-targeted Akt2 and Akt3. Oncogene **20:**4419-23.

73. **Montagne, J., M. J. Stewart, H. Stocker, E. Hafen, S. C. Kozma, and G. Thomas.** 1999. Drosophila S6 kinase: a regulator of cell size. Science **285:**2126-9.

74. **Morey, C., and W. Bickmore.** 2006. Sealed with a X. Nat Cell Biol **8:**207-9.

75. **Mothe-Satney, I., G. J. Brunn, L. P. McMahon, C. T. Capaldo, R. T. Abraham, and J. C. Lawrence, Jr.** 2000. Mammalian Target of Rapamycin-dependent Phosphorylation of PHAS-I in Four (S/T)P Sites Detected by Phospho-specific Antibodies. J. Biol. Chem. **275:**33836-33843.

76. **Na, S. Y., A. Patra, Y. Scheuring, A. Marx, M. Tolaini, D. Kioussis, B. A. Hemmings, T. Hunig, and U. Bommhardt.** 2003. Constitutively active protein kinase B enhances Lck and Erk activities and influences thymocyte selection and activation. J Immunol **171:**1285-96.

77. **Nakatani, K., D. A. Thompson, A. Barthel, H. Sakaue, W. Liu, R. J. Weigel, and R. A. Roth.** 1999. Up-regulation of Akt3 in estrogen receptor-deficient breast cancers and androgen-independent prostate cancer lines. J Biol Chem **274:**21528-32.

78. **Okumura, E., T. Fukuhara, H. Yoshida, S. Hanada Si, R. Kozutsumi, M. Mori, K. Tachibana, and T. Kishimoto.** 2002. Akt inhibits Myt1 in the signalling pathway that leads to meiotic G2/M-phase transition. Nat Cell Biol **4:**111-6.

79. **Olefsky, J. M., and J. J. Nolan.** 1995. Insulin resistance and non-insulin-dependent diabetes mellitus: cellular and molecular mechanisms. Am J Clin Nutr **61:**980S-986S.

80. **Patra, A. K., S. Y. Na, and U. Bommhardt.** 2004. Active protein kinase B regulates TCR responsiveness by modulating cytoplasmic-nuclear localization of NFAT and NF-kappa B proteins. J Immunol **172:**4812-20.

81. **Pedrero, J. M., D. G. Carracedo, C. M. Pinto, A. H. Zapatero, J. P. Rodrigo, C. S. Nieto, and M. V. Gonzalez.** 2005. Frequent genetic and biochemical alterations of the PI 3-K/AKT/PTEN pathway in head and neck squamous cell carcinoma. Int J Cancer **114:**242-8.

82. **Peng, X. D., P. Z. Xu, M. L. Chen, A. Hahn-Windgassen, J. Skeen, J. Jacobs, D. Sundararajan, W. S. Chen, S. E. Crawford, K. G. Coleman, and N. Hay.** 2003. Dwarfism, impaired skin development, skeletal muscle atrophy, delayed bone development, and impeded adipogenesis in mice lacking Akt1 and Akt2. Genes Dev **17:**1352-65.

83. **Petersen, K. F., and G. I. Shulman.** 2006. Etiology of insulin resistance. Am J Med **119:**S10-6.

84. **Potter, C. J., L. G. Pedraza, and T. Xu.** 2002. Akt regulates growth by directly phosphorylating Tsc2. Nat Cell Biol **4:**658-65.

85. **Prentki, M., and C. J. Nolan.** 2006. Islet beta cell failure in type 2 diabetes. J Clin Invest **116:**1802-12.

86. **Raho, G., V. Barone, D. Rossi, L. Philipson, and V. Sorrentino.** 2000. The gas 5 gene shows four alternative splicing patterns without coding for a protein. Gene **256:**13-7.

87. **Rathmell, J. C., R. L. Elstrom, R. M. Cinalli, and C. B. Thompson.** 2003. Activated Akt promotes increased resting T cell size, CD28-independent T cell growth, and development of autoimmunity and lymphoma. Eur J Immunol **33:**2223-32.

88. **Raught, B., F. Peiretti, A. C. Gingras, M. Livingstone, D. Shahbazian, G. L. Mayeur, R. D. Polakiewicz, N. Sonenberg, and J. W. Hershey.** 2004. Phosphorylation of eucaryotic translation initiation factor 4B Ser422 is modulated by S6 kinases. Embo J **23:**1761-9.

89. **Roux, P. P., B. A. Ballif, R. Anjum, S. P. Gygi, and J. Blenis.** 2004. Tumor-promoting phorbol esters and activated Ras inactivate the tuberous sclerosis tumor suppressor complex via p90 ribosomal S6 kinase. Proc Natl Acad Sci U S A **101:**13489-94.

90. **Ruvinsky, I., and O. Meyuhas.** 2006. Ribosomal protein S6 phosphorylation: from protein synthesis to cell size. Trends Biochem Sci **31:**342-8.

91. **Sano, H., S. Kane, E. Sano, C. P. Miinea, J. M. Asara, W. S. Lane, C. W. Garner, and G. E. Lienhard.** 2003. Insulin-stimulated phosphorylation of a Rab GTPase-activating protein regulates GLUT4 translocation. J Biol Chem **278:**14599-602.

92. **Sansal, I., and W. R. Sellers.** 2004. The biology and clinical relevance of the PTEN tumor suppressor pathway. J Clin Oncol **22:**2954-63.

93. **Sarbassov, D. D., S. M. Ali, and D. M. Sabatini.** 2005. Growing roles for the mTOR pathway. Curr Opin Cell Biol **17:**596-603.

94. **Sarbassov, D. D., D. A. Guertin, S. M. Ali, and D. M. Sabatini.** 2005. Phosphorylation and regulation of Akt/PKB by the rictor-mTOR complex. Science **307:**1098-101.

95. **Saucedo, L. J., X. Gao, D. A. Chiarelli, L. Li, D. Pan, and B. A. Edgar.** 2003. Rheb promotes cell growth as a component of the insulin/TOR signalling network. Nat Cell Biol **5:**566-71.

96. **Schlegel, J., G. Piontek, and H. D. Mennel.** 2002. Activation of the anti-apoptotic Akt/protein kinase B pathway in human malignant gliomas in vivo. Anticancer Res **22:**2837-40.

97. **Schubert, M., D. P. Brazil, D. J. Burks, J. A. Kushner, J. Ye, C. L. Flint, J. Farhang-Fallah, P. Dikkes, X. M. Warot, C. Rio, G. Corfas,**

and M. F. White. 2003. Insulin receptor substrate-2 deficiency impairs brain growth and promotes tau phosphorylation. J Neurosci **23:**7084-92.

98. **Schwertfeger, K. L., J. L. McManaman, C. A. Palmer, M. C. Neville, and S. M. Anderson.** 2003. Expression of constitutively activated Akt in the mammary gland leads to excess lipid synthesis during pregnancy and lactation. J Lipid Res **44:**1100-12.

99. **Schwertfeger, K. L., M. M. Richert, and S. M. Anderson.** 2001. Mammary gland involution is delayed by activated Akt in transgenic mice. Mol Endocrinol **15:**867-81.

100. **Sesti, G., M. Federici, M. L. Hribal, D. Lauro, P. Sbraccia, and R. Lauro.** 2001. Defects of the insulin receptor substrate (IRS) system in human metabolic disorders. Faseb J **15:**2099-111.

101. **Shayesteh, L., Y. Lu, W. L. Kuo, R. Baldocchi, T. Godfrey, C. Collins, D. Pinkel, B. Powell, G. B. Mills, and J. W. Gray.** 1999. PIK3CA is implicated as an oncogene in ovarian cancer. Nat Genet **21:**99-102.

102. **Shima, H., M. Pende, Y. Chen, S. Fumagalli, G. Thomas, and S. C. Kozma.** 1998. Disruption of the p70(s6k)/p85(s6k) gene reveals a small mouse phenotype and a new functional S6 kinase. Embo J **17:**6649-59.

103. **Shioi, T., J. R. McMullen, P. M. Kang, P. S. Douglas, T. Obata, T. F. Franke, L. C. Cantley, and S. Izumo.** 2002. Akt/protein kinase B promotes organ growth in transgenic mice. Mol Cell Biol **22:**2799-809.

104. **Stolovich, M., H. Tang, E. Hornstein, G. Levy, R. Cohen, S. S. Bae, M. J. Birnbaum, and O. Meyuhas.** 2002. Transduction of growth or mitogenic signals into translational activation of TOP mRNAs is fully reliant on the phosphatidylinositol 3-kinase-mediated pathway but requires neither S6K1 nor rpS6 phosphorylation. Mol Cell Biol **22:**8101-13.

105. **Suzuki, A., J. L. de la Pompa, V. Stambolic, A. J. Elia, T. Sasaki, I. del Barco Barrantes, A. Ho, A. Wakeham, A. Itie, W. Khoo, M. Fukumoto, and T. W. Mak.** 1998. High cancer susceptibility and embryonic lethality associated with mutation of the PTEN tumor suppressor gene in mice. Curr Biol **8:**1169-78.

106. **Tamemoto, H., T. Kadowaki, K. Tobe, T. Yagi, H. Sakura, T. Hayakawa, Y. Terauchi, K. Ueki, Y. Kaburagi, S. Satoh, and et al.** 1994. Insulin resistance and growth retardation in mice lacking insulin receptor substrate-1. Nature **372:**182-6.

107. **Tschopp, O., Z. Z. Yang, D. Brodbeck, B. A. Dummler, M. Hemmings-Mieszczak, T. Watanabe, T. Michaelis, J. Frahm, and B. A. Hemmings.** 2005. Essential role of protein kinase B gamma (PKB gamma/Akt3) in postnatal brain development but not in glucose homeostasis. Development **132:**2943-54.

108. **Tuttle, R. L., N. S. Gill, W. Pugh, J. P. Lee, B. Koeberlein, E. E. Furth, K. S. Polonsky, A. Naji, and M. J. Birnbaum.** 2001. Regulation of pancreatic beta-cell growth and survival by the serine/threonine protein kinase Akt1/PKBalpha. Nat Med **7:**1133-7.

109. **Viglietto, G., M. L. Motti, P. Bruni, R. M. Melillo, A. D'Alessio, D. Califano, F. Vinci, G. Chiappetta, P. Tsichlis, A. Bellacosa, A. Fusco, and M. Santoro.** 2002. Cytoplasmic relocalization and inhibition of the cyclin-dependent kinase inhibitor p27(Kip1) by PKB/Akt-mediated phosphorylation in breast cancer. Nat Med **8:**1136-44.

110. **Walker, K. S., M. Deak, A. Paterson, K. Hudson, P. Cohen, and D. R. Alessi.** 1998. Activation of protein kinase B beta and gamma isoforms by insulin in vivo and by 3-phosphoinositide-dependent protein kinase-1 in vitro: comparison with protein kinase B alpha. Biochem J **331 (Pt 1):**299-308.

111. **Warram, J. H., B. C. Martin, A. S. Krolewski, J. S. Soeldner, and C. R. Kahn.** 1990. Slow glucose removal rate and hyperinsulinemia precede the development of type II diabetes in the offspring of diabetic parents. Ann Intern Med **113:**909-15.

112. **Withers, D. J., D. J. Burks, H. H. Towery, S. L. Altamuro, C. L. Flint, and M. F. White.** 1999. Irs-2 coordinates Igf-1 receptor-mediated beta-cell development and peripheral insulin signalling. Nat Genet **23:**32-40.

113. **Withers, D. J., J. S. Gutierrez, H. Towery, D. J. Burks, J. M. Ren, S. Previs, Y. Zhang, D. Bernal, S. Pons, G. I. Shulman, S. Bonner-Weir, and M. F. White.** 1998. Disruption of IRS-2 causes type 2 diabetes in mice. Nature **391:**900-4.

114. **Xu, X., M. Sakon, H. Nagano, N. Hiraoka, H. Yamamoto, N. Hayashi, K. Dono, S. Nakamori, K. Umeshita, Y. Ito, N. Matsuura, and M. Monden.** 2004. Akt2 expression correlates with prognosis of human hepatocellular carcinoma. Oncol Rep **11:**25-32.

115. **Yamada, E., S. Okada, T. Saito, K. Ohshima, M. Sato, T. Tsuchiya, Y. Uehara, H. Shimizu, and M. Mori.** 2005. Akt2 phosphorylates Synip to regulate docking and fusion of GLUT4-containing vesicles. J Cell Biol **168:**921-8.

116. **Yang, J., P. Cron, V. Thompson, V. M. Good, D. Hess, B. A. Hemmings, and D. Barford.** 2002. Molecular mechanism for the regulation of protein kinase B/Akt by hydrophobic motif phosphorylation. Mol Cell **9:**1227-40.

117. **Yang, Z. Z., O. Tschopp, N. Di-Poi, E. Bruder, A. Baudry, B. Dummler, W. Wahli, and B. A. Hemmings.** 2005. Dosage-dependent effects of Akt1/protein kinase Balpha (PKBalpha) and Akt3/PKBgamma on thymus, skin, and cardiovascular and nervous system development in mice. Mol Cell Biol **25:**10407-18.

118. **Yang, Z. Z., O. Tschopp, M. Hemmings-Mieszczak, J. Feng, D. Brodbeck, E. Perentes, and B. A. Hemmings.** 2003. Protein kinase B alpha/Akt1 regulates placental development and fetal growth. J Biol Chem **278:**32124-31.

119. **Zhang, Y., X. Gao, L. J. Saucedo, B. Ru, B. A. Edgar, and D. Pan.** 2003. Rheb is a direct target of the tuberous sclerosis tumour suppressor proteins. Nat Cell Biol **5:**578-81.

120. **Zhou, B. P., Y. Liao, W. Xia, B. Spohn, M. H. Lee, and M. C. Hung.** 2001. Cytoplasmic localization of p21Cip1/WAF1 by Akt-induced phosphorylation in HER-2/neu-overexpressing cells. Nat Cell Biol **3:**245-52.

V. ACKNOWLEDGEMENTS

I would like to thank….

…Dr. Brian A. Hemmings for giving me the unique opportunity to do my Ph.D. in his laboratory and for his invaluable support throughout this work. His enthusiasm for science and his critical scientific thinking have been a guide for me to develop my scientific and intellectual skills. I am extremely grateful for the vast experience I gained in his lab on all aspects of scientific research.

…Alex Hergovich, Derek Brazil, and the many other people at FMI who have helped me during my Ph.D. study with a lot of constructive advice and encouragement.

…Debby Hynx for her fantastic support and expertise in conducting *in vivo* experiments; and also for management of our mice strains.

…Prof. Nancy Hynes and Prof. Christoph Moroni for agreeing to be on my thesis committee as Ko-Referentin and Fakultaetsverantwortlicher, respectively, and for their constructive advice during our meetings.

…Prof. Matthias Wymann and Prof. Patrick Matthias for agreeing to function as external expert and chairman, respectively, on my thesis exam.

…Krebsliga Schweiz (Oncosuisse) for supporting this work (KFS 1167-09-2001 and KFS 01002-02-2000).

VI. APPENDIX

Part 1:

Dissecting the physiological functions of CTMP1 and CTMP2 proteins by generation and analysis of loss-of-function mice models.

Dummler B, Brazil DP, Hemmings BA.

(Fragmental project containing unpublished results)

Dissecting the physiological functions of CTMP1 and CTMP2 proteins by generation and analysis of loss-of-function mice models

Introduction

Among the plethora of PKB binding partners, our group identified the C-terminal modulator protein (CTMP1), as a novel PKB-binding protein. Recently, we also identified and cloned a CTMP1-related protein, CTMP2. Both CTMP1 and CTMP2 are conserved in higher eukaryotes but not present in drosophila or C.elegans (Fig. 1).

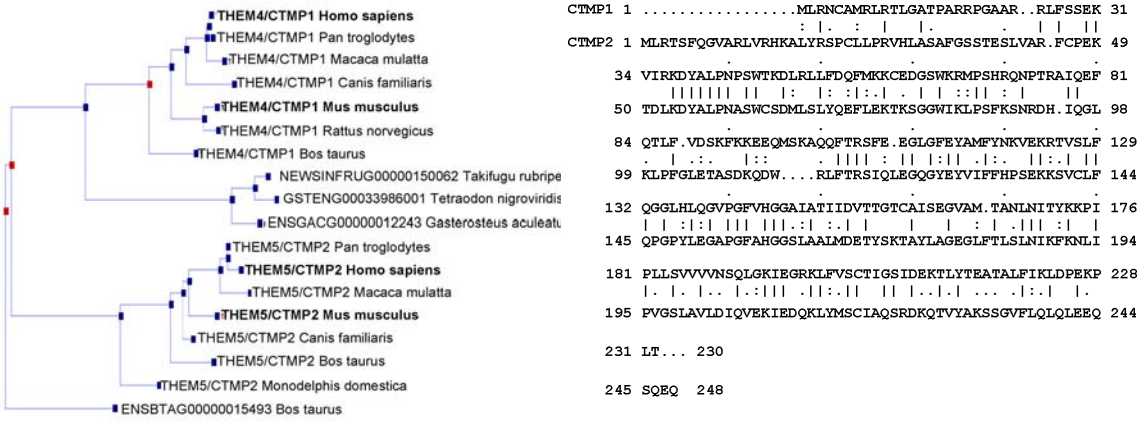

Fig. 1. (Left) Conservation of CTMP proteins across species (from www.ensembl.org, GeneTreeView). (Right) Sequence alignment of mouse CTMP1 and CTMP2. The two proteins have ~30% sequence identity and >50% similarity.

CTMP1 and CTMP2 have also been termed THEM4 (thioesterase superfamily member 4) and THEM5 (thioesterase superfamily member 5), respectively, because they contain a putative thioesterase domain called 4HBT[6] domain (4-

[6] 4HBT is an enzyme found in Pseudomonas and catalyzes the final step in the biosynthesis of 4-hydroxybenzoate from 4-chlorobenzoate as part of the bacterial 2,4-dichlorobenzoate degradation pathway. A 4HBT domain is also present in other mammalian proteins, such as thioesterase superfamily member 2 (THEM2) or acyl-CoA thioesterases (Acot7, Acot11, Acot12) that catalyze the hydrolysis of acyl-CoAs to free fatty acid and coenzyme A (CoASH).

hydroxybenzoyl-CoA thioesterase domain). The most N-terminal ~25 amino acid residues of both CTMP1 and CTMP2 are predicted to function as a mitochondrial targeting sequence (TargetP software from Emanuelsson *et al.*, 2000). Cell fractionation and immunoctyochemistry showed clearly that the major cellular pool of hCTMP1 protein is localized in the mitochondria (Fig. 2; Tintignac *et al.*, unpublished).

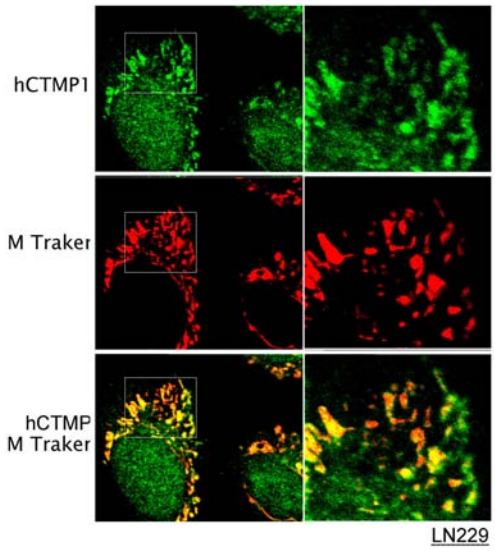

Fig. 2. The major pool of endogenous CTMP1 is localized in the mitochondria. Endogenous CTMP1 co-localizes with MitoTracker dye, a mitochondrial-selective fluorescent label (from L.Tintignac).

In most cases, the mitochondrial targeting sequence of an imported protein is proteolytically removed during or after the entry of the protein into the mitochondrion. Cleavage is mediated by the mitochondrial processing peptidase (MPP) that recognizes a consensus sequence characterized by an Arg in position -2 or -3 relative to the cleavage site. CTMP1 contains a highly probable MPP-cleavage site following the mitochondrial targeting sequence, with cleavage occurring after amino acid residue 36 and 27 for hCTMP1 and mCTMP1, respectively; in CTMP2 this cleavage site is not conserved and there is only a low predicted probability for MPP to cleave after residue 35. Cleavage of CTMP1 can be detected by immunoblotting and the introduction of point mutations within the MPP cleavage site abolishes proteolytic processing of

CTMP1 (Tintignac *et al.*, unpublished). In summary, these findings suggest that CTMP1 protein (and very likely also CTMP2), is synthesized as a 27kDa precursor in the cytosol, translocated into the mitochondria and processed by the MPP in a 25kDa mature protein (missing the 36 first amino acids).

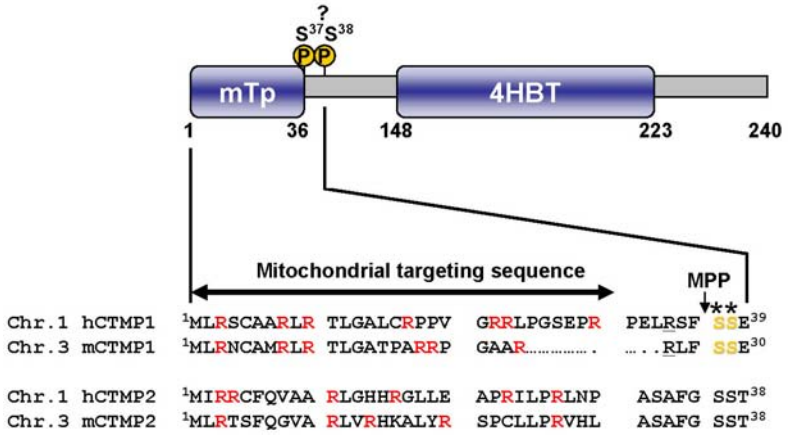

Fig. 3. Domain structure of CTMP proteins. Both CTMP1 and CTMP2 contain an N-terminal, ~25 amino acid residues long, mitochondrial targeting peptide (mTp) and a 4HBT domain. In CTMP1 this peptide is followed by a MPP (mitochondrial processing peptidase) cleavage site. Mitochondrial targeting sequences do not share distinct consensus sequences but display common physicochemical properties, they are rich in positively charged residues (mainly Arg) and have the potential to form an amphiphilic helical structure. (*) indicates potential phosphorylation sites. Ser37 and Ser38 were identified as *in-vivo* phosphorylation sites following pervanadate treatment in hCTMP1.

When containing an N-terminal tag, such as FLAG or HA, CTMP proteins do not translocate to the mitochondria but remain mostly in the cytosol. Presumably, the tag is interfering with recognition of the mitochondrial targeting sequence. Such cytosolic CTMP binds to PKB at the plasma membrane and reduces PKB activity by preventing its phosphorylation (65). Furthermore, cells transformed with v-Akt[7] undergo phenotypic reversion when CTMP is stably expressed, due to decreased PKB activity, and also exhibit significantly

[7] The transforming oncogene v-Akt is the viral homolog of PKB. V-akt encodes a fusion protein between the viral protein Gag and full-length cellular PKBα. The viral gag domain in v-Akt possesses a myristoylation signal that mediates targeting of the fusion protein to the plasma membrane, leading to constitutive activation of PKB. CCL64 mink lung cells stably expressing v-Akt (AKT8 cells) form tumors when injected into nude mice.

reduced tumor-forming ability in nude mice (65). Therefore, CTMP is predicted to serve a tumor suppressor-like role by virtue of its negative regulation of PKB in cells. A recent report supports this function of CTMP as a tumor-suppressor-like protein. Knobbe *et al.* found significantly reduced CTMP1 mRNA expression in 40% of primary glioblastomas and reduced mRNA levels were closely associated with hypermethylation of the CTMP1 promoter (53). This suggests that downregulation of CTMP1 expression is an important molecular mechanism involved in the pathogenesis of glioblastoma.

Biochemical characterization of the interaction between PKB and CTMP1 showed that CTMP1 binds to the most C-terminal ~15 amino acids of PKB (Hanada *et al.*, unpublished). This sequence contains the Ser473 phosphorylation site, which has to be phosphorylated for maximal activity of PKB. It is likely, that binding of CTMP1 to Ser473 blocks the access for activating kinases and thereby inhibits Ser473 phosphorylation. Of the three PKB isoforms, both CTMP1 and CTMP2 appear to preferentially bind PKBα (Hanada *et al.*, unpublished). Furthermore, CTMP1 and CTMP2 form homo- and heterodimers in cells through the conserved 4HBT-domain found in both proteins (Hanada *et al.*, unpublished).

Results and discussion

Physiological function of CTMP1

CTMP1 protein is highly expressed in brain, heart, liver, kidney and testis in wild type mice (Fig. 4). This protein expression pattern of CTMP1 differs slightly from the mRNA expression pattern previously described in human tissues (63) but is consistent with high expression in brain, kidney, and testis.

To dissect CTMP1 gene function in a vertebrate model, we have generated mice deficient in CTMP1 (Fig. 5). CTMP1 knockout mice were viable and fertile and did not display any gross abnormalities. Histomorphological analysis

showed increased erythropoiesis and granulopoiesis in spleen [8] and bone marrow of CTMP1$^{-/-}$ mice; in some knockout animals this was accompanied with a marked increase in spleen weight (data not shown, collaboration with Daniel Roth and Anne Provencher-Bolliger, Novartis).

Wild type tissue	CTMP1 protein expression
Brain	+++
Heart	++
Lung	-
Liver	++
Spleen	-
Kidney	++
Skel. Muscle	+/-
Fat	-
Testis	+++
MEFs	+/-
ES cells	+/-

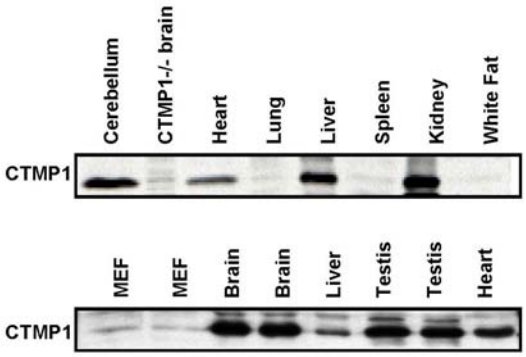

Fig. 4. Detection of CTMP1 protein in tissue and cell lysates shows high expression in brain, liver, kidney, heart, and testis. Table (left) summarizes results from various experiments where CTMP1 expression was detected in wild type tissue and cell line lysates by immunoblotting with anti-CTMP1 antibody (Ab99390). Expression levels: +++: high; ++: medium; +/- very low; - not detectable.

Interestingly, we could not detect any CTMP1 protein expression in spleen tissue lysates, indicating that these findings may be a secondary effect due to some other disturbance. So far, changes in the hematopoietic system appear to be the major phenotype of CTMP1$^{-/-}$ mice.

As we have previously observed that CTMP1 can inhibit PKB phosphorylation, we expected that the absence of CTMP1 protein in the mutant mice would lead to increased phosphorylation of PKB. To investigate this hypothesis, we examined steady-state phospho-PKB levels in mutant mice in tissues that exhibit high CTMP1 expression in wild type mice. In all examined tissues (brain, heart, liver, and kidney) no difference in PKB phospho-Ser473 levels

[8] In mice hematopoiesis not only occurs in the bone marrow but also at extramedullary sites, especially in the spleen.

could be observed in CTMP1$^{-/-}$ compared to CTMP1$^{+/+}$ mice (data not shown). Next, we generated primary cultures of mouse embryonic fibroblasts (MEFs) to study inducible PKB activation in an in vitro cellular system. MEFs were deprived of serum over night and then stimulated with 10% fetal calf serum (FCS) which leads to a clear induction of PKB phosphorylation (Fig. 6). Induction of PKB phospho-Ser473 and phospho-Thr308 was similar in both CTMP1$^{+/+}$ and CTMP1$^{-/-}$ MEF clones. Thus, CTMP1 ablation does not affect PKB phosphorylation in these cells.

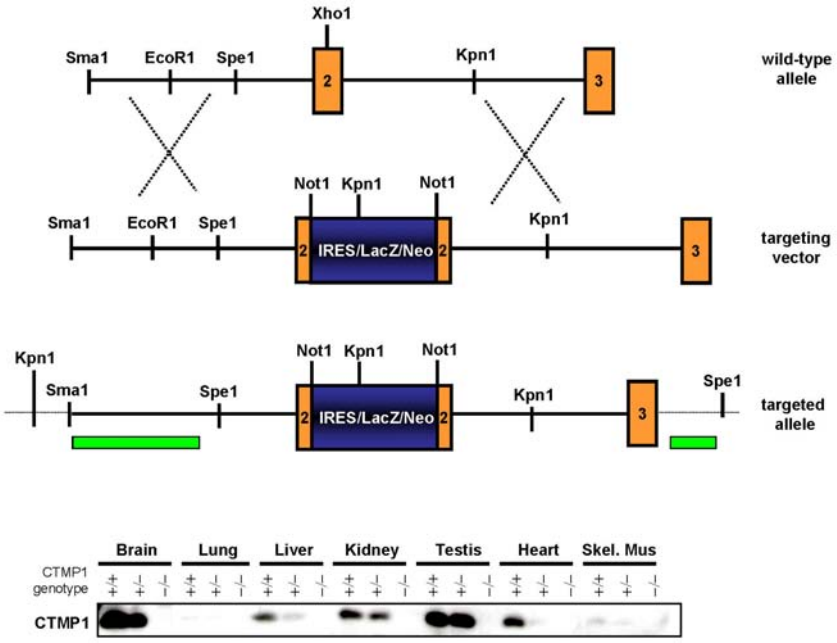

Fig. 5. Targeted disruption of CTMP1 in mice (Brazil et al., unpublished). Homologous recombination with the targeting vector results in disruption of exon 2 in the CTMP1 gene and introduces a translational frame shift (green boxes: internal and external probes). In mice homozygous for the targeted allele, expression of CTMP1 protein was not detectable with CTMP1-specific antibody (bottom, Ab99390). Thus, the targeted disruption resulted in a functional null allele.

Considering the intracellular localization of CTMP1, we are now investigating whether CTMP1-mediated inhibition of PKB may take place upon its release from the mitochondria under apoptosis inducing conditions (A. Parcellier and L. Tintignac, unpublished). Alternatively, we cannot exclude that the *in vivo* function of CTMP1 differs from its function observed in previous overexpression studies with N-terminally tagged (cytosolic) CTMP1.

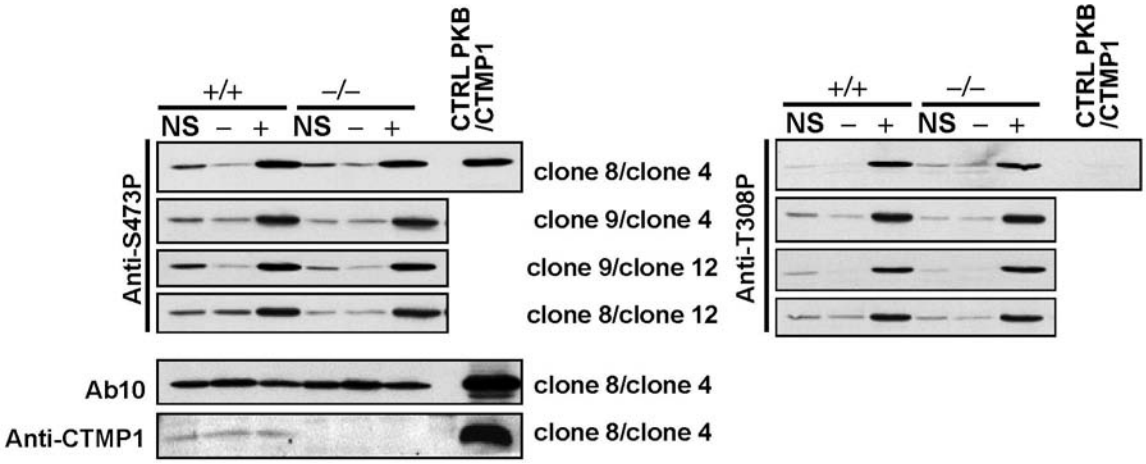

Fig. 6. Activation of PKB in CTMP1$^{-/-}$ MEFs. CTMP1$^{-/-}$ (clone 4 and 12) and CTMP1$^{+/+}$ (clone 8 and 9) MEFs were generated from littermate E12.5 embryos. MEFs (passage 4) growing in 10% FCS (NS), serum-deprived over night (-), and stimulated after serum-deprivation with 10% FCS for 20' (+), were blotted with anti-Phospho-Ser473 (left) and anti-Phospho-Thr308 antibody (right). Protein expression levels of PKB and CTMP1 were detected with Ab10 and Ab99390, respectively.

We also analyzed gene expression patterns in two tissues with high CTMP1 expression, brain and kidney, to detect whether CTMP1-deficiency leads to changes in gene expression (Table 1). In both brain and kidney of CTMP1$^{-/-}$ mice, erythroid differentiation regulator (Edr) was upregulated more than 2-fold. This is a autocrine factor produced in many tissues and released from cells in response to various stressful conditions. It may promote cell survival and growth (31). Other genes whose expression was changed in CTMP1$^{-/-}$ mice in both organs are growth arrest specific 5 (Gas5) and inactive X specific transcripts (Xist), expression of both genes was significantly upregulated. The RNAs of these two genes are assumed to be non-protein-coding RNAs. Xist is implicated in the process of X-inactivation(74); whether gas5 RNA has any regulatory function is not clear (86). Strongly upregulated in CTMP1$^{-/-}$ kidney was also 3-β-hydroxy-delta(5)-steroid dehydrogenase type 2. Hydroxy-steroid-dehydrogenases play crucial roles in the biosynthesis of all classes of hormonal steroids; 3-β-hydroxy-delta(5)-steroid dehydrogenase type 2 is mainly expressed in liver and kidney.

Physiological function of CTMP2

The mild phenotype observed in CTMP1$^{-/-}$ mice may be due to a compensation by the recently identified CTMP1-paralogue CTMP2. We first wanted to assess in which tissues CTMP2 is expressed in mice and whether its expression is upregulated in CTMP1$^{-/-}$ mice. CTMP2 mRNA levels were analyzed by Northern blotting and semi-quantitative RT-PCR (Fig. 7).

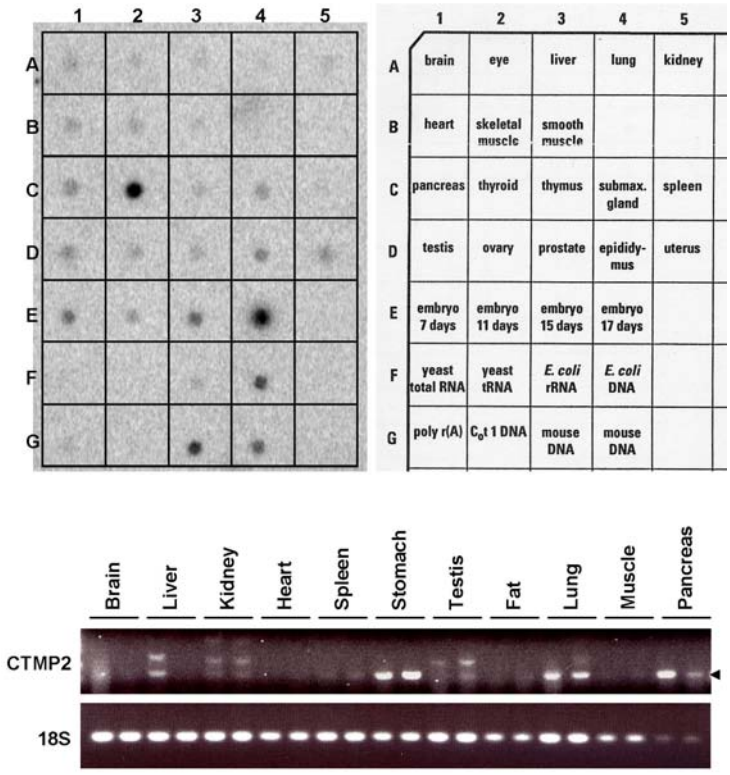

Fig. 7. mRNA expression levels of CTMP2 in various tissues. (Top) A commercial northern blot (RNA Master Blot, Clonetech) was hybridized with cDNA probe for mCTMP2. (Bottom) RNA was purified from indicated organs (first lane CTMP1$^{-/-}$ and second lane CTMP1$^{+/+}$). Reverse transcription was performed to obtain cDNA from which CTMP2 cDNA was amplified with forward primer 5'-CAC AGA GTC CCT GGT TGC AAG AT-3' and reverse primer 5'-GGC CCT GGA TAT GAT CTC TGT TG-3'. The resulting product is ~180 bp; forward primer stretches over exon1/exon2 border. A control PCR on mCTMP2 plasmid DNA resulted in a product on the same height as indicating arrow head. In a second wild type mouse, expression of CTMP2 in cDNA of heart could also be detected (data not shown). 18s internal control primers: forward 5'-CCT GGA TAC CGC AGC TAG GA-3' and reverse 5'-GCG GCG CAA TAC GAA TGC CCC-3'.

CTMP2 expression could be detected in various tissues (mainly liver, kidney, stomach, lung, pancreas, thyroid gland) and overall tissue distribution shows partial overlap with CTMP1 expression. From the preliminary results it appears that CTMP2 mRNA is not generally upregulated in CTMP1$^{-/-}$ tissues (Fig. 7). Whether the difference in CTMP2 mRNA levels between CTMP1$^{-/-}$ and CTMP1$^{+/+}$ liver is real or incidental needs to be confirmed with further experiments.

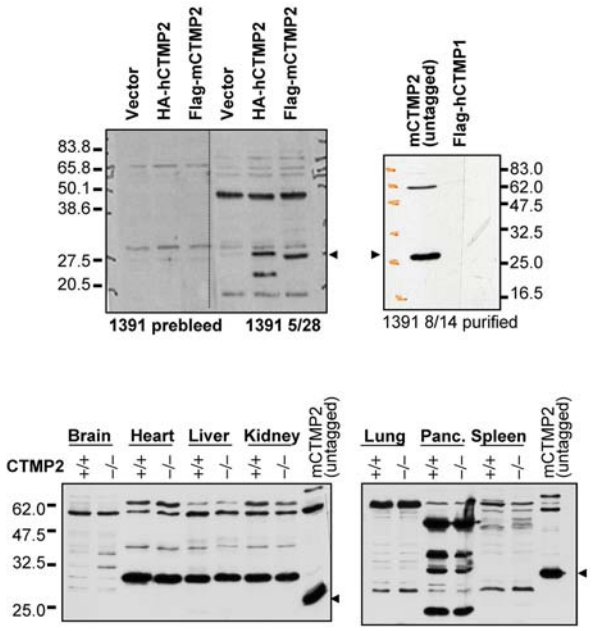

Fig. 8. Purification of antibody against CTMP2. (A) Crude serum from immunized rabbit (project D2515-s, immunization with peptide SPO22501 from hCTMP2 sequence) was purified on peptide column (bleed batch 8/14, rabbit #B1391) Low pH elution contained antibody fraction recognizing overexpressed CTMP2 of both human and mouse origin. Antibody is specific for CTMP2 and does not recognize CTMP1 (right). (B) Antibody was tested on indicated tissue lysates of CTMP2$^{+/+}$ and CTMP$^{-/-}$ mice. It appears not to recognize endogenous CTMP2 as no band of appropriate size could be detected that would be absent in the CTMP2$^{-/-}$ tissues. Last lane on both blots contains untagged mCTMP2 expressed in 293HEK cells as size control. Of note, all visible bands recognized by the purified antibody could be titrated away by peptide competition.

To be able to assess CTMP2 protein levels, we generated a polyclonal CTMP2 peptide antibody. This antibody was purified on a peptide column and recognizes both human and mouse CTMP2 when overexpressed in cell lines

(Fig. 8). However, in various tests with this antibody we could not reliably detect endogenous CTMP2.

To investigate the physiological function of CTMP2, we generated mice deficient in CTMP2 by targeted disruption of the CTMP2 gene. In the targeted alleles, the protein coding part of exon 1 and exon 2 are deleted, ablating the ATG start codon and introducing a frame shift in the remaining coding sequence (Fig. 9). CTMP2$^{-/-}$ mice are viable and fertile and do not display any gross abnormalities. These mice are currently analyzed in more detail and preliminary observations show prominently enlarged preputial glands in the males with high penetrance. Preputial glands are highly modified, paired sebaceous glands that are only found in rodents and release pheromones to the urine. In males they are located anterior to the male prepuce between body wall and skin. The released pheromones have attractant function towards females and are connected with the social status of the male: preputial hypertrophy correlates with aggressiveness and dominance whereas preputial atrophy correlates with subordinate behavior (36, 43).

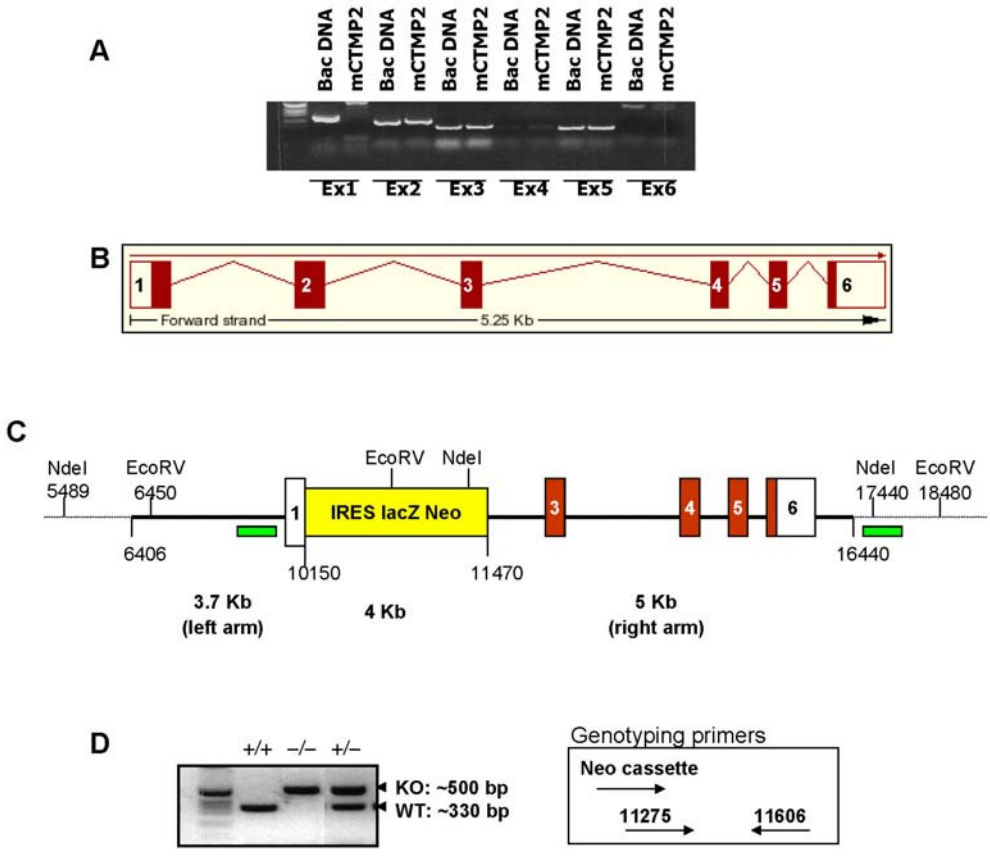

Fig. 9. Targeted disruption of mCTMP2 gene by homologous recombination. (A) Presence of mCTMP2 genomic DNA in BAC clone was verified by PCR of individual exons (cloned mCTMP2 cDNA is positive control). BAC clone was used as PCR template for generating left and right homology region of targeting vector. (B) Transcript structure of mCTMP2 gene in mice. White areas represent untranslated regions (from Ensembl database). (C) Targeted mCTMP2 allele. A targeting vector was generated that contains a 3.7 kb 5' homology region, an IRES/lacZ/neo cassette, and a 5 kb 3' homology region. A genomic DNA fragment of about 1.3 kb, including the ATG start codon in exon 1 and the full sequence of exon2, is deleted in the targeting vector. The targeting vector was linearized with NotI and electroporated into 129/Ola ES cells. Screening of ES cell clones was performed by Southern Blotting. DNA was digested with EcoRV and probed with an external probe (green box spanning sequence 16980-17663). An internal probe was then used on NdeI digested DNA (green box spanning sequence 9652-10154) for further characterization of ES cell clones positive for homologous recombination. Correctly targeted ES cells were used to generate chimeras. Male chimeras were mated with wild type C57BL/6 females to obtain $CTMP2^{+/-}$ mice, which were intercrossed to produce CTMP2 homozygous mutants. **(D)** Progeny were genotyped for the presence of a targeted allele by multiplex PCR. The following primers were used for genotyping: P1-as 5'-GCA GCA GGC TGA ACT GAC TGA GG-3'; P2/KO-s 5'- GCT GCC TCG TCC TGC AGT TCA TTC-3''; P3/WT-s 5'-CAG GCG GCT GGA TTA AAC TAC C-3'. One reaction amplifies a 500 bp fragment from the targeted allele and the second reaction amplifies a 330 bp fragment from the wild type allele.

There are several issues to address as next steps in the analysis of these mice. First, it needs to be confirmed that mouse CTMP proteins localize to the mitochondria as their human orthologues. Next, it is important to obtain an anti-CTMP2 antibody that recognizes endogenous protein. Also, targeted CTMP2 alleles contain an NLS-lacZ expression reporter cassette and X-gal staining can thus be used to assess CTMP2 gene expression in tissues of these mice. As redundancy between CTMP1 and CTMP2 may be the reason for the mild phenotypes of the individual knockouts, it would also be interesting to generate CTMP1/CTMP2 double knockout mice.

Table 1. Gene expression analysis in brain and kidney of CMTP1 mutant and wild type mice

Kidney				
Expression lower in CTMP1$^{-/-}$				
Affymetrix Probe	**CTMP1$^{-/-}$ kidney: normalized expression average and range**	**CTMP1$^{+/+}$ kidney: normalized expression average and range**	**Fold Change**	**Gene Name**
104617_at	230.2 (177.6 to 267.6)	845.2 (600.7 to 1,180.5)	0.27	RIKEN cDNA 0610005C13 gene
93059_at	115.9 (107.2 to 122.4)	260.3 (200.0 to 395.6)	0.45	RIKEN cDNA 2610204K14 gene
101574_f_at	146.5 (117.9 to 166.2)	310.1 (160.2 to 468.7)	0.47	serine protease inhibitor 1-5
94338_g_at	275.1 (193.9 to 383.2)	573.2 (502.1 to 670.5)	0.48	growth arrest specific 2
103421_at	139.5 (106.9 to 191.9)	267.2 (236.1 to 340.8)	0.52	stromal cell derived factor receptor 2
92252_at	82.2 (63.0 to 120.5)	156.5 (131.9 to 172.5)	0.52	cholecystokinin A receptor
101572_f_at	120.6 (92.7 to 153.2)	228.0 (113.3 to 386.8)	0.53	serine protease inhibitor 1-1
94426_at	111.9 (84.4 to 154.5)	198.3 (164.5 to 247.8)	0.56	RIKEN cDNA 6330575P11 gene
95439_at	402.9 (266.1 to 652.6)	708.1 (595.3 to 847.8)	0.57	arylacetamide deacetylase (esterase)
93045_at	1,872.6 (1,252.3 to 3,197.5)	3,233.4 (2,684.5 to 4,298.3)	0.58	ATP-binding cassette, sub-family D (ALD), member 3
93109_f_at	263.6 (262.1 to 265.5)	449.6 (223.1 to 760.3)	0.59	serine protease inhibitor 1-4
104495_f_at	1,230.4 (956.2 to 1,849.0)	1,946.2 (1,855.8 to 2,063.6)	0.63	kallikrein 5
101289_f_at	2,324.6 (1,886.6 to 3,142.9)	3,648.7 (3,325.4 to 3,954.1)	0.64	kallikrein 1-related peptidase b16
100061_f_at	5,452.7 (4,470.4 to 7,652.1)	8,497.6 (7,961.0 to 9,461.3)	0.64	kallikrein 6
102947_at	820.5 (665.1 to 1,196.7)	1,273.2 (1,214.6 to 1,327.7)	0.64	solute carrier family 22 (organic cation transporter), member 2
161637_f_at	458.0 (375.0 to 647.6)	709.1 (635.8 to 775.8)	0.65	kallikrein 5
101950_at	150.6 (138.9 to 174.1)	232.5 (212.6 to 245.4)	0.65	semaF cytoplasmic domain associated protein 2
96072_at	1,999.5 (1,835.9 to 2,221.2)	3,062.8 (2,836.9 to 3,253.7)	0.65	lactate dehydrogenase 1, A chain
101565_f_at	317.0 (266.0 to 350.3)	476.7 (305.3 to 658.0)	0.66	serine protease inhibitor 1-3
95775_f_at	3,910.8 (3,195.5 to 4,939.4)	5,733.4 (5,208.8 to 6,465.3)	0.68	kallikrein 1
100329_at	162.5 (159.4 to 168.0)	237.7 (90.1 to 495.9)	0.68	serine protease inhibitor 1-4
101576_f_at	270.7 (234.4 to 299.0)	389.8 (208.1 to 705.6)	0.69	serine protease inhibitor 1-2
Expression higher in CTMP1$^{-/-}$				
101659_at	2,490.5 (2,124.3 to 2,962.8)	378.1 (248.0 to 534.2)	6.59	hydroxysteroid dehydrogenase-2, delta<5>-3-β
98531_g_at	1,026.0 (817.3 to 1,153.0)	162.0 (83.7 to 508.2)	6.33	growth arrest specific 5
101532_g_at	1,345.7 (875.1 to 2,365.3)	304.7 (133.5 to 1,335.3)	4.42	aldolase 2, B isoform
160799_at	444.6 (367.7 to 501.2	168.1 (64.9 to 315.1)	2.64	ESTs, Weakly similar to A47643

				hypothetical protein - mouse (fragment) [M.musculus]
103534_at	2,110.3 (862.9 to 4,953.2)	930.5 (349.5 to 1,526.3)	2.27	hemoglobin, β adult major chain
102234_at	202.6 (172.1 to 260.1)	92.4 (87.9 to 98.2)	2.19	RIKEN cDNA 1810037I17 gene
98525_f_at	2,155.9 (1,893.8 to 2,558.3)	999.0 (681.2 to 1,388.4)	2.16	erythroid differentiation regulator
161835_at	1,022.0 (914.1 to 1,197.9)	483.1 (362.1 to 776.2)	2.12	calbindin-D9K
96215_f_at	614.8 (452.0 to 798.4)	297.6 (250.0 to 402.8)	2.07	Mus musculus, clone IMAGE:3983821, mRNA, partial cds
93435_at	104.9 (70.4 to 161.2)	52.1 (31.3 to 75.1)	2.01	cytochrome P450, family 24, subfamily a, polypeptide 1
95430_f_at	502.0 (418.6 to 565.1)	251.9 (135.9 to 421.1)	1.99	DNA segment, Chr 9, Wayne State University 18, expressed
99126_at	1,038.5 (748.4 to 1,281.1)	548.2 (358.4 to 712.0)	1.89	inactive X specific transcripts
160375_at	812.6 (401.7 to 1,480.8)	453.3 (215.1 to 780.4)	1.79	carbonic anhydrase 3
100443_at	578.0 (564.4 to 590.0)	331.2 (249.3 to 448.9)	1.75	branched chain aminotransferase 2, mitochondrial
102049_at	425.8 (262.4 to 1,029.4)	250.4 (159.7 to 519.2)	1.70	pyruvate dehydrogenase kinase, isoenzyme 4
160918_at	1,200.5 (1,148.5 to 1,229.2)	732.4 (511.2 to 990.4)	1.64	calbindin-D9K
160306_at	665.2 (459.6 to 910.3)	408.0 (290.7 to 543.8)	1.63	thyroid hormone responsive SPOT14 homolog (Rattus)
101451_at	150.5 (105.6 to 227.9)	95.8 (80.4 to 133.0)	1.57	paternally expressed 3
94224_s_at	299.1 (282.7 to 325.2)	190.6 (160.8 to 260.4)	1.57	interferon activated gene 205
104445_at	190.3 (172.5 to 202.4)	124.4 (116.9 to 138.9)	1.53	RIKEN cDNA 4631408O11 gene
99104_at	363.8 (194.3 to 580.2)	238.9 (132.6 to 321.7)	1.52	adipocyte complement related protein
94689_at	411.6 (351.0 to 537.0)	274.2 (257.8 to 303.7)	1.50	expressed sequence C79248
101027_s_at	926.9 (867.0 to 1,003.1)	620.7 (589.9 to 670.4)	1.49	pituitary tumor-transforming 1
104444_at	262.1 (173.0 to 362.9)	176.3 (163.6 to 187.2	1.49	RIKEN cDNA 9430098E02 gene
98473_at	312.2 (240.2 to 402.8)	212.1 (172.7 to 268.5)	1.47	arginase type II
104513_at	248.0 (180.9 to 298.7)	170.6 (145.1 to 188.7)	1.45	RIKEN cDNA 2410004N09 gene
102108_f_at	727.9 (666.0 to 787.7)	509.6 (376.8 to 680.8)	1.43	myosin heavy chain IX
93497_at	367.4 (328.9 to 454.2)	257.8 (177.7 to 483.1)	1.43	complement component 3
99643_f_at	387.8 (326.5 to 529.7)	275.0 (194.4 to 458.5)	1.41	carboxypeptidase E

Brain

Expression lower in CTMP1$^{-/-}$

Affymetrix Probe	CTMP1$^{-/-}$ brain: normalized expression average and range	CTMP1$^{+/+}$ brain: normalized expression average and range	Fold change	Gene Name
93059_at	134.4 (121.7 to 148.3)	398.8 (335.8 to 554.9)	0.34	RIKEN cDNA 2610204K14 gene
98332_at	151.1 (149.8 to 153.0)	315.8 (266.1 to 370.6)	0.48	potassium inwardly-rectifying

				channel, subfamily J, member 9
94426_at	131.3 (98.2 to 221.9)	272.6 (232.5 to 370.1)	0.48	RIKEN cDNA 6330575P11 gene
94767_at	1,372.3 (1,230.5 to 1,563.7)	2,806.7 (2,421.0 to 3,417.8)	0.49	ribosomal protein S11
96629_at	189.8 (174.1 to 200.6)	343.0 (209.8 to 510.8)	0.55	DNA segment, Chr 7, Roswell Park 2 complex, expressed
92943_at	556.1 (532.9 to 597.6)	890.3 (716.2 to 1,001.2)	0.62	glutamate receptor, ionotropic, AMPA1 (alpha 1)
98600_at	73.6 (67.5 to 76.9)	117.6 (110.5 to 125.0)	0.63	S100 calcium binding protein A11 (calizzarin)
99608_at	296.9 (260.2 to 366.3)	427.7 (409.3 to 441.9)	0.69	peroxiredoxin 2
93656_g_at	148.7 (141.7 to 154.8)	213.5 (180.5 to 250.3)	0.70	upstream transcription factor 1
104343_f_at	524.0 (492.4 to 561.0)	744.9 (699.3 to 800.7)	0.70	phospholipase A2, group XII
104598_at	407.5 (356.1 to 500.8)	579.0 (557.4 to 611.8)	0.70	dual specificity phosphatase 1
160901_at	225.4 (206.1 to 239.9)	319.2 (305.5 to 340.6)	0.71	FBJ osteosarcoma oncogene
100307_at	225.4 (207.6 to 260.7)	315.8 (247.9 to 370.4)	0.71	nuclear factor I/X
Expression higher in CTMP1$^{-/-}$				
98531_g_at	806.9 (783.9 to 854.6)	175.7 (97.3 to 476.4)	4.59	growth arrest specific 5
102234_at	299.1 (242.0 to 414.5)	128.9 (119.4 to 141.5)	2.32	RIKEN cDNA 1810037I17 gene
98525_f_at	1,109.8 (982.5 to 1,222.2)	523.8 (423.1 to 682.2)	2.12	erythroid differentiation regulator
97752_at	267.4 (232.8 to 337.7)	135.8 (82.6 to 177.0)	1.97	Mus musculus, clone IMAGE:4507176, mRNA
99126_at	195.9 (145.5 to 247.4)	105.7 (82.9 to 120.4)	1.85	inactive X specific transcripts
160173_at	1,308.8 (1,144.0 to 1,541.3)	790.4 (536.9 to 1,076.2)	1.66	maternally expressed gene 3
98946_at	170.3 (146.0 to 221.3)	107.9 (76.6 to 135.2)	1.58	WD-40-repeat-containing protein with a SOCS box 1
96215_f_at	255.3 (219.9 to 284.0)	169.5 (125.6 to 244.8)	1.51	Mus musculus, clone IMAGE:3983821, mRNA, partial cds
160172_at	807.7 (607.5 to 1,185.3)	537.2 (479.2 to 576.0)	1.50	maternally expressed gene 3
102870_at	997.8 (844.7 to 1,325.1)	664.5 (597.4 to 705.7)	1.50	RIKEN cDNA 5930418K15 gene
93274_at	594.6 (538.2 to 645.7)	398.2 (280.3 to 512.7)	1.49	CDC-like kinase
160316_at	125.4 (112.1 to 150.2)	86.1 (72.3 to 95.1)	1.46	heterogeneous nuclear ribonucleoprotein U

RNA was extracted from whole brains and kidneys of 3-month-old female CTMP$^{+/+}$ and CTMP$^{-/-}$ mice. Microarray analysis was performed on three individual organs per genotype using murine Affymetrix GeneChipsTM (U74). Changes ≤ 1.4-fold were considered insignificant.

VI. APPENDIX

Part 2:

Functional characterization of human RSK4, a new 90-kDa ribosomal S6 kinase, reveals constitutive activation in most cell types.

Dummler B, Hauge C, Silber J, Yntema HG, Kruse LS, Kofoed B, Hemmings BA, Alessi DR, Frodin M.

J Biol Chem 2005, 280(14):13304-13314

THE JOURNAL OF BIOLOGICAL CHEMISTRY
Vol. 280, No. 14, Issue of April 8, pp. 13304–13314, 2005
Printed in U.S.A.

Functional Characterization of Human RSK4, a New 90-kDa Ribosomal S6 Kinase, Reveals Constitutive Activation in Most Cell Types*

Received for publication, July 20, 2004, and in revised form, December 17, 2004
Published, JBC Papers in Press, January 4, 2005, DOI 10.1074/jbc.M408194200

Bettina A. Dümmler‡§¶, Camilla Hauge‡§‖, Joachim Silber‡, Helger G. Yntema, Lars S. Kruse‡, Birte Kofoed‡, Brian A. Hemmings‡‡, Dario R. Alessi§§, and Morten Frödin‡‖¶¶**

*From the ‡Department of Clinical Biochemistry, Glostrup Hospital, 2600 Glostrup, Denmark, the **Department of Human Genetics, University Medical Centre St. Raboud, P. O. Box 9101, Nijmegen 6500 HB, the Netherlands, the ‡‡Friedrich Miescher Institute, Maulbeerstrasse 66, CH-4558 Basel, Switzerland, §§Medical Research Council Protein Phosphorylation Unit, School of Life Sciences, Medical Sciences Institute/Wellcome Trust Biocentre Complex, University of Dundee, Dow Street, Dundee DD1 5EH, Scotland, United Kingdom, and the ‖Kinase Signalling Laboratory, Biotech Research and Innovation Centre, Fruebjergvej 3, 2100 Copenhagen Ø, Denmark*

The 90-kDa ribosomal S6 kinases (RSK1–3) are important mediators of growth factor stimulation of cellular proliferation, survival, and differentiation and are activated via coordinated phosphorylation by ERK and 3-phosphoinositide-dependent protein kinase-1 (PDK1). Here we performed the functional characterization of a predicted new human RSK homologue, RSK4. We showed that RSK4 is a predominantly cytosolic protein with very low expression and several characteristics of the RSK family kinases, including the presence of two functional kinase domains and a C-terminal docking site for ERK. Surprisingly, however, in all cell types analyzed, endogenous RSK4 was maximally (constitutively) activated under serum-starved conditions where other RSKs are inactive due to their requirement for growth factor stimulation. Constitutive activation appeared to result from constitutive phosphorylation of Ser^{232}, Ser^{372}, and Ser^{389}, and the low basal ERK activity in serum-starved cells appeared to be sufficient for induction of ~50% of the constitutive RSK4 activity. Finally experiments in mouse embryonic stem cells with targeted deletion of the *PDK1* gene suggested that PDK1 was not required for phosphorylation of Ser^{232}, a key regulatory site in the activation loop of the N-terminal kinase domain, that in other RSKs is phosphorylated by PDK1. The unusual regulation and growth factor-independent kinase activity indicate that RSK4 is functionally distinct from other RSKs and may help explain recent findings suggesting that RSK4 can participate in non-growth factor signaling as for instance p53-induced growth arrest.

The 90-kDa ribosomal S6 kinases (RSKs)[1] are serine kinases that are activated by growth factors and many polypeptide hormones via the Ras-dependent mitogen-activated protein (MAP) kinase cascade composed of Raf, MEK, and extracellular signal-regulated kinase (ERK) (Refs. 1 and 2; for a review, see Ref. 3). RSKs contain two functional protein kinase domains, and in mammals three widely expressed homologues (RSK1, RSK2, and RSK3) have been identified. Many studies suggest that RSKs are central mediators of ERK in regulation of cellular division, survival, and differentiation via phosphorylation of numerous intracellular proteins. For instance, RSK mediates ERK-induced G_2/M phase progression in meiosis I (4) and metaphase arrest in meiosis II (5, 6) of *Xenopus laevis* oocytes, which may in part occur via phosphorylation of the $p34^{cdc2}$-inhibitory kinase Myt1 (7) and the protein kinase Bub1 (8), respectively. In somatic cell types, RSK may stimulate cell division through phosphorylation of substrates like $p27^{Kip1}$ (9) and glycogen synthase kinase-3 (10–12); protein synthesis and cell growth through substrates like elongation factor 2 kinase (13), glycogen synthase kinase-3 (10–12), transcription initiation factor IA (14), and tuberous sclerosis complex-2 protein (15); cell survival through Bad (16); and transcription through substrates like c-Fos (17) and estrogen receptor (18). Experiments with PC12 cells suggest that RSK is a key mediator of ERK in neurotrophin-induced neuronal differentiation (19). Finally genetic evidence from human and mouse has identified an important role for RSK2 in osteoblast differentiation and function through phosphorylation of activating transcription factor-4 (20) and in stimulation of white adipose tissue mass via an unknown mechanism (21). RSK is related to the mitogen- and stress-activated protein kinases (MSK1 and MSK2), which also contain two kinase domains. MSK, however, is activated by the ERK family as well as by p38 family MAP kinases and thereby functions in signal transduction of growth factors as well as of cellular stress stimuli like UV/radioactive irradiation and proinflammatory cytokines (22, 23).

The substrates of RSK are phosphorylated by the N-terminal kinase (NTK) domain (24–27) whose activity is regulated by

* The work was supported by grants from the Novo Nordisk Foundation (to M. F.), the Danish Medical Research Council (Grant No. 52-00-1162 to M. F.), the Danish Cancer Research Foundation (to M. F.), and the *Krebsliga Schweiz* (Grant KSF-01002-02-2000/OCS 1167-09-2001 to B. A. D.). The costs of publication of this article were defrayed in part by the payment of page charges. This article must therefore be hereby marked "*advertisement*" in accordance with 18 U.S.C. Section 1734 solely to indicate this fact.

§ Both authors contributed equally to this study.
¶ Present address: The Friedrich Miescher Inst., Maulbeerstrasse 66, CH-4558 Basel, Switzerland.
¶¶ To whom correspondence should be addressed: Biotech Research and Innovation Centre, Fruebjergvej 3, DK-2100 Copenhagen Ø, Denmark. E-mail: morten.frodin@bric.dk.

[1] The abbreviations used are: RSK, 90-kDa ribosomal S6 kinase; MSK, mitogen- and stress-activated kinase; ERK, extracellular signal-regulated kinase; MEK, mitogen-activated protein kinase/extracellular signal-regulated kinase kinase; MAP, mitogen-activated protein; NTK, N-terminal kinase; PDK1, 3-phosphoinositide-dependent protein kinase-1; HA, hemagglutinin; HEK, human embryonic kidney; CHO, Chinese hamster ovary; EGF, epidermal growth factor; PMA, phorbol 12-myristate 13-acetate; MAPK, mitogen-activated protein kinase; JNK, c-Jun N-terminal kinase; ES, embryonic stem; IR, insulin receptor; Ab, antibody; GST, glutathione *S*-transferase; PBS, phosphate-buffered saline; EST, expressed sequence tag.

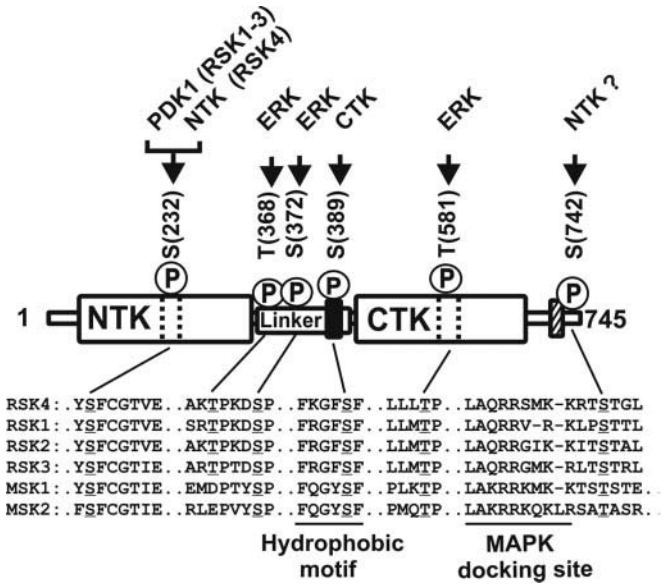

FIG. 1. **Predicted structure and phosphorylation sites of RSK4.** RSK4 is predicted to contain two functional protein kinase domains (NTK and C-terminal kinase (*CTK*)) connected by a regulatory linker region. The *black box* indicates the hydrophobic motif, and the *hatched box* indicates the MAPK docking site. The locations of six phosphorylation sites (*P*) are shown along with the kinases that appear to phosphorylate these sites in RSK family members as evidenced by the present and previous studies. Amino acid alignment of all human RSK/MSK family members shows conservation of the phosphorylated serine or threonine residues (*underlined*) and the surrounding sequence. The overall amino acid identity/similarity of RSK4 and RSK1–3 is 72/81, 76/85, and 73/83%, respectively.

the C-terminal kinase domain and a linker region between the two kinase domains (Fig. 1). The activation mechanism of RSK is complex and involves sequential phosphorylation of four regulatory sites (28), which are Ser^{232}, Ser^{372}, Ser^{389}, and Thr^{581}, using RSK4 numbering. First ERK, bound to a C-terminal MAP kinase docking site (29, 30), phosphorylates Ser^{372} in the linker and Thr^{581} in the activation loop of C-terminal kinase (28, 31). Phosphorylation of Thr^{581} activates C-terminal kinase, which thereafter autophosphorylates RSK at Ser^{389}, located in a so-called hydrophobic motif in the linker (32). Phosphorylation of Ser^{389} in the hydrophobic motif generates a transient docking site that recruits as well as stimulates the activity of 3-phosphoinositide-dependent protein kinase-1 (PDK1) (25), which then phosphorylates Ser^{232} in the activation loop of the NTK of RSK (33, 34). After dissociation of PDK1 from RSK, the Ser^{386}-phosphorylated hydrophobic motif interacts with a binding pocket within the NTK domain and thereby activates the NTK in synergy with phospho-Ser^{232} (35). The phosphorylation of Ser^{372} enhances the activity of the NTK by a yet unknown mechanism (28, 33). Apart from these four activating sites, Thr^{368} is phosphorylated by ERK, but the site has not been found to regulate kinase activity (28). Moreover Ser^{742} appears to be phosphorylated by the activated NTK (28, 36), which results in decreased affinity of RSK for ERK, serving as an intramolecular feedback inhibitory mechanism that operates in RSK1 and RSK2 but not in RSK3 (36). The activation mechanism of MSK is thought to be very similar to that of RSK except for two features (22, 23, 37–39). First, the MAP kinase docking site can interact with both ERK and p38 MAP kinase, explaining why MSK is activated by two MAP kinase pathways. Second, the activation loop of the NTK is not phosphorylated by PDK1 but probably via autophosphorylation.

Recently a search for the mental retardation gene in a complex disease locus at Xq21 resulted in the discovery of a gene encoding a new RSK/MSK homologue (40), which contains all the structural hallmarks of this kinase family (Fig. 1). Due to highest amino acid sequence identity to RSKs, the kinase was named RSK4 (gene symbol *RPS6KA6*), but no functional studies were performed to confirm the relationship. Although RSK4 was found to be deleted in several patients with alterations in Xq21, a definitive link to mental retardation could not be established. At present, the only characterization performed with RSK4 is the demonstration of RSK4 mRNA expression in various human (40) and fetal mouse (41) tissues. Very recently, a short interfering RNA screen targeting 7,914 human genes identified five genes, including *RSK4*, whose transcripts were required for growth arrest induced by the p53 tumor suppressor protein (42). This finding suggests that RSK4 has a function in growth inhibition and opens the possibility that RSK4 is a tumor suppressor protein. Moreover an expression screen with mouse mRNAs in *X. laevis* embryos showed that RSK4 expression can disrupt mesoderm formation induced by the fibroblast growth factor-Ras-ERK signaling pathway (43). RSK4 was therefore proposed to be an inhibitor rather than a mediator of growth factor signal transduction. However, the two recent studies provided no characterization of the RSK4 protein, its kinase activity, or regulation. Since RSK1–3 are activated by growth factors it is currently enigmatic how RSK4 can be an inhibitor of growth factor signal transduction and a mediator of p53, which is a transcription factor.

In this study, we characterized RSK4 and demonstrated that RSK4 is distinct from other RSKs by being constitutively activated in serum-starved cells in the absence of growth factor. Our data suggested that constitutive activity was due to constitutive phosphorylation of Ser^{232}, Ser^{372}, and Ser^{389} induced in part by very low basal levels of ERK activity and in part by less well defined mechanisms that may include enhanced autophosphorylation ability of RSK4 compared with other RSKs. The constitutive, growth factor-independent activity of RSK4 may help explain how RSK4 can participate in non-growth factor signaling, such as p53-induced growth arrest.

EXPERIMENTAL PROCEDURES

Antibodies to RSK4 (sc-17178) were from Santa Cruz Biotechnology, Inc. (Santa Cruz, CA). Two different lots, C112 and H152, were used, and both were found to be specific as shown in the experiment depicted in Fig. 2*B*. Antibodies to RSK2 (sc-1430), the PDK1 phosphorylation site in RSK (sc-12445-R), MSK1 (sc-9392), lamin A/C (sc-7292), and the influenza hemagglutinin (HA) epitope tag (sc-805, used for immunocytochemistry and immunoblotting) were also from Santa Cruz Biotechnology, Inc. Antibodies to the phosphorylated hydrophobic motif (06-826) and the regulatory ERK phosphorylation site in the linker (06-824) of RSK were from Upstate Biotechnology (Lake Placid, NY). Antibody to phospho-Thr^{581}, raised against RSK2, is described in Ref. 44. Anti-HA Ab used for immunoprecipitation was from the 12CA5 mouse hybridoma cell line. Antibody to p63/CLIMP-63 (45) was kindly provided by Dr. Hans-Peter Hauri (Basel, Switzerland). Antibody to α-tubulin was from the YL1/2 mouse hybridoma cell line. Epidermal growth factor (EGF) was from PreproTech Inc. (Rocky Hill, NJ). S6 peptide (RRLSSLRA) and cross-tide (GRPRTSSFAEG) were synthesized by K. J. Ross-Petersen AS (Copenhagen, Denmark). U0126 was from Promega (Madison, WI). SB203580 was from Calbiochem. [γ-^{32}P]ATP was from Amersham Biosciences. Other chemicals were from Sigma.

Plamid Constructs—HA-RSK2 (mouse) and HA-RSK3 (human) in the mammalian expression vector pMT2 (2) were kindly provided by Dr. Christian Bjørbæk (Beth Israel Deaconess Medical Center, Boston, MA). To generate pMT2-HA-RSK4, the entire human RSK4 coding sequence was PCR-amplified using pTL10Flag-RSK4 (see below) as template and primers introducing a 5′ XhoI site just prior to the start codon and a 3′ KpnI site after the stop codon. RSK2 was excised from pMT2-HA-RSK2 using XhoI and KpnI and replaced with the PCR product digested with the same enzymes. HA-RSK1 (rat) in pMT2 (46) was kindly provided by Dr. Joseph Avruch. HA-MSK1 in pMT2 is described in Ref. 25. To generate pTL10-Flag-RSK4, Marathon Ready human fetal brain cDNA (Clontech) was used as template to PCR-amplify the human RSK4 coding region (amino acids 1–745) with primers introducing a 5′ BamHI site just prior to the start codon and a 3′

EcoRI site after the stop codon. The PCR product was cloned into the pCR2.1 vector (Topo TA cloning kit, Invitrogen). RSK4 was then excised from the pCR2.1 vector using BamHI and cloned into the BamHI site of the mammalian expression vector pTL10Flag, modified from psG5 (47), resulting in N-terminal fusion of the FLAG epitope tag. pMT2-HA-RSK3* was generated by PCR amplification of the HA tag and residues 1–40 of RSK2 with a 3′ primer introducing a SalI site and a 5′ primer annealing upstream of the PstI site in pMT2. The PCR product was digested with PstI and SalI and used to replace the corresponding first 31 residues of RSK3 in pMT2 digested with PstI and XhoI. Point mutations were introduced in RSK4 using the QuikChange™ (Stratagene) mutagenesis procedure, and the entire coding region was sequenced to confirm that no other mutations were introduced. HA-RSK4-(1–730) and HA-RSK2-(1–725) in pMT2 were generated by introducing a stop codon after residues 730 and 725, respectively, in the wild-type constructs using QuikChange. To generate wild-type and T581A HA-RSK4-(371–745) in pMT2, the sequence encoding residues 371–745 of RSK4 was PCR-amplified with primers introducing a 5′ XhoI site just prior to residue 371 and a 3′ KpnI site after the stop codon using wild-type RSK4 and RSK4-T581A, respectively, as a template. RSK2 was excised from pMT2-HA-RSK2 using XhoI and KpnI and replaced with either of the two PCR products digested with the same enzymes. To generate glutathione *S*-transferase (GST)-JNK2α2, the JNK2α2 (48) coding sequence was amplified by PCR with primers introducing a 5′ BamHI and a 3′ NotI site, and the digested PCR product was cloned into the mammalian expression vector pEBG in-frame with GST. The expression construct for HA-c-Jun is described in Ref. 49.

Transfection, Stimulation, and Immunoprecipitation—All cell lines were cultured in Dulbecco's modified Eagle's medium supplemented with 10% fetal bovine serum at 37 °C in atmospheric air with 5% CO_2. Medium for wild-type and PDK1-deficient mouse embryonic stem (ES) cells (37) also contained 10 ng/ml leukemia inhibitory factor and 0.1 mM 2-mercaptoethanol. For transfection, ~90% confluent cells in 9.6-cm^2 wells were incubated with 4 μg of DNA and 11 μl of Lipofectamine 2000 reagent (Invitrogen) as described in the manufacturer's protocol. Transfection of ES cells was scaled up to 56-cm^2 culture dishes. Serum starvation was performed by two washes with serum-free Dulbecco's modified Eagle's medium, aspiration, and incubation in serum-free Dulbecco's modified Eagle's medium. Phorbol 12-myristate 13-acetate (PMA), anisomycin, U0126, and SB203580 were added from 1,000× stock solutions in Me_2SO. Cells were harvested by washing with phosphate-buffered saline (PBS) and solubilization for 15 min in 500 μl of lysis buffer (1% Triton X-100, 150 mM NaCl, 50 mM Tris-HCl (pH 7.4), 1 mM Na_3VO_4, 5 mM EDTA, 25 mM sodium fluoride, 10 nM calyculin A, 1 mM phenylmethylsulfonyl fluoride, 10 μM leupeptin, 10 μM pepstatin, and 200 kallikrein inhibitor units/ml aprotinin) on ice. Subsequent manipulations were performed at 0–4 °C. Cell extracts were clarified by centrifugation for 5 min at 14,000 × *g*, and the supernatant was incubated for 90 min with antibody with the addition of 20 μl of 50% protein G-agarose beads (Santa Cruz Biotechnology, Inc.) during the final 30 min. For GST fusion protein pull-down assays, glutathione-Sepharose 4B (Amersham Biosciences) was used. Agarose bead-antibody complexes were precipitated by centrifugation, washed five times with lysis buffer, drained, and dissolved in SDS-PAGE sample buffer (2% sodium dodecyl sulfate, 62 mM Tris (pH 6.8), 10% glycerol, 5% 2-mercaptoethanol, 0.1% bromphenol blue). For kinase assays, the final two washes were with 1.5× kinase assay buffer (30 mM Tris-HCl (pH 7.4), 10 mM $MgCl_2$, 1 mM dithiothreitol).

Kinase Assays—Agarose beads with immunoprecipitated kinase were drained with a syringe and resuspended in 20 μl of 1.5× kinase assay buffer. The kinase reaction was initiated by the addition of 10 μl (final concentrations) of ATP (100 μM, 0.5 μCi of [γ-^{32}P]ATP) and 800 μM S6 peptide (RSK assays) or 166 μM cross-tide (MSK assays). After 10 min at 30 °C (the reaction was linear with time), 20 μl of the supernatant was removed with a Hamilton syringe (leaving behind precipitated kinase) and spotted onto phosphocellulose paper (Whatman p81) that was washed four to five times with 150 mM orthophosphoric acid. [^{32}P]phosphate incorporated into protein substrate was quantified on a STORM™ PhosphorImager using ImageQuant™ software (Amersham Biosciences). Due to the low activity, a reaction blank (an assay performed without antibody during immunoprecipitation) was performed for all the conditions in endogenous RSK4 and MSK1 assays and subtracted from the respective kinase assay values.

In Vitro Activation of RSK—Endogenous RSK4 or RSK2, immunopurified from ~3 × 10^6 serum-starved embryonic kidney (HEK) 293 cells per assay point, were incubated for 30 min at 30 °C with 50 μM MgATP in the absence or presence of 50 ng of active ERK2 (Upstate Biotechnology) and 50 ng of active PDK1 (35) in 20 μl of 1.5× kinase assay buffer. Thereafter the kinase activity of RSK4 and RSK2 was determined as described under "Kinase Assays" except that in the present assay the blank reaction contained ERK2 and PDK1.

Immunocytochemistry—Subconfluent cells cultured on gelatin-coated glass coverslips were transfected with pMT2-HA-RSK4. One day after transfection, cells were fixed in 4% (w/v) paraformaldehyde for 15 min followed by permeabilization with 0.2% (v/v) Triton X-100 for 5 min and blocking in 10% horse serum for 20 min. Cells were then incubated for 60 min at 37 °C with rabbit anti-HA antibody diluted 1:500 in PBS. After washing with PBS, cells were incubated for 45 min at 37 °C with fluorescein isothiocyanate-conjugated anti-rabbit antibody (F0511, Sigma) diluted 1:300 in PBS. Coverslips were then washed with PBS, mounted with Vectashield mounting medium (Vector Laboratories Inc., Burlingame, CA), and analyzed in a laser scanning confocal microscope (Leica).

Cell Fractionation—HEK293F cells were harvested in cold PBS, pelleted, and resuspended in hypotonic RSB buffer (10 mM HEPES (pH 6.2), 10 mM NaCl, 1.5 mM $MgCl_2$, inhibitors as for lysis buffer above). The cell suspension was incubated for 30 min at 4 °C and then homogenized by 20 strokes in a tight fitting homogenizer. The homogenate was centrifuged at 375 × *g* (2 min), and the pellet was washed twice with RSB buffer and then resuspended in lysis buffer (50 mM Tris (pH 8.0), 250 mM NaCl, 1% Triton X-100, inhibitors as for lysis buffer above) to generate the nuclear fraction. The supernatant was centrifuged for 60 min at 150,000 × *g*. The resulting pellet was washed once in RSB buffer and then resuspended in lysis buffer to generate the membrane fraction, whereas the supernatant of this centrifugation represented the cytosolic fraction. All procedures were carried out at 4 °C.

Immunoblotting—Immunoblotting was performed as described previously (33) except that the membrane was blocked in Bailey's Irish Cream liquor in immunoblots using phosphospecific Abs or anti-RSK4 Ab.

RESULTS

We first cloned the predicted coding sequence of the human *RSK4* gene into the mammalian expression vector pMT2, which resulted in fusion of the 9-amino acid HA epitope tag to the N terminus of RSK4. In transiently transfected human HEK293 cells, the RSK4 cDNA expressed a single protein product that was of the same size as a putative endogenous RSK4 protein immunoprecipitated from non-transfected HEK293 cells with an antibody directed to the C-terminal sequence of human RSK4 (Fig. 2*A*). To investigate the specificity of the anti-RSK4 Ab, we tested its ability to precipitate each of the four RSK homologues. To perform this experiment, we first had to generate a soluble mutant of RSK3 because >95% of wild-type RSK3 is lost to the insoluble fraction during clearing of crude cell lysates before immunoprecipitation (Ref. 2 and our data not shown). By constructing and analyzing RSK3-RSK2 chimeras, an RSK3 mutant (RSK3*), in which the N-terminal 40 amino acids derive from RSK2, was found to be soluble and was used for the experiment. N-terminally HA-tagged forms of the four RSKs were transiently expressed in COS7 cells, and cell lysate from each transfection was split and subjected to immunoprecipitation with anti-RSK4 Ab and anti-HA Ab, respectively. Anti-HA immunoblotting on the precipitates showed that the anti-RSK4 Ab precipitated RSK4 only (Fig. 2*B*). Similar experiments showed that the Ab also does not interact with MSK1 or MSK2 (data not shown). Using the anti-RSK4 Ab, we detected expression of RSK4 protein in lysates from human U2OS osteosarcoma cells, BJ fibroblasts, Ln405 glioblastoma cells, and monkey COS7 kidney fibroblasts (Fig. 2*C*), whereas no RSK4 was detected in HeLa and Chinese hamster ovary (CHO) cells (data not shown). Immunoblotting on lysates of adult mouse tissues showed RSK4 expression in whole brain, heart, cerebellum, kidney, and skeletal muscle, whereas the remaining tissues analyzed showed no detectable RSK4 (Fig. 2*C*). Typically 10 times more cells were required to perform an immunoprecipitation/immunoblot experiment with endogenous RSK4 compared with other endogenous RSKs, although we estimate that the anti-RSK4 Ab has quite high avidity based on experiments like the one depicted in Fig. 2*B*. RSK4 therefore appears to be expressed at much lower levels than other RSKs.

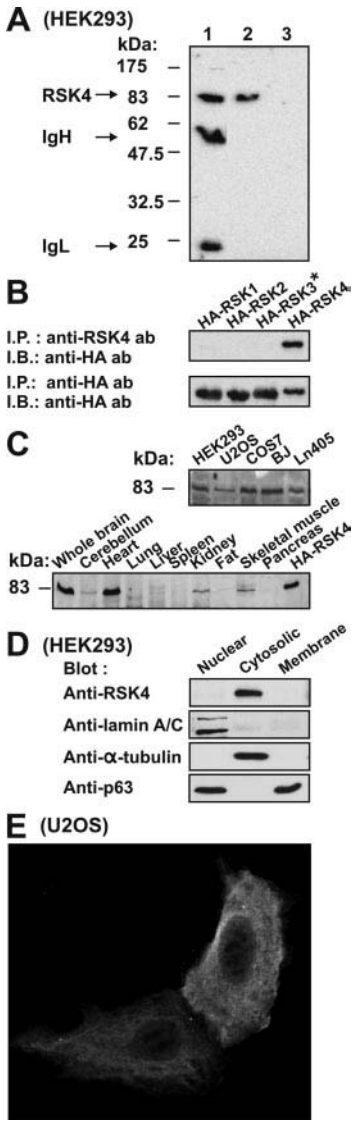

FIG. 2. **Expression of endogenous and recombinant RSK4 protein in various cell lines and mouse tissues.** *A*, anti-RSK4 immunoblot was performed on endogenous RSK4 immunoprecipitated from ≈10^7 HEK293 cells (*lane 1*) or on crude lysates from ≈10^4 HEK293 cells transfected with plasmid expressing HA-tagged RSK4 (*lane 2*) or with empty plasmid (*lane 3*). *B*, COS7 cells were transfected with plasmid expressing HA-tagged RSK1, RSK2, RSK3*, or RSK4. After 20 h, the cells were lysed, and the lysates were split in two parts that were subjected to immunoprecipitation with anti-RSK4 Ab (*upper panel*) or with anti-HA Ab (*lower panel*). Thereafter all the precipitates were subjected to immunoblotting with anti-HA Ab. To ensure higher amounts of RSK1–3 compared with RSK4 in the precipitates, the amounts of lysates were used in the ratio 3(RSK1):1(RSK2):1(RSK3*):1(RSK4). *C*, anti-RSK4 immunoblot was performed on ≈50 μg of total protein from various cell lines (*left panel*) or from various adult mouse tissues (*right panel*). The *last lane* in the *right panel* is lysate from COS7 cells transfected with plasmid expressing HA-tagged RSK4. *D*, lysates of the nuclear, cytosolic, or membrane fraction of HEK293 cells were subjected to immunoblotting using antibody against RSK4 or antibodies against marker proteins for the various fractions. *E*, U2OS cells were transfected with plasmid expressing HA-RSK4. After 18 h, including a final 4-h serum starvation period, the cells were fixed and immunostained with Ab to the HA tag. A confocal micrograph is shown. *I.P.*, immunoprecipitate; *I.B.*, immunoblot; *IgL*, Ig light; *IgH*, Ig heavy.

RSK4 immunoblotting on the nuclear, cytosolic, or membrane fraction of HEK293 cells suggested that RSK4 is localized to the cytoplasm (Fig. 2*D*). Control blots showed the expected distribution of the marker proteins lamin A/C, α-tubulin, and p63 in the various cell fractions. A predominantly cytosolic localization of RSK4 was confirmed by immunocytochemistry and confocal microscopy to HA-RSK4 transiently expressed in various cell types (Fig. 2*E*). However, a weak nuclear RSK4 signal was also observed, suggesting that a minor fraction of cellular RSK4 may be localized to the nucleus. This fraction might have leaked to the cytoplasmic fraction during the cell fractionation experiment depicted in Fig. 2*D*. The subcellular distribution of transiently expressed RSK4 was not affected by exposure of the cells to a variety of stimuli that activate MAP kinase pathways. These stimuli included 20 nM EGF or 150 nM PMA for 10, 20, 30, or 60 min; 120 J of UV irradiation and analysis after 20, 40, or 60 min or 2, 4, 7, or 10 h; and 10 μg/ml anisomycin for 30 or 60 min (data not shown). We noted an optimal bipartite nuclear localization signal in a loop within the N-terminal kinase domain of RSK4: ^{325}KRHLFFANIDWDKLYKR^{341}. Although this nuclear localization signal is conserved in all RSKs, it does not appear to be functional since the low nuclear RSK4 signal in transfected cells was not affected by its mutation as in the triple mutant RSK4-K325Q/R326A/K337A (data not shown).

To investigate how the kinase activity of RSK4 is regulated, endogenous RSK4 was immunoprecipitated and assayed from serum-starved HEK293 cells after exposure, or not, to EGF and/or U0126, a specific inhibitor of MEK1 (50). The anti-RSK4 Ab precipitated RSK4 to the same extent under all the conditions (Fig. 3*A*, *lower left panel*). Surprisingly the kinase activity of RSK4 was only slightly stimulated by EGF (Fig. 3*A*, *lower left panel*). In contrast, the activity of RSK2 precipitated from the same cell lysates was stimulated 10-fold by EGF as expected (Fig. 3*A*, *lower right panel*) and as previously demonstrated with RSK1, RSK2, and RSK3 in HEK293 cells (36). Moreover ERK, assayed on the same cell lysates, was robustly activated by EGF (Fig. 3*A*, *upper panel*). Incubation with U0126 for 2 h reduced the basal and EGF-stimulated kinase activity of RSK4 by 40–50%. This demonstrates the involvement of the MEK-ERK pathway in activation of RSK4 and also suggests that the very low level of ERK activity in unstimulated cells is sufficient to induce significant activation of RSK4 but not of RSK2. Serum starvation for 18 h, instead of 4 h as in Fig. 3, did not increase the responsiveness of RSK4 to growth factor stimulation nor did incubation for 18 h with U0126 or PD98059, another specific MEK1 inhibitor (51), decrease the activity of RSK4 by more than 50% (data not shown). In agreement with the activity measurements, EGF induced a profound electrophoretic mobility shift in RSK2 (Fig. 3*A*, *lower right panel*) most likely due to profound EGF-induced phosphorylation of RSK2. In contrast, EGF induced no significant mobility shift in RSK4 (Fig. 3*A*, *lower left panel*), suggesting that no significant phosphorylation was induced. Results identical to those shown in Fig. 3*A* were obtained by exposure of HEK293 cells to PMA, which is another strong activator of the ERK pathway in this and other cell types (data not shown). Intriguingly also in other cell types analyzed under serum-starved conditions, the activity of endogenous RSK4 was not significantly increased by EGF or PMA but was 30–50% inhibited by U0126. In contrast, RSK2 precipitated from the same cell lysates was robustly stimulated by EGF or PMA. Fig. 3, *B–D*, shows the results of such experiments with U2OS osteosarcoma cells, BJ fibroblasts, and COS7 cells. These experiments indicate that RSK4 is constitutively activated in cells.

Control experiments showed that one single protein that was reactive with the anti-RSK4 Ab was precipitated in the above experiments, and this protein was competed out by incubation of the anti-RSK4 Ab with the peptide used to raise the Ab (blocking peptide) (Fig. 3*E*). Note that the band indicated by an *asterisk* derives from the blocking peptide reagent and not from the cell lysate since it is present in a precipitation performed

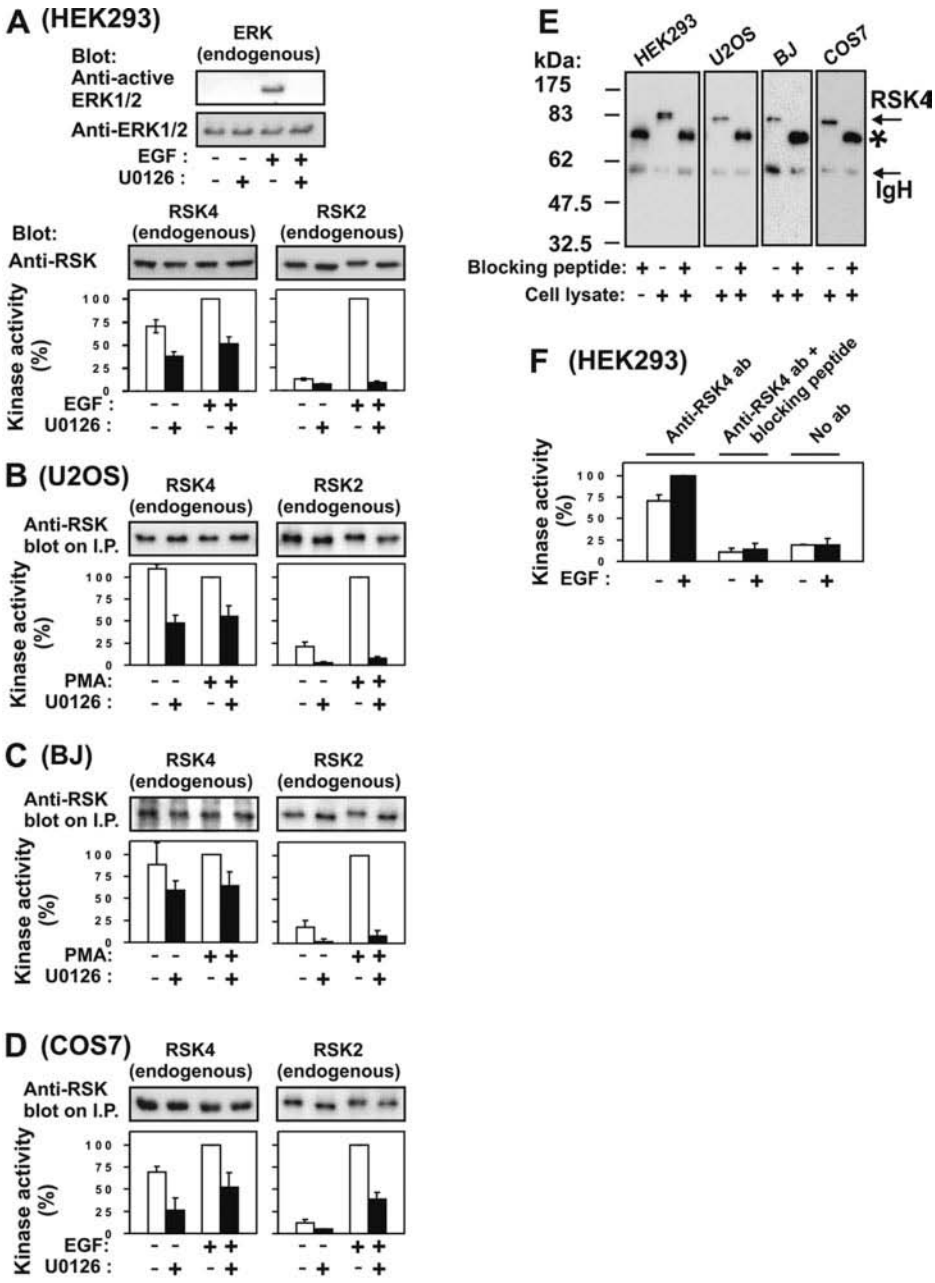

FIG. 3. **Endogenous RSK4 is constitutively activated in many cell types in a partly U0126-sensitive manner.** *A*, HEK293 cells were serum-starved for 2 h and then incubated for 2 h with 10 μM U0126 or vehicle. Thereafter the cells were exposed, or not, for 20 min to 20 nM EGF and lysed. *Lower panels*, the lysates were split 8:1 and subjected to immunoprecipitation with anti-RSK4 Ab and anti-RSK2 Ab, respectively. The precipitates were subjected to kinase assay using S6 peptide as a substrate or to immunoblotting with the indicated Abs. Kinase activity is expressed as percent, and data are means ± S.D. of three independent experiments. *Upper panel*, aliquots of preprecipitation lysates were subjected to immunoblotting with antibody to active ERK or to ERK. *B*, RSK4 and RSK2 activity in U2OS cells was analyzed as in *A* except that cells were stimulated with 150 nM PMA or vehicle for 10 min. *C*, RSK4 and RSK2 activity in BJ cells was analyzed as in *A* except that cells were stimulated with 150 nM PMA or vehicle for 10 min. *D*, RSK4 and RSK2 activity in COS7 cells was analyzed as in *A*. *E*, lysates of HEK293, U2OS, BJ, or COS7 cells were subjected to immunoprecipitation with anti-RSK4 Ab or with anti-RSK4 Ab preadsorbed to the peptide used to generate the Ab (blocking peptide). The band indicated by an *asterisk* derives from the blocking peptide reagent and not from the cell lysate. *F*, RSK4 activity in HEK293 cells was analyzed as in *A* except that immunoprecipitations were also performed with anti-RSK4 Ab preadsorbed to blocking peptide as well as without any Ab as indicated in the panel. *IgH*, Ig heavy; *I.P.*, immunoprecipitate.

with omission of cell lysate (Fig. 3*E*, *lane 1*). Moreover the S6 peptide kinase activity present in HEK293 immunoprecipitates was reduced by 80–90% when the precipitations were performed with anti-RSK4 Ab incubated with blocking peptide or by omission of the anti-RSK4 Ab (Fig. 3*F*), confirming that kinases other than RSK4 account for only a minor fraction of the S6 peptide kinase activity. In fact, all the data with endogenous RSK4 kinase activity presented in this study have been adjusted by subtraction of a reaction blank, which was determined by performing parallel immune complex kinase assays with omission of the anti-RSK4 Ab in each experiment. We therefore conclude that the kinase activity measured in the experiments derives from RSK4.

To investigate the activity and regulation of RSK4 expressed from the RSK4 cDNA clone, HEK293 cells were transiently transfected with plasmid expressing HA-RSK4 or HA-RSK2 for comparison. Exogenous RSK4 and RSK2 responded to EGF and U0126 in basically the same way as the endogenous kinases except that a 2-fold stimulation of exogenous RSK4 was observed in response to EGF (Fig. 4*A*). To determine the specific kinase activity of RSK4 compared with that of RSK2, immunoprecipitations for kinase assays were titrated to precipitate similar amounts of HA-RSK4 and HA-RSK2 from transiently transfected COS7 cells. As shown in Fig. 4*B*, RSK4 has in fact higher specific activity than RSK2 when measured against S6 peptide, the most frequently used *in vitro* RSK substrate, or against cross-tide, derived from glycogen synthase kinase-3β and containing Ser^9, which is a physiological RSK phosphorylation site (37). Using full-length glycogen synthase kinase-3β as a substrate, similar results were obtained (data not shown). When correlating for RSK protein levels, the specific activity of RSK4 was 10–20-fold higher than that of RSK2 in serum-starved COS7 cells and 2–3-fold higher than that of RSK2 in EGF-treated COS7 cells. As observed with HEK293 cells, exogenous RSK4 could be stimulated 2–3-fold by EGF in COS7 cells in contrast to the endogenous RSK4, which was not stimulated by EGF in these cell types, as shown in Fig. 3. It should be noted that the above *in vitro* results do not imply that S6 protein or glycogen synthase kinase-3 are physiological substrates of RSK4 but only reflect that the proteins contain

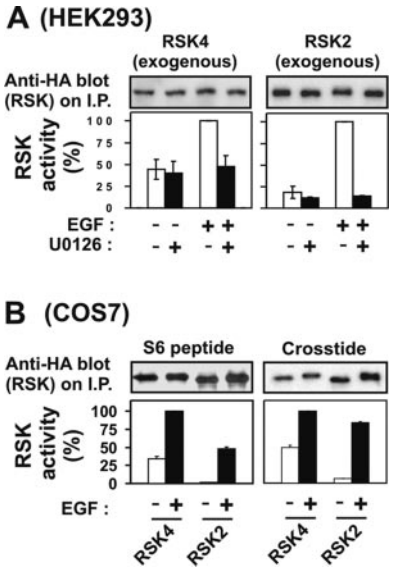

FIG. 4. **Kinase activity of recombinant RSK4.** HEK293 or COS7 cells were transfected with plasmid expressing HA-tagged RSK4 or RSK2. After 20 h, the cells were serum-starved for 2 h and then incubated for 2 h with 10 μM U0126 or vehicle where indicated in the panels. Thereafter the cells were exposed, or not, for 20 min to 20 nM EGF and lysed. The lysates were subjected to immunoprecipitation with anti-HA Ab, and the precipitates were subjected to kinase assay or to immunoblotting with Ab to the HA tag. *A*, kinase activity, determined using S6 peptide as a substrate, is expressed as percent, and data are means ±S.D. of three independent experiments. *B*, to obtain similar amounts of precipitated RSK2 and RSK4, 2.4-fold less cell lysate was used for immunoprecipitation of RSK2 compared with that used for RSK4. The precipitates were subjected to kinase assay using S6 peptide or cross-tide as a substrate or to immunoblotting with Ab to the HA tag. Kinase activity is expressed as percent of maximal RSK4 activity, and data are means ±S.D. of triplicate determinations from one representative experiment of three. *I.P.*, immunoprecipitate.

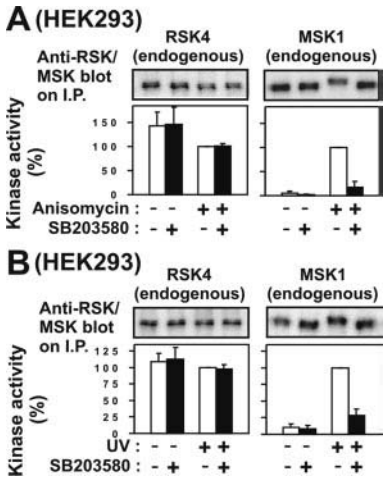

FIG. 5. **RSK4 activity is not affected by activators or inhibitors of stress-activated MAP kinase pathways.** HEK293 cells were serum-starved for 2 h and incubated for 2 h with 10 μM SB203580 or vehicle. Thereafter the cells were exposed, or not, for 60 min to 10 μg/ml anisomycin (*A*) or to 200 J of UV irradiation and lysed after 20 min (*B*). The lysates were split 8:1 and subjected to immunoprecipitation with anti-RSK4 Ab and anti-MSK1 Ab, respectively. The precipitates were subjected to kinase assay using S6 peptide (for RSK4) or cross-tide (for MSK1) as a substrate or to immunoblotting with Ab to RSK4 or MSK1. Kinase activity is expressed as percent, and data are means ± S.D. of three independent experiments. *I.P.*, immunoprecipitate.

the minimal consensus sequence (Arg-*X*-*X*-Ser), which allows *in vitro* phosphorylation by RSK family kinases as well as by several other kinases related to RSKs.

We next investigated whether RSK4, like MSK, might be regulated via stress-stimulated MAPK pathways. Endogenous RSK4 was therefore immunoprecipitated from HEK293 cells exposed to either of two distinct stress stimuli, anisomycin and UV irradiation, that strongly activate p38 and JNK family kinases. As shown in Fig. 5, *A* and *B*, the stress stimuli did not increase the activity of RSK4. Moreover SB203580, a specific inhibitor of p38α and -β MAPKs (52), had no effect on the kinase activity of RSK4. Serving as a control for the various treatments, the kinase activity of MSK1 was strongly stimulated by anisomycin or UV irradiation and was profoundly inhibited by SB203580. Note that treatment with anisomycin reduced precipitable RSK4 kinase activity apparently by decreasing the RSK4 protein level, which may be due to the ability of anisomycin to inhibit protein synthesis. Also in U2OS cells, the activity of RSK4 was not affected by UV irradiation or SB203580 (data not shown).

The experiments depicted in Figs. 3–5 were performed with cell cultures of 80–95% confluency that contained a mixture of growing and contact-inhibited cells. To investigate whether the activity of RSK4 varies as a function of growth status, RSK4 was immunoprecipitated from equal amounts of exponentially growing or contact-inhibited HEK293 cells and assayed for kinase activity. As shown in Fig. 6, RSK4 had similar activity in growing and arrested HEK293 cells. Moreover RSK4 activity was not affected by growth factor stimulation or by stress stimulation of the growing or arrested cells. Similar results were obtained in COS7 cells (data not shown).

The involvement of ERK in activation of RSK4 was supported by the finding that RSK4 can co-immunoprecipitate ERK1 from lysates of transiently transfected COS7 cells (Fig. 7*A*). In contrast, the mutant RSK4-(1–730) with deletion of the C-terminal 15 residues, which contain the predicted MAPK docking site, did not precipitate ERK1, showing that the MAPK docking site is functional. Interestingly RSK4 co-precipitated from 2 to 3 times as much ERK1 as did similar amounts of RSK2 (Fig. 7*A*). Finally RSK4 showed no ability to co-immunoprecipitate with p38α or JNK2α2 (Fig. 7, *B* and *C*). As controls, p38α and JNK2α2 co-immunoprecipitated with MSK1 and c-Jun, respectively. Thus, these results provide further evidence that RSK4 is regulated by ERK-type MAP kinases but not by stress-activated MAP kinases.

The results presented in Figs. 3–7 support the intriguing conclusion that endogenous RSK4 is maximally (constitutively) activated in serum-starved cells and suggest that the low basal ERK activity is responsible for inducing at least 30–50% of the RSK4 activity under these conditions. RSK4 is thereby markedly distinct from other RSKs, which require growth factor stimulation to obtain significant kinase activity. To further investigate the basis of constitutive RSK4 activity, endogenous RSK4 and RSK2 were precipitated from HEK293 cells and analyzed with phosphospecific antibodies to the three phosphorylation sites known from analysis of RSK1 (28) and RSK2 (33, 35) to directly stimulate catalytic activity, *i.e.* Ser^{232}, Ser^{372}, and Ser^{389}. This analysis revealed that RSK4 had a very similar level of phosphorylation in serum-starved and EGF-stimulated cells at all three sites (Fig. 8*A*). By contrast in RSK2, EGF stimulated phosphorylation 2-fold at Ser^{232} and >10-fold at Ser^{372} and Ser^{389} in a U0126-sensitive manner. The 40–50% reduction of RSK4 kinase activity by U0126 (Fig. 3*A*) was not paralleled by a 40–50% reduction of phosphorylation of one particular site by U0126 in Fig. 8*A*. Conceivably U0126 induces a small decrease of phosphorylation at perhaps all of the sites, which is difficult to detect by immunoblotting but which together result in 50% reduction of kinase activity, which can readily be measured by the very accurate kinase assay.

We next subjected endogenous RSK4 or RSK2, immunopre-

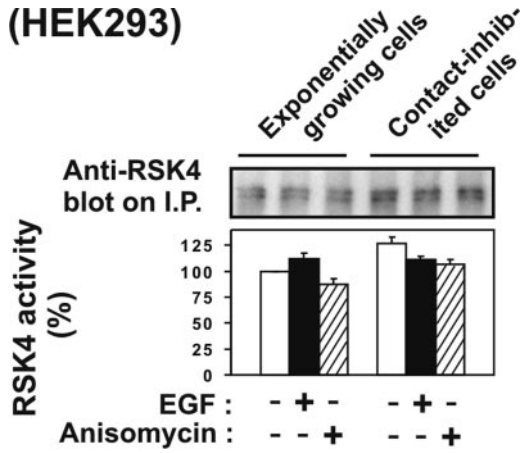

FIG. 6. **Endogenous RSK4 is constitutively activated in exponentially growing and contact-inhibited cells.** Exponentially growing HEK293 cells (used at 30–40% confluency) or contact-inhibited HEK293 cells (used 2 days after reaching confluency) were exposed for 20 min to 20 nM EGF or for 60 min to 10 μg/ml anisomycin or left untreated and then lysed. Cell lysates were normalized for protein and subjected to immunoprecipitation with anti-RSK4 Ab. The precipitates were subjected to kinase assay using S6 peptide as a substrate or to immunoblotting using anti-RSK4 Ab. Kinase activity is expressed as percent, and data are means ± S.D. of three independent experiments. *I.P.*, immunoprecipitate.

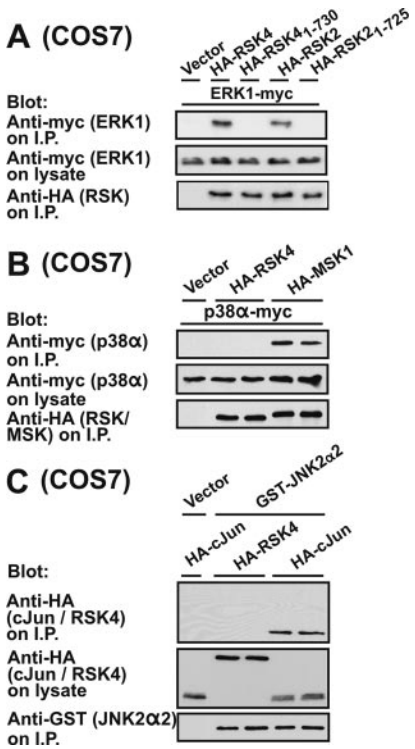

FIG. 7. **RSK4 can form a complex with ERK but not with p38 or JNK in cells.** COS7 cells were transfected with plasmid expressing Myc-tagged ERK1 (*A*) or Myc-tagged p38α (*B*) together with plasmid expressing wild type or deletion mutants of HA-RSK4, HA-RSK2, or HA-MSK1 or with empty vector as indicated in the panels. After 20 h, the cells were lysed, and cell lysates were subjected to immunoprecipitation with Ab to the HA tag. Aliquots of the precipitates and the preprecipitation lysates were subjected to immunoblotting with Ab as indicated. To obtain equal amounts of precipitated RSK4 compared with RSK2 and MSK1, 2.4- and 5-fold less cell lysate was used for immunoprecipitation of RSK2 and MSK1, respectively, compared with that used for RSK4. *C*, COS7 cells were transfected with plasmid expressing HA-c-Jun or HA-RSK4 together with plasmid expressing GST-JNK2α2 or empty vector. To obtain similar expression of HA-c-Jun and HA-RSK4, HA-c-Jun plasmid was diluted 1:3 with empty vector. After 20 h, the cells were lysed, and cell lysates were subjected to precipitation of GST proteins using glutathione-agarose beads. Aliquots of the precipitates and the preprecipitation lysates were subjected to immunoblotting with Ab as indicated. All experiments were performed three times with similar results. *I.P.*, immunoprecipitate.

cipitated from serum-starved HEK293 cells, to *in vitro* phosphorylation by active ERK2 and PDK1 and thereafter measured the kinase activity of the two RSKs. The activity of RSK2 was increased 4-fold by incubation with ERK2 and PDK1, whereas the activity of RSK4 was not affected (Fig. 8*B*). In conclusion, the results presented in Fig. 8, *A* and *B*, strongly suggest that endogenous RSK4 is constitutively activated in serum-starved cells because it is maximally phosphorylated at the key activating sites.

Phosphoblot analysis was also performed on exogenous RSK4 and RSK2 transiently expressed in COS7 cells. RSK4 was phosphorylated at Ser^{232} to the same extent in starved and EGF-stimulated cells, whereas RSK2 showed a 3–4-fold induction of this site in response to EGF (Fig. 8*C*, *upper panel*). RSK4 also showed high basal phosphorylation of Ser^{389} and Thr^{581} as compared with RSK2. By contrast, RSK4 showed no basal phosphorylation of Ser^{372}. In exogenous RSK4, the phosphorylation of Ser^{372}, Ser^{389}, and Thr^{581} was induced or further increased by EGF, probably explaining why the kinase activity of exogenous RSK4 can be stimulated to a modest degree by EGF in COS7 cells in contrast to the endogenous RSK4. However, exogenous RSK4 still showed high basal kinase activity in COS7 cells that appears to result from high basal phosphorylation of Ser^{232} and Ser^{389}.

Analysis of RSK4 point mutants surprisingly revealed that phosphorylation of the predicted PDK1 site, Ser^{232}, was not affected by mutation of Ser^{389} in the predicted PDK1 docking site (Fig. 8*C*, *upper panel*). By contrast in RSK2, mutation of the corresponding serine in the PDK1 docking site (Ser^{386}) completely abolished phosphorylation of the PDK1 phosphorylation site (Fig. 8*C*, *upper panel*). Also unexpectedly, mutation of Thr^{581} only slightly decreased the ability of EGF to induce phosphorylation of Ser^{389}. To investigate whether this is due to an inability of the C-terminal kinase of RSK4 to be activated via phosphorylation of Thr^{581}, we analyzed EGF-induced activation of the isolated C-terminal kinase domain with the linker including the Ser^{389} site (RSK4-(371–745)). As shown in Fig. 8*C* (*lower panel*), EGF promoted wild-type RSK4-(371–745), but not RSK4-(371–745)-T581A, to autophosphorylate at Ser^{389}. This shows that the C-terminal kinase of RSK4 is functional. Kinase assays showed that mutation of Ser^{389} profoundly decreased the kinase activity of RSK4, suggesting that this phosphorylation site has a major role in the basal as well as EGF-stimulated catalytic activity of RSK4 (Fig. 8*C*). By contrast, kinase assays on mutants of Thr^{581} and Ser^{372} suggested that these sites have no role in the basal activity of exogenous RSK4 in COS7 cells but contribute to the EGF-stimulated activity.

Only in one of eight cell lines tested did RSK4 show a low basal activity compared with stimulated kinase activity. Thus, in CHO cells stably transfected with the insulin receptor (IR) (53), the activity of exogenous RSK4 was stimulated about 5-fold by insulin. No endogenous RSK4 protein could be detected in CHO-IR cells (data not shown). Since endogenous RSK4 was not stimulated in any cell type tested, the stimulation in CHO-IR cells may not be physiological. However, this cell line was considered suitable for further analysis of the role of the individual phosphorylation sites in regulation of the catalytic activity of RSK4 due to the low basal *versus* stimulated activity. Wild-type RSK4 and mutants of the six phosphorylation sites identified in RSKs were expressed and assayed in CHO-IR cells. Stimulation of RSK4 activity by insulin was mediated by ERK since it was completely abolished by U0126

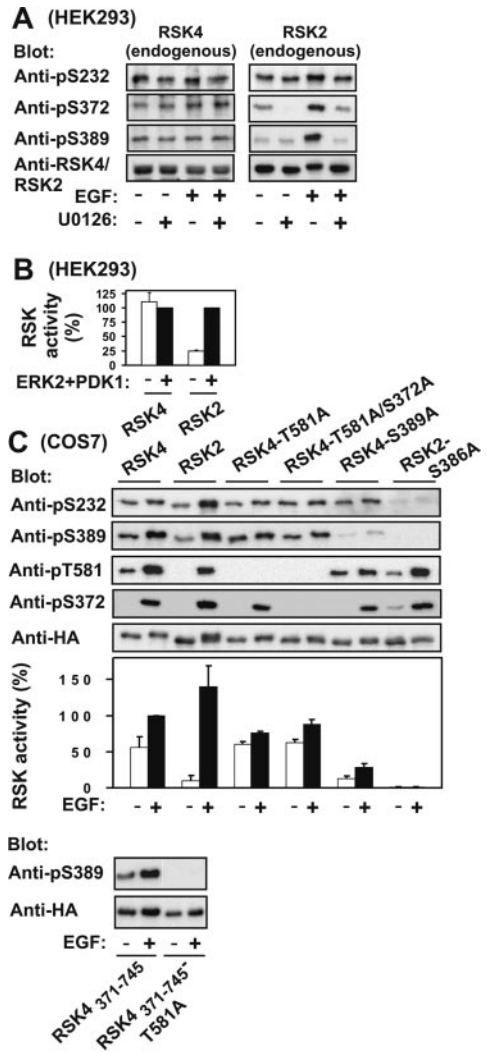

FIG. 8. **Constitutive activation of endogenous RSK4 in serum-starved cells is due to constitutive phosphorylation.** *A*, endogenous RSK4 or RSK2 was immunoprecipitated from serum-starved HEK293 cells treated as described in the legend to Fig. 3*A* and subjected to immunoblotting with phosphospecific Abs to Ser^{232}, Ser^{372}, or Ser^{389}. The experiment was performed three times with similar results. *B*, HEK293 cells were serum-starved for 4 h and then lysed. Endogenous RSK4 or RSK2 was immunoprecipitated from the cell lysates and incubated for 30 min with MgATP in the absence or presence of active ERK2 and active PDK1. Thereafter the kinase activity of RSK4 and RSK2 was determined using S6 peptide as a substrate and expressed as percent of the activity after incubation with ERK2 and PDK1. *C*, COS7 cells were transfected with plasmid expressing wild-type or mutant HA-RSK4 or HA-RSK2. After 20 h and a final 4-h serum starvation period, cells were exposed, or not, for 20 min to 20 nM EGF and then lysed. The lysates were subjected to immunoprecipitation with Ab to the HA tag. Aliquots of the precipitates were subjected to immunoblotting with the Abs indicated in the panel or to kinase assay using S6 peptide as a substrate. Kinase activity is expressed as percent of maximal RSK4 activity, and data are means ± S.D. of three independent experiments. *pT*, phosphothreonine; *pS*, phosphoserine.

(Fig. 9*A*, *left panel*) and insensitive to SB203580 (data not shown). Mutation of Thr^{368} did not affect RSK4 kinase activity as shown for the corresponding Thr in RSK1 (28) and RSK2.[2] Individual mutation of Ser^{372} and Thr^{581} decreased the activity of RSK4 by 30%, whereas the double mutant S372A/T581A showed 80% reduced activity. Mutation of Ser^{389} most profoundly reduced RSK4 activity, whereas mutation of Ser^{742} had no effect. The RSK4-S232A mutant was not included in Fig. 9*A* due to low expression, but the mutant was completely devoid of kinase activity, indicating that Ser^{232} phosphorylation is strictly required for activation of RSK4. Since individual mutation of the sites corresponding to Ser^{372} and Thr^{581} were previously shown to abolish PMA-induced activity of RSK1 in COS1 cells (28), we analyzed these RSK1 mutants in CHO-IR cells. Compared with RSK4, these two sites individually contributed considerably more to activation of RSK1, although their mutation did not abolish kinase activity (Fig. 9*A*, *right panel*). Phosphoimmunoblot analysis of RSK4 from CHO-IR cells showed that, as in COS7 cells, mutation of Ser^{389} did not abolish phosphorylation of Ser^{232}, although a 2-fold reduction was observed (Fig. 9*B*). Also as in COS7 cells, mutation of Thr^{581} had only a small effect on insulin-stimulated phosphorylation of Ser^{389}, explaining why the T581A mutation had only a small effect on kinase activity.

The finding that mutation of the PDK1 docking site in RSK4 did not significantly affect phosphorylation of Ser^{232} could indicate that, unlike RSK1–3 (33, 34, 37), RSK4 does not require PDK1 for activation. To address this question, RSK4 was transiently expressed in wild-type mouse ES cells or in mouse ES cells with targeted disruption of both *PDK1* alleles (37) and thereafter analyzed with respect to kinase activity and phosphorylation of Ser^{232}. As shown in Fig 10*A*, exogenous RSK4 had similar activity in wild-type and PDK1-deficient ES cells and showed similar phosphorylation of Ser^{232}. In contrast, endogenous RSK2 showed greatly decreased kinase activity and phosphorylation at the PDK1 site in PDK1-deficient ES cells (Fig. 10*A*). To obtain maximal RSK2 activity, the ES cells were treated with PMA in these experiments, but RSK4 had similar activity in PMA-treated and untreated cells (data not shown). To investigate whether RSK4 may autophosphorylate at Ser^{232}, PDK1-deficient ES cells were transfected with RSK4 mutants (RSK4-K105A or RSK4-P242A/E243A) in which the NTK had been inactivated by mutation of critical residues conserved in virtually all kinases. These mutants had minimal kinase activity and showed profoundly decreased phosphorylation at Ser^{232} compared with wild-type RSK4 (Fig 10*B*), suggesting that RSK4 can autophosphorylate at Ser^{232}. Finally, like exogenous RSK4, endogenous RSK4 showed equal phosphorylation of Ser^{232} in wild-type and PDK1-deficient ES cells (Fig. 10*C*). In conclusion, RSK4 is markedly distinct from other RSKs in that it does not require PDK1 for phosphorylation of Ser^{232} and activation.

DISCUSSION

We performed the first functional characterization of the putative new RSK family member RSK4. Our data showed that RSK4 is a functional protein kinase that belongs to the RSK, rather than MSK, family since RSK4 interacts with and is regulated by ERK, whereas no evidence for regulation by stress-activated MAP kinases was obtained. However, our data also showed that RSK4 has important features that clearly distinguish it from other RSK proteins. Thus, RSK4 has growth factor-independent, constitutive activity in many cell types and does not require PDK1 for activation. These features imply that RSK4 has different signaling properties and is functionally distinct from other RSKs.

The constitutive activity of RSK4 appears to result from constitutive phosphorylation of key activating sites. Thus, endogenous RSK4 showed the same level of phosphorylation of Ser^{232}, Ser^{372}, and Ser^{389} in starved and growth factor-stimulated cells, and mutational analysis demonstrated that these sites are important in stimulation of kinase activity. In a simple explanation for the constitutive activation, the expression level (and/or the rate of dephosphorylation) of RSK4 is so low that the basal activity of a highly expressed activating kinase is sufficient to induce maximal phosphorylation of RSK4. This is

[2] C. J. Jensen and M. Frödin, unpublished observation.

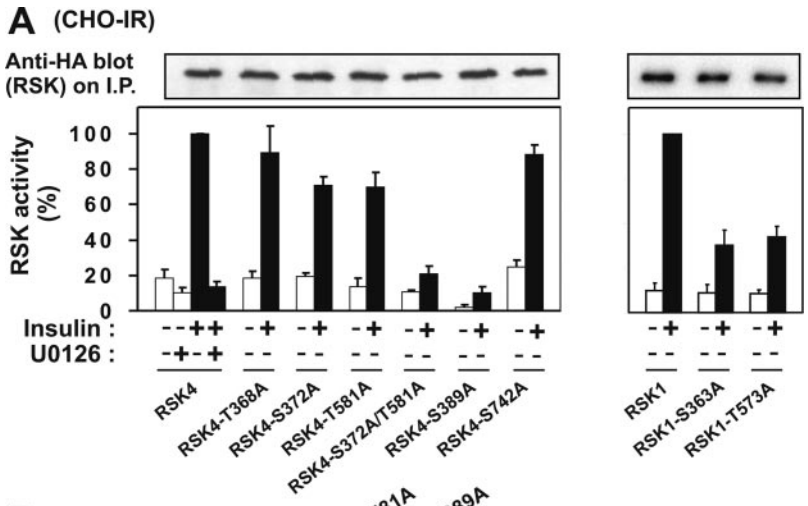

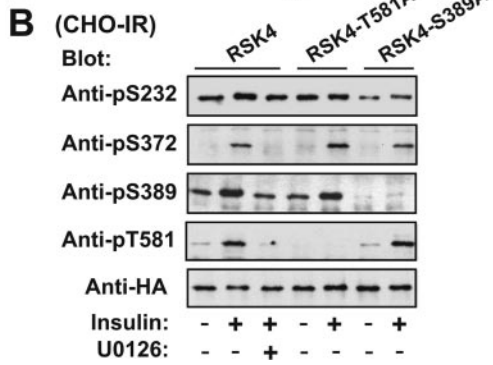

FIG. 9. **Role of individual phosphorylation sites in regulation of RSK4 kinase activity.** *A*, CHO-IR cells were transfected with plasmid expressing wild-type or mutant HA-RSK4 or HA-RSK1. After 36 h and a final 4-h serum starvation period, cells were exposed, or not, for 15 min to 150 nM insulin and then lysed. The lysates were subjected to immunoprecipitation with Ab to the HA tag. Aliquots of the precipitates were subjected to kinase assay using S6 peptide as a substrate or to immunoblotting with Ab to the HA tag (only precipitates from starved cells are shown). Kinase activity is expressed as percent, and data are means ± S.D. of at least three independent experiments. *B*, wild-type and mutant HA-RSK4 were expressed and purified from CHO-IR cells as described in *A* and subjected to immunoblotting with the Abs indicated in the panel. The experiment was performed three times with similar results. *I.P.*, immunoprecipitate; *pT*, phosphothreonine; *pS*, phosphoserine.

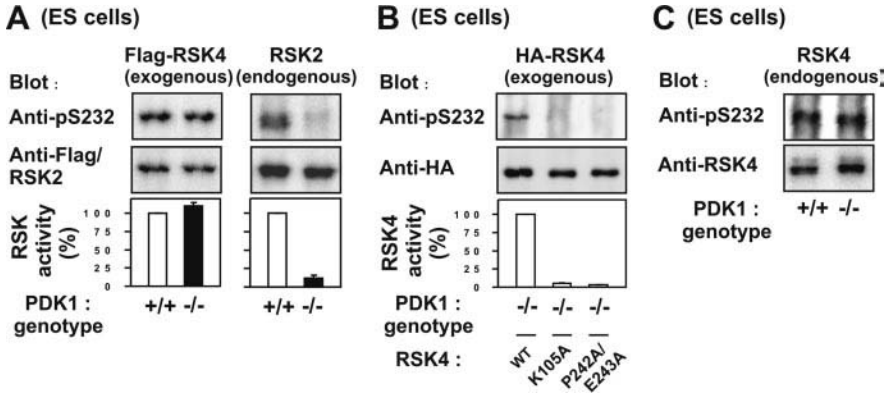

FIG. 10. **RSK4 does not require PDK1 for phosphorylation of Ser232 or activation.** *A*, for RSK4, wild-type (+/+) or PDK1-deficient (−/−) mouse ES cells were transfected with plasmid expressing FLAG-tagged RSK4. After 18 h, the cells were exposed to 150 nM PMA for 20 min and then lysed. The lysates were subjected to immunoprecipitation with Ab to the FLAG tag. The precipitates were subjected to kinase assay using S6 peptide as a substrate followed by the addition of SDS-PAGE sample buffer to the precipitates and immunoblotting with Ab to Ser(P)^{232} or the FLAG tag. To obtain equal amounts of precipitated RSK4 from the two ES cell lines, more lysate from −/− cells than from +/+ cells was used for immunoprecipitation since the −/− cells were transfected with low efficiency. Kinase activity is expressed as percent, and data are means ± S.D. of triplicate determinations. For RSK2, endogenous RSK2 was precipitated with anti-RSK2 Ab from ≈10^7 non-transfected PDK1(+/+) or PDK1(−/−) ES cells exposed for 20 min to 150 nM PMA and then analyzed as described for RSK4. The experiments were performed four times with similar results. *B*, PDK1-deficient (−/−) ES cells were transfected with plasmid expressing wild-type or mutant HA-tagged RSK4. HA-RSK4 was precipitated using anti-HA Ab and analyzed as described in *A*. To obtain similar amounts of precipitated RSK4, 5-fold less cell lysate was used for immunoprecipitation of wild-type compared with mutant RSK4 as the mutants showed decreased expression. Kinase activity is expressed as percent, and data are means ± range of two independent experiments. *C*, approximately 10^7 wild-type (+/+) or PDK1-deficient (−/−) ES cells were exposed to 150 nM PMA for 20 min and then lysed. Endogenous RSK4 was precipitated with anti-RSK4 Ab and subjected to immunoblotting with Ab to Ser(P)^{232} or to RSK4. The experiment was performed twice with similar results. *pS*, phosphoserine; *WT*, wild type.

likely to be partly the case since the basal activity of ERK contributed to at least 30–50% of the activity of endogenous RSK4 as evidenced by U0126 sensitivity, although basal ERK activity was very low, amounting to less than 5% of the EGF-stimulated ERK activity (Fig. 3*A* and data not shown). In addition, ERK is a very abundant kinase with an estimated concentration of 1–3 μM in mammalian cells (54), whereas RSK4 has very low expression as discussed below. The above explanation is also indirectly supported by the finding that, in the case of overexpressed RSK4 in COS7 cells, the basal activity of endogenous ERK was not sufficient to induce maximal phosphorylation of the ERK sites in RSK4 conceivably due to high amounts of RSK4 relative to ERK.

The experiments with exogenous RSK4 in COS7 cells also

suggested that the U0126-insensitive (*i.e.* apparently ERK-independent) RSK4 activity derives from phosphorylation of Ser^{232} and Ser^{389} since the RSK4-S372A/T581A mutant with all regulatory ERK sites mutated showed considerable basal phosphorylation of Ser^{232} and Ser^{389} as well as considerable basal kinase activity. Mutational analysis furthermore confirmed that Ser^{232} and Ser^{389} are the most important phosphorylation sites in stimulation of RSK4 catalytic activity. This is not surprising since the two sites are conserved in many kinases of the so-called AGC kinase superfamily, which includes RSK, MSK, protein kinase B (PKB), p70 S6 kinase, and serum- and glucocorticoid-inducible kinase, where the two sites have an essential and synergistic effect on kinase activation (35). An absolute requirement for PDK1 in phosphorylation of the activation loop in the NTK of RSK1–3 has been demonstrated biochemically (33, 34) and genetically (37, 55). It is therefore surprising that PDK1 is not required for Ser^{232} phosphorylation and activation of RSK4 as demonstrated here genetically in PDK1-deficient ES cells. Instead RSK4 may autophosphorylate at Ser^{232} as indicated by the reduced Ser^{232} phosphorylation observed in the catalytically inactive RSK4 mutants in PDK1-deficient ES cells. Our results, however, do not exclude that PDK1 may contribute to phosphorylation of Ser^{232} in PDK1 wild-type cells.

Mutational analysis also suggested that phosphorylation of Ser^{372} and Thr^{581} plays a more modest role in stimulation of RSK4 kinase activity than does phosphorylation of Ser^{232} and Ser^{389}. In insulin-stimulated CHO-IR cells, double mutation of Ser^{372} and Thr^{581} had a much greater effect on RSK4 kinase activity than did the single mutations, suggesting that the sites can compensate for each other. It is possible that the unexpected phospho-Thr^{581}-independent phosphorylation of Ser^{389} induced by insulin in the T581A mutant (Fig. 9*B*) could contribute to the apparent compensating function of the two sites, but the mechanism behind this observation is unknown.

Based on this and previous studies on the RSK activation mechanism, a model for constitutive activation of endogenous RSK4 in serum-starved cells is proposed. Constitutive activation is due to maximal phosphorylation of Ser^{232}, Ser^{372}, and Ser^{389} of which Ser^{232} and Ser^{389} synergize to stabilize the NTK in the active conformation thereby inducing about 80% of the RSK4 activity. The low basal ERK activity is responsible for induction of at least 50% of the RSK4 activity via maximal phosphorylation of Ser^{372} and Thr^{581}. Phosphorylation of Ser^{372} directly stimulates the activity of the NTK, whereas phosphorylation of Thr^{581} stimulates NTK by promoting partial phosphorylation of Ser^{389}, and this event may possibly enhance autophosphorylation of Ser^{232}. The remaining 50%, apparently ERK-independent, RSK4 activity derives from phosphorylation of Ser^{232} and Ser^{386}, which may be catalyzed by autophosphorylation by the NTK and the C-terminal kinase, respectively, although a contribution from additional kinases cannot be excluded.

Two recent studies suggest that RSK4 may have unique cellular functions compared with RSK1–3. In the first study, a short interfering RNA screen was carried out to identify mediators of p53-induced growth arrest, and it was discovered that knock-down of RSK4 abolishes p53-dependent G_1 cell cycle arrest induced either by conditional activation of p53 or by DNA damage via ionizing irradiation (42). It was also demonstrated that RSK4 knock-down strongly suppressed expression of mRNA for the cyclin-dependent kinase inhibitor $p21^{cip1}$, a major component of the antiproliferative response to p53. However, the regulation and mechanism of action of RSK4 in the p53 response was not addressed. In the present study, we found no regulation of RSK4 by UV irradiation, which also induces DNA damage and p53 activation, or by p53 transfection in U2OS or BJ cells, the two cell types analyzed in the study mentioned above. Thus, no change in RSK4 activity or subcellular distribution was detected within 8 h after UV irradiation nor did UV irradiation or transfection with p53 plasmid increase the RSK4 protein level within 24 h, although a robust growth arrest was observed (data not shown). It is therefore possible that RSK4 may function as an indirect mediator of p53 in induction of downstream effectors for instance by phosphorylating a protein in the p53 transcriptional activation complex on the $p21^{cip1}$ promotor or by stimulating $p21^{cip1}$ mRNA stability in the cytoplasm. The constitutive activity of RSK4 demonstrated here would enable RSK4 to function as such an indirect mediator of p53 signaling.

In the second study, a functional screen of mouse mRNAs showed that injection of RSK4, but not RSK1–3, transcripts into *X. laevis* one-cell embryos disrupted the subsequent formation of mesoderm, which is induced by the fibroblast growth factor-Ras-ERK pathway (43). The mechanism of inhibition was not resolved, but the inhibitory action appeared to take place at a level downstream of Ras, resulting in reduced phosphorylation of MEK and ERK at the activating sites. In early mouse development, RSK4 shows particularly high mRNA expression in extraembryonic tissue, and RSK4 expression is inversely correlated with the presence of active ERK as detected by anti-active ERK immunostaining. The authors proposed that RSK4 is an inhibitor, rather than a mediator, of growth factor signal transduction via the Ras-ERK pathway in selected cellular contexts. This hypothesis would require that activation of RSK4 can occur in a growth factor-independent manner. In the present study, we found evidence for growth factor-independent activation of RSK4 that may occur via low basal levels of ERK activity and/or autophosphorylation.

Although a quantitative analysis was not performed, the low signal in kinase assays and immunoblots of endogenous RSK4 suggests that RSK4 may be expressed at 10–20 times lower levels than other RSKs in most cell types. This conclusion is supported by the extraordinarily low number of human RSK4 expressed sequence tags (ESTs) in the public data bases. Thus, as of January 2005, Unigene listed 16 RSK4 ESTs, 289 RSK1 ESTs, 282 RSK2 ESTs, and 351 RSK3 ESTs (www.ncbi.nlm.nih.gov/entrez/query.fcgi?db=unigene), indicating that low RSK4 protein expression is due to low RSK4 mRNA levels. In agreement with this conclusion, Kohn *et al.* (41) noted that RSK4 shows relatively broad but low expression compared with RSK2 in fetal mouse tissues. Since RSK4 appears to be constitutively activated in cells and may function to suppress Ras-ERK signal transduction and cell proliferation, the expression level of RSK4 may be low in most cell types to allow cell growth. Conversely up-regulation of RSK4 expression may be one mechanism to restrict cell growth. It can further be speculated that the biological activity of RSK4 is regulated primarily at the level of expression rather than at the level of catalytic activity, the major level of regulation of RSK1–3.

Acknowledgments—We gratefully acknowledge reagents provided by Dr. Joseph Avruch (Boston, MA), Dr. Karine Merienne (Strasbourg, France), and Dr. Tuula Kallunki (Copenhagen, Denmark) that were important for conducting this study.

REFERENCES

1. Sturgill, T. W., Ray, L. B., Erikson, E., and Maller, J. L. (1988) *Nature* **334,** 715–718
2. Zhao, Y., Bjorbak, C., and Moller, D. E. (1996) *J. Biol. Chem.* **271,** 29773–29779
3. Frodin, M., and Gammeltoft, S. (1999) *Mol. Cell. Endocrinol.* **151,** 65–77
4. Gross, S. D., Lewellyn, A. L., and Maller, J. L. (2001) *J. Biol. Chem.* **276,** 46099–46103
5. Gross, S. D., Schwab, M. S., Lewellyn, A. L., and Maller, J. L. (1999) *Science* **286,** 1365–1367
6. Bhatt, R. R., and Ferrell, J. E., Jr. (1999) *Science* **286,** 1362–1365

7. Palmer, A., Gavin, A. C., and Nebreda, A. R. (1998) *EMBO J.* **17,** 5037–5047
8. Schwab, M. S., Roberts, B. T., Gross, S. D., Tunquist, B. J., Taieb, F. E., Lewellyn, A. L., and Maller, J. L. (2001) *Curr. Biol.* **11,** 141–150
9. Fujita, N., Sato, S., and Tsuruo, T. (2003) *J. Biol. Chem.* **278,** 49254–49260
10. Cohen, P., and Frame, S. (2001) *Nat. Rev. Mol. Cell. Biol.* **2,** 769–776
11. Sutherland, C., Leighton, I. A., and Cohen, P. (1993) *Biochem. J.* **296,** 15–19
12. Stambolic, V., and Woodgett, J. R. (1994) *Biochem. J.* **303,** 701–704
13. Wang, X., Li, W., Williams, M., Terada, N., Alessi, D. R., and Proud, C. G. (2001) *EMBO J.* **20,** 4370–4379
14. Zhao, J., Yuan, X., Frodin, M., and Grummt, I. (2003) *Mol. Cell* **11,** 405–413
15. Roux, P. P., Ballif, B. A., Anjum, R., Gygi, S. P., and Blenis, J. (2004) *Proc. Natl. Acad. Sci. U. S. A.* **101,** 13489–13494
16. Bonni, A., Brunet, A., West, A. E., Datta, S. R., Takasu, M. A., and Greenberg, M. E. (1999) *Science* **286,** 1358–1362
17. Murphy, L. O., Smith, S., Chen, R.-H., Fingar, D. C., and Blenis, J. (2002) *Nat. Cell Biol.* **4,** 556–564
18. Joel, P. B., Smith, J., Sturgill, T. W., Fisher, T. L., Blenis, J., and Lannigan, D. A. (1998) *Mol. Cell. Biol.* **18,** 1978–1984
19. Silverman, E., Frodin, M., Gammeltoft, S., and Maller, J. L. (2004) *Mol. Cell. Biol.* **24,** 10573–10583
20. Yang, X., Matsuda, K., Bialek, P., Jacquot, S., Masuoka, H. C., Schinke, T., Li, L., Brancorsini, S., Sassone-Corsi, P., Townes, T. M., Hanauer, A., and Karsenty, G. (2004) *Cell* **117,** 387–398
21. El-Haschimi, K., Dufresne, S. D., Hirshman, M. F., Flier, J. S., Goodyear, L. J., and Bjorbaek, C. (2003) *Diabetes* **52,** 1340–1346
22. Deak, M., Clifton, A. D., Lucocq, L. M., and Alessi, D. R. (1998) *EMBO J.* **17,** 4426–4441
23. Pierrat, B., da Silva Correia, J., Mary, J.-L., Tomas-Zuber, M., and Lesslauer, W. (1998) *J. Biol. Chem.* **273,** 29661–29671
24. Leighton, I. A., Dalby, K. N., Caudwell, F. B., Cohen, P. T. W., and Cohen, P. (1995) *FEBS Lett.* **375,** 289–293
25. Frodin, M., Jensen, C. J., Merienne, K., and Gammeltoft, S. (2000) *EMBO J.* **19,** 2924–2934
26. Bjørbæk, C., Zhao, Y., and Moller, D. E. (1995) *J. Biol. Chem.* **270,** 18848–18852
27. Fisher, T., and Blenis, J. (1996) *Mol. Cell. Biol.* **16,** 1212–1219
28. Dalby, K. N., Morrice, N., Caudwell, F. B., Avruch, J., and Cohen, P. (1998) *J. Biol. Chem.* **273,** 1496–1505
29. Gavin, A.-C., and Nebreda, A. R. (1999) *Curr. Biol.* **9,** 281–286
30. Smith, J. A., Poteet-Smith, C. E., Malarkey, K., and Sturgill, T. W. (1999) *J. Biol. Chem.* **274,** 2893–2898
31. Sutherland, C., Campbell, D. G., and Cohen, P. (1993) *Eur. J. Biochem.* **212,** 581–588
32. Vik, T. A., and Ryder, J. W. (1997) *Biochem. Biophys. Res. Commun.* **235,** 398–402
33. Jensen, C. J., Buch, M.-B., Krag, T. O., Hemmings, B. A., Gammeltoft, S., and Frodin, M. (1999) *J. Biol. Chem.* **274,** 27168–27176
34. Richards, S. A., Fu, J., Romanelli, A., Shimamura, A., and Blenis, J. (1999) *Curr. Biol.* **9,** 810–820
35. Frodin, M., Antal, T. L., Dummler, B. A., Jensen, C. J., Deak, M., Gammeltoft, S., and Biondi, R. M. (2002) *EMBO J.* **21,** 5396–5407
36. Roux, P. P., Richards, S. A., and Blenis, J. (2003) *Mol. Cell. Biol.* **23,** 4796–4804
37. Williams, M. R., Arthur, J. S., Balendran, A., van der Kaay, J., Poli, V., Cohen, P., and Alessi, D. R. (2000) *Curr. Biol.* **10,** 439–448
38. Tomas-Zuber, M., Mary, J.-L., and Lesslauer, W. (2000) *J. Biol. Chem.* **275,** 23549–23558
39. Tomas-Zuber, M., Mary, J.-L., Lamour, F., Bur, D., and Lesslauer, W. (2001) *J. Biol. Chem.* **276,** 5892–5899
40. Yntema, H. G., van den Helm, B., Kissing, J., van Duijnhoven, G., Poppelaars, F., Chelly, J., Moraine, C., Fryns, J. P., Hamel, B. C., Heilbronner, H., Pander, H. J., Brunner, H. G., Ropers, H. H., Cremers, F. P., and van Bokhoven, H. (1999) *Genomics* **62,** 332–343
41. Kohn, M., Hameister, H., Vogel, M., and Kehrer-Sawatzki, H. (2003) *Gene Expr. Patterns* **3,** 173–177
42. Berns, K., Hijmans, E. M., Mullenders, J., Brummelkamp, T. R., Velds, A., Heimerikx, M., Kerkhoven, R. M., Madiredjo, M., Nijkamp, W., Weigelt, B., Agami, R., Ge, W., Cavet, G., Linsley, P. S., Beijersbergen, R. L., and Bernards, R. (2004) *Nature* **428,** 431–437
43. Myers, A. P., Corson, L. B., Rossant, J., and Baker, J. C. (2004) *Mol. Cell. Biol.* **24,** 4255–4266
44. Merienne, K., Jacquot, S., Zeniou, M., Pannetier, S., Sassone-Corsi, P., and Hanauer, A. (2000) *Oncogene* **19,** 4221–4229
45. Schweizer, A., Rohrer, J., Jeno, P., DeMaio, A., Buchman, T. G., and Hauri, H. P. (1993) *J. Cell Sci.* **104,** 685–694
46. Grove, J. R., Price, D. J., Banerjee, P., Balasubramanyam, A., Ahmad, M. F., and Avruch, J. (1993) *Biochemistry* **32,** 7727–7738
47. Green, S., Issemann, I., and Sheer, E. (1988) *Nucleic Acids Res.* **16,** 369
48. Kallunki, T., Su, B., Tsigelny, I., Sluss, H. K., Derijard, B., Moore, G., Davis, R., and Karin, M. (1994) *Genes Dev.* **8,** 2996–3007
49. Kallunki, T., Deng, T., Hibi, M., and Karin, M. (1996) *Cell* **87,** 929–939
50. Favata, M. F., Horiuchi, K. Y., Manos, E. J., Daulerio, A. J., Stradley, D. A., Feeser, W. S., Van Dyk, D. E., Pitts, W. J., Earl, R. A., Hobbs, F., Copeland, R. A., Magolda, R. L., Scherle, P. A., and Trzaskos, J. M. (1998) *J. Biol. Chem.* **273,** 18623–18632
51. Alessi, D. R., Cuenda, A., Cohen, P., Dudley, D. T., and Saltiel, A. R. (1995) *J. Biol. Chem.* **270,** 27489–27494
52. Cuenda, A., Rouse, J., Doza, Y. N., Meier, R., Cohen, P., Gallagher, T. F., Young, P. R., and Lee, J. C. (1995) *FEBS Lett.* **364,** 229–233
53. Myers, M. G., Backer, J. M., Siddle, K., and White, M. F. (1991) *J. Biol. Chem.* **266,** 10616–10623
54. Ferrell, J., and James E. (1996) *Trends Biochem. Sci.* **21,** 460–466
55. Collins, B. J., Deak, M., Arthur, J. S., Armit, L. J., and Alessi, D. R. (2003) *EMBO J.* **22,** 4202–4211

VI. APPENDIX

Part 3:

Vom Labor zum Krankenbett: Wie die Grundlagenforschung zur Entwicklung neuer Krebsmedikamente führt.

Dummler B, Hemmings BA.
Krebsforschung in der Schweiz 2005, 46-55. Review.
Editor: Wolfgang Wettstein
Publisher: Oncosuisse

Vom Labor zum Krankenbett: Wie die Grundlagenforschung zur Entwicklung neuer Krebsmedikamente führt

Bettina A. Dümmler[1], and Brian A. Hemmings[1,2]

[1]Friedrich Miescher Institut für Biomedizinische Forschung, Maulbeerstrasse 66, CH-4058, Basel

[2]Korrespondenz-Adresse:

Brian A. Hemmings
Friedrich Miescher Institut für Biomedizinische Forschung
Maulbeerstrasse 66
CH-4058, Basel
Schweiz
Tel.: (41)-61-697-4872
Fax: (41)-61-697 3976
Email: brian.hemmings@fmi.ch

Viele neue Erkenntnisse aus der Grundlagenforschung haben in den letzten Jahren zu konkreten Erfolgen im Bereich der Krebsbehandlung geführt. Unser zunehmendes Wissen darüber, wie aus gesunden Zellen Krebszellen entstehen können, ermöglicht die Entwicklung von spezifischen Medikamenten, welche weniger Nebenwirkungen zeigen als herkömmliche Chemotherapien. Mehrere neue Techniken, die in Forschungslaboratorien entstanden sind, werden nun im klinischen Bereich der Diagnostik eingesetzt.

Mit der Entschlüsselung des menschlichen Erbguts stehen erstmals Informationen über die Genstruktur aller menschlichen Gene zur Verfügung. Durch so genannte Hochdurchsatztechnologien kann diese immense Datenmenge für die molekulare Analyse von Krankheiten nutzbar gemacht werden. In einem einzigen Experiment kann in einem Gewebe oder einer Blutprobe die Expression von hunderten von Proteinen oder tausenden von Genen untersucht werden. Die Verfügbarkeit solcher Technologien hat die

biomedizinische Forschung fundamental verändert. Im Prinzip ist es heute möglich, präzise zu analysieren, welche Gene oder Proteine in einer Zelle eines bestimmten Typs oder Zustandes exprimiert werden, und welche nicht. Diese Information wird als "Expressionsprofil" des Zelltyps bezeichnet. Ein Bereich der Krebsforschung, in welchem diese Technologien intensiv genutzt werden, ist die Suche nach neuen Tumormarkern.

Tumormarker sind Stoffe, hauptsächlich Proteine, die sich bei der Entstehung und dem Wachstum von bösartigen Tumoren bilden. Indem man die Expressionsprofile von Krebszellen mit denjenigen von gesunden Zellen vergleicht, können viele solche potenzielle Marker identifiziert werden. Durch den spezifischen Nachweis eines verlässlichen Markermoleküls, zum Beispiel im Serum des Patienten oder in entsprechenden Gewebebiopsien, ist eine Diagnose in einem frühen Krebsstadium möglich. Neben verbesserter Diagnostik erlauben Hochdurchsatzverfahren aber auch eine zunehmend auf den einzelnen Patienten zugeschnittene Behandlung. Auf Grund von genetischen Unterschieden können zum Beispiel gewisse Medikamente bei einem Patienten wirkungsvoll sein, bei einem anderen jedoch keine oder eine unerwünschte Wirkung zeigen. So genannte Gentests können bei Patienten Verträglichkeit und Wirksamkeit für gewisse Medikamente im vornherein abklären.

Die Entwicklung effizienterer und besser verträglicher Krebsmedikamenten ist ein weiterer Forschungsschwerpunkt. Toxische Nebenwirkungen treten unter anderem bei allen Medikamenten auf, welche nicht nur Krebszellen, sondern auch das gesunde Gewebe angreifen. In den letzten Jahren wurden selektive Krebsmedikamente entwickelt, die ein höheres Potenzial zur Unterscheidung von Tumor- und Nichttumorzellen besitzen. Ein solcher neuer therapeutischer Ansatz ist der zielgerichtete Transport eines therapeutisch wirkenden Stoffes ins Tumorgewebe, zum Beispiel mit Hilfe von tumorspezifischen Antikörpern. Ein anderer innovativer Therapieansatz ist die selektive Inhibierung von Signaltransduktionswege innerhalb der Krebszellen. Fortschritte in der Grundlagenforschung haben hier zur Identifikation zahlreicher molekularer Angriffspunkte ('drug targets') geführt, für welche selektive Wirkstoffe entwickelt

werden können. Solche Angriffspunkte sind Proteine, die zum Beispiel an der Vermehrung der Krebszellen oder an der Entwicklung neuer Blutgefässe (Angiogenese) im Tumorgewebe beteiligt sind.

In diesem Beitrag möchten wir an einigen Beispielen erläutern, wie Ergebnisse aus der Grundlagenforschung Eingang in die klinische Praxis finden und damit den Patienten zugute kommen.

Früherkennung durch Tumormarker and Proteinmuster

Bei Krebs spielt das frühe Erkennen der Erkrankung eine entscheidende Rolle. Bisher basierte eine Diagnose hauptsächlich auf der mikroskopischen Untersuchung von Gewebeproben. Manche Krebserkrankungen sind jedoch bis zu dem Zeitpunkt, an dem ein solcher Nachweis möglich ist, schon weit fortgeschritten und können häufig nicht mehr erfolgreich behandelt werden. In der Grundlagenforschung werden deshalb grosse Anstrengungen unternommen, um verlässliche Tumormarker zu identifizieren. Tumormarker sind Substanzen, meist Proteine, die bei Krebserkrankungen im Blut oder in anderen Körperflüssigkeiten erstmals oder in größerer Menge nachweisbar sind. In der klinischen Praxis können Serumproben von Patienten auf solche Tumormarker untersucht werden, um Krebserkrankungen frühzeitig zu erkennen.

Konzeptionell stützt sich dieses diagnostische Verfahren auf die veränderte Expression von Genen und Proteinen, die mit der Krebsentstehung einhergehen. Über solche molekularen Veränderungen weiss man in der Grundlagenforschung immer besser Bescheid. Zudem können mittels neuer Hochdurchsatzverfahren zahlreiche im Erkrankungszustand unterschiedlich exprimierte Proteine identifiziert werden. Diese Fortschritte haben zur Aufdeckung einer Reihe neuer Tumormarker-Kandidaten geführt (1,2). Prostataspezifisches Antigen (PSA) ist ein gutes Beispiel für einen etablierten Tumormarker. PSA ist ein Protein das von der Prostata sezerniert wird. Die Entdeckung, dass die Serumkonzentration von PSA bei Prostatakrebs erhöht ist, hat die Diagnostik von Prostatakrebs drastisch verbessert. Seit über zehn

Jahren werden nun Messungen der Serumkonzentration von PSA routinemässig für die Früherkennung und Überwachung von Prostatakrebs genutzt. Ausserdem sind einige neue Tumormarker identifiziert worden, welche die Diagnose von Prostatakrebs weiter verbessern könnten, zum Beispiel humanes Kallikrein 2 (hK2) (3) und Prostataspezifisches Membran Antigen (PSMA) (4).

Eine weitere vielversprechende Perspektive für die klinische Diagnostik bietet die Untersuchung von Proteinmustern ('proteomic pattern analysis'). Diese Methode fokussiert nicht auf die Identifikation eines einzelnen Tumormarkers, sondern erfasst das Gesamtbild der Veränderungen in den Protein- und Peptidzusammensetzungen (6). Mit einer auf Massenspektrometrie basierenden Technologie kann beispielsweise eine Abbildung des Proteinmusters einer Serumprobe aufgezeichnet werden. Für diese Methode ist keine Identifikation der einzelnen Komponenten notwendig. Vielmehr wird ein für "Krebserkrankung" charakteristisches Proteinmuster etabliert, welches dann mit dem Proteinmuster der Serumprobe eines Patienten verglichen wird.

Eine kürzlich publizierte Pilotstudie benutzte dieses neuartige diagnostische Verfahren zur Erkennung von Tumoren in Eierstöcken (7). Bei dieser Krebsart ist eine Frühdiagnose besonders dringlich. Tumore der Eierstöcke werden oft zu spät erkannt und haben dann nur noch geringe Heilungschancen. Bei rechtzeitiger Erkennung könnten jedoch die meisten Patienten durch einen operativen Eingriff geheilt werden. In der erwähnten Pilotstudie wurden durch Proteinmuster-Analysen Tumore der Eierstöcke mit einer Effizienz von über 90% erkannt. Die Proteinmuster-Analysen in der Tumordiagnostik steckt zwar noch in den Anfängen, sie könnte sich aber in naher Zukunft zu einer effizienten diagnostischen Methode entwickeln.

Gentests und Massgeschneiderte Behandlungen

Warum reagieren Patienten unterschiedlich auf eine Behandlung? Und wie finden wir die optimale Behandlung für den einzelnen Patienten? Die Antwort liegt zu einem grossen Teil in der Genetik. Kleine genetische Unterschiede

können nicht nur das Risiko, an Krebs zu erkranken, und den klinischen Verlauf der Krebserkrankung beeinflussen, sondern können auch dramatische Auswirkung auf die Wirksamkeit und Verträglichkeit von Medikamenten haben (8). Der Einbezug der Genetik in die Krebsbehandlung fördert eine individuell angepasste Medizin, welche eine Maximierung der Effizienz und Minimierung von toxischen Nebenwirkungen erlaubt. Dabei sollten sowohl der genetisch Hintergrund des Patienten, als auch die genetische Klassifizierung des Tumors berücksichtigt werden.

Gentests können das Erbgut von Patienten auf häufige Mutationen (so genannte Polymorphismen) in Genen überprüfen, welche zum Beispiel die Verstoffwechselung der Medikamente regulieren. Solche Tests stehen vor allem dann zur Diskussion, wenn ein Medikament verordnet werden soll, bei dem gravierende Nebenwirkungen auftreten können. Ein gutes Beispiel für eine solche Situation ist die Behandlung mit 6-Mercaptopurin (6MP). Dies ist ein effizientes Medikament um Leukämie bei Kindern zu behandeln. Die Behandlung mit 6MP ist jedoch bei Patienten mit vererbten Mutationen in TPMT, einem Gen, das die Verstoffwechselung von 6MP beeinflusst, extrem toxisch. Für Patienten, welche in beiden Genkopien von TPMT eine Mutation tragen, ist die Einnahme von 6MP lebensgefährlich (9). Es ist relativ einfach, Patienten auf eine Mutation in einem einzelnen Gen zu überprüfen. Schwieriger wird es, wenn wie für die meisten Krebsmedikamente, zahlreiche genetische Polymorphismen die Wirksamkeit und Verträglichkeit beeinflussen.

Ein neues Verfahren, welches die parallele Analyse von zahlreichen Genen ermöglicht, ist die Microarray Technologie. Microarray Chips, auch Genchips genannt, bestehen aus einer soliden Oberfläche, beispielsweise aus Glas, auf der tausende von verschiedenen DNA Molekülen (so genannte DNA- oder Oligonukleotid-Proben) in einer systematische Anordnung platziert sind (Abb. 1). Jede einzelne Probe besteht aus einem einmaligen genau definierten Genabschnitt. Anhand eines solchen Microarrays kann untersucht werden. welche Gene in einer Zelle transkribiert werden. Microarray Technologie kann unter anderem (mit auf diesen Zweck angepassten DNA Proben) dazu benutzt werden, genetische Polymorphismen im Erbgut eines Patienten abzuklären.

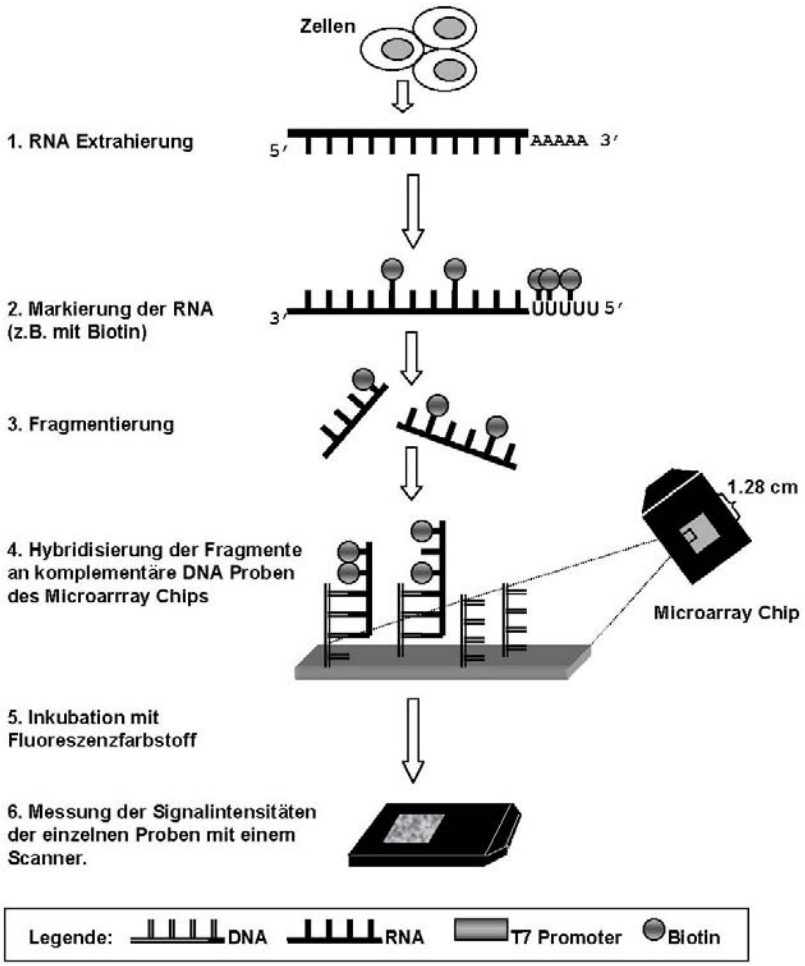

Abb. 1. Microarray Technologie. Microarray Chips ermöglichen die simultane Expressionsanalyse von zehntausenden von Genen in einem einzigen Assay. Als erster Schritt wird RNA aus biologischem Material (z.B. Blut oder Gewebe) extrahiert. Diese RNA wird danach über mehrere Zwischenschritte markiert (z.B. mit Biotin) und in kürzere Fragmente zerstückelt. Die RNA Fragmente werden dann mit dem Microarray Chip inkubiert. Ein Microarray Chip enthält sogenannte DNA Proben, kurze Gensequenzen von tausenden von verschiedenen Genen, welche auf einem Träger immobilisiert sind. Ein einziger Microarray Chip kann heute mit bis zu 450'000 verschiedenen DNA Proben bestückt werden, wobei jede Probe auf dem Chip eine genau bekannte Sequenz und Lokalisation hat. Oft ist so ein Chip nicht viel grösser als 1 cm^2. Die Anordnung und Zusammensetzung der Proben auf solchen Chips können bei der Herstellung dem Verwendungszweck angepasst werden. Die markierten RNA Fragmente hybridisieren während der Inkubation an komplementäre DNA Proben auf dem Microarray. Die gebundene RNA kann z.B. mit einem an Streptavidin-gekoppelten Fluoreszenzfarbstoff detektiert werden. Für jede Probe wird mit einem Scanner die Lichtintensität des Fluoreszenzfarbstoffes gemessen. Diese ist proportional zur Anzahl gebundener RNA Transkripte und es ist damit möglich die relative Menge der Transkripte eines spezifischen Gens zu bestimmen.

Eine andere Anwendung für Microarray Technologie ist die genetische Klassifizierung von Tumoren. Neben genetischen Polymorphismen im Erbgut der Patienten ist die molekulare Heterogenität der Tumore ein weiterer Hauptgrund für die interindividuelle Variation in der Arzneimittelwirkung. Tumorentwicklung ist ein komplexer Prozess, und auch wenn Tumore, die aus demselben Zelltyp entstanden sind, gewisse gemeinsame Charakteristika haben, gibt es dennoch grosse Variationen auf der molekularen und genetischen Ebene. Bis jetzt ist die mikroskopische Untersuchung von Tumorbiopsien der goldene Standard für Diagnose und Klassifizierung. Sie beruht ausschliesslich auf dem morphologischen Erscheinungsbild des Tumors. Morphologisch ähnliche Tumore können jedoch unterschiedliche molekulare Veränderungen aufweisen, die den klinischen Prozess und die Ansprechbarkeit auf Medikamente wesentlich bestimmen. Mit Microarray Technologie ist eine molekulare Tumorklassifizierung anhand von Genexpressionsprofilen möglich, welche die herkömmlichen Diagnoseverfahren komplementieren kann (10). Die prognostische und therapeutische Beurteilung eines Tumors wird dadurch signifikant verbessert und ermöglicht eine Behandlung die besser auf den individuellen Patienten abgestimmt ist.

Molekulare Angriffspunkte und tumorspezifische Antikörper in der Krebsbehandlung

Zwar hat sich die Chemotherapie bei bestimmten Krebsarten als ausserordentlich wirkungsvoll erwiesen, doch wird ihre Effizienz häufig durch erhebliche Nebenwirkungen behindert. Die meisten zytotoxischen Wirkstoffe, die in der Chemotherapie eingesetzt werden, wirken auf DNA und Tubulin, das heisst, ihre Wirkung beschränkt sich nicht auf Krebszellen, sondern sie greifen alle sich häufig teilenden Zellen im Körper an. Eine neue Behandlungsmöglichkeit hat sich nun mit der Entwicklung von zielgerichteten Wirkstoffen eröffnet, welche spezifisch bestimmte zelluläre Proteine blockieren, die an der Tumorentstehung beteiligt sind. Solche Proteine können Plasmamembranrezeptoren sein, Komponenten von intrazellulären

Signaltransduktionswegen, Zellzyklus-regulierende Proteine, oder auch Proteine und Signalstoffe, welche in der Angiogenese wichtig sind.

Eine wichtige Klasse von Proteinen, auf welche viele der neuen Wirkstoffe ausgerichtet sind, bilden die Proteintyrosinkinasen (PTKs) (Tabelle 1).

Tabelle 1

Proteinkinase-Hemmer in klinischer Entwicklung

Hemmer	Firma	Zielkinase(n)
Flavopiridol	Aventis	Cdks
PD184352 (CI 1040)	Pfizer	MEK
RAD001	Novartis	mTOR
CCI779	Wyeth-Ayerst	mTOR
E7070	Eisai	Cdks
Cyc202	Cyclacel	Cdks
Bryostatin-I	Bristol Myers Squibb	PKC
PKC412	Novartis	PKC, VEGFR2, PDGFR, Flt-3
UCN-01	NCI	PKC and Chk1
ISIS 3521 (antisense)	ISIS	PKC-α
GEM231 (antisense)	Hybridon	PKA
BIRB0796	Boehringer Ingelheim	p38
SCIO-469	Scios	p38
BAY 43-9006	Bayer	c-raf
CEP-1347	Cephalon	Jun
LY-333531	Eli Lilly	PKC-β
Gleevec (Glivec, Imatinib, STI571)	Novartis	ABL, KIT, PDGFR
PTK787/ZK222584	Novartis/Schering AG	VEGFR2, KIT, PDGFR
PKI166	Novartis	EGFR and HER-2
AG013726	Agouron	VEGFR2, PDGF-R
KRN633	Kirin	VEGFR1/2, KIT
CHIR 200131	Chiron	VEGFR1/2, FGFR, PDGFR
Tarceva (Erlotinib, OSI-774)	Roche/Genentech/OSI	EGFR
CI-1033 (PD183805)	Pfizer/Warner-Lambert	EGFR and HER-2
CP-547632	Pfizer	VEGFR2, FGFR
EKB-569	Wyeth-Ayerst	EGFR and HER-2
GW-2016	GlaxoSmithKline	EGFR and HER-2
SU5416	SUGEN/Pharmacia	VEGFR2
SU6668	SUGEN/Pharmacia	VEGFR2 (PDGFR, FGFR)
SU11248	SUGEN/Pharmacia	VEGFR, PDGFR, KIT, Flt-3
ZD 6474	AstraZeneca	VEGFR2 and EGFR
Iressa (Gefitinib, ZD 1839)	AstraZeneca	EGFR
CEP-701	Cephalon	Trk
Angiozyme ®	Ribozyme	VEGFR1 (Flt-1)

Abkürzungen: ABL: Abelson; Cdk: cyclin-dependent kinase; Chk1: checkpoint kinase 1; EGFR: Epidermal growth factor receptor; FGFR: fibroblast growth factor receptor; Flt: FMS-like tyrosine kinase; MEK: mitogen-activated protein kinase kinase; PDGFR: platelet-derived growth factor receptor; PKA: protein kinase A; PKC: protein kinase C; VEGF-R: vascular endothelial growth factor receptor.

PTKs sind Enzyme, welche andere Proteine modifizieren, indem sie Phosphatgruppen auf deren Tyrosin-Reste übertragen (Phosphorylierung).

Durch solche Phosphorylierungen können PTKs die Funktion anderer Proteine aktivieren oder deaktivieren. Häufig belegen PTKs deshalb eine Schlüsselposition innerhalb intrazellulärer Signaltransduktionswege und kontrollieren zahlreiche zelluläre Prozesse wie Wachstum, Stoffwechsel, Differenzierung, und Apoptose der Zelle (Abb. 2).

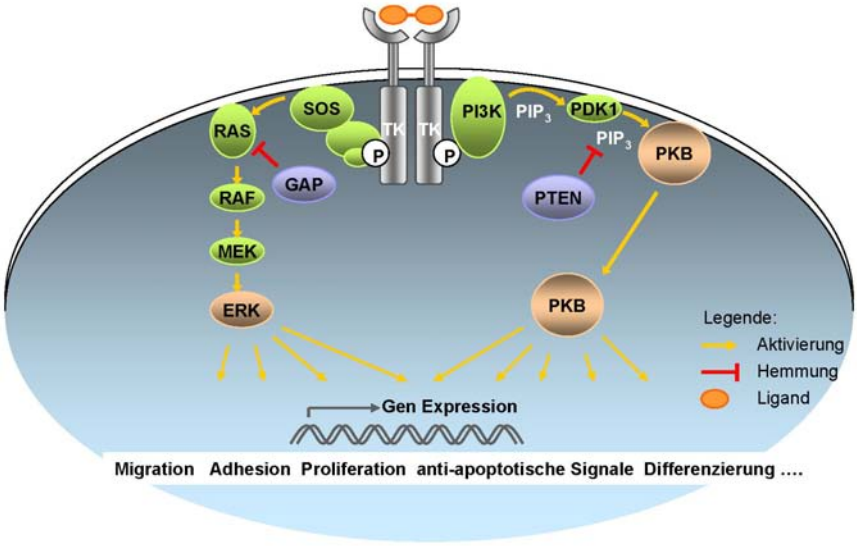

Abb. 2. Signaltransduktionswege von Rezeptor-Tyrosinkinasen. Receptor-Tyrosinkinasen wie z.B. PDGFR (platelet-derived growth factor receptor), EGFR (epidermal growth factor receptor) und HER-2, enthalten eine extrazelluläre Rezeptor-Domäne, welche den Ligand bindet, und eine intrazelluläre Tyrosinkinase-Domäne (TK). Beim Binden eines Liganden dimerisieren die Rezeptoren, und ihre intrazelluläre Tyrosinkinase-Domänen werden aktiviert durch Phosphorylierung (P). Spezifische intrazelluläre Signalproteine werden darauf zu den aktivierten Rezeptoren rekrutiert und induzieren verschiedene Signaltransduktionswege. Zwei wichtige solche Signaltransduktionswege sind hier illustriert: der RAS/ERK Signalweg (links) und der PI3K/PKB Signalweg (rechts). Viele Proteine in diesen Signalwegen sind Proteinkinasen (z.B. RAF, MEK, ERK, PDK1, and PKB). Abhängig vom zellulären Zusammenhang und dem Ligand-Rezeptor-Paar, definieren diese Signaltransduktionswege verschiedenste physiologische Vorgänge wie Zellproliferation, Differenzierung, Migration oder Apoptose. Wird dieses abgestimmte Netzwerk durch Überexpression oder Genmutationen in wichtigen Signalmolekülen gestört, kann dies zu pathophysiologischen Veränderungen wie beispielsweise Krebs führen. (Abkürzungen: ERK: extracellular signal-regulated kinase; GAP: GTPase activating protein; MEK: Mitogen-activated protein kinase kinase; PDK1: 3-phosphoinositide-dependent kinase; PI3K: phosphoinositol 3-kinase; PIP_3: phosphatidylinositol 3,4,5-trisphosphate; PKB: Protein kinase B; PTEN: Phosphatase and tensin homolog deleted on chromosome 10; SOS: son of sevenless).

In einer gesunden Zelle wird genau kontrolliert, wo und für wie lange eine solche Schlüsselposition-PTK aktiv ist. In Krebszellen ist die Aktivität von PTKs jedoch aufgrund von Mutationen oder anderen genetischen Veränderungen oft ausser Kontrolle. Die Konsequenz ist ein deregulierter Signaltransduktionsweg, der zur unkontrollierter Vermehrung der Zelle und zur Entstehung maligner Tumore führen kann. Im menschlichen Genom sind über 90 PTKs bekannt und viele von diesen sind bei Krebserkrankungen als Onkogene identifiziert worden (11). Das Verständnis der physiologischen Regulation von PTKs und der molekularen Mechanismen, welche eine onkogene Aktivierung von PTKs bewirken, ist ein wichtiges Anliegen der Grundlagenforschung- und die Voraussetzung für die Entwicklung von auf PTKs ausgerichteten Medikamenten.

Zahlreiche niedermolekulare synthetische Wirkstoffe, welche PTKs hemmen, sind zur Zeit in der klinischen Entwicklung (Tabelle 1) (12,13). Das Krebsmedikament Gleevec (Glivec, imatinib mesylate, vorher STI571) ist ein beeindruckendes Beispiel für die erfolgreiche Therapie von Krebserkrankungen mit einem Tyrosinkinase-Hemmer (14). Gleevec wird für die Behandlung von chronisch myeloischer Leukämie (CML), einer Form von Blutkrebs, bei dem es zu exzessiver Vermehrung von weissen Blutkörperchen kommt, verewendet. Die leukämischen Zellen fast aller CLM Patienten weisen eine spezifische chromosomale Anomalie auf: eine reziproke Translokation von genomischer DNA zwischen den Chromosomen 9 und 22 (das dadurch veränderte Chromosom 22 ist bekannt als Philadelphia-Chromosom). Durch diese Umlagerung geraten auf Chromosom 22 zwei Gene - das Gen für die Proteintyrosinkinase Abelson (ABL) und das Gen für break-point cluster region (BCR) - in unmittelbare Nachbarschaft,. Als Produkt entsteht ein abnormes BCR-ABL Fusionsprotein mit erhöhter Tyrosinkinase-Aktivität, welches die Blutzellen dazu antreibt, sich ungebremst zu teilen. Diese Erkenntnisse aus der Grundlagenforschung, die BCR-ABL als zentralen Verursacher von CML identifizierten, lieferten der medizinischen Forschung einen molekularen Angriffspunkt für den nun gezielt ein Wirkstoff entworfen werden konnte.

Die Entwicklung des Medikaments Gleevec begann mit einem willkürlichen Screen für Tyrosinkinasehemmer. Dabei wurde eine erste geeignete Prototyp-Substanz gefunden, die mehrere Tyrosinkinasen hemmte, darunter auch BCR-ABL. Die gefundene Substanz wurde daraufhin durch chemische Veränderungen optimiert und daraus entstand der Wirkstoff Gleevec, ein spezifischer und potenter Hemmer von drei Kinasen, nämlich (BCR-)ABL, platelet-derived growth factor receptor (PDGFR) und c-KIT. Tests in Zellkulturen und Mausmodellen zeigten, dass Gleevec gezielt BCR-ABL induzierte Zellproliferation hemmen kann, ohne gesunde Zellen anzugreifen (15,16). Solche Experimente führten zu ersten klinischen Tests, welche die Wirksamkeit von Gleevec in der Behandlung von CML bestätigen konnten. In der Schweiz erhielt das Medikament schliesslich im April 2002 die Zulassung (17). Gleevec setzt neue Standards für Krebstherapien, die gezielt molekulare Signaltransduktionswege hemmen. Es wurde seither nicht nur für die Behandlung von CML gebraucht, sondern hat sich auch bei bestimmten anderen Krebserkrankungen, bei welchen ABL, c-KIT oder PDGFR eine kritische Rolle in der Pathogenese spielen, bewährt (18).

Ein anderer Therapieansatz für einen zielgerichteten Angriff auf Krebszellen ist der Gebrauch von tumorspezifischen monoklonalen Antikörpern (19). Eine erste Herausforderung war hier die Entwicklung von verträglichen Antikörpern. Erste Antikörperkonstrukte stammten von Mäusen und verursachten teilweise starke Abstossungsreaktionen, da das menschliche Immunsystem diese als Fremdproteine erkennt. Durch die Entwicklung von genetisch veränderten Mäusen und anderen Technologien wurde es möglich, so genannte "humanisierte" Maus-Antikörper (zu 95% human und zu 5% murin) oder sogar vollständig humane Antikörper zu produzieren. Diese sind gut verträglich und für den therapeutischen Gebrauch geeignet. Im Gegensatz zu den oben erwähnten niedermolekularen synthetischen Wirkstoffen, können Antikörper jedoch nicht ins Zellinnere eindringen und deshalb nur solche tumorspezifische Zielproteine angreifen, die an der Zelloberfläche zugängliche sind. Therapeutische Antikörper haben einen einzigartigen Wirkungsmechanismus um Tumorzellen zu bekämpfen: sie mobilisieren körpereigene Abwehrzellen (natürliche Killerzellen) und Komplement-Proteine des Immunsystems, welche

vom gebundenen Antikörper dazu aktiviert werden die Tumorzelle abzutöten. In den Fällen, in denen das Zielprotein des Antikörpers ein Wachstumsfaktor-Rezeptor ist, kann die Bindung des Antikörpers auch dessen Signaltransduktion blockieren oder verändern. Therapeutische Antikörper können zudem auch mit einer zytotoxischen Substanz (z.B. Radioisotope oder Toxine) gekoppelt werden, welche dann spezifisch dem Tumor zugeführt wird.

Tabelle 2

Therapeutische Antikörper in klinischer Entwicklung

Antikörper	**Firma**	**Zielkinase(n)**
Cetuximab (Erbitux, IMC-225)	ImClone & Merck KgaA	chimeric mAb against EGFR
Herceptin (Trastuzumab)	Genentech	humanized mAb against HER-2
Bevacizumab (Avastin, RhuMAb)	Genentech	humanized mAb against VEGF
ABX-EGF	Abgenix/Immunex	humanized mAb against EGFR
MDX-447 (EMD 82633)	MEdarex	humanized mAb against EGFR
MV833	EORTC	humanized mAb against VEGFR
IMC-1C11	ImCone	chimeric mAb against VEGFR
CDP 860	Celltech	humanized mAb against PDGFR

Mehrere therapeutische Antikörper für verschiedene Krebserkrankungen befindend sich zur Zeit in klinischen Testphasen oder sind bereits zugelassen (Tabelle 2). Ein Beispiel für einen zugelassenen therapeutischen Antikörper, welcher ebenfalls eine PTK als Zielprotein hat, ist Herceptin (Trastuzumab). Herceptin wird in der Behandlung von Brustkrebs verwendet (20,21). Die Suche nach genetischen Veränderungen bei Brustkrebs, wies in den Tumoren von 25-30% der Patientinnen eine Überexpression des Wachstumsfaktor-Rezeptors HER-2 (human epidermal growth factor receptor-2, ErbB2/Neu) nach.

HER-2 ist ein Transmembranprotein mit einer extrazellulären Rezeptordomäne und einer intrazellulären Domäne mit Tyrosinkinase-Aktivität, durch welche Proliferationssignale an den Zellkern weitergeleitet werden können (Abb. 2). Überexpression von HER-2 führt in Zellen zu unkontrollierter Proliferation und ist bei Brustkrebs mit einem aggressiveren Tumorphänotyp und schlechteren Heilungschancen verbunden (22).

Es wurden deshalb viele Wirkstoffe entwickelt, die spezifisch auf HER-2 ausgerichtet sind (Tabelle 1 und 2). Im Gegensatz zu BCR-ABL, ist HER-2 an der Zelloberfläche zugänglich und kann von therapeutischen Antikörpern erreicht werden. Herceptin, ein humanisierter monoklonaler Antikörper ist gegen die extrazelluläre Komponente des HER-2 Proteins gerichtet und zeigt effiziente Wirkung in der Behandlung von HER-2-überexprimierenden Brusttumoren.

Zielgerichtete Therapien mit niedermolekularen synthetischen Hemmern oder therapeutischen Antikörpern haben ein grosses Potenzial für die Krebsbehandlung. Die Grundlagenforschung ist hier essenziell, um geeignete, mit der Krebsentstehung und –ausbreitung relevante Proteine zu identifizieren.

Schlussfolgerung

Innerhalb weniger Jahre wurden sowohl in der Diagnostik als auch im Therapiebereich grosse Fortschritte erzielt. Innovative Technologien und das zunehmend bessere Verständnis der molekularen Mechanismen, die der Entstehung eines Tumors zugrunde liegen, haben zur Entdeckung zahlreicher Tumormarker und molekularer Angriffspunkte für zielgerichtete therapeutische Wirkstoffe geführt. Eine neue Generation von antineoplastischen Wirkstoffen wurde entwickelt, welche die molekulare Basis von Krebs bekämpft. In den nächsten paar Jahren wird die Entwicklung hochspezifischer Krebsmedikamente voraussichtlich exponentiell ansteigen. PTKs und Signaltransduktions-Kinasen im Allgemeinen bilden eine wichtige Gruppe von Zielproteinen für spezifische Krebsmedikamente. Die klinische Wirksamkeit von Gleevec belegt eindrucksvoll den Nutzen und das Potenzial von Kinasehemmern in der Krebsbehandlung. Pharmazeutische Unternehmen fokussieren deshalb über ein Drittel ihrer Medikamentenforschung im Bereich der Krebsbehandlung auf Kinasehemmer.

Die Behandlung mit hochspezifischen Krebsmedikamenten setzt jedoch eine sorgfältige Abklärung beim Patienten voraus. So muss geprüft werden, ob es wahrscheinlich ist, dass der betreffende Patient auf ein spezifisches

Medikament anspricht (oder schädigende Nebenwirkungen erleiden müsste). Eine solche Abklärung erfordert eine genetische und molekulare Analyse des Tumors und des Patienten. Ansatzweise ist dies zum Beispiel schon Praxis bei Herceptin: Das Medikament wird nur an solche Brustkrebs-Patientinnen abgegeben, bei welchen eine Überexpression von HER-2 in den Tumoren nachgewiesen wurde. Zukünftige Therapien könnten aus Kombinationsbehandlungen von mehreren zielgerichteten Medikamenten bestehen, die in Krebszellen komplementär den selben Signaltransduktionsweg blockieren. Fortgesetzte intensive Grundlagenforschung ist notwendig um die zellulären Signalnetzwerke, welche die Krebsentwicklung antreiben, weiter zu entschlüsseln, und den Weg für neue therapeutische Ansätze zu bahnen.

Referenzen:

(1) Negm, R.S., Verma, M., Srivastava, S. (2002). The promise of tumormarkers in cancer screening and detection. Trends Mol Med, 8, 288-293. Review.

(2) Wu, W., Hu, W., and Kavanagh, J.J. (2002). Proteomics in cancer research. Int J Gynecol Cancer, 12, 409-423. Review.

(3) Darson, M.F., Pacelli, A., Roche, P., Rittenhouse, H.G., Wolfert, R.L., Young, C.Y., Klee, G.G., Tindall, D.J., Bostwick, D.G. (1997). Human glandular kallikrein 2 (hK2) expression in prostatic intraepithelial neoplasia and adenocarcinoma: a novel prostate cancer marker. Urology, 49, 857-862.

(4) Silver, D.A., Pellicer, I., Fair, W.R., Heston, W.D., Cordon-Cardo, C. (1997). Prostate specific membrane antigen expression in normal and malignant human tissues. Clin Cancer Res, 3, 81-85.

(6) Conrads, T.P., Zhou, M., Petricoin III, E.F, Liotta, L., Veenstra, T.D. (2003). Cancer diagnosis using proteomic patterns. Expert Rev Mol Diagn, 3, 411-420. Review.

(7) Petricoin, E.F., Ardekani, A.M., Hitt, B.A., Levine, P.J., Fusaro, V.A., Steinberg, S.M., Mills, G.B., Simone, C., Fishman, D.A., Kohn, E.C., Liotta, L.A.

(2002). Use of proteomic patterns in serum to identify ovarian cancer. Lancet, 359, 572-577.

(8) Watters, J.W., McLeod, H.L. (2003). Cancer pharmacogenomics: current and future applications. Biochim Biophys Acta, 1603, 99-111. Review.

(9) McLeod, H.L., Krynetski, E.Y., Relling, M.V., Evans, W.E. (2000). Genetic polymorphism of thiopurine methyltransferase and its clinical relevance for childhood acute lymphoblastic leukemia. Leukemia, 14, 567-72. Review.

(10) Liefers, G.-J., Tollenaar, R.A.E.M. (2002). Cancer genetics and their applications to individualised medicine. Eur J Cancer, 38, 872-879. Review.

(11) Blume-Jensen, P., Hunter, T. (2001). Oncogenic kinase signalling. Nature, 411, 355-365. Review.

(12) Laird, A.D., Cherrington, J.M. (2002). Small molecule tyrosine kinase inhibitors: clinical development of anticancer agents. Expert Opin Investig Drugs, 12, 51-64. Review.

(13) Fabbro, D., Parkinson, D., Matter, A. (2002). Protein tyrosine kinase inhibitors: new treatment modalities? Curr Opin Pharmacol, 2, 374-81. Review.

(14) Capdeville, R., Buchdunger, E., Zimmermann, J., Matter, A. (2002). Glivec (STI571, imatinib), a rationally developed, targeted anticancer drug. Nat Rev, 1, 493-502.

(15) Buchdunger, E., Zimmermann, J., Mett, H., Meyer, T., Muller, M., Druker, B.J., Lydon, N.B. (1996). Inhibition of the Abl protein-tyrosine kinase in vitro and in vivo by a 2-phenylaminopyrimidine derivative. Cancer Res, 56, 100-104.

(16) Druker, B.J., Tamura, S., Buchdunger, E., Ohno, S., Segal, G.M., Fanning, S., Zimmermann, J., Lydon, N.B. (1996). Effects of a selective inhibitor of the Abl tyrosine kinase on the growth of Bcr-Abl positive cells. Nat Med, 2, 561-566.

(17) Kantarjian, H., Sawyers, C., Hochhaus, A., Guilhot, F., Schiffer, C., Gambacorti-Passerini, C., Niederwieser, D., Resta, D., Capdeville, R., Zoellner, U., Talpaz, M., Druker, B., Goldman, J., O'Brien, S.G., Russell, N., Fischer, T., Ottmann, O., Cony-Makhoul, P., Facon, T., Stone, R., Miller, C., Tallman, M., Brown, R., Schuster, M., Loughran, T., Gratwohl, A., Mandelli, F., Saglio, G., Lazzarino, M., Russo, D., Baccarani, M., Morra, E.; International STI571 CML

Study Group (2002). Hematologic and cytogenetic responses to imatinib mesylate in chronic myelogenous leukemia. N Engl J Med, 346, 645-652.

(18) Dagher, R., Cohen, M., Williams, G., Rothmann, M., Gobburu, J., Robbie, G., Rahman, A., Chen, G., Staten, A., Griebel, D., Pazdur, R. (2002). Approval summary: imatinib mesylate in the treatment of metastatic and/or unresectable malignant gastrointestinal stromal tumors. Clin Cancer Res, 8, 3034-3038.

(19) Harris, M. (2004). Monoclonal antibodies as therapeutic agents for cancer. Lancet Oncology, 5, 292-302.

(20) Carter, P., Presta, L., Gorman, C.M., Ridgway, J.B., Henner, D., Wong, W.L., Rowland, A.M., Kotts, C., Carver, M.E., Shepard, H.M. (1992). Humanization of an anti-p185HER2 antibody for human cancer therapy. Proc Natl Acad Sci U S A, 89, 4285-4289.

(21) Cobleigh, M.A., Vogel, C.L., Tripathy, D., Robert, N.J., Scholl, S., Fehrenbacher, L., Wolter, J.M., Paton, V., Shak, S., Lieberman, G., Slamon, D.J. (1999). Multinational study of the efficacy and safety of humanized anti-HER2 monoclonal antibody in women who have HER2-overexpressing metastatic breast cancer that has progressed after chemotherapy for metastatic disease. J Clin Oncol, 17, 2639-2648.

(22) Slamon, D.J., Clark, G.M., Wong, S.G., Levin, W.J., Ullrich, A., McGuire, W.L. (1987). Human breast cancer: correlation of relapse and survival with amplification of the HER-2/neu oncogene. Science, 235, 177-182.